Modelling of Phase Transformations and Properties in Steel Weld Metal

By

Kazutoshi Ichikawa

Darwin College, Cambridge

Department of Materials Science and Metallurgy

Pembroke Street

Cambridge CB2 3QZ

A dissertation submitted for the degree of

Doctor of Philosophy

at the University of Cambridge

February 1999

PREFACE

This dissertation is submitted as a Ph. D. thesis in the University of Cambridge. The investigation described here was carried out under the supervision of Dr H. K. D. H. Bhadeshia, in the Department of Materials Science and Metallurgy, University of Cambridge between October 1994 and October 1996. This work is to the best of my knowledge original and has been carried out without collaboration, except where acknowledgements and references are specially made to the contrary. Neither this, nor any substantially similar dissertation has been or is being submitted for any degree, diploma or other qualification at any other university or institution. The work has been presented in the following publications:

K. Ichikawa, H. K. D. H. Bhadeshia and D. J. C. MacKay, *Science and Technology of Welding and Joining*, 1996, 1, pp. 43–50.

K. Ichikawa and H. K. D. H. Bhadeshia, *Mathematical modelling of weld phenomena 3*, Ed. H. Cerjak, The Institute of Materials, 1997, pp. 181–198.

K. Ichikawa and H. K. D. H. Bhadeshia, *Mathematical modelling of weld phenomena 4*, Ed. H. Cerjak, The Institute of Materials, 1998, pp. 302–320.

T. Kasuya, K. Ichikawa, M. Fuji and H. K. D. H. Bhadeshia, *Materials Science and Technology*, 1998, *in press*.

Kazutoshi Ichikawa
Darwin College

ACKNOWLEDGEMENTS

I would like to thank Professor Alan Windle for the provision of laboratory facilities in the Department of Materials Science and Metallurgy at the University of Cambridge. I would also like to express my gratitude to my supervisor Dr H. K. D. H. Bhadeshia, FRS for his invaluable assistance and boundless enthusiasm. I have learnt from him during the course of my study not only materials science but also how a scientist should be. I am also very grateful to follow members of my research group for their friendship, kindness and help. Dr David MacKay, at the Darwin College, gave me invaluable guidance with the use of his classification neural network model. I wish to exprèss my special thanks to Dr Hidetoshi Fujii (now at the Osaka University, Japan), in our research group, for his help on operating the neural network programs.

I gratefully acknowledge Dr Tasuku Huwa, Emeritus Professor of Tohoku University in Japan and Dr. Nobutaka Yurioka, the Research Fellow at Nippon Steel Corporation for giving me the opportunity to study in the University of Cambridge. Dr Yurioka especially led me to the attractive scientific world of welding when he was a visiting professor at Nagoya University, Japan. I also wish to thank Dr Chuich Katoh, Mr Masao Fuji and Dr Shigeru Ohkita for allowing me to work on the modelling of weld phenomena at the Welding & Joining Research Center, Nippon Steel Corporation.

I am indebted to many members of the Welding & Joining Research Center, Nippon Steel Corporation for assistance with my work; Dr Yukihiko Horii (now at the Japan Power Engineering and Inspection Corporation), Dr Tadashi Kasuya, Dr Toshihiko Koseki (now at the Oita R&D Laboratories) and Mr. Kazuhiro Kojima. Mr Kazuhiro Kojima, a senior researcher, helped me with the experiments in this study. Dr Yukihiko Horii taught me the importance of welding technology in modern steel fabrication. I am grateful to Dr Tadashi Kasuya for his useful discussions. I am also grateful to Dr Toshihiko Koseki for his invaluable discussion and help in using Thermo-Calc. I am also indebted to grants from the Personnel Division of Nippon Steel Corporation, and would like to acknowledge here the generosity of the organisation for the financial support.

I wish to express my thanks to Miyuki, my wife for her dedicated support to my life in Cambridge. I am also grateful to my lovely children Mami and "Tommy" Tomohiro. Without their encouragement, this thesis could not be completed. Finally, I deeply thank my parents for their cordial encouragement throughout the years.

ABSTRACT

The purpose of the work in this thesis was to formulate a model for the prediction of microstructure and mechanical properties of steel weld metals.

Existing work on the modelling of steel welds is reviewed in Chapter 1. The review includes important metallurgical features of steel welds of relevance to modelling.

Previous work on allotriomorphic ferrite formation requires certain empirical corrections. The work presented in Chapter 2 reduces the arbitrary use of correction factors which, as a bonus, also allows the estimation of ferrite grain size. In addition, solidification-induced segregation is taken into account. The transformation model works very well for carbon, manganese and nickel containing steel welds.

It is now extremely important that any welding process has a high productivity. This not only means that the process should be automated, but also that the rate of weld metal deposition should be as large as possible. To obtain data on large heat input welding, the cooling characteristics and microstructure of experimental welds were measured as reported in Chapter 3. Quantitative metallographic data from the large heat input welds have been compared against theory and some discrepancies are discussed.

Allotriomorphic ferrite formation is frequently accompanied by that of Widmanstätten ferrite. In the past, such *simultaneous* transformations have been modelled by arbitrarily stopping one transformation to permit the next in the sequence to commence (Chapter 4). This does not reflect reality so a new model has been implemented.

Estimation of the inclusion characteristics in weld metals was attempted through thermodynamic calculations in Chapter 5. Reasonable agreement is found between the calculations and experimental observations. Phase stability exerts a significant influence on the inclusions in steel welds.

Data on solidification cracking in steel welds have been analysed using a classification neural network in Chapter 6. It has been possible to express quantitatively, the effect of variables such as the chemical composition and welding conditions, on the cracking tendency. The ability of the network to express the relationship in a suitably nonlinear form is shown to be vital in reproducing known phenomena.

Appendices contain the statistical analysis of measurement of microstructure and some analytical solutions which relate real and extended volumes in simultaneous transformations. Datasets and programs developed in this work are also listed in the appendices.

CONTENTS

CHAPTER TWO Modelling of Allotriomorphic Ferrite Transformation in Steel Welds

CHAPTER THREE Application of the Ferrite Transformation Model to Large Heat-Input Welds

CHAPTER FOUR Simultaneous Transformation to Allotriomorphic and Widmanstätten Ferrite in Steel Welds

NOMENCLATURE

a_c	Side-length of hexagonal prism
Ac_1	Temperature at which ferrite+cementite becomes ferrite+austenite during heating
Ae_3	Temperature separating the ferrite+austenite and austenite phase field
a_{out}	Variable in the equation calculating the output in a neural network; $a_{out} = \sum_i w_i^{(2)} h_i + \theta^{(2)}$
a_1^γ	Activity of carbon on austenite
A	Constant
A_{wn}	Coefficient in Fourier series, $A_{wn} = U_{wn}^2/(U_{wn}^2 - h_p^2 d_w^2 + 2h_p d_w)$
A_{pn}	Coefficient in Fourier series, $A_{pn} = U_{nn}^2/(U_{pn}^2 - h_p^2 d_p^2 + 2h_p d_p)$
b	Interatomic spacing in the boundary plane of austenite
B	Constant
c_0	Initial composition
c_3	Constant, $c_3 = \tan(30°)$
c_C	Carbon concentration, moles per unit volume
$\overline{c}_C$	Average carbon concentration, moles per unit volume
c_j	Concentration of component j in matrix at arbitrary time and position, moles per unit volume
$\overline{c}_j$	Average concentration of component j in matrix, moles per unit volume
$c_j^{\gamma\alpha}$	Concentration of component j in austenite which is in equilibrium with ferrite, moles per unit volume
$c_j^{\alpha\gamma}$	Concentration of component j in ferrite which is in equilibrium with austenite, mole per unit volume
c^{liq}	Concentration of alloying element in liquid which is equilibrium with solid
c^{sol}	Concentration of alloying element in solid which is equilibrium with liquid
$c_C^{\gamma\theta}$	Carbon concentration in gamma which is in equilibrium with cementite, moles per unit volume
$c_C^{\theta\gamma}$	Carbon concentration in cementite which is in equilibrium with austenite, moles per unit volume
C	Constant
C_1, C_2	Empirical constant derived by fitting experimental cooling curves to the equation for three dimensional heat flow by Svensson *et al.* [1986]

C_3	Constant obtained by fitted with experimental results
C_4	Constant obtained by fitted with experimental results
d_a	Mean two-dimensional inclusion diameter
d_p	Heat transfer coefficient at plate surface, $d_p = \alpha_p/\lambda$
d_V	Mean three-dimensional inclusion diameter
d_w	Heat transfer coefficient at weld surface, $d_w = \alpha_w/\lambda$
$\overline{d}_\alpha$	Nominal ferrite grain diameter
D	Diffusivity of carbon in austenite, a function of the concentration of carbon x_C^γ and the substitutional alloying elements in austenite
$\overline{D}$	Weighted average diffusivity of carbon in austenite
D_B	Boundary diffusion coefficient
D_{eff}	Effective diffusion coefficient related to boundary or volume diffusion, which depends on the coherency state of the nucleus
D_{jk}	Term of diffusion coefficients of component j, related with component k
D_s	Diffusion coefficient in the solid
D_V	Volume diffusion coefficient
f	Integral function as a function of θ, $\eta_{l/t}$, α_1, I_B and t
ΔF^*	Activation free energy
$FATT$	Fracture appearance brittle/ductile transition temperature
G	Lengthening rate of Widmanstätten ferrite
G_r	Isotropic growth rate of a particle
ΔG_2	Free energy change per unit of ferrite accompanying ferrite growth with carbon partitioning during growth
ΔG_3	Free energy change for nucleation
ΔG_{crit}^f	Critical activation free energy of ferrite nucleation per atom for nucleation on faces of austenite grains
ΔG_m	Maximum free energy change accompanying the formation of 1 mol of nucleating ferrite
ΔG_m^V	Maximum volume free energy change accompanying the formation of a nucleus in a large amount of matrix phase
ΔG_N	Driving force necessary for nucleation of shear transformations
ΔG_S	Strain energy change per unit volume of ferrite
G_{SB}	Stored energy of bainite (about 400 J mol^{-1})
ΔG_V	Free energy change per unit volume

	for ferrite nucleation from supersaturated austenite
G_{WB}	Stored energy of Widmanstätten ferrite (about 50 J mol^{-1})
$\Delta^{\circ}G(X)$	Gibbs free energy change per mole in transforming the pure element X from the delta ferrite to liquid to the liquid state
G_{Zener}	Zener ordering energy
G_{α}	Gibbs free energy of ferrite
G_{γ}	Gibbs free energy of austenite
$\Delta G^{\gamma\rightarrow\alpha}$	Free energy change accompanying the diffusionless formation of ferrite from austenite
$\Delta G_c^{\gamma\rightarrow\alpha'}$	Critical amount of free energy change for martensitic transformation
$\Delta G^{\gamma\rightarrow\gamma'+\alpha}$	Free energy change accompanying ferrite growth without substitute elements partitioning; carbon partitioning during growth
h	Planck constant
h_c	Height of hexagonal prism
h_p	Plate thickness
H	Enthalpy
i	General variables (*e.g.* , positive integer or oxide denotation)
I	Welding current
I_{α}^{B}	Grain boundary steady state nucleation rate of allotriomorphic ferrite per unit area of austenite boundary; $I_{\alpha}^{B} = I_{\alpha}^{B_f} + I_{\alpha}^{B_e} + I_{\alpha}^{B_c}$
$I_{\alpha W}^{B}$	Grain boundary steady state nucleation rate of Widmanstätten ferrite per unit area of austenite boundary.
$I_{\alpha}^{B_c}$	Steady state rate of nucleation of allotriomorphic ferrite on grain boundary corners per unit area of boundary
$I_{\alpha}^{B_e}$	Steady state rate of nucleation of allotriomorphic ferrite on grain boundary edges per unit area of boundary
$I_{\alpha}^{B_f}$	Steady state rate of nucleation of allotriomorphic ferrite on grain boundary faces per unit area of boundary
j	General variables (*e.g.*, arbitrary component in alloy, positive integer or nitride denotation)
k	General variables (*e.g.*, arbitrary component in alloy ($k \neq j$) or positive integer)
k_B	Boltzmann constant
k_0	Equilibrium partition coefficient

$k_0(X)$	Equilibrium partition coefficient of alloying element X
K_0	0 order of 2nd kind of Bessel function
K_1	Constant term in the equation which defines the critical driving force $\Delta G_c^{\gamma \rightarrow \alpha'}$ for martensitic transformation
K_1^α	Fraction of atomic sites on grain boundary which can support nucleation
K_2^α	Empirical multiplication factor for ΔG_{crit}^f
L	Length of the solidifying system
$\overline{L}$	Mean lineal intercept of austenite grain
$\overline{L}_i$	Intercept measurement from inclined sections
$\overline{L}_l$	Intercept measurement from longitudinal sections
$\overline{L}_t$	Intercept measurement from transverse sections
L_{tn}	A lineal intercept measured in the transverse section in a direction normal to the major axes of grains
$\overline{L}_{tn}$	Mean lineal intercept measured in the transverse section in a Direction normal to the major axes of grain sections
L_V	Mean surface-surface spacing of the inclusions
n	Number of division for the fraction solidified; positive integer
N	Number of measurement in lineal intercept or point counting
N_{com}	Number of the models in the committee in the neural network
N_a	Number of particles per unit area
N_A	AvogadroÕs number
N_B	Total number of ferrite grains nucleated during the transformation per unit volume of austenite
N^f	Number of face sites per unit area of boundary
N_V	Number of particles per unit volume
O	Area of any plane surface parallel to a particular austenite boundary
$[O]$	Oxygen concentration in weld metal in wt.%
O_b	Area of a particular austenite grain boundary
O_B	Total austenite grain boundary area
O_α	Actual area defined as the sum of the areas of intersection of the allotriomorphic ferrite discs with a plane parallel to a particular austenite boundary
$O_{\alpha+\alpha_W}$	Actual area defined as the sum of the areas of intersection of the allotriomorphic and Widmanstätten ferrite discs with a plane parallel to a particular austenite

	boundary
O^e_α	Extended area defined as the sum of the areas of intersection of the allotriomorphic ferrite discs with a plane parallel to a particular austenite boundary
$O^e_{\alpha+\alpha_W}$	Extended area defined as the sum of the areas of intersection of the allotriomorphic and Widmanstätten ferrite discs with a plane parallel to a particular austenite boundary
$O^e_{\alpha_W}$	Extended area defined as the sum of the areas of intersection of the and Widmanstätten ferrite discs with a plane parallel to a particular austenite boundary
Q	Heat input per unit length of weld
Q'	Constant obtained by fitting with experimental results
Q_{act}	Activation free energy per atom for crossing the austenite/ferrite nucleus interface
Q_p	Effective heat input per unit time, $Q_p = \eta IV$
r	Distance from point heat source
R_m	Distance from a centre of weld bead right-angled to a welding direction for three dimensional heat flow
R	Universal gas constant
s	Shear component of the strain for a transformation
S	Entropy
$[S]$	Sulphur concentration in weld metal in wt.%
S_c	Theoretical critical spacing for which the velocity of the pearlite reaction becomes zero
S_l	Combined width of ferrite and cementite lamellae
S_V	Austenite grain boundary surface per unit volume
S^α	Width of ferrite lamella in pearlite
S^θ	Width of cementite lamella in pearlite
t	Time
δt	Short time interval
t_0	Solidification time needed to complete the solidification in the very small solidifying system assuming the growth rate of solid is constant
t_2	Time required to achieve a degree of transformation at a Temperature T_2 which is equal to ξ_1 obtained during isothermal transformation at the Temperature T_1 where $T_2 < T_1$

$t_a(T)$	Isothermal time required to transform a certain fraction of at a arbitrary temperature
t_m	Target for the mth dataset in the neural network
t_W	Time after welding
T	Absolute temperature
T_∞	Ambient temperature
T_h	Temperature at which austenite first transform to ferrite during continuous cooling
T_M	Melting temperature
T_W	Temperature at weldment at (X_m, R_m) for three dimensional heat flow and at (X_m, Y_m) for two dimensional heat flow
T_1	A temperature
T_2	A temperature; $T_2 < T_1$
U_{pn}	Eigenvalues satisfying $\tan U_{pn} = 2h_p d_p U_{pn}/(U_{pn}^2 - h_p^2 d_p^2)$
U_{wn}	Eigenvalues satisfying $\tan U_{wn} = 2h_p d_w U_{wn}/(U_{wn}^2 - h_p^2 d_w^2)$
v	Rate at which a planer interface moves
v_i	Volume fraction of the products i; $v_i = v_i/V_{total}$
v_i^e	Extended volume fraction of the products i; $v_i^e = v_i^e/V_{total}$
v_s	Travel speed
V	Voltage
V_i	Volume of the products i
V_i^e	Extended volume of the products i
V_s	Fraction solidified
V_{total}	Total volume
V_V	Volume fraction of inclusions
V_x	Volume fraction of microstructural component x
V_α	Volume fraction of allotriomorphic ferrite
$V_{\alpha+\alpha_W}$	Volume fraction of allotriomorphic ferrite and Widmanstätten ferrite
$\overline{V_\alpha}$	Total average volume fraction of allotriomorphic ferrite through the segregation segments in weld
V_α^b	Allotriomorphic allotriomorphic ferrite volume originating one grain boundary
V_α^e	Total extended volume of allotriomorphic ferrite
$V_{\alpha+\alpha_W}^e$	Extended volume of allotriomorphic ferrite and Widmanstätten ferrite
$V_{\alpha'}$	Volume fraction of martensite

V_α^{act}	Actual volume of the ferrite
w	Moving coordinate, $w = x_p - v_S t_W$
w	Neural network parameters
w_i	Weight percent of an element i
W	Number of octahedral interstices around a single such interstice
$w_{ij}^{(1)}$	Weight connecting the ith hidden unit (h_i) and jth input in the neural network ($j = 1, 2, 3, \ldots, n$, where n is a number of input units)
$w_i^{(2)}$	Weight connecting the output and ith hidden unit (h_i) in the neural network ($i = 1, 2, 3, \ldots, n$, where n is a number of hidden units)
$W_{nitride,j}$	Weight of nitride j in 1 mol of the system
$W_{oxide,i}$	Weight of oxide i in 1 mol of the system
W_{slag}	Weight of slag in 1 mol of the system
W_{total}	Molar weight of the system
x	Input variables
$[X]'$	Converted concentration of the element X in oxides in wt.%; $[Si]' + [Mn]' + [Al]' + [Ti]' \approx 100$
$[X]_{original}$	Original silicon concentration in oxides in wt.%; $[Si]_{original} + [Mn]_{original} + [Al]_{original} + [Ti]_{original} \leq 100$
x_p, y_p, z_p	Coordinates fixed to a plate
$\overline{x}_C$	Average carbon concentration of alloy, mole fraction
x	Input variable in the neural network
x_C	Carbon concentration, mole fraction
x_j	Input variables in the neural network ($j = 1, 2, 3, \ldots, n$, where n is a number of input units)
x_{max}	Maximum value of the input variable series of x in the neural network
x_{min}	Minimum value of the input variable series of x in the neural network
x_N	Normalised value of an input variable x in the neural network; $x_N = (x - x_{\min})/(x_{\max} - x_{\min}) - 0.5$
x_C^α	Concentration of carbon in ferrite, mole fraction
$x_{C_m}^\alpha$	Ferrite nucleus carbon concentration which gives the maximum free energy change for the formation of 1 mol of nucleating ferrite, mole fraction
x_C^γ	Concentration of carbon in austenite, mole fraction
$x_C^{\alpha\gamma}$	Carbon concentration in ferrite which is in equilibrium with austenite,

	mole fraction
$x_C^{\gamma\alpha}$	Carbon concentration in austenite which is in equilibrium with ferrite, mole fraction
X	Arbitrary substitutional alloying element
X_m	Coordinate which has an origin at a moving point heat source
y	Coordinate, *e.g.*, distance between austenite grain boundary and arbitrary plane parallel to the boundary
y_m	Calculated output for the mth dataset in the neural network
$\overline{y}$	Single prediction made by a committee by averaging the prediction of of each model in the neural network
$y(x, w)$	Neural network output
y_γ	Coordinate normal to a diagonal line of the equilateral hexagonal section of columnar austenite grain
Y_m	Distance from a centre of weld bead right-angled to a welding direction for two dimensional heat flow
z	Coordinate normal to interface plane
z'	Constant obtained by fitted with experimental results
z_n	Total volume fraction transformed of n product phases
z_n^e	Total extended volume fraction transformed of n product phases
Z	Half-thickness of allotriomorphic ferrite
α_0	Dimensionless coefficient for back-diffusion
α'	Dimensionless coefficient for interdendritic back-diffusion
α_1	Parabolic-thickening rate constant for one-dimensional growth
α_p	Surface conductivity at plate
α_w	Surface conductivity at weld
β	Aspect ratio of β
Γ_m	Activity coefficient
δ	Dilatational component of the strain for a transformation
ζ_α	Actual volume of allotriomorphic ferrite divided by its equilibrium volume; $\zeta_\alpha = V_\alpha/(V_{total}\phi)$
$\zeta_{\alpha+\alpha W}$	Actual volume of allotriomorphic and Widmanstätten ferrite divided by their equilibrium volume
$\zeta_{\alpha W}$	Actual volume of Widmanstätten ferrite divided by it equilibrium volume

θ	Parameter; $\theta = y/(\alpha_1 t^{1/2})$
η	Arc efficiency
η_α	Ratio of length to thickness of allotriomorphic ferrite (taken as 3.0)
H	A function of carbon concentration
Θ	Ratio of the number of carbon atoms x_1 to the total number of solvent atoms; $\Theta = x_1/(1 - x_1)$
κ	Thermal diffusivity
λ	Thermal conductivity
λ_V	Mean center-center spacing of the inclusions
λ_γ	Distance between (002) austenite planes
μ_C^α	Chemical potential of carbon in ferrite
μ_C^γ	Chemical potential of carbon in austenite
μ_{Fe}^α	Chemical potential of iron in ferrite
μ_{Fe}^γ	Chemical potential of iron in austenite
ξ_1	A specific value of volume fraction isothermally transformed during a time period $\Delta\tau_1$ at a Temperature T_1
ξ_2	A specific value of volume fraction isothermally transformed during a time period $t_2 + \Delta\tau_2$ at a Temperature T_2
ξ_a	A specific value of volume fraction of ferrite transformed
ρ_{Fe}	Density of iron
$\rho_{nitride,j}$	Density of nitride j
$\rho_{oxide,i}$	Density of oxide i
ρ_{slag}	Density of slag
σ	Austenite/ferrite nucleus interfacial energy per unit area
σ_n	Total amount of n transformed products; $\sigma_n = \sum_{j=1}^{n} v_j$
σ_n^e	Total amount of n transformed products; $\sigma_n^e = \sum_{j=1}^{n} v_j^e$
σ_B	Tensile strength
σ_L	Standard deviation in the size distribution of L_{tn}
σ_W	Hyperparameters measuring the model perceived significance of each input variable in affecting the output in the neural network
τ	Incubation time
τ_S	Time taken to establish a steady–state nucleation rate
$\Delta\tau_1$	Time spent at the temperature T_1

$\Delta\tau_2$	Time spent at the temperature T_2
ϕ	Equilibrium volume fraction of ferrite; $\phi = (x^{\gamma\alpha} - \overline{x})/(x^{\gamma\alpha} - x^{\alpha\gamma})$
Φ	Ensemble average interstitial site exclusion parameter
Ω	Solute supersaturation
ω_γ	Nearest neighbour carbon-carbon interaction energy in austenite

CHAPTER ONE

Introduction and Literature Review

1.1 Aim of the Project

A number of new and high performance structural steels have recently been developed [*e.g.*, Horii *et al.*, 1995c]. These steels are fabricated using arc welding which is a very reliable and efficient joining technique compared with other methods such as riveting and bolting. Weldments define the overall performance of steel structures since they focus stress by representing mechanical, geometrical and chemical discontinuities. Hence, in order to exploit the new steels effectively, it is necessary to undertake a parallel development of welding materials.

The development of welding materials can be a very complex process in which so many essential factors have to be satisfied at the same time (Fig. 1-1).

Adequate mechanical properties, including the tensile strength and toughness, must be achieved in weld metal over the range of service temperatures. Some actual examples of strength and toughness characteristics for novel structural steels will be discussed in the next section.

Many types of welding materials have to be developed even for one specification of a newly developed steel. This is to deal with all the usual welding techniques, positions and conditions encountered during construction. Welding materials for shielded metal arc welding (SMAW), gas metal arc welding (GMAW) and submerged arc welding (SAW) are required as a minimum. Much higher heat input welding techniques such as electroslag welding (ESW) and electrogas welding (EGW) are sometimes needed in order to achieve higher deposition rate for vertical welding used during for ship building and civil engineering applications.

Weld metal microstructures determine the mechanical properties of the weld metal. A metallurgical model of weld microstructure evolution is thus important both as a contribution to basic research and in order to decrease the number of variables that need to be considered during the development of welding materials.

The purpose of the work presented in this thesis was to formulate a metallurgical model for the prediction

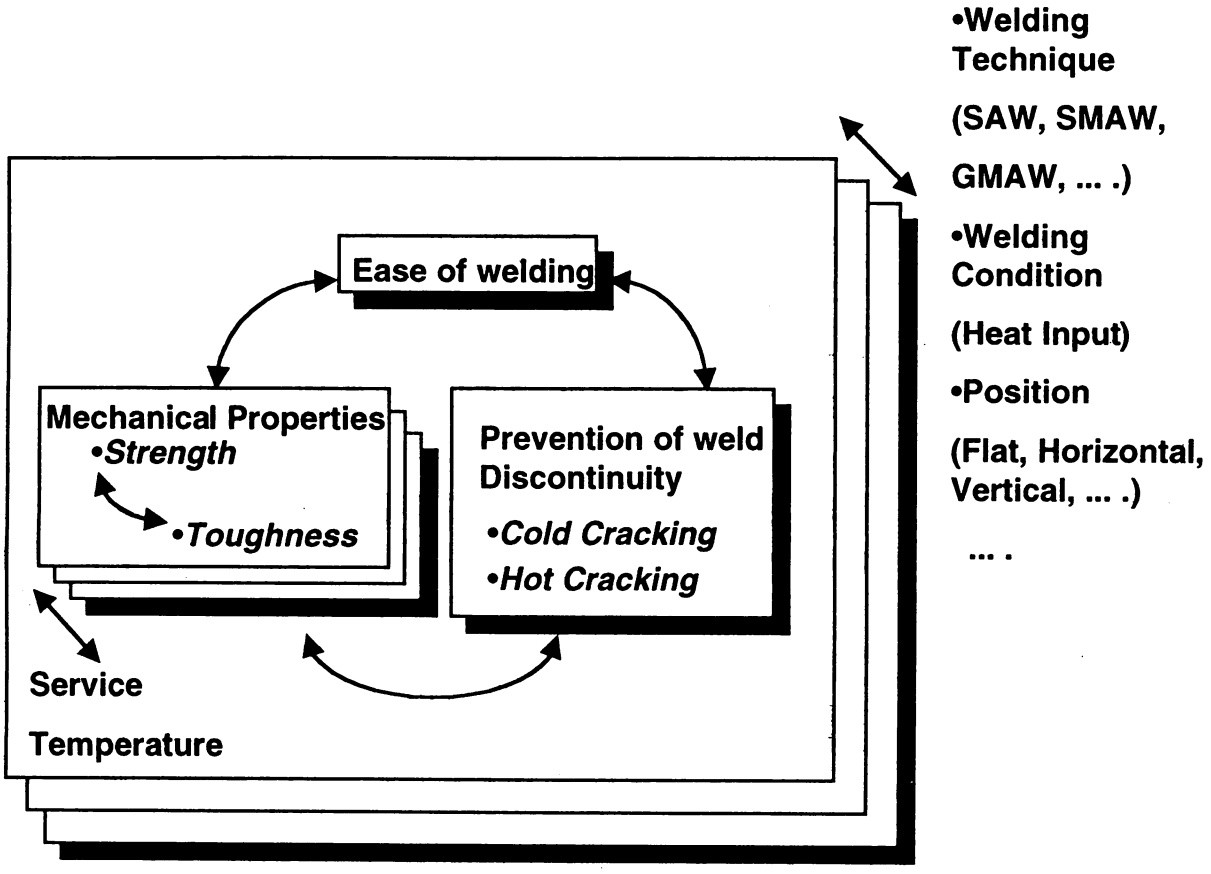

Fig. 1-1 : Schematic illustration showing the features involved during the development of steel welding materials.

of microstructure and properties of steel weld metal, such as solidification cracking susceptibility in the weld metal. Such models already exist but it will be demonstrated that there are a number of significant difficulties which have not yet been resolved.

1.2 Recent Developments in Wrought Steel

Oil and natural gas exploitation is being extended to the cryogenic and abyssal regions where the steel structures must have sufficient toughness and strength at the low temperatures. Penstocks for hydro-electric power generation systems, oil-transport piping and oil-refining equipment are most efficiently operated at high pressures. Fig. 1-2 summarises the requirements for the energy-related industries [Horii 1995a; Horii *et al.*, 1995c] .

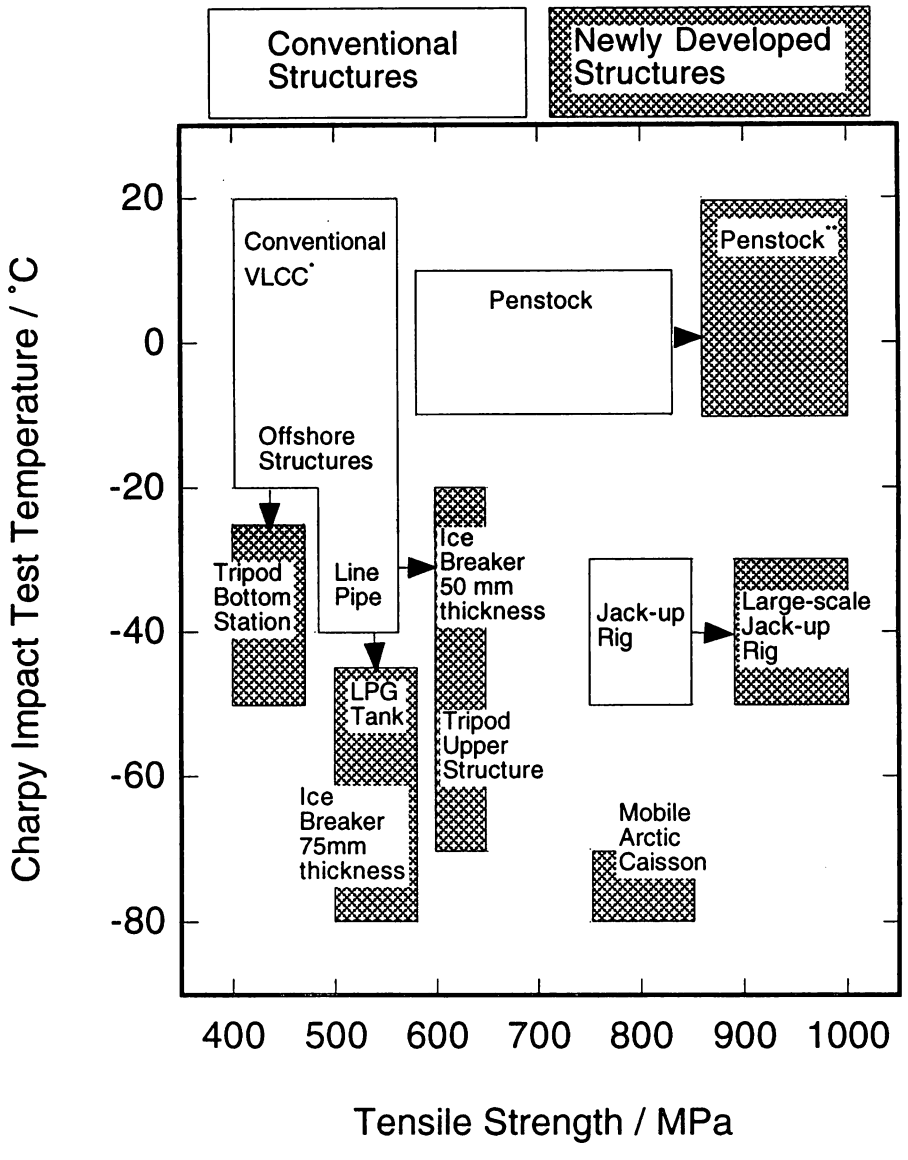

Fig. 1-2 : Relationship between tensile strength and Charpy test temperature in the energy-related industries (after Horii 1995a; Horii *et al.*, 1995c). Where VLCC* means Very Large Crudeoil Carrier and Penstock** means Steel pipe for conveying water from dam to water-turbine at hydroelectric power station.

These metallurgical characteristics must be achieved at an affordable cost and hence the use of high

tensile steel with an ultimate tensile strength in the range 780–980 MPa.

Although Fig. 1-2 only shows the strength and toughness requirements for low temperature service, heat- resistant steels which are employed at elevated temperatures are also in demand. Heat-resistant alloys such as the classic 2.25Cr-1Mo steel, are used widely for pressure vessels in power stations or in petroleum and chemical plant due to its outstanding mechanical properties at elevated temperatures. Many power plant built twenty or thirty years ago are at present reaching the end of their design lives. This has led to the development of the *modified* 2.25Cr-1Mo steel which is microalloyed with niobium and vanadium to improve tensile and creep rupture strength [*e.g.*, Shimomura *et al.*, 1988; Ichikawa *et al.*, 1995]. The modified steel has been standarised under ASME CASE 2098-1 [1991]. These steels must retain strength but also toughness in cold climates. ASME CASE 2098-1 in fact specifies a tensile strength of 586 to 758 MPa and an average Charpy V-notch toughness of 54 J at 255 K.

There is another novel low-alloy heat-resistant steel developed for pressurised fluidised bed combustion (PFBC) boiler [Ohhama *et al.*, 1995]. PFBC power generation systems are being implemented for high efficiency thermal power electricity generation with low environmental pollution. Table 1-1 shows the required mechanical properties for any steel designated for the PFBC system. Several difficulties exist in the development of welding materials for this PFBC system.

Table 1-1 : Required specifications of weld metal properties for Pressurised Fluidised Bed Combustion Boiler.

Post Weld Heat Treatment Condition	Tensile Strength at Room Temperature and 350℃ / MPa	V-notch Charpy Absorbed Energy at -30℃ / J
As-welded	>610	>47
580℃, 13.5hrs	>610	>47

The mechanical properties should be satisfactory in both the as-welded condition and after post-weld heat treatment (PWHT) at 580 °C. There are also problems in maintaining good weldability in these high strength steels. In order to decrease the number of passes during the welding process and to

improve the productivity, a narrow welding gap and groove preparation is employed. This increases the risk of solidification cracking. Enhanced tensile strength and restrain by the heavy section increase the carbon equivalent of the steel and increases the risk of hydrogen-induced cold-cracking.

Building construction materials represent one of the most common applications of structural steel. However, unless fire protection is provided, conventional steel structures cannot maintain the required strength in dangerous circumstances. This is one of the disadvantages of steel structures and many countries therefore regulate for fire protection. Recently a fire resistant (FR) steel has been developed which has better mechanical properties at elevated temperatures [Sakumoto *et al.*, 1992; Ichikawa *et al.*, 1996]. The FR steel can sustain its yield strength at temperatures up to 600 °C, over two-thirds of the strength specified for the room temperature. Besides the requirement to retain strength at high temperatures, this steel also satisfies the conventional standard for rolled steels for welded structures. Japan Industrial Standard [JIS G3106] for example specifies 490 to 610 MPa as the tensile strength at room temperature, 17 % elongation and 27 J as the average Charpy V-notch energy at 0 °C. These required properties are satisfied by the about 0.5wt.% molybdenum addition and micro-alloying of niobium [Chijiiwa *et al.*, 1993]. Welding materials for shielded metal arc, submerged arc and electroslag welding have also been developed for this steel. Their weld metals also satisfy the above requirements.

1.3 Microstructures in Steel Welds

1.3.1 Microstructural Zones

There is a well-defined gradient of microstructure from the weld metal to the heat-affected zone as a function of the distance from the fusion boundary in a one-pass weldment (Fig. 1-3) [*e.g.*, Honeycombe and Bhadeshia, 1995].

Matsuda [1972] categorised the weld microstructural zones and their properties into the following seven regions according to the peak temperature range encountered.

1. Deposited Weld Metal

Peak temperature over 1500 °C (melting temperature). Melted and solidified weld metal.

2. Coarse Grained Zone

Peak temperature over 1250 °C. Part of heat affected zone where the austenite grains are coarsened. The resulting increase in hardenability can lead to an increase in hardness and can cause cold-cracking.

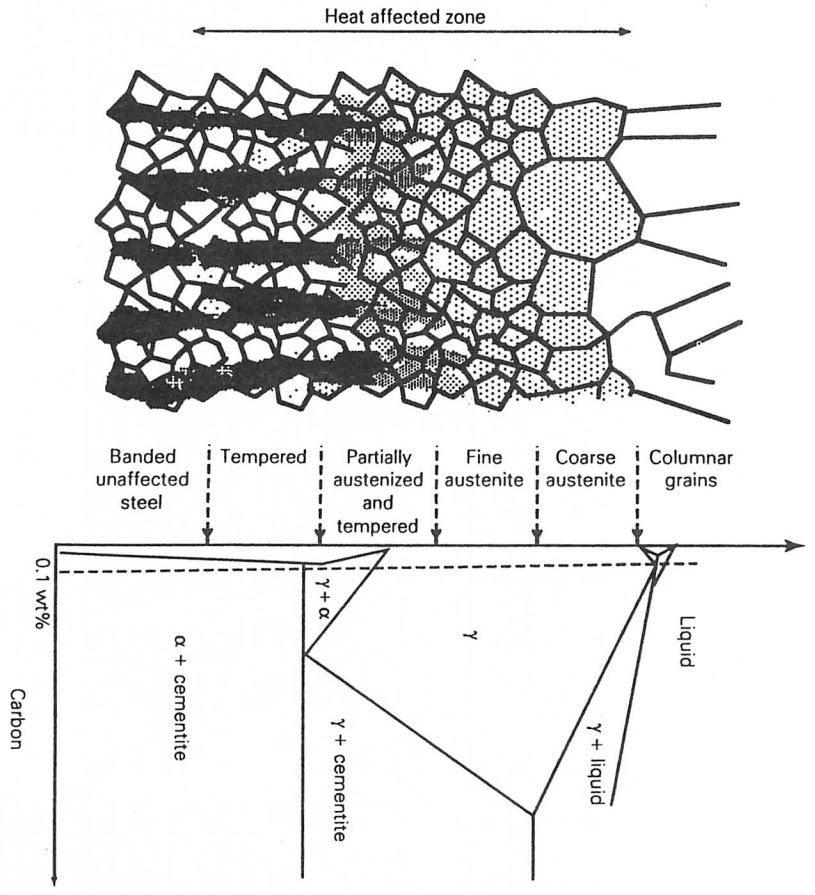

Fig. 1-3 : Schematic illustration showing microstructural gradient in a steel weldment (after Honeycombe and Bhadeshia [1995]).

3. Mixed Grain Zone

Peak temperature from 1100 to 1250 °C. Intermediate zone between the coasened grained and grain-refined zone.

4. Grain-refined Zone

Peak temperature from 900 to 1100 °C. The austenite grains are fined. Mechanical properties, *e.g.* toughness, are fairly good in this zone.

5. Globular Pearlite Zone

Peak temperature from 750 to 900 °C. The pearlite is spherodised or reaustenitised. Toughness is good when the weld cooling rate is low but is often poor when the cooling rate is high due to the formation

of martensite.

6. Embrittled Zone

Peak temperature is from 300 to 750 °C. Steels are occasionally embrittled during heat treatment in this temperature range, either due to the segregation of impurities to austenite grain boundaries or due to the precipitation of carbides.

7. Unaltered Basemetal

Peak temperature from room temperature to 300 °C. The microstructure in this region is not heat-affected.

1.3.2 Classification of the Microstructures in Steel

The microstructures in steel and characteristics of their transformations have been thoroughly reviewed by Bhadeshia [1992] (Fig. 1-4). All varieties of ferrite which grow by displacive mechanism have the form of plates (Table 1-2). The displacive transformations cause the shape of the transformed region to change, the change being an invariant-plane strain with the large shear (s) [Watson and McDougall, 1973; Sandvik, 1982; Swallow and Bhadeshia, 1996; Wayman, 1964; Dunne and Wayman, 1971, Bhadeshia, 1998] (Table 1-2), while the shear component of strain in reconstructive transformation is 0.

Table 1-2 : Approximate values of the shear (s) and dilatational (δ) components of strain for a variety of transformation products in steels (after Bhadeshia, 1998).

Transformation	s	δ	Morphology	Reference
Widmanstätten ferrite	0.36	0.03	Thin plates	[Watson and McDougall, 1973]
Bainite	0.22	0.03	Thin plates	[Sandvik, 1982] [Swallow and Bhadeshia, 1996]
Martensite	0.24	0.03	Thin plates	[Wayman, 1964] [Dunne and Wayman, 1971]
Allotriomorphic ferrite	0	0.03	irregular	[Bhadeshia, 1998]
Idiomorphic ferrite	0	0.03	equiaxed	

The microstructures observed in as-deposited low-alloy steel welds normally consist of allotriomorphic

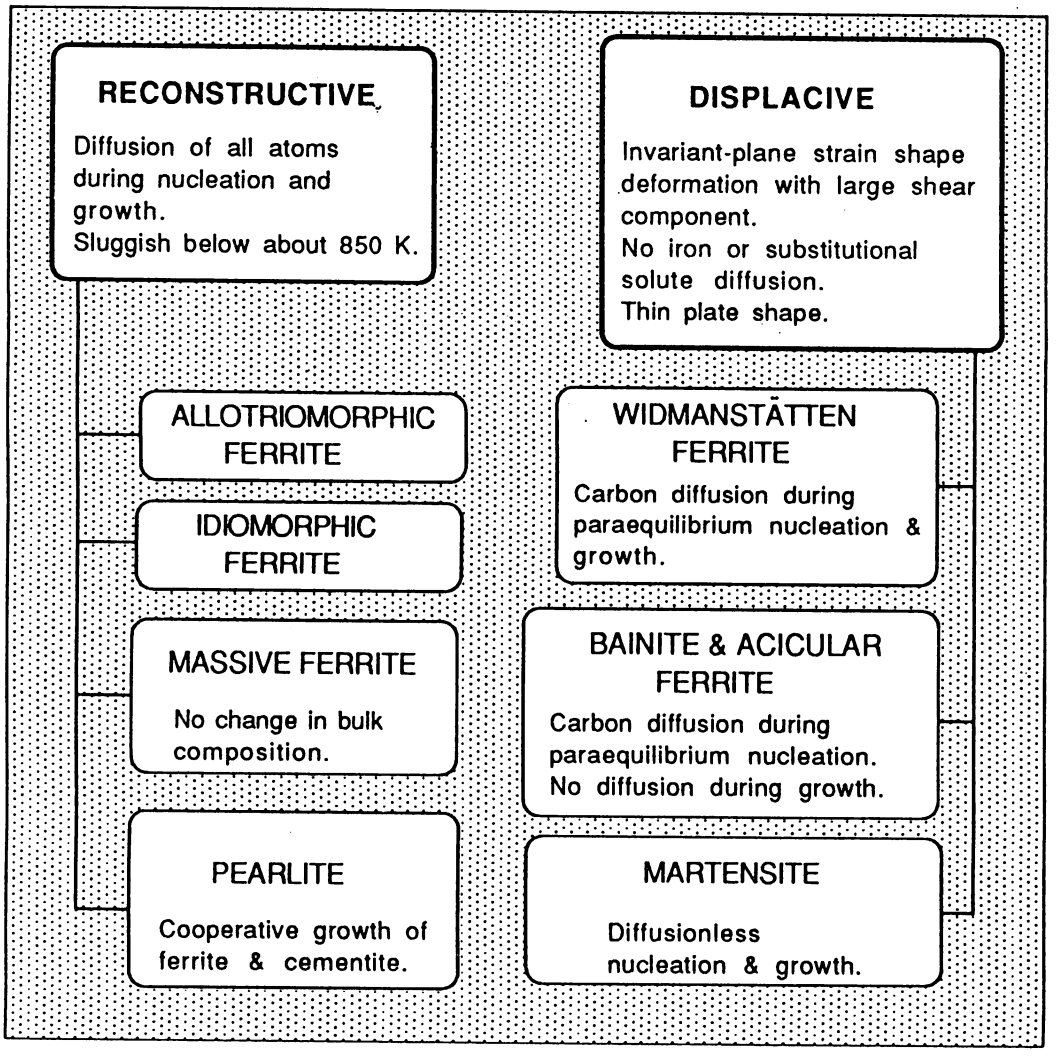

Fig. 1-4 : Classification of steel microstructures (after Bhadeshia [1992]).

ferrite α, Widmanstätten ferrite α_W, acicular ferrite α_a, bainite α_b and microphases which include the so-called martensite-austenite constituent (MAC) and degenerate pearlite [Bhadeshia and Svensson, 1993]. Bainite can be distinguished into lower bainite α_{lb} and upper bainite α_{ub} due to the difference in the distribution of carbides. The detailed aspects of the microstructures are reviewed below. A deeper mathematical description will be discussed in the Chapters that follow. Although massive ferrite can

be observed in Fe-C alloys, this microstructure will not be reviewed because it is hardly observed in conventional arc welds or indeed in the vast majority of steels.

1.3.3 Allotriomorphic Ferrite

Ferrite which grows by a reconstructive mechanism can be categorised into two main morphologies: allotriomorphic ferrite and idiomorphic ferrite [Dubé, 1948, Aaronson, 1955, Dubé *et al.*, 1958]. Allotriomorphic ferrite is the first phase to form on austenite grain boundaries during the cooling of a steel weld below the Ae_3 temperature [Bhadeshia, 1985c]. Here Ae_3 is an equilibrium $\gamma \rightarrow \gamma' + \alpha$ transformation temperature. Because of its high formation temperature, the transformation involves the diffusion of all atoms during the nucleation and growth processes. Allotriomorphic ferrite is therefore classified as a reconstructive transformation [Bhadeshia, 1985c].

Allotriomorphic ferrite reduces the toughness of welds [Mori *et al.*, 1981; 1982a; Horii and Ohkita, 1991]. Mori *et al.* investigated the effect of allotriomorphic ferrite fraction (V_α) and tensile strength (σ_{UTS}) on the fracture appearance transition temperature ($FATT$) of steel welds [1982]. They derived an empirical equation which can estimate the $FATT$ as a function of volume fraction and tensile strength of allotriomorphic ferrite, for V_α up to 0.4 and σ_{UTS} between 55.7 and 69.7 kgf mm^{-2} (546 and 683 MPa):

$$FATT\,(^\circ\mathrm{C}) = 140V_\alpha + 1.5\sigma_{UTS}\left(\mathrm{kgf\,mm^{-2}}\right) - 187 \qquad (1-1)$$

Some recent work contradicts this general impression that allotriomorphic ferrite should be avoided and indicates that some allotriomorphic ferrite is a desirable constituent of weld microstructure. It is well known that titanium and boron containing steel welds are often susceptible to embrittlement by intragranular fracture at the columnar austenite grain boundaries [Lazor and Kerr,1980; Kayali *et al.*, 1984; Sneider and Kerr, 1984; Abson, 1987; Kluken and Grong, 1993]. Lazor and Kerr [1980] and Kayali *et al.* [1984] have reported such failure in welds containing only of acicular ferrite. Ichikawa *et al.* [1996] examined the mechanical properties of large heat input submerged arc welds designed for fire-resistant steel. They demonstrated that the ductility of the welds at the high temperature (550 to 650 °C) deteriorated sharply in the absence of allotriomorphic ferrite (Fig. 1-5).

The intergranular fracture, with respect to prior austenite grain boundaries, became intragranular when some allotriomorphic ferrite was introduced into the microstructure. In a study of the heat-affected zone in weldments of steel tube for power transmission towers, Iezawa *et al.* [1993], demonstrated that zinc embrittlement depends on the allotriomorphic ferrite content, which in turn varied with the boron concentration. The absence of allotriomorphic ferrite at the prior austenite grain boundaries clearly made them more sensitive to zinc infiltration, proving again that these prior austenite boundaries have

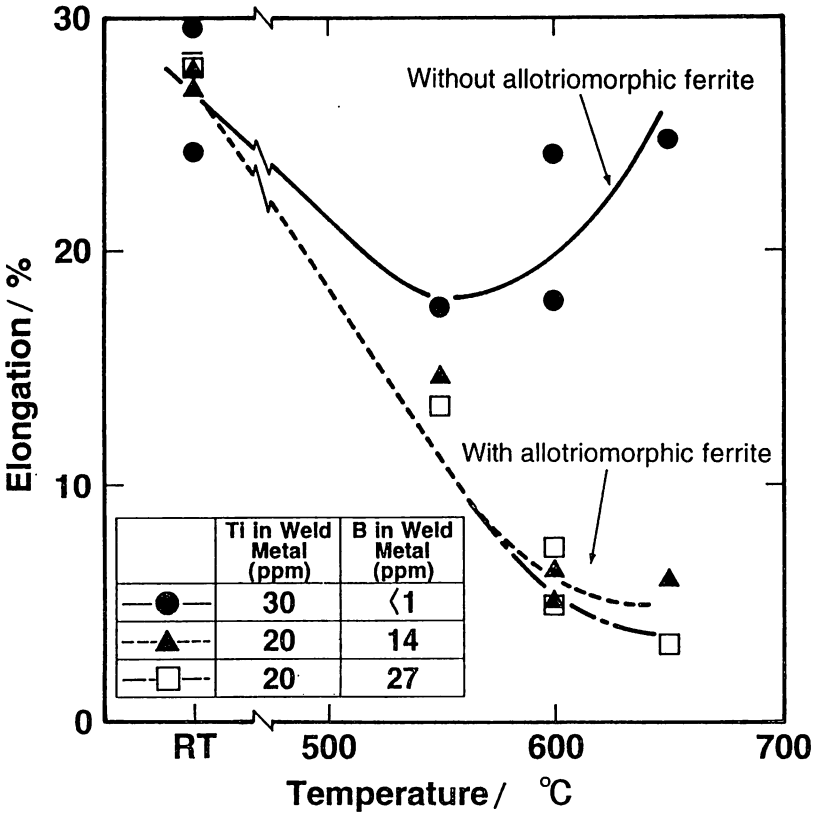

Fig. 1-5 : Influence of microstructure on the ductility of fire-resistant steel weld metal (after Ichikawa *et al.* [1996]).

a high-energy structure which is susceptible to wetting and impurity segregation [Bhadeshia, 1995b]. Watanabe *et al.* demonstrated that the introduction of allotriomorphic ferrite to austenite boundaries in

martensitic steel can improve hydrogen induced delayed intergranular cracking [1996].

All these advantageous characteristics of allotriomorphic ferrite on the properties are consistent with its reconstructive nature of the transformation and can be explained comprehensively. Bhadeshia and Svensson [1993] explained that a vestige of austenite grain boundary remains when the transformation products are all displacive and that in presence of impurities this can lead to intragranular failure with respect to the prior austenite grain boundaries. They thus suggested that allotriomorphic ferrite disrupts the original austenite boundaries entirely and removes the sites for the segregation of impurities.

Allotriomorphic ferrite in steel has, because of its technological importance, been studied from the point of view of both practical aspects and fundamental transformation theory. Therefore most of the research on the modelling of the transformation in steels has focused on allotriomorphic ferrite. The present study also deals mainly with the allotriomorphic transformation. The detailed transformation mechanism, thermodynamic and kinetic aspects will be discussed in Chapter 2.

1.3.4 Idiomorphic Ferrite

Idiomorphic ferrite in steel has a faceted shape with the faces belonging to its crystalline form and normally forms intragranularly [Dubé, 1948] Fig. 1-6 shows an example of idiomorphic ferrite in Fe-0.1C-2.3Si-1.4Mn-2Cr-0.9Mo (wt.%) cast alloy [Ichikawa, 1997].

Bhadeshia [1985c] suggested that idiomorphic ferrite is taken to be that which has a roughly equiaxed morphology. Idiomorphic ferrite is not often observed in steel weld metal. That is because reconstructive ferrite normally starts at the high energy austenite boundaries and forms allotriomorphs. Nevertheless, it may occur in weld metals which are cooled slowly such as during thermit welding since its metallurgical process is similar to ingot casting.

1.3.5 Pearlite

Pearlite is a lamellar mixture of ferrite and cementite (Fe_3C) which is formed by eutectoid transformation. The eutectoid carbon concentration in Fe-C alloys is 0.765 wt.%. This microstructure is industrially very important especially for higher carbon concentration steel welds. Uchino, for example, reported the existence of a eutectoid pearlite microstructure during the arc welding of railway steel [1997]. He mentioned that at the carbon concentration of 0.78 wt.% fine lamellar pearlite was observed and may have contributed to the improvement of wear resistance.

Pearlite usually nucleates at the austenite grain boundaries. The nucleation rate of pearlite is two orders of magnitude smaller than that of allotriomorphic ferrite [Jones and Bhadeshia, 1997a].

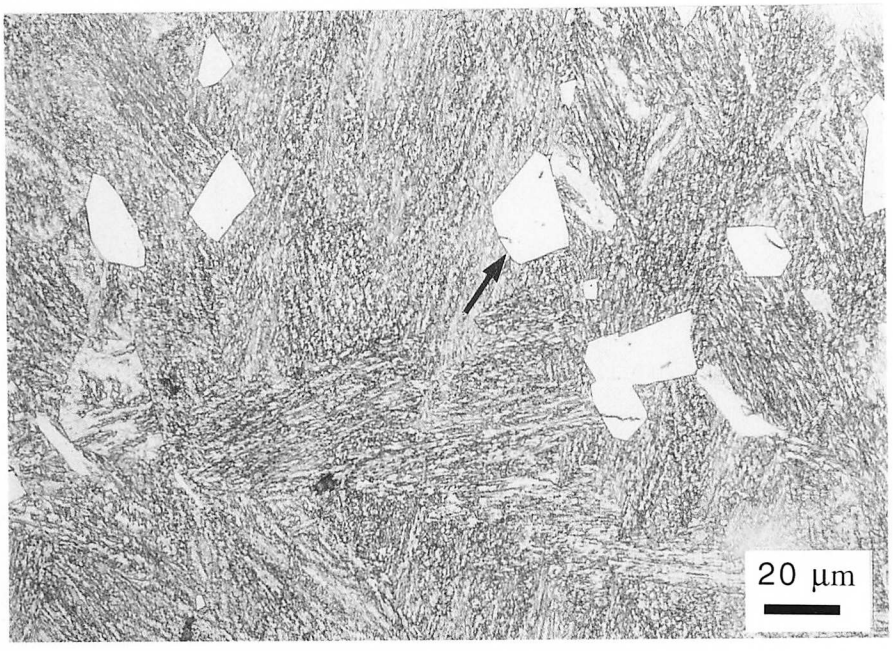

Fig. 1-6 : An example of idiomorphic ferrite in Fe-0.1C-2.3Si-1.4Mn-2Cr-0.9Mo (wt.%) cast alloy [Ichikawa, 1997].

The growth rate of the pearlite in a binary steel is expected to be constant since the average carbon concentration in the product phases (ferrite and cementite) is equal to the composition in the matrix phases far ahead of the advancing interface [Puls and Kirkaldy, 1972]. The composition is found to be uniform within each lamella and the ratio of the thickness of ferrite and cementite is uniquely determined by the original matrix austenite carbon concentration and the lever rule [Puls and Kirkaldy, 1972]. Based on these observations and assuming that the growth of pearlite occurs with local equilibrium at the transformation front and is controlled by the diffusion of carbon in austenite, Zener [1946] obtained the following expression which describes the growth rate;

$$v_p = \frac{D}{S_l}\frac{\phi_R}{k_p}\left(1 - \frac{S_c}{S_l}\right) \qquad (1-2)$$

where D is a diffusivity of carbon in austenite, k_p is a geometrical factor and is equal to 0.72 for Fe-C, S_l is the combined width of ferrite and cementite lamellae, and S_c is the theoretical critical spacing

for which the velocity of the reaction becomes zero. ϕ_R is a relative supersaturation and is given by [Hillert, 1957];

$$\phi_R = \frac{\left(c_C^{\gamma\alpha} - c_C^{\gamma\theta}\right)}{\left(c_C^{\theta\gamma} - c_C^{\alpha\gamma}\right)} \frac{S^2}{S^\alpha S^\theta} \qquad (1-3)$$

where $c_C^{\gamma\alpha}$ and $c_C^{\gamma\theta}$ are the carbon concentrations in austenite on the austenite/ferrite and at the austenite/cementite interface respectively. $c_C^{\theta\gamma}$ and $c_C^{\alpha\gamma}$ are the carbon concentrations in cementite and ferrite respectively, when they are in equilibrium with austenite. S^α and S^θ are the widths of ferrite and cementite lamellae respectively. Zener [1946] and Hillert [1957] assumed that the system stabilises at that spacing for which the velocity is a maximum and obtained the following expression [Puls and Kirkaldy, 1972].

$$S_l = 2S_c = \frac{4\sigma^{\alpha\theta} T_E}{\Delta H_v \Delta T} \qquad (1-4)$$

where $\sigma^{\alpha\theta}$ is the surface energy of the ferrite/cementite phase boundary and ΔH_v is the change in enthalpy per unit volume between austenite and pearlite. T_E is the eutectoid temperature and ΔT the magnitude of the undercooling below T_E.

1.3.6 Widmanstätten Ferrite

Widmanstätten ferrite is a plate-like variety of ferrite which forms at temperatures below that of allotriomorphic ferrite and above that at which bainite forms. Watson and McDougall [1973] proposed that the transformation mechanism is displacive; however the transformation can occur at a relatively small driving force because the strain energy due to its displacive transformation mechanism is mitigated by the cooperative growth of two mutually accommodating variants of ferrite [Bhadeshia, 1981a; 1985b; 1988]. This also leads to the wedge-like shape of Widmanstätten ferrite.

The displacive transformation mechanism of Widmanstätten ferrite has been uniquely confirmed by Shipway and Bhadeshia [1997] who showed that the transformation is stabilised if the austenite is plastically deformed prior to transformation. Only displacive transformation can be retarded by plastic deformation. The amount of Widmanstätten ferrite decreased when the austenite was deformed as the accumulated debris of dislocations interfered with the motion of the glissile Widmanstätten ferrite/austenite interface. Deformation does increase the number density of nucleation sites and hence leads to a refined microstructure. This evidence is consistent with the growth of Widmanstätten ferrite by a mechanism which is displacive. Yang and Chang [1997] also showed that the number of crystallographic variants of Widmanstätten ferrite is reduced by an applied compressive stress. They concluded that all their own experimental results can be interpreted in terms of the invariant plane-strain displacive mechanism for Widmanstätten ferrite.

The strain energy of the composite Widmanstätten ferrite plate is therefore small at about 50 J mol^{-1}, compared with that of bainite which is about 400 J mol^{-1} [Bhadeshia, 1981a].

Spanos and Hall [1996] summarised three possible mechanisms of Widmanstätten ferrite formation (Fig. 1-7).

Fig. 1-7a shows a morphological instability mechanism. This model assumes the formation of Widmanstätten ferrite by the continuous development of growth instabilities at the ferrite/ austenite boundaries of allotriomorphs. Townsend and Kirkaldy [1968] demonstrated reasonable agreement between experimental and calculated Widmanstätten ferrite spacing applying the Mullins-Sekerka theory [1963] but this analysis is of little use because the velocity during the diffusion-controlled growth of the original flat interface varies with time. Townsend and Kirkaldy arbitrarily set this velocity to particular values in order to reach agreement between experimental results and theory.

Aaronson and Wells [1956] suggested that sympathetic nucleation of Widmanstätten ferrite on allotriomorphic ferrite crystal (Fig. 1-7b) led to *secondary sawteeth* in which there are ferrite/ferrite boundaries between the sawtooth and the allotriomorph.

The third mechanism (Fig. 1-7c) suggested is that some *primary* Widmanstätten ferrite particles initially nucleate directly from the austenite boundary and then quickly physically impinge along the austenite boundary forming an apparent allotriomorph. The adjacent nucleation of *secondary* Widmanstätten ferrite plates along the broad interfaces of *primary* Widmanstätten ferrite may also be possible. Spanos *et al.* investigated these hypothesis using transmission electron microscopy (TEM), scanning electron microscopy (SEM), electron back scattering pattern (EBSP) analysis and optical microscopy. They demonstrated that groups of Widmanstätten ferrite plates and the allotriomorphs from which they nucleate are not composed of monolithic single crystals which are formed by morphological instability mechanism. It should be emphasised that none of these proposed mechanisms accounts for the shape deformation accompanying the transformation to Widmanstätten ferrite.

Enomoto [1991a; 1991b] has developed finite difference computer model for the demonstration of the transition from allotriomorph to Widmanstätten ferrite based on growth by the ledge mechanism. If the supersaturation Ω is low ($\Omega = 0.3$), successively nucleated ferrite steps coalescence to the first step and grow slowly forming a plane interface. If Ω is low ($\Omega = 0.65$), initially nucleated few steps grow toward the matrix and subsequently nucleated steps coalescence at the back of the growing ferrite. However, the calculations depend critically on the ready availability of steps, which is an adjustable parameter in the theory.

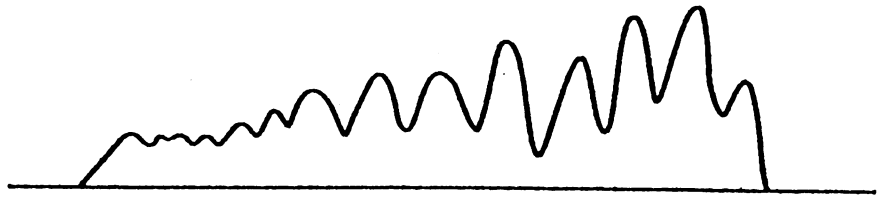

(*a*)

(*b*)

(*c*)

Fig. 1-7 : Schematic illustrations showing the three possible models of formation of Widmanstätten ferrite (after Spanos and Hall [1996]). (a) A morphological instability model, (b) "sympathetic" nucleation model on interface of pre-existing allotriomorph. and (c) rapid physical impingement model of primary Widmanstätten ferrite.

The tendency of Widmanstätten ferrite to form in packets might be detrimental to toughness and fatigue

properties of steel [Dieter, 1976; Grong and Matlock, 1986].

1.3.7 Bainite

Bainite is non-lamellar mixture of ferrite plates and cementite. It occurs in the temperature range between pearlite and martensite are formed by isothermal decomposition of austenite [Hehemann, 1970]. Thus bainite can be observed in weld metals, for example, in chromium alloyed steel weld metals which is used at elevated temperatures. Fig. 1-8 shows an example of the bainitic microstructure observed in modified 2.25Cr-1Mo steel submerged-arc weld metal [Ichikawa *et al.*, 1995].

Advanced high strength steel welds also often show bainitic microstructures [Devletian *et al.*,1995; 1996, Blackburn *et al.*, 1996; Fiore, 1996]. Devletian *et al.* have recently studied the welding of high strength low-alloyed (HSLA) steels using ultra low carbon bainitic (ULCB) steel [1995]. They reported good strength and toughness for steels having a yield strength level of 100 ksi (690 MPa), 80 ksi (550 MPa) and 65 ksi (450 MPa) (namely HSLA-100, HSLA-80 and HSLA-65 respectively) using ultra low carbon bainitic steel welds. They also suggested that the ultra low carbon bainitic steel welds are relatively insensitive to the cooling rate over the range $18\,^{\circ}\mathrm{C\,s^{-1}}$ to $6\,^{\circ}\mathrm{C\,s^{-1}}$.

Bainite is a displacive transformation, nucleating at austenite grain boundaries and forming as aggregates (sheaves) of small platelets or laths (sub-units) of ferrite. An invariant-plane strain shape deformation with a large shear component accompanies the growth of bainite. There is no diffusion of iron or substitutional solute elements during nucleation and growth. Carbon, however, must diffuse during paraequilibrium nucleation but does not appear to do so during growth [Bhadeshia, 1981a].

Bainite can be distinguished into upper and lower bainite by its transformation mechanism and mechanical properties. The bainitic ferrite is free of carbides in upper bainite, where carbides grow from the regions of carbon-enriched residual austenite which are trapped between the sub-units of ferrite. By contrast bainitic ferrite in lower bainite contains plate-like particles of carbide [Bhadeshia and Christian, 1990]. Upper bainite is often observed in alloyed steel welds with tensile strength in the range 65 to $75\,\mathrm{kgf\,mm^{-2}}$ (637 to 735 MPa). This microstructure has a relatively low toughness compared with acicular ferrite because upper bainite grows in packets of plates with a common cleavage plane [Horii, 1989].

Bainite should be able to form by a diffusionless transformation mechanism at a temperature just below T_0 temperature where the austenite and ferrite of the same composition have identical free energy [Bhadeshia and Edmonds, 1980]. Additional free energy is necessary to account for the strains associated with the mechanism of transformation. A further temperature T_0', which incorporates a strain

that the strain energy term due to the shape change is about 400 J mol^{-1} [Bhadeshia, 1981a]. The growth of bainitic ferrite ceases at the maximum volume fraction θ_b when the carbon concentration of the residual austenite reaches the T_0' concentration [Bhadeshia and Edmonds, 1979].

The nucleation mechanisms of bainite and Widmanstätten ferrite are identical [Bhadeshia, 1981a]. The activation energy for the nucleation is a linear function of the maximum chemical free energy change involved ΔG_m [Bhadeshia, 1982b] (The derivation of ΔG_m will be discussed in section *1.4.5.5.*). The nucleation rate of bainitic ferrite per unit volume $I^B_{\alpha_b}$ at any temperature T Kelvin can be thus written by [Bhadeshia, 1982b];

$$I^B_{\alpha_b} = C_1 \exp\left[-(C_2 + C_3 \Delta G_m)/(RT)\right] \qquad (1-5)$$

where C_1, C_2 and C_3 are empirical constants and R is the gas constant. If the bainite nucleation rate at the Widmanstätten ferrite start-temperature W_S is given by $I^B_{W_S}$, equation (1-5) can be rewritten as;

$$I^B_{\alpha_b} = I^B_{W_S} \exp\left[-\frac{C_2 \Delta T}{RTW_S} - \frac{C_3}{R}\left(\frac{\Delta G_m}{T} - \frac{G_N}{W_S}\right)\right] \qquad (1-6)$$

where $C_2 = 27910$ J mol^{-1}, $C_3 = 3.679$ [Rees and Bhadeshia, 1992].

ΔT: supercooling, $\Delta T = W_S - T$,

G_N: the minimum necessary free energy change for the displacive nucleation of ferrite.

This equation for the nucleation rate can be rearranged to give [Rees and Bhadeshia, 1992];

$$I^B_{\alpha_b} = K_{W1} \exp\left(-\frac{K_{W2}}{RT} - \frac{K_{W2} \Delta G_m}{rRT}\right) \qquad (1-7)$$

where $K_{W1} = \left(\overline{L} K'_{W1}\right)^{-1}$, with K'_{W1} being an empirical constant and $\overline{L}$ the mean linear intercept of a series of random lines which intersect with the austenite grain boundaries. K_{W2} is an empirical constant. Typical values of K'_{W1} and K_{W2} can be seen in [Rees and Bhadeshia, 1992].

The overall transformation rate of bainite $d\xi_b/dt$ is then given by [Rees and Bhadeshia, 1992];

$$\frac{d\xi_b}{dt} = \frac{uK_1}{\theta_b}(1-\xi_b)(1+\beta\theta_b\xi_b)\exp\left[-\frac{K_2}{RT}\left(1+\frac{\Delta G^0_m}{r}\right)+\Gamma_2\xi_b\right] \qquad (1-8)$$

where

ξ_b: normalised volume fraction of bainite; $\xi_b = v_b/\theta_b$ where v_b and θ_b are the actual and maximum volume fraction of bainite respectively,

β: an empirical autocatalysis constant ($\beta = 200$),

ΔG^0_m: initial value of ΔG_m;

$\Delta G_m = \Delta G^0_m [1 - (C_4\theta_b\xi_b/C_3)]$ where $C_3 = 3.679$ and $C_4 = 11$ are empirical constants,

Γ_2 is $K_{W2}\left(\Delta G^0_m - G_N\right)/(rRT)$ where r is 2540 J mol^{-1}.

Thus in total there are six fitting constants (*i.e.*, C_2, C_3, C_4, K'_{W1}, K_{W2} and β) for describing the overall transformation rate of bainite with the approximation by Rees and Bhadeshia.

1.3.8 Acicular Ferrite

Acicular ferrite is, in general, a desirable microstructural component in low-alloy steel welds. It has excellent strength and toughness [Ito and Nakanishi, 1975; Abson *et al.*, 1979; Cochrane and Kirkwood, 1979; Mori *et al.*, 1981]. The finely dispersed nucleation sites in weld metals give the observed chaotic distribution of acicular ferrite plate. This microstructure confers excellent toughness to the welds because cleavage cracks are then frequently deflected [Ohkita *et al.*, 1986].

Acicular ferrite forms at temperatures where reconstructive transformations are relatively sluggish and give way to displacive transformations [Bhadeshia and and Svensson, 1993]. It is similar to bainite; *i.e.*, carbon diffusion occurs during paraequilibrium nucleation but not during its growth [Bhadeshia, 1992]. In fact, Rees and Bhadeshia [1994] have demonstrated that the universal nucleation function, which describes the minimum driving force for detectable nucleation of acicular ferrite, is virtually identical to that of bainite in ordinary steels and in weld metals. On the other hand acicular ferrite is known to nucleate heterogeneously [Ito and Nakanishi, 1975] on non-metallic of inclusions inside austenite grains, while bainite nucleates on the austenite grain surfaces.

Weld metals, although protected by fluxes or inert gases, usually contain large quantities of oxides which become the heterogeneous nucleation sites for ferrite [Horii, 1989]. The nature of inclusions is important for the formation of acicular ferrite. For example, Horii *et al.* [1995b] demonstrated that small additions of titanium to weld metal promote the formation of $(\mathrm{Mn,Ti})(\mathrm{Al,Ti})_2\mathrm{O}_4$. There is no general theory for the potency of ferrite nucleation sites. Several researchers have proposed necessary features of inclusions as acicular ferrite nucleation sites. For example, Mori *et al.* [1981], Mills *et al.* [1987], Thewlis [1989a; b] supposed that inclusion surfaces which have low misfit with ferrite accelerate ferrite nucleation. Devillers *et al.* [1984] suggested that strain in the matrix austenite around oxides accelerates nucleation. They showed that aluminium-manganese silicate display the lowest thermal expansion coefficient in compounds they examined and that they are therefore the most likely to create significant strains and contribute the nucleation. Jang and Indacochea [1987] assumed the significance of the size of non-metallic inclusions due to the presence of 0.6 μm and smaller inclusions within fine acicular ferrite. Gregg and Bhadeshia [1994a; 1994b] have established a technique that allows the systematic study of the ability of oxides and other compounds to simulate the nucleation of bainite on mineral surfaces. They showed, using this technique, that TiO_2, $\mathrm{Ti}_2\mathrm{O}_3$ and TiO are all effective in enhancing the formation of bainite in the adjacent steel by a variety of mechanisms. They also

demonstrated that TiN by contrast is ineffective as a nucleation substrate for bainite. They categorised minerals into three groups I, II and III (Table 1-3).

Table 1-3 : Relative efficacy of the minerals for stimulating bainite nucleation, after Gregg and Bhadeshia, 1994a.

Group I (effective)	Group II (effective)	Group III (ineffective)
TiO_2	Ti_2O_3	TiN
PbO_2	TiO	$MnAl_2O_4$
MnO_2		γ-Al_2O_3
SnO_2		α- Al_2O_3
WO_3		NbC
MoO_3		$CaTiO_3$
V_2O_5		$SrTiO_3$
KNO_3		MnS

Minerals in Group I , including TiO_2 and MnO_2, are oxygen sources which cause local decarburisation on the adjacent steel matrix and hence stimulate transformation since a reduction of carbon reduces the stability of austenite. Ti_2O_3 in Group II absorbs manganese from the austenite matrix, thereby reducing its hardenability, and hence stimulating ferrite nucleation; manganese absorption could not be observed on TiO in the group. Minerals in Group III, including TiN and $MnAl_2O_4$, were found to be ineffective. Zhang *et al.* [1996] applied a similar technique as Gregg and Bhadeshia and examined ferrite nucleation potencies of pure polycrystal ceramics (VN, ViN, TiO, VN, AlN and Al_2O_3). They showed VN to be most effective in stimulating ferrite nucleation whereas TiO was least effective.

The inoculation of steel welds with these effective non-metallic particles to produce acicular ferrite is often combined with the addition of boron [Mori *et al.*, 1981]. Boron segregates at austenite grain boundaries, reduces their energy and thus suppresses allotriomorphic ferrite formation. Whereas the effect of boron on the effectiveness of austenite grain surfaces as heterogeneous nucleation sites is well established, its corresponding effect of inclusions as heterogeneous sites is not completely clear. Yamamoto *et al.* [1996] discussed the interaction between Ti_2O_3 and boron. They suggested that the Ti_2O_3 contains cation vacancies which contribute to the preferential nucleation of other phases (*e.g.*, MnS and TiN). They explained the detailed mechanism is that the frequency of lattice vibration at vacancy sites of Ti_2O_3 interface is considered to increase after vacancies are filled with atoms in the

matrix around Ti_2O_3 by which vibration entropy increases. Due to this, both interfacial free energy and internal energy of Ti_2O_3 decrease with the diffusion of atoms into Ti_2O_3. The resulting Mn-depleted zone at the Ti_2O_3/austenite boundaries reduces hardenability whereas TiN decreases the interfacial energy for ferrite nucleation. They also suggested that whereas boron segregates to the austenite grain surfaces, it does not do so at the Ti_2O_3/γ boundaries because it is absorbed by the Ti_2O_3. The Ti_2O_3 therefore retains its ability to stimulate ferrite nucleation even in the presence of boron. This means that the addition of boron will enhance the significance of inclusions as ferrite nucleation sites.

Zhang and Farrar [1996] suggested two types of nucleation and growth modes on the inclusions; the growth direction of the acicular ferrite laths parallel or normal to the nucleating surface of the inclusion. The former mode results in the "boxing in" of the inclusion whereas the latter leads to the enclosure of the inclusions within ferrite plates. Ferrite plates nucleated on inclusions may in turn stimulate others, a phenomena known as autocatalytic nucleation [Ricks *et al.*, 1982].

Yang and Bhadeshia [1989] showed the clusters of acicular ferrite plates in high strength steel weld metal form in such a way that adjacent plates tend to have a similar orientation in space because it is easier to form plates with approximately the same orientation.

Farrar and Zhang [1995] showed that higher nickel contents in weld metal resulted in sharper acicular ferrite laths with larger aspect ratios and that reducing the oxygen content increases the acicular ferrite lath aspect ratio. The former effect has been explained by Singh and Bhadeshia [1998] who demonstrated quantitatively that the reduction in driving force and the increase in the strength of the austenite due to the addition of nickel, both decrease the thickness of acicular ferrite plates. A reduction in the oxygen content is expected to increase the aspect ratio because the smaller number density of nucleation sites allows the plates to lengthen without hindrance.

1.3.9 Martensite

Martensitic microstructures can be observed in high-strength-low-alloy (HSLA) steel welds with relatively low heat input [Fonda *et al.*, 1995]. The high hardness of martensite can make the weld susceptible to cold cracking, requiring the use of preheating to reduce the cooling rate. The use of preheat unfortunately reduces productivity. Ikeda and Oi and their co-workers have recently developed welding materials for a tensile strength of 980 MPa steel with low cold cracking susceptibility for the application to penstock [Ikeda *et al.*, 1997; Oi *et al.*, 1997]. They identified that, for example, it is necessary to keep the weld metal Vickers hardness below 380 in order to reduce the preheat required to less than 75 °C for shielded metal arc welding.

Solidification induced chemical segregation can lead to the formation of coarse blocky laths of martensite and bainite along the solidification or transformation sub-boundaries [Garland and Kirkwood, 1975; Grong and Matlock, 1986]. Banded microstructures of martensite can sometimes be observed along the primary solidification boundaries due to the local increase in hardenability caused by chemical segregation. An example was shown by Buck [1984] in the submerged arc welding weld metal for Ni-Cr-Mo alloyed steel.

Martensite grows without diffusion with a cooperative movement of atoms during the transformation from austenite. Several empirical equations have been proposed for predicting the martensite transformation start temperature (M_S) as a function of the steel composition [Payson and Savage, 1944; Carapella, 1944; Rowland and Lyle, 1945; 1946; Grange and Stewart, 1946; Nehrenberg, 1946; Steven and Haynes, 1956; Andrews, 1965]. These relations have been summarised by Cool [1996]. There also is an equation by Hollomon and Jaffe, which includes the effects of aluminium, cobalt and vanadium while it does not include silicon [1947]. These empirical equations work very well for most practical purposes as long as they are not overly extrapolated.

Yurioka *et al.* [1987] and Okumura [1990] have presented empirical equations representing the martensite fraction $V_{\alpha'}$ as a function of the chemical composition and cooling time $\Delta t_{800\rightarrow500}$ between 800 to 500 °C and equations giving the hardness of the heat affected zone. According to their description, $V_{\alpha'}$ can be calculated by;

$$V_{\alpha'} = 0.5 - 0.455 \arctan(X) \qquad (1-9)$$

where

$$X\,(\text{radian}) = 4\frac{\log(\Delta t_{800\rightarrow500}) - \log(\Delta t_M)}{\log(\Delta t_B) - \log(\Delta t_M)} - 2$$

where Δt_M is the critical cooling time of 800 to 500 °C for which 100% martensite is obtained and Δt_B is the cooling time for which the maximum fraction of bainite is obtained;

$$\log(\Delta t_M) = 4.60 CE_I - 2.08 \qquad (1-10)$$

$$\log(\Delta t_B) = 2.69 CE_{III} - 0.321 \qquad (1-11)$$

where CE_I and CE_{III} are empirical carbon equivalents given by;

$$CE_I = C_P + \frac{w_{\text{Si}}}{24} + \frac{w_{\text{Mn}}}{6} + \frac{w_{\text{Cu}}}{15} + \frac{w_{\text{Cr}}\left(1 - 0.16\sqrt{w_{\text{Cr}}}\right)}{8} + \frac{w_{\text{Mo}}}{4} + \Delta H \qquad (1-12)$$

$$CE_{III} = C_P + \frac{w_{\text{Mn}}}{3.6} + \frac{w_{\text{Cu}}}{20} + \frac{w_{\text{Ni}}}{9} + \frac{w_{\text{Cr}}}{5} + \frac{w_{\text{Mo}}}{4} \qquad (1-13)$$

where w_i weight percent of element i. C_P is a function of the carbon concentration;

$$C_P = w_{\text{C}}, \text{ for } w_{\text{C}} \leq 0.3 \text{ wt.\%}$$

$$C_P = \frac{w_C}{6} + 0.25, \text{ for } w_C > 0.3 \text{ wt.\%}$$

ΔH is a function of boron concentration (w_B);

$$\Delta H = 0, \text{ for } w_B \leq 0.0001 \text{ wt.\%}$$

$$\Delta H = 0.03, \text{ for } w_B = 0.0002 \text{ wt.\%}$$

$$\Delta H = 0.06, \text{ for } w_B = 0.0003 \text{ wt.\%}$$

$$\Delta H = 0.09, \text{ for } w_B \geq 0.0004 \text{ wt.\%}$$

These equations can be applied for cooling time about $0.1 \leq \Delta t_{800 \rightarrow 500} \leq 100$ and compositions $w_C < 0.8$ wt.%, $w_{Si} < 1.2$ wt.%, $w_{Mn} < 2$ wt.%, $w_{Cu} < 0.9$ wt.%, $w_{Ni} < 10$ wt.%, $w_{Cr} < 10$ wt.% and $w_{Mo} < 2$ wt.% [Yurioka *et al.*, 1987; Okumura, 1990].

A thermodynamic approach is also available for estimating the M_S temperature as a function of alloying element concentration [Kaufmann and Cohen, 1958; Bhadeshia 1981b; c; Ghosh and Olson, 1993; 1994; Ishida, 1995]. Kaufmann and Cohen [1958] presented $\Delta G^{\gamma \rightarrow \alpha'}$ as;

$$\Delta G^{\gamma \rightarrow \alpha'} = \Delta G^{\gamma \rightarrow \alpha} + G_{Zener} \qquad (1-14)$$

where $\Delta G^{\gamma \rightarrow \alpha'}$ is the free energy change from austenite to body-centered tetragonal martensite, $\Delta G^{\gamma \rightarrow \alpha}$ is the corresponding free energy change from austenite to body-centered cubic ferrite and G_{Zener} is the Zener ordering energy which arises because the carbon atoms in ferritic iron can order on one of the three available sublattices of octahedral interstitial site. The ordering changes the lattice symmetry from body-centred cubic to body-centred tetragonal, when M_S is below the ordering temperature T_C [Fisher, 1949];

$$T_C\,(K) = \frac{T\,(1 - x_C)}{28080 x_C} \qquad (1-15)$$

where x_C is mole fraction of carbon. Martensitic transformation starts when the metal is cooled to a temperature where a critical amount of free energy change $\Delta G_c^{\gamma \rightarrow \alpha'}$ for diffusionless transformation is achieved. *i.e.*, [Kaufmann and Cohen, 1958];

$$\Delta G^{\gamma \rightarrow \alpha'}\,\{M_S\} = \Delta G_c^{\gamma \rightarrow \alpha'} \qquad (1-16)$$

$\Delta G_c^{\gamma \rightarrow \alpha'}$ is approximately -900 to -1300 J mol^{-1} for low alloy steels, but is strictly a function of the strength of the austenite. $\Delta G_c^{\gamma \rightarrow \alpha'}$ thus varies with the alloy concentration.

Ghosh and Olson [1993, 1994] therefore expressed the critical driving force as a function of concentration in a manner consistent with the solid solution strengthening effect of each element in austenite;

$$\begin{aligned} -\Delta G_c^{\gamma \rightarrow \alpha'} \quad &= K_1 + 4009 w_C^{0.5} + 1879 w_{Si}^{0.5} + 1980 w_{Mn}^{0.5} + 172 w_{Ni}^{0.5} + 1418 w_{Mo}^{0.5} \\ &+1618 w_V^{0.5} + 752 w_{Cu}^{0.5} + 714 w_W^{0.5} + 1653 w_{Nb}^{0.5} + 3097 w_N^{0.5} - 352 w_{Co}^{0.5} \end{aligned} \qquad (1-17)$$

where K_1 is a constant which includes the combined effects of the interfacial and strain energy terms. The maximum concentrations for equation (1-17) are approximately 2 wt.% for carbon and nitrogen, 0.9 wt.% for vanadium and about 2–28 wt.% for all the other alloying elements [Ghosh and Olson, 1993; 1994; Olson, 1995; Cool and Bhadeshia, 1996].

1.3.10 Microphases

Small quantities of "martensite-austenite-constituents" (MAC) can be detrimental to the toughness of welds. Horii *et al.* [1990] revealed that second heating cycle to 550°C can improve the reheated weld metal toughness due to the decomposition of the martensite-austenite-constituents to cementite. Martensite-austenite-constituent formation at the intercritically reheated grain-coarsened heat-affected zone has been well investigated [Nakao *et al.*, 1985]. Fig. 1-9 shows the course of events [Nakao *et al.*, 1985; Horii, 1989];

1. austenite is nucleated on carbides and on any existing martensite-austenite-constituents on the prior austenite boundaries just above Ac_1 (Temperature at which ferrite+cementite becomes ferrite+austenite during heating) during the reheating caused by welding,
2. carbon concentration of austenite is enriched and becomes homogeneously distributed,
3. carbon is partitioned from ferrite to austenite leading to an increase its concentration during cooling,
4. the carbon-enriched austenite transforms to partly martensite, the remainder being retained.

Retention of martensite-austenite-constituents in weld metal however has not been studied very well from a point of view of the modelling.

1.4 Modelling of Transformations in Steel Welds

1.4.1 Introduction

Weld processes involve a large number of physical phenomena over a range of temperatures in a very short time during continuous cooling from elevated temperatures. Very few of these can be neglected (*e.g.*, segregation of carbon) in order to convincingly represent the welding process. A few of the phenomena include the treatment of thermal history, solidification-induced segregation, austenite grain structure and finally solid-state transformations. Olson *et al.* [1993], for example, mentioned a generic additive function that represents the factors which affect the transformations in steel welds. Such a function should include terms that describe the following aspects which might be important in determining weld metal microstructure:

1. alloying element hardenability effects,

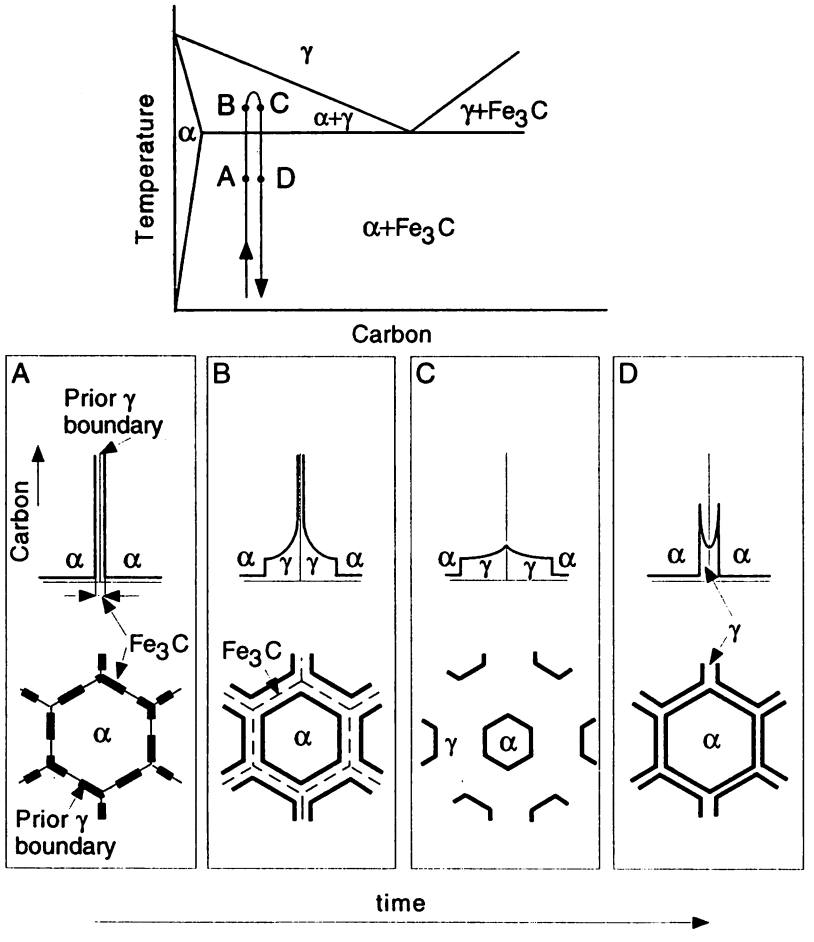

Fig. 1-9 : Schematic illustration showing the mechanism of martensite-austenite constituent formation in the reheated region of steel weldment (after Nakao *et al.* [1985] and Horii [1989].

2. interactions of solute partitioning effects and weld metal inclusion formation with phase transformations,
3. weld metal chemical composition changes due to electrochemical reactions,
4. microstructural changes due to heat input and cooling rate variations,
5. compositional gradient effects during solidification.

They did not indicate how such functions may be derived and there is no justification for the implied additivity of the different factors.

Most of the microstructural modelling has been based on phase transformation theory [*e.g.*, Bhadeshia *et al.*, 1985a] and has been applied to the microstructural modelling of base steel [Saito, 1997]. The

following part of this chapter thus focuses on analytical models which are metallurgically interesting. Other methodologies also have been recently proposed for microstructures and mechanical properties. Bhadeshia *et al.* [1995] have applied Bayesian neural network analysis for the prediction of impact toughness of C–Mn steel arc welds. Application of this technique to the prediction of weld solidification cracking will be discussed in a later Chapter. Umemoto [1995] and his co-workers [Kusunoki and Umemoto, 1996] have proposed another methodology that estimates the strength of single-phase (*i.e.*, pearlite) from the driving force of the phase transformation calculated by the thermodynamics. They assumed that strength of materials is a function of "free energy remaining in the structure (ΔG_{st})" which includes grain boundary, dislocation and elastic strain energy of matrix and interfacial and elastic strain energy on precipitates and matrix interfaces. Assuming that the (ΔG_{st}) is proportional to the driving force, they have shown that the yield strength prediction agrees fairly well with th experiment. By this method, any quantitative measurement of microstructures is not necessary but it still needs some empiricism to relate the chemical driving force and (ΔG_{st}) and to have numerical expression of the strength of materials as a function of ΔG_{st}.

1.4.2 Thermal History of Welds

The estimation of weld thermal history is important since the microstructure depends on the cooling rate. It also influences cold-cracking which depends on the hardness achieved in the heat affected zone. Hence, a large number of studies have been reported on the prediction of weld cooling curves involving various degrees of empiricism. Rosenthal [1941] and Adams [1958] obtained analytical solutions for a moving point heat source, neglecting radiation and heats of transformation:

for three dimensional heat flow,

$$T_W - T_\infty = \frac{Q_P v_S}{4\pi\lambda\kappa} \cdot \frac{\exp\left[X_m - \sqrt{X_m^2 + R_m^2}\right]}{\sqrt{X_m^2 + R_m^2}} \qquad (1-18)$$

and for two dimensional heat flow,

$$T_W - T_\infty = \left(Q_P 2\pi\lambda h_p\right) \exp\left(X_m\right) K_0\left(\sqrt{X_m^2 + Y_m^2}\right) \qquad (1-19)$$

where

$$X_m = v_S x_p \,(2\kappa)$$

$$R_m = v_S \sqrt{\left(y_p^2 + z_p^2\right)} \Big/ (2\kappa)$$

$$Y_m = v_S y_p / (2\kappa)$$

x_p, y_p, z_p: coordinates fixed to the plate (m),

X_m: coordinate which has an origin at a moving point heat source (m),

R_m: a distance from the centre of the weld bead normal to the welding direction for three-dimensional heat flow (m),

Y_m: a distance from the centre the weld bead normal to the welding direction for two-dimensional heat flow (m),

T_W: temperature at weldment at (X_m, R_m) for three-dimensional heat flow and at (X_m, Y_m) for two-dimensional heat flow (m),

T_∞: far field temperature (K),

Q_p: effective heat input per unit time $\left(\mathrm{J\ s^{-1}}\right)$, $Q_p = \eta IV$,

η: arc energy transfer efficiency,

I: welding current (A),

V: voltage (V),

v_s: travel speed $\left(\mathrm{m\ s^{-1}}\right)$,

λ: thermal conductivity $\left(\mathrm{J\ s^{-1}\ m\ K}\right)$,

κ: thermal diffusivity $\left(\mathrm{m^2\ s^{-1}}\right)$,

h_p: plate thickness (m),

K_0: Bessel function of zero order and second kind of .

These equations are used frequently in combination with empirical fitting for the prediction of weld cooling characteristics. Yurioka *et al.* [1985] derived an exact solution for the three-dimensional heat flow due to a moving point heat source on a preheated plate with finite thickness, accounting for heat transfer from the plate surface:

$$\begin{aligned} T_W\left(x_p, y_p, z_p, t_W\right) = T_\infty + \frac{Q_P}{\pi\lambda h_p}\exp\left(-\frac{v_S w}{2\kappa}\right)\sum_{n=0}^{\infty} A_{wn}\left(\cos\frac{U_{wn}z_p}{h_p} + \frac{h_p d_w}{U_{wn}}\sin\frac{U_{wn}z_p}{h_p}\right) \\ \times K_0\left(\frac{r}{h_p}\sqrt{U_{wn}^2 + \left(\frac{v_S h_p}{2\kappa}\right)^2}\right) \\ + 2\left(T_i - T_\infty\right)\sum_{n=0}^{\infty} A_{pn}\left(\cos\frac{U_{pn}z_p}{h_p} + \frac{h_p d_p}{U_{pn}}\sin\frac{U_{pn}z_p}{h_p}\right) \\ \times\left(\frac{\sin U_{pn}}{U_{pn}} - \frac{h_p d_p\left(\cos U_{pn} - 1\right)}{U_{pn}^2}\right)\exp\left(-\frac{\kappa U_{pn}^2}{h_p}t_W\right) \end{aligned} \qquad (1-20)$$

where

$$r = \sqrt{w^2 + y_p^2 + z_p^2}$$

w: moving coordinate, $w = x_p - v_s t_W$ (m),

r: distance from point heat source (m),

t_W: time after welding (s),

T_i: initial temperature of plate or preheat temperature (K),

α_w: weld surface heat transfer conductivity to ambience $\left(\mathrm{J\ m^{-2}\ K\ s}\right)$,

α_p: plate surface heat transfer conductivity to ambience $\left(\mathrm{J\ m^{-2}\ K\ s}\right)$,

d_w: heat transfer coefficient at weld surface $\left(\mathrm{m^{-1}}\right)$, $d_w = \alpha_w/\lambda$,

d_p: heat transfer coefficient at plate surface $\left(\mathrm{m^{-1}}\right)$, $d_p = \alpha_p/\lambda$,

U_{wn}: eigenvalues satisfying $\tan\left(U_{wn}\right) = 2h_p d_w U_{wn}/(U_{wn}^2 - h_p^2 d_w^2)$,

U_{pn}: eigenvalues satisfying $\tan\left(U_{pn}\right) = 2h_p d_p U_{pn}/(U_{pn}^2 - h_p^2 d_p^2)$,

A_{wn}: coefficient in Fourier series, $A_{wn} = U_{wn}^2/\left(U_{wn}^2 - h_p^2 d_w^2 + 2h_p d_w\right)$,

A_{pn}: coefficient in Fourier series, $A_{pn} = U_{pn}^2/\left(U_{pn}^2 - h_p^2 d_p^2 + 2h_p d_p\right)$.

Since the derivation is more representative of real welds, this solution is often used in practice. Kasuya *et al.* [1993] have derived further solutions for weld heat flow: a moving heat source inside the plate without neglecting plate surface heat transfer (Model I); an instantaneous line heat source (Model II); and local preheating (Model III). For instance, contours of fusion line and phase transformation lines as well as thermal history of large heat input submerged arc welding (SAW) and electrogas welding (EGW) were predicted accurately using Model I.

Above solutions have been applied successfully for the prediction of heat affected zone properties, such as maximum hardness. Bhadeshia *et al.* [1985a] found that similar solutions (by Rosenthal) were unsuitable for application to the weld fusion zone. They used instead an empirical adaptation for three dimensional heat flow [Svensson *et al.*, 1986] based on an approximation by Weisman [Welding Handbook, 1981]:

$$\frac{dT_W}{dt_W} = \frac{C_1}{Q\eta}\left(T_W - T_i\right)^{C_2} \qquad (1-21)$$

where

Q: heat input per unit length of weld $\left(\mathrm{J\ m^{-1}}\right)$,

C_1, C_2: empirical constants derived by fitting against experimental cooling curves to the equation.

They found that this equation properly represents the cooling conditions as long as the constants C_1 and C_2 are adjustable. Note that there is no position dependence in equation 1-21 so that it is assumed that fusion zone cools at a uniform rate.

1.4.3 Modelling of Chemical Segregation during Solidification

Welds solidify more rapidly than conventional castings and therefore can be prone to chemical segre-

gation, particularly of substitutional alloying elements. This can influence their subsequent solid-state transformation behaviour. For example, Gretoft *et al.* [1985] suggested that segregation can significantly increase the allotriomorphic ferrite content because the ferrite nucleates more easily in solute-depleted regions.

Solidification-induced segregation can be modelled by assuming that;

1. there is no concentration gradient ahead of the solid/liquid interface (*i.e.*, uniform liquid composition),
2. there is a flat solid/liquid interface,
3. the partition coefficient is the same as from the phase diagram,
4. the densities of the solid and liquid phases are identical.

Using these assumptions, Clyne and Kurz [1981] derived the following equations in order to estimate segregation for one dimensional growth of solid phase:

$$\frac{c^{liq}}{c_0} = \{1 - (1 - 2a'k_0)\, V_s\}^{-(1-k_0)/(1-2a'k_0)} \qquad (1-22)$$

with

$$a' = a_0 \left[1 - \exp\left(-\frac{1}{a_0}\right)\right] - 0.5 \exp\left(-\frac{1}{2a_0}\right)$$

where a_0 is a dimensionless diffusion time given by $a_0 = (D_s t_0)/L^2$

D_s: diffusion coefficient in the solid,

t_0: time needed to complete solidification assuming that the solidification rate is constant,

L: length of the solidifying system,

c^{liq}: concentration of alloying element in liquid phase,

c_0: initial composition,

V_s: fraction solidified,

k_0: equilibrium partition coefficient.

The concentration of the solute in the solid, c^{sol} can be obtained from the phase diagram as:

$$c^{sol} = k_0 c^{liq} \qquad (1-23)$$

where

c^{sol}: concentration of alloying element in solid phase.

If solid-state diffusion is neglected, a' becomes zero and equation 1-22 becomes:

$$\frac{c^{liq}}{c_0} = (1 - V_s)^{k_0 - 1} \qquad (1-24)$$

The concentration in the solid is thus:

$$c^{sol} = k_0 c_0 (1 - V_s)^{k_0 - 1} \qquad (1-25)$$

This equation (1-25) is a special case of equation (1-22) and is identical to the classical "Scheil equation" [1942]. If solid-state diffusion is rapid or if the diffusion boundary layer is large, a' tends towards a value of 0.5, in which case:

$$\frac{c^{liq}}{c_0} = \frac{1}{1 - (1 - k_0) V_s} \qquad (1-26)$$

This equation corresponds to the well known "lever rule" [Kurz and Fisher, 1992].

These calculations (equations 1-22 to 26) require the equilibrium coefficients k_0 for the partition of solute elements between the solid and liquid phases. Using thermodynamics, the equilibrium partition can be shown to be [Kirkaldy *et al.*, 1978]:

$$k_0 = \exp\{\Delta^\circ G/(RT)\} \qquad (1-27)$$

where $\Delta^\circ G$ is the Gibbs free energy change per mole in transforming the pure solute from the delta ferrite to the liquid state, R is the universal gas constant and T is the absolute temperature.

1.4.4 The Austenite Grain Structure

The austenite grain boundary surface per unit volume S_V influences the rate at which allotriomorphic ferrite nucleates and grows [Bhadeshia *et al.*, 1987]. Nucleation is also possible on grain boundary edges and corners. However, in steel welds, nucleation on the edges and corners can be ignored because the austenite grain size is large enough and since since ferrite formation starts at relatively high supersaturations [Bhadeshia *et al.*, 1985a; 1987].

The columnar austenite grain geometry typical of welds can be represented approximately by a space-filling array of hexagonal prisms, each of which has a side-length of "a_c" and the height of "h_c" as illustrated in Fig. 1-10 [Bhadeshia and Svensson, 1993].

The mean lineal intercept of the austenite grain $\overline{L}$ is an average of measurements from several differently oriented sections. For example, Bhadeshia *et al.* [1986a] derived:

$$\overline{L} = \frac{\overline{L}_t + \overline{L}_l + \overline{L}_i}{3} \qquad (1-28)$$

where $\overline{L}_t$, $\overline{L}_l$ and $\overline{L}_i$ are intercept measurements from the transverse (*i.e.*, the plane $abcd$ in Fig. 1-11), longitudinal (*i.e.*, the plane which contains line gh and is parallel to the plane bce) and inclined sections (*i.e.*, the plane $abef$) respectively.

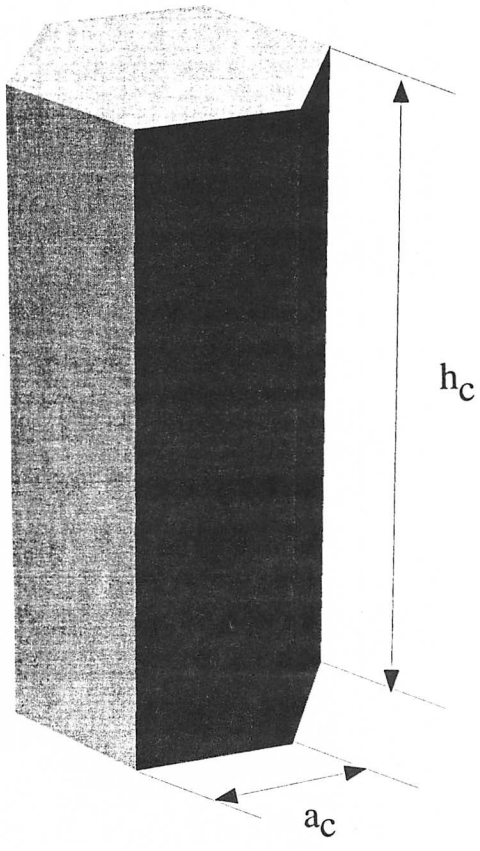

Fig. 1-10 : A space-filling hexagonal prism represents the austenite grain geometry (after Bhadeshia *et al.* [1993]).

According to Underwood [1970], this $\overline{L}$ is given by:

$$\overline{L} = \frac{12^{0.5} a_c h_c}{3^{0.5} a_c + 2h_c} \qquad (1-29)$$

For weld deposits, the austenite grains are elongated $h_c \gg a_c$, so that

$$\overline{L} = 3^{0.5} a_c \qquad (1-30)$$

S_V can be calculated from [DeHoff and Rhines, 1968]:

$$S_V = \frac{2}{\overline{L}} \qquad (1-31)$$

However, because of the directional microstructure of welds, the lineal intercepts, such as , $\overline{L}_t$, $\overline{L}_l$ and $\overline{L}_i$, are a function of scan orientation relative to the microstructure [Bhadeshia *et al.*, 1986a]. Thus,

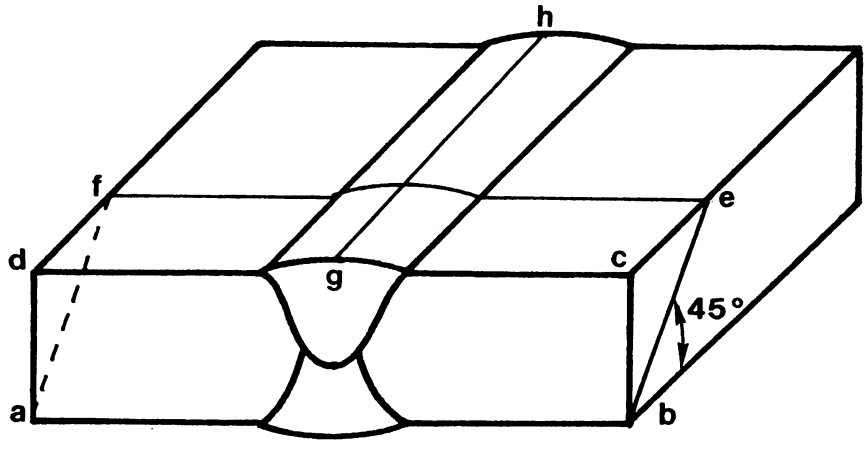

Fig. 1-11 : Diagram illustrating the different sections on which austenite grain sizes are measured. The line gh is the weld centre-line. The plane $abcd$ represents the transverse section. The plane $abef$ represents the inclined section. The plane which contains line gh and is parallel to the plane bce represents the longitudinal section. After Bhadeshia *et al.* [1986a].

experimentally, the austenite grain size of weld metal has conventionally represented by a mean lineal intercept determined by superimposition of scaling line on transverse sections (*i.e.*, the plane *abcd* in Fig. 1-11), not in a random orientation relative to the microstructure, but in a direction normal to the major axes of the grain sections (hereafter, that is defined as $\overline{L}_{tn}$) [Bhadeshia *et al.*, 1986a].

The theoretical prediction of austenite grain size in steel welds is still impossible. For instance, an experiment by Babu *et al.* [1991] demonstrated that influence of the crystallographic texture of the base metal on the austenite grain size in weld deposits. Approximate empirical regression equations exist which can help estimating the mean lineal intercept $\overline{L}_{tn}$ as a function of the chemical composition and

heat input Q [Svensson *et al.*, 1986]:

$$\overline{L}_{tn}\,(\mu\mathrm{m}) = 64.5 - 445.8w_{\mathrm{C}} + 138.6w_{\mathrm{Si}} - 7.591w_{\mathrm{Mn}} + 16\,(Q, \mathrm{kJ\ mm^{-1}}) \qquad (1-32)$$

This equation can be applied for $0.044 < w_{\mathrm{C}} < 0.152$, $0.25 < w_{\mathrm{Si}} < 0.41$, $0.60 < w_{\mathrm{Mn}} < 1.93$ in weight percent and $0.6 < Q < 4.3$.

1.4.5 Metallurgical Model for Allotriomorphic Ferrite Formation

1.4.5.1 Thermodynamics

Thermodynamics indicates that a substance takes its state in which the free energy is minimum at a certain temperature and pressure. The Gibbs free energy is:

$$G = H - TS \qquad (1-33)$$

where H and S are enthalpy and entropy respectively. During equilibrium between austenite and ferrite in pure iron:

$$G_{\gamma} = G_{\alpha} \qquad (1-34)$$

where G_{γ} and G_{α} are Gibbs free energies of austenite and ferrite respectively. For a steel (Fe – C alloy) the carbon concentration is an additional variable. G_{γ} can then be represented by:

$$G_{\gamma} = (1 - x_C^{\gamma})\,\mu_{Fe}^{\gamma} + x_C^{\gamma}\mu_C^{\gamma} \qquad (1-35)$$

where x_C^{γ} is the concentration of carbon in austenite, μ_{Fe}^{γ} is the chemical potential of iron in austenite and μ_C^{γ} is the chemical potential of carbon in austenite.

Similarly, G_{α} is given by:

$$G_{\alpha} = (1 - x_C^{\alpha})\,\mu_{Fe}^{\alpha} + x_C^{\alpha}\mu_C^{\alpha} \qquad (1-36)$$

Notice that in these equations the free energy of the phase is in effect partitioned between contributions from the two components iron and carbon. Equilibrium between phases is now defined by the equality of chemical potentials:

$$\mu_{Fe}^{\gamma} = \mu_{Fe}^{\alpha} \text{ and } \mu_C^{\gamma} = \mu_C^{\alpha} \qquad (1-37)$$

This is illustrated in Fig. 1-12 where the top diagram shows the case where phases of composition x_C^{γ} and x_C^{α} are not at equilibrium. The equilibrium state is illustrated in Fig. 1-12b, where the common tangent construction is seen to be consistent with equations 1-37.

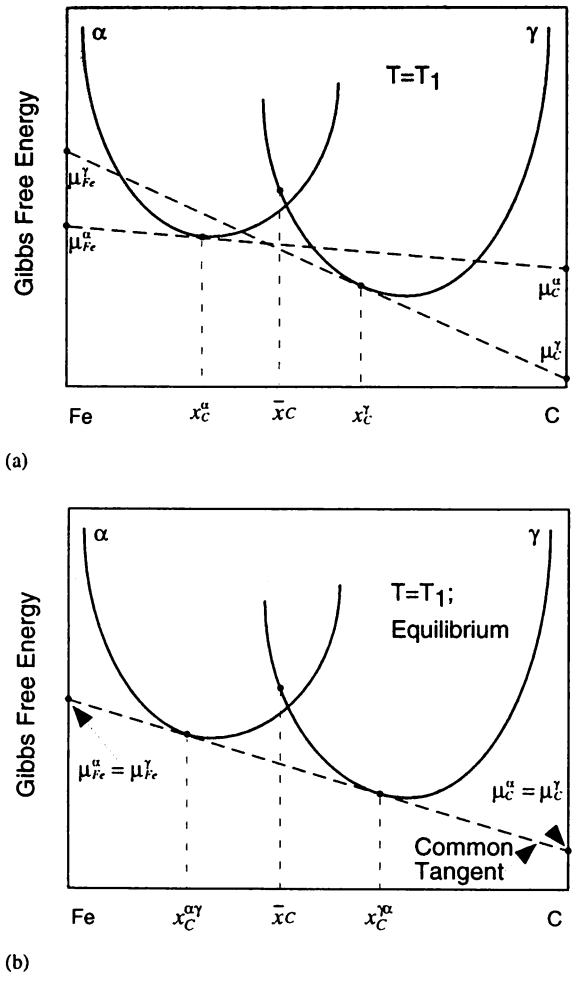

Fig. 1-12 : Common tangent construction giving the equilibrium compositions of austenite and ferrite at a fixed temperature $T = T_1$ (after Bhadeshia [1995a]). Where $\overline{x}$ is average carbon concentration of the matrix austenite.

1.4.5.2 One-dimensional Growth Kinetics

Industrial steel welds may contain a number of substitutional alloying elements such as silicon and manganese in addition to interstitial carbon. A kinetic analysis therefore requires a consideration of multicomponent alloy systems. For simplicity, we consider a ternary Fe-C-X system, where X is a substitutional solute.

Suppose that a planar austenite/ferrite interface moves with a speed v in the direction z, normal to the interface plane. Mass conservation at the interface requires that [Hillert, 1953; Kirkaldy, 1958; Purdy *et al.*, 1964; Coates, 1973]:

$$(c_1^{\gamma\alpha} - c_1^{\alpha\gamma})\, v = -D_{11}\, \nabla c_1 - D_{12}\, \nabla c_2 \qquad (1-38)$$

$$(c_2^{\gamma\alpha} - c_2^{\alpha\gamma})\, v = -D_{22}\nabla c_2 - D_{21}\nabla c_1 \qquad (1-39)$$

where

$c_j^{\gamma\alpha}$: concentration of component j in austenite which is in equilibrium with ferrite, moles per unit volume,

$c_j^{\alpha\gamma}$: concentration of component j in ferrite which is in equilibrium with austenite, moles per unit volume,

c_j: concentration of component j at an arbitrary time and position in the matrix, moles per unit volume,

D_{jk}: defines the dependence of the flux of component j due to the gradient in the concentration of component k.

For motion of semi-infinite matrix, the interface position Z along the co-ordinate z is then given by;

$$Z = \alpha_1 t^{0.5} \qquad (1-40)$$

where $Z = 0$ at $t = 0$, α_1 is a parabolic-thickening rate constant for one-dimensional growth, and t is the time. The interface velocity is therefore $v = \alpha_1/(2\sqrt{t})$. The derivation of α_1 will be discussed in section *1.4.5.8.*

Manganese is a typical substitutional solute in steel welds so that the Fe-C-Mn system will be considered here. Equations 1-38 and 1-39 may be approximated by (subscript 1 ≡ carbon and 2 ≡ manganese) :

$$(c_1^{\gamma\alpha} - c_1^{\alpha\gamma})\, v = -D_{11}\nabla c_1 \qquad (1-41)$$

$$(c_2^{\gamma\alpha} - c_2^{\alpha\gamma})\, v = -D_{22}\nabla c_2 \qquad (1-42)$$

if cross-diffusion effects can be neglected. Since $D_{11} \gg D_{22}$, it is not in general possible to satisfy these equations simultaneously. This means that the tie-line defining interface compositions has to be chosen such that it either reduces the gradient of carbon to compensate for the large D_{11}, or makes the gradient of manganese very large to compensate for the small D_{22}.

Fig. 1-13 schematically illustrates isothermal section of the Fe-C-Mn phase diagram with the average alloy composition defined as $\bar{c}_1$ and $\bar{c}_2$ [Coates, 1973; Bhadeshia, 1985c].

For the low supersaturation case, if a tie-line is chosen such that $c_1^{\gamma\alpha} \approx \bar{c}_1$ the gradient of carbon is reduced greatly to compensate for its large diffusivity. For the alloy identified A, this would entail the choice of tie-line *cd* such that the activity of carbon in the austenite at the interface is the same as that of carbon far away from the interface. Ferrite growth by this mechanism is called "Partitioning Local

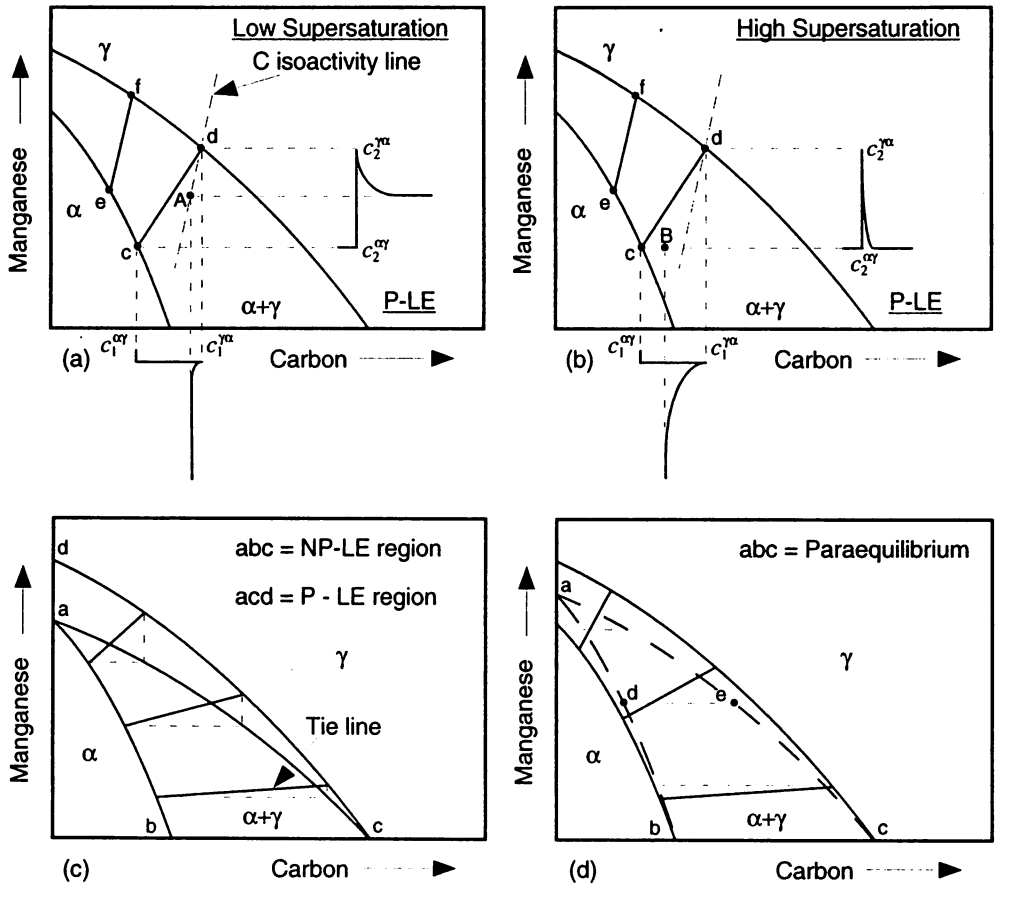

Fig. 1-13 : Schematic isothermal sections of the Fe - C - Mn system, describing ferrite growth under local equilibrium and paraequilibrium at the austenite/ferrite interface [Coates, 1973; Bhadeshia, 1985c]. (a) Growth with Partitioning Local Equilibrium (PLE) mechanism. (b) Growth with Negligible Partitioning Local Equilibrium (NPLE) mechanism. (c) Division of the ferrite + austenite field into domains where either the PLE or the NPLE mechanism can operate. (d) The paraequilibrium phase field within the equilibrium phase field.

Equilibrium (PLE)" mechanism, because $c_2^{\alpha\gamma}$ is quite different from $\overline{c}_2$. In the case of Fe – C – Mn system, this mechanism gives a considerable partitioning of manganese into austenite and subsequent long range diffusion of manganese into austenite [Coates, 1973].

Another choice of tie-line makes it possible for $c_2^{\alpha\gamma} \rightarrow \overline{c_2}$ (*e.g.*, line *cd* for alloy B in Fig. 1-13b). The gradient of c_2 is then drastically increased since only very small amounts of manganese can be partitioned into the austenite. In this high supersaturation case, the flux of manganese atoms at the interface correspondingly increases and manganese diffusion can then keep pace whilst carbon with satisfying the mass conservation conditions of equations 1-41 and 1-42 [Bhadeshia, 1985c]. This ferrite growth mechanism has been defined as "Negligible Partitioning Local Equilibrium (NPLE)" mechanism since the manganese content of the ferrite approximately equals the bulk concentration. Therefore, this mechanism gives little manganese partitioning into the austenite [Coates, 1973].

Fig. 1-13c shows the division of the austenite + ferrite phase field into regions where either the PLE or NPLE mechanism can operate exclusively [Bhadeshia, 1985c].

1.4.5.3 Paraequilibrium

The concept of "paraequilibrium" describes the kinetically constrained case in which the carbon atoms at the austenite/ferrite interface are in local equilibrium but the substitutional solutes do not redistribute during the transformation. The normal equilibrium phase diagram no longer applies. With the paraequilibrium phase diagram , there is only one possible choice of tie-line for any specified alloy (*e.g.*, tie-line *de* in Fig. 1-13d) [Hultgren, 1951].

1.4.5.4 Calculation of the TTT Diagram

A method of the estimating the Time-Temperature-Transformation (TTT) diagram for arbitrary steel has been derived by Bhadeshia using a theory due to Russell [1969]. Theory for the incubation period τ_S, defined as the time taken to establish a steady-state nucleation rate for a coherent nucleus, is given by:

$$\tau_S \propto \frac{T}{(\Delta G_m^V)^3 D_B} \qquad (1-43)$$

Whereas that for an incoherent nucleus is:

$$\tau_S \propto \frac{T}{(\Delta G_m^V)^2 D_V} \qquad (1-44)$$

where ΔG_m^V is the maximum *volume* free energy change accompanying the formation of a nucleus in a large amount of matrix phase, D_B is a boundary diffusion coefficient and D_V is a volume diffusion

coefficient. These relations can be generalised as [Bhadeshia, 1982a]:

$$\tau_S \propto \frac{T}{(\Delta G_m^V)^p D_{eff}} \qquad (1-45)$$

where D_{eff} now becomes an effective diffusion coefficient which depends on the coherency state of the nucleus, as does the exponent p.

Bhadeshia [1982a] pragmatically identified the incubation period with the time required to detect isothermal transformation, and also made the activation energy for diffusion temperature dependent to obtain:

$$\ln\left|\frac{\tau_S (\Delta G_m)^p}{T^{z'}}\right| = \frac{Q'}{RT} + C_4 \qquad (1-46)$$

where ΔG_m is the chemical free energy change accompanying the formation of 1 mol of nucleating ferrite† and z', Q', C_4 are constants obtained by fitting with experimental results. The derivation of ΔG_m will be discussed in following section *1.4.5.5*.

Bhadeshia obtained $p = 4$, $Q' = 0.6031 \times 10^{-6}$J mol^{-1}, $C_4 = 1.905$ and $z' = 20$ for reconstructive transformations, and $p = 5$, $Q' = 0.2432 \times 10^{-6}$J mol^{-1}, $C_4 = 1.350$ and $z' = 20$ for displacive transformations in steel.

The "C" curves calculated in this way have as their upper limits the temperature. For allotriomorphic ferrite, this is simple because transformation becomes possible once the Ae_3 temperature is reached. To deal with the displacive transformations, Bhadeshia [1981a; 1982a] considered the driving force ΔG_N is necessary nucleate shear transformations such as Widmanstätten ferrite and bainite. On the basis of thermodynamic analysis of transformation-start-temperatures he proposed that the following simultaneous equations have to be satisfied for the shear transformation nucleation.

the initiation of Widmanstätten ferrite:

$$\Delta G_m < \Delta G_N \qquad (1-47)$$

$$\Delta G^{\gamma\rightarrow\gamma'+\alpha} < -G_{SW} \qquad (1-48)$$

where $\Delta G^{\gamma\rightarrow\gamma'+\alpha}$ is free energy change accompanying the growth of ferrite without substitute elements partitioning; carbon partitioning during the growth. G_{SW} is stored energy of Widmanstätten ferrite and is about 50 J mol^{-1}.

† In the equations 1-43 to 45, the maximum free energy change for the nucleation is represented in *per volume* of ferrite and is designated by ΔG_m^V but here it is represented with ΔG_m in *per mole* by multiplying ΔG_m^V by the molar volume of ferrite.

Bainite would initiate at a higher undercooling because:

$$\Delta G_m < \Delta G_N \qquad (1-49)$$

$$\Delta G^{\gamma\rightarrow\alpha} < -G_{SB} \qquad (1-50)$$

where $\Delta G^{\gamma\rightarrow\alpha}$ is the free energy change accompanying the diffusionless formation of ferrite from austenite, without any change in chemical composition and G_{SB} is stored energy of bainite and is about 400 J mol^{-1}.

ΔG_N in the above equations is only dependent on the temperature and can be for any steel established as follows.

$$\Delta G_N \left(\text{J mol}^{-1}\right) = 3.25175\,(T-273) - 2183 \qquad (1-51)$$

1.4.5.5 The Free Energy Change during Nucleation

Some important thermodynamic parameters for nucleation are reviewed in this section and illustrated diagrammatically [Bhadeshia, 1992].

$\Delta G^{\gamma\rightarrow\alpha}$ in Fig. 1-14a, which is given by the distance on the free energy axis, represents the free energy change accompanying the diffusionless formation of ferrite from austenite, without any change in chemical composition.

Fig. 1-14b shows the net free energy change $\Delta G^{\gamma\rightarrow\gamma'+\alpha}$ for the decomposition of austenite into an equilibrium mixture of ferrite and austenite of compositions $x_C^{\alpha\gamma}$ and $x_C^{\gamma\alpha}$ respectively. However the free energy change per unit of ferrite is now ΔG_2. ΔG_2 is given by dividing $\Delta G^{\gamma\rightarrow\gamma'+\alpha}$ by the equilibrium mole fraction of ferrite $((x_C^{\gamma\alpha} - \overline{x}_C)/(x_C^{\gamma\alpha} - x_C^{\alpha\gamma}))$.

With ΔG_2, it is assumed that the ferrite has its equilibrium composition as given by the common tangent construction illustrated in Fig. 1-14b. Thus there is significant composition change in the austenite that remains untransformed. However, nucleation involves the formation of very small amount of ferrite, so that the austenite hardly changes its chemical composition. Consequently, the free energy change for nucleation is given by drawing a tangent to the austenite free energy curve at $\overline{x}_C$ and estimating ΔG_3 if the ferrite nucleus is of composition x_C^{α}, Fig. 1-14c. However, the maximum free energy change available for nucleation is clearly ΔG_m, by finding the appropriate ferrite nucleus composition $x_{C_m}^{\alpha}$ when the ferrite nucleus composition is that obtained by using the parallel tangent construction illustrated in Fig. 1-14c.

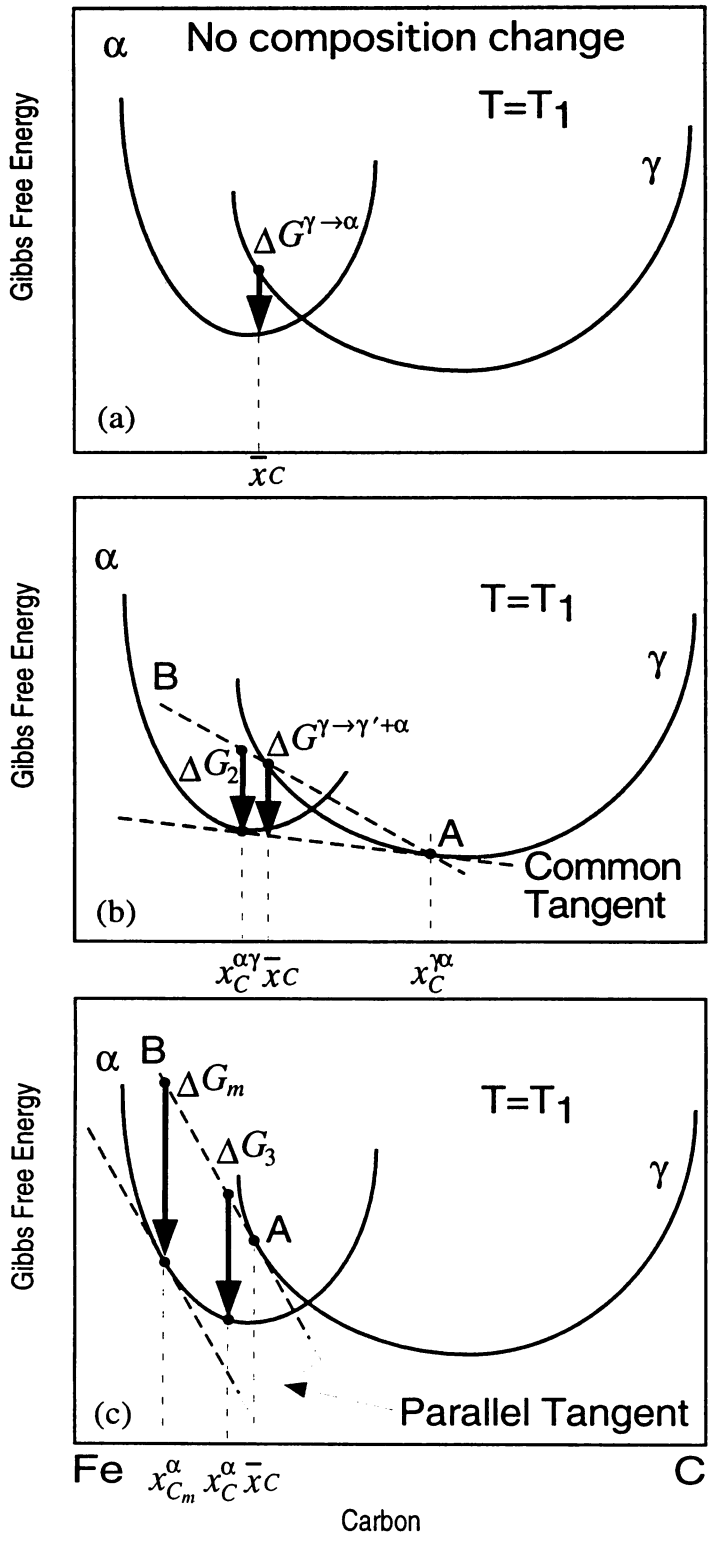

Fig. 1-14 : Schematic diagrams illustrating the free energy changes during the nucleation and growth of ferrite from austenite of composition $\overline{x}_C$. (a) Partitionless transformation. (b) Decomposition of austenite into a mixture of ferrite and enriched austenite. (c) Parallel tangent construction giving the maximum free energy change accompanying nucleation.

1.4.5.6 Additivity Rule

Actual welding phenomena involve continuous cooling so that methods are required to translate from isothermal transformation behavior to anisothermal reaction.

Scheil [1935] proposed the "additivity rule" in which transformation should be considered to commence during continuous cooling when the sum of the ratio of time to incubation time reaches unity. Assuming that isothermal time $t_a\,(T)$ is required to transform a certain fraction ξ_a at an arbitrary temperature T, the criterion of the transformation start time t is then:

$$\int_0^t \frac{dt}{t_a\,(T)} = 1 \qquad (1-52)$$

This additivity rule can only be justified under the "isokinetic assumption". A reaction can only be "isokinetic" if nucleation and growth rates are proportional each other as a function of temperature [Avrami, 1940] or if all the nucleation sites have been exhausted (*i.e.*, "site saturation") [Cahn, 1956b].

1.4.5.7 Nucleation Rate

Classical nucleation theory gives the steady state rate of nucleation of allotriomorphs on grain boundary faces per unit area of boundary as [Christian, 1975]:

$$I_\alpha^{B_f} = N^f \frac{k_B T}{h} \exp\left\{ \frac{-\left(\Delta G_{crit}^f + Q_{act}\right)}{RT} \right\} \qquad (1-53)$$

where

N^f: number of face sites per unit area of boundary,

k_B: Boltzmann constant,

h: Plank constant,

ΔG_{crit}^f: critical activation free energy of ferrite nucleation per atom for nucleation on faces of austenite grains,

Q_{act}: activation free energy per atom for crossing the austenite/ferrite nucleus interface.

The detailed derivation of the value of ΔG_{crit}^f will be discussed in Chapter 2. The activation energy per mol for self-diffusion of iron in the ferrite phase is 2.5×10^5 J mol^{-1} [Handbook of Chemistry and Physics, 1977]. Then the value of Q_{act} is:

$$Q_{act} \approx (2.5 \times 10^5)/N_A \ (\text{ J atom}^{-1}) \qquad (1-54)$$

where N_A is the Avogadro's number. This approximation is justified because the interface is likely to be coherent at the nucleation stage.

1.4.5.8 Modelling of Growth Kinetics

The half-thickness Z of an allotriomorph of ferrite which has formed during continuous cooling transformation may be calculated by integration [Bhadeshia, 1985a]:

$$Z = \int_0^{t_1} 0.5\alpha_1 t^{-0.5} dt \qquad (1-55)$$

where the alloy reaches the temperature at which austenite being to transform to ferrite at $t = 0$, and the temperature at which the transformation stops at $t = t_1$ during continuous cooling.

Therefore, it is necessary to determine the rate constant α_1. Considering the simplest one dimensional ferrite growth model, the half thickness Z is given by equation 1-40. Fick's second law for the matrix becomes:

$$\frac{\partial c_C}{\partial t} = \frac{\partial \left\{ \overline{D} (\partial c_C / \partial z) \right\}}{\partial z} \qquad (1-56)$$

where the boundary conditions are $c_C = c_C^{\gamma\alpha}$ at $z = Z(t)$, and $c_C = \bar{c}_C$ at $t = 0$, where

c_C: carbon concentration, mole per unit volume,

$c_C^{\gamma\alpha}$: carbon concentration in austenite which is in equilibrium with ferrite, mole *per* unit volume,

$\bar{c}_C$: average carbon concentration, mole per unit volume,

$\overline{D}$: weighted average diffusivity of carbon in austenite.

The weighted average diffusivity of carbon in austenite $\overline{D}$ is obtained by [Trivedi and Pound, 1967]:

$$\overline{D} = \int_{x_C^{\gamma\alpha}}^{\bar{x}_C} \frac{D\left(x_C^{\gamma}\right)}{\bar{x}_C - x_C^{\gamma\alpha}} dx_C^{\gamma} \qquad (1-57)$$

where D is the diffusivity of carbon in austenite and is a function of the concentration of carbon in austenite x_C^{γ} and of the substitutional alloying elements. Siller and McLellan obtained the following expression for the diffusion coefficient [1969; 1970].

$$D\left(x_1, T\right) = \frac{k_B T}{h} \left(\exp \frac{-\Delta F^*}{k_B T} \right) \frac{\lambda_\gamma^2}{3\Gamma_m} H\left(\Theta\right) \qquad (1-58)$$

with

$$\frac{H\left(\Theta\right)}{a_1^{\gamma}} = 1 + \left\{ \frac{W\left(1+\Theta\right)}{1 - \left(0.5W+1\right)\Theta + \left(0.25W^2 + 0.5W\right)\left(1-\Phi\right)\Theta^2} \right\} + \left(1+\Theta\right) \frac{1}{a_1^{\gamma}} \frac{da_1^{\gamma}}{d\Theta}$$

$$\Phi = 1 - \exp(-\omega_\gamma / k_B T)$$

where

W: number of octahedral interstices around a single such interstice,

ΔF^*: an activation free energy,

Γ_m: activity coefficient,

λ_γ : distance between {002} austenite planes,

ω_γ : nearest neighbour carbon-carbon interaction energy in austenite,

Θ: ratio of the number of carbon atoms x_1 to the total number of solvent atoms; $\Theta = x_1/(1-x_1)$,

a_1^γ activity of carbon in austenite.

Bhadeshia [1981d] found $\Delta F^*/k_B = 21230$ K and $\ln\{\Gamma_m/\lambda_\gamma^2\} = 31.84$ K.

Babu and Bhadeshia [1995] demonstrated that with the appropriate activity functions, this procedure also works very well for Fe-C-X (X = Mn, Ni, Si, Al, W, Cr, Mo and Co) alloys, the exception being Fe-C-Cr alloy, for reasons which are not clear, there is a relatively large discrepancy observed between the calculated and experimental data.

Conservation of mass at the moving interface gives:

$$(c_C^{\alpha\gamma} - c_C^{\gamma\alpha})\left(\frac{\alpha_1 t^{-1/2}}{2}\right) = \overline{D}\left(\frac{\partial c_C}{\partial z}\right)_{z=Z} \qquad (1-59)$$

where

$c_C^{\alpha\gamma}$: carbon concentration in ferrite which is in equilibrium with austenite, mole per unit volume.

Equations 1-40, 1-56 and 1-59 can be solved simultaneously [Zener 1949; Dubé, 1948; Atkinson, 1967] to give an implicit relation for α_1:

$$\frac{\bar{c}_C - c_C^{\gamma\alpha}}{c_C^{\alpha\gamma} - c_C^{\gamma\alpha}} = \left(\frac{0.25\pi}{\overline{D}}\right)^{\frac{1}{2}} \alpha_1 \left\{\exp\left[\frac{\alpha_1^2}{4\overline{D}/\pi}\right]\right\}\left\{1 - \mathrm{erf}\left[\frac{\alpha_1}{2\overline{D}^{1/2}}\right]\right\} \qquad (1-60)$$

Note that the concentrations c, in mole per unit volume, are frequently replaced by mole fractions.

The volume fraction of ferrite V_α can be estimated from the half-thickness Z and the geometry of the austenite grains. For the columnar austenite grains representation of welds, and assuming a uniform value of Z, it can be shown that [Bhadeshia, 1985a]:

$$V_\alpha = \frac{4Zc_3(a_c - Zc_3)}{a_c^2} \qquad (1-61)$$

where $c_3 = \tan(30°)$. This procedure has been extensively demonstrated to work well, but only when the calculated fraction is multiplied by an empirical factor about 2 [Bhadeshia, 1985a]. It is believed that this consistent underestimation of V_α is caused by the neglect of nucleation, since equation (1-61) relies on the existence of an infinitely thin uniform layer of ferrite surface at the austenite grain surface for $t = 0$ (Fig. 1-15a).

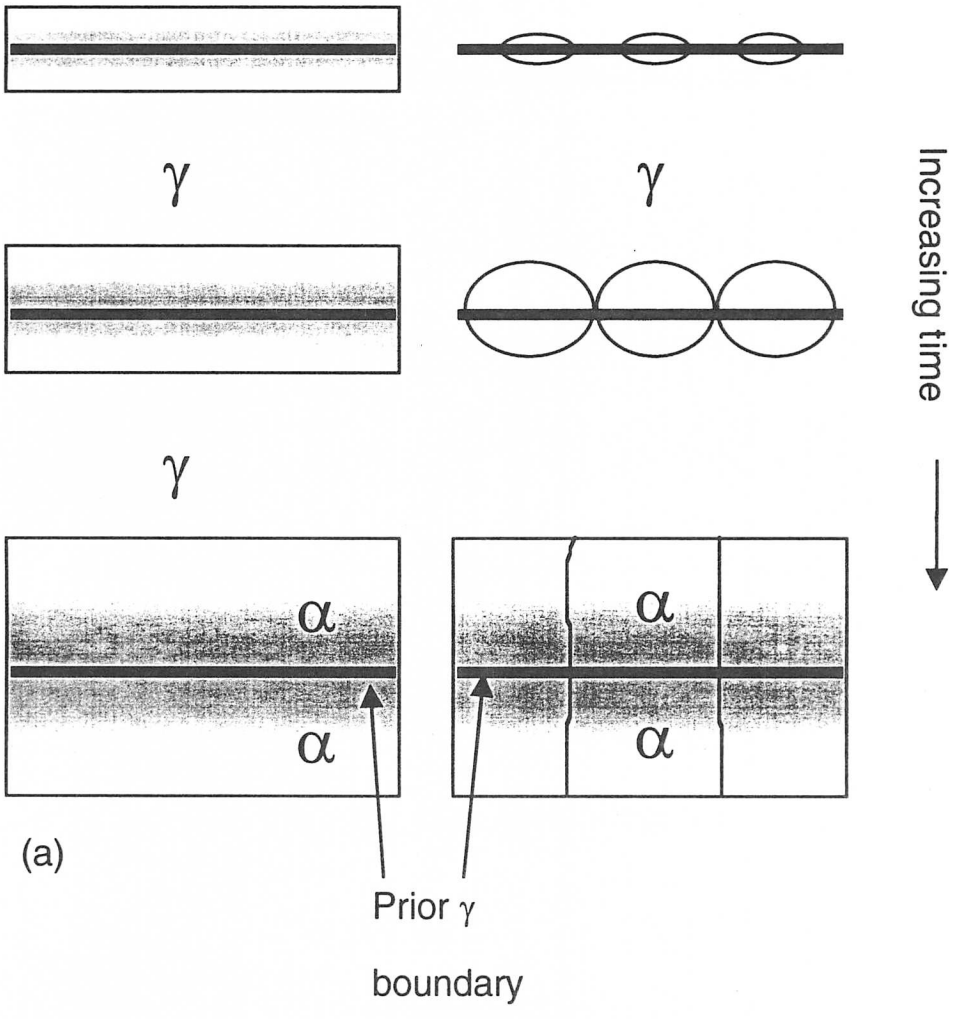

Fig. 1-15 : Schematic diagrams illustrating allotriomorphic ferrite formation [Bhadeshia *et al.*, 1985a] (a) and modified [Bhadeshia *et al.*, 1987] as is the one in reality (b).

To cope with nucleation, Bhadeshia *et al.* [1987] used Avrami theory (Fig. 1-15b):

$$-\ln\{1-\zeta_\alpha\} = \frac{2S_V}{\phi}\alpha_1 t^{0.5} f\left(\theta, \eta_\alpha\alpha_1, I_\alpha^B, t\right) \qquad (1-62)$$

where

$$f\left(\theta, \eta_\alpha\alpha_1, I_\alpha^B, t\right) = \int_0^1 \left[1-\exp\left\{-0.5\pi I_\alpha^B \left(\eta_\alpha\alpha_1\right)^2 t^2 \left(1-\theta^4\right)\right\}\right] d\theta$$

$$\zeta_\alpha = V_\alpha^{act} / \left(V_{total}\phi\right)$$

$$\theta = y/(\alpha_1 t^{0.5})$$

S_V: austenite grain surface per unit volume,

V_α^{act}: actual volume of the ferrite,

V_{total}: total volume,

ϕ: equilibrium volume fraction of ferrite; $\phi = \left(x_C^{\gamma\alpha} - \overline{x}_C\right) / \left(x_C^{\gamma\alpha} - x_C^{\alpha\gamma}\right)$,

I_α^B: total nucleation rate of allotriomorph,

η_α: ratio of length to thickness of allotriomorphic ferrite (taken as 3.0),

y: distance between austenite grain boundary and an arbitrary plane parallel to the boundary.

The total grain boundary steady state nucleation rate of ferrite per unit area of austenite boundary I_α^B can be expressed as [Cahn, 1956a]:

$$I_\alpha^B = I_\alpha^{B_f} + I_\alpha^{B_e} + I_\alpha^{B_c} \qquad (1-63)$$

where $I_\alpha^{B_e}$ is the nucleation rate on grain boundary edges and $I_\alpha^{B_c}$ is the nucleation rate on grain boundary corners.

However, as mentioned previously, nucleation on the edges and corners can be ignored in the case of welds, so that $I_\alpha^B \approx I_\alpha^{B_f}$. For site saturation takes place, equation 1-62 simplifies to:

$$-\ln\left(1-\zeta_\alpha\right) = \frac{2S_V}{\phi}\alpha_1 t^{0.5} \qquad (1-64)$$

Then volume fraction of allotriomorphic ferrite V_α can be given by:

$$V_\alpha = \frac{V_\alpha^{act}}{V_{total}} = \phi\zeta_\alpha \qquad (1-65)$$

The theory has not yet been applied in full to experimental data.

1.4.5.9 Ferrite Grain Size

Predicting the ferrite size is very important because mechanical properties, such as toughness and yield strength are a function of grain size. The nominal ferrite grain diameter $\overline{d}_\alpha$ is defined by the ASTM

method [ASTM designation E 112-82] as the square root of the average area of a grain on a section observed. $\overline{d}_\alpha$ can be deduced by [Umemoto *et al.*, 1984]:

$$\overline{d}_\alpha\,(\mathrm{m}) = \left(\frac{2}{3N_B}\right)^{1/3} \qquad (1-66)$$

where N_B is the total number of ferrite grains nucleated during the transformation per unit volume of austenite.

1.5 Summary

The mechanisms of phase transformations in low-alloy steels have been summarised with emphasis on the microstructures of welds. It is evident that a great deal of progress has been made in this general area of microstructural calculation. Nevertheless, there remain significant difficulties.

Welds are prone to chemical segregation during solidification which should affect the subsequent transformation behaviour. A solidification model should therefore be incorporated into the transformation model.

The theoretical prediction of austenite grain size in steel welds is still impossible. Only empirical regression equations exist which can help estimating the mean lineal intercept of the austenite grains as a function of the chemical composition and heat input.

The detailed theory developed for the modelling of nucleation and growth of allotriomorphic ferrite in steel welds has not yet been applied in full to experimental data and needs to be assessed.

CHAPTER TWO

Modelling of Allotriomorphic Ferrite Transformation in Steel Welds

2.1 Introduction

Allotriomorphic ferrite (α) is the first phase to form from the austenite when a low–alloy steel weld cools below its equilibrium $\gamma \rightarrow \gamma + \alpha$ transformation temperature (Ae_3). It nucleates at the columnar austenite grain boundaries. Because these boundaries are easy diffusion paths, they soon become decorated with thin, continuous layers of ferrite [Honeycombe and Bhadeshia, 1995]. The ferrite grows by a reconstructive mechanism in which all the atoms diffuse, but only the carbon partitions between the residual austenite and the growing ferrite. This is because the cooling rate of welds is too high to permit any long–range diffusion of substitutional solutes. Thus, the layers of ferrite thicken by a paraequilibrium mechanism at a rate which is controlled by the diffusion of carbon in the austenite ahead of the transformation interface [Bhadeshia *et al.*, 1993]. The purpose of this chapter is to describe a new model for the calculation of this phase, whose importance is discussed first in order to set the computations into context.

As discussed in Chapter 1, it has in the past been accepted that allotriomorphic ferrite is bad for weld metal toughness because it offers little resistance to cleavage crack propagation. The mechanical properties, especially toughness, improve as allotriomorphic ferrite is progressively replaced by acicular ferrite. Nevertheless, there is growing evidence [Lazor and Kerr, 1980; Sneider and Kerr, 1984; Kayari *et al.*, 1984; Abson, 1987; Bhadeshia and Svensson, 1993; Ichikawa *et al.*, 1996] that some allotriomorphic ferrite must be retained in the microstructure in order to disrupt the austenite grain boundaries and hence reduce the chances of impurity–induced embrittlement phenomena at the prior austenite grain boundaries in the final microstructure.

To avoid failure at the prior austenite grain boundaries, it is therefore necessary to decorate them with allotriomorphic ferrite. But this layer of ferrite must be thin so that it does not in its own right lead to a deterioration in toughness. The requirement to strictly control the allotriomorphic ferrite content in turn necessitates accuracy and a high level of reliability in any design calculations. A previous model

for allotriomorphic ferrite [Bhadeshia *et al.*, 1985a] is not adequate since it suffers from two significant problems. The first is that nucleation is not explicitly included in the analysis, which assumes the existence of an infinitely thin and uniform layer of ferrite at all the austenite grain surfaces at the point where ferrite formation first begins. The model cannot therefore deal with discontinuous layers, or predict a ferrite grain size. The second difficulty is that all the predictions have to be corrected empirically by a factor of about two.

Bhadeshia *et al.* [1987] presented the theory for a more sophisticated approach to the calculation of allotriomorphic ferrite, but did not at the time exploit the model. The purpose of the present work is to fully apply the theory to weld deposits.

2.2 Transformation from Homogeneous Austenite

The following is a method allowing the calculation of grain size and transformation kinetics. Many of the theoretical details have been reviewed by Christian [1975] and subsequently by Bhadeshia [1985c].

Allotriomorphic ferrite nucleation is considered to occur at the austenite grain surfaces. The austenite grain size is defined by the amount of grain surface per unit volume S_V. The shape of the austenite grains (equiaxed or columnar) determines the specific relation between S_V and standard stereological measurements.

Each allotriomorph, prior to site–saturation, is modelled as a disc parallel to the austenite grain boundary plane on which it nucleated. The allotriomorph has a half–thickness Z and radius $\eta_\alpha Z$, where η_α is an aspect ratio of the allotriomorph. η_α is considered constant and taken to equal 3 because the lengthening and thickening process are actually coupled [Bradley *et al.*, 1977; Reed and Bhadeshia, 1992]. The aspect ratio is considered to be constant because in reality, lengthening and thickening are coupled processes, at least prior to impingement along the austenite grain boundary plane. Impingement may include both hard impingement which is physical contact between particles nucleated at different locations, and soft–impingement which represents the overlap of concentration (or heat) fields of different particles.

The analysis presented below follows the method of Cahn [1956a] and Avrami [1939], for the calculation of isothermal reaction kinetics. It assumes diffusion–controlled growth in which the proportionality constant relating the thickness of the allotriomorph to time is α_1, the one–dimensional parabolic thickening rate constant. The detailed calculation of α_1 as a function of the alloy chemistry, diffusion coefficient *etc.* has been described in Chapter 1. Nucleation at grain edges or corners is ignored, so that

the analysis only applies at high supersaturations. The general theory of overall transformation kinetics is reviewed by Christian [1975].

Consider any plane surface of total area O parallel to a particular boundary; the extended area O_α^e is defined as the sum of the areas of intersection of the discs with this plane. The instant of time when a particular allotriomorph nucleates is called the incubation time τ. It follows that the change dO_α^e in O_α^e due to a disc nucleated in the interval $t = \tau$ and $t = \tau + d\tau$ is:

$$\begin{aligned} dO_\alpha^e &= \pi O_b I_\alpha^B [(\eta_\alpha \alpha_1)^2 (t-\tau)] d\tau \quad \text{for} \quad \alpha_1 (t-\tau)^{0.5} > y \\ dO_\alpha^e &= 0 \quad \text{for} \quad \alpha_1 (t-\tau)^{0.5} < y \end{aligned} \tag{2-1}$$

where y is the distance between the boundary and an arbitrary plane parallel to the boundary and O_b is the area of the particular grain boundary. The nucleation rate per unit area of austenite grain boundary is I_α^B.

Bearing in mind that only particles nucleated for $\tau > (y/\alpha_1)^2$ can contribute to the extended area intersected by the plane at y, the whole extended area is given by:

$$\begin{aligned} O_\alpha^e &= \int_0^{t-(y/\alpha_1)^2} (\eta_\alpha \alpha_1)^2 \pi O_b I_\alpha^B (t-\tau) d\tau \\ &= 0.5 \pi O_b I_\alpha^B (\eta_\alpha \alpha_1)^2 t^2 [1 - \theta^4] \end{aligned} \tag{2-2}$$

where $\theta = y/(\alpha_1 t^{0.5})$.

The relationship between the extended and the actual areas is given by [Christian, 1975; Cahn, 1956a]:

$$\frac{O_\alpha^e}{O} = -\ln\{1 - \frac{O_\alpha}{O}\} \tag{2-3}$$

where O_α is actual area defined as the sum of the areas of intersection of the discs with a plane parallel to a particular austenite boundary. Assuming that there is no interference from other boundaries, the total volume V_α^b of material originating from this grain boundary is obtained by integrating for all y between negative and positive infinity; in terms of θ, the integral amounts to:

$$\begin{aligned} V_\alpha^b &= \int_0^1 2 O_b \alpha_1 t^{0.5} (1 - \exp\{-O_\alpha^e / O_b\}) d\theta \\ &= \int_0^1 2 O_b \alpha_1 t^{0.5} (1 - \exp\{-0.5 \pi I_\alpha^B (\eta_\alpha \alpha_1)^2 t^2 [1 - \theta^4]\}) d\theta \\ &= 2 O_b \alpha_1 t^{0.5} f\{\theta, \eta_\alpha \alpha_1, I_\alpha^B, t\} \end{aligned} \tag{2-4}$$

where

$$f\{\theta, \eta_\alpha \alpha_1, I_\alpha^B, t\} = \int_0^1 (1 - \exp\{-0.5 \pi I_\alpha^B (\eta_\alpha \alpha_1)^2 t^2 [1 - \theta^4]\}) d\theta$$

If the total grain boundary area is $O_B = \sum O_b$, then by substituting O_B for O_b in the above equation the total extended volume V_α^e of material emanating from all boundaries is found. This is an *extended* volume because allowance was not made for impingement of discs originating from different boundaries. Thus,

$$V_\alpha^e = 2O_B(\alpha_1 t^{0.5}) f\{\theta, \eta_\alpha \alpha_1, I_\alpha^B, t\} \qquad (2-5)$$

and if V_{total} is the total volume, and S_V the austenite grain surface per unit volume, then:

$$\frac{V_\alpha^{act}}{V_{total}\phi} = 1 - \exp\{-V_\alpha^e/(V_{total}\phi)\} \qquad (2-6)$$

where $\phi = (x^{\gamma\alpha} - \overline{x})/(x^{\gamma\alpha} - x^{\alpha\gamma})$. It follows that

$$-\ln\{1-\zeta_\alpha\} = \frac{2S_V}{\phi}\alpha_1 t^{0.5} f\{\theta, \eta_\alpha \alpha_1, I_\alpha^B, t\} \qquad (2-7)$$

(*i.e.*, equation 1-62) where ζ_α is the volume of ferrite divided by its equilibrium volume (*i.e.*, $V_\alpha^{act}/(V_{total}\phi)$).

2.3 Austenite Grain Structure of Welds

For an equiaxed grain structure, standard stereological theory [DeHoff and Rhines, 1968] gives

$$S_V = \frac{2}{\overline{L}} \qquad (2-8)$$

where $\overline{L}$ is the mean lineal intercept measured by projecting randomly oriented test lines on random sections of the microstructure.

The austenite grain structure of welds is highly anisotropic, consisting of columnar grains. The grain surface per unit volume, S_V has to be related to the usual experimental measurement, $\overline{L}_{tn}$, which represents the mean lineal intercept measured on the transverse section of a weld, in a direction normal to the major grain axis.

It has been demonstrated that the columnar grains can be represented by space–filling hexagonal prisms. A cross–section of such a grain is illustrated in Fig. 2-1.

Given the way in which $\overline{L}_{tn}$ is measured, it can be assumed that the test lines are always parallel to one side of the hexagonal cross–section. It follows that

$$\begin{aligned} \overline{L}_{tn} &= \frac{\int_0^{a_c \cos 30^\circ} \{2a_c - 2y_c/\tan 60^\circ\} dy_c}{a_c \cos 30^\circ} \\ &= 1.5a_c \end{aligned} \qquad (2-9)$$

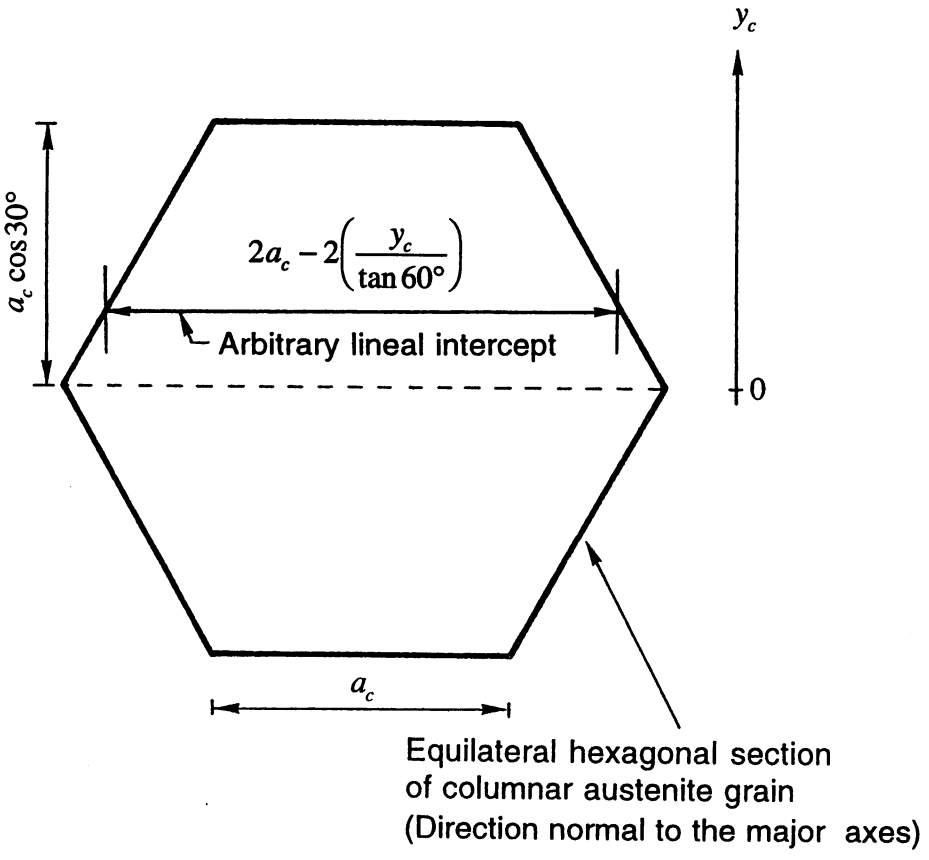

Fig. 2-1 : The hexagonal cross–section of a columnar austenite grain which is assumed to have the shape of a hexagonal prism in three dimensions.

It then follows from equations 1-30, 1-31 and 2-9 that:

$$S_V \simeq \frac{2}{\sqrt{3}a_c} \quad \text{so that} \quad S_V = \frac{\sqrt{3}}{\overline{L}_{tn}} \qquad (2-10)$$

2.4 Grain Boundary Nucleation Rate

Classical nucleation theory [Christian, 1975] gives the nucleation rate per unit area as

$$I_\alpha^{Bf} = N^f \frac{k_B T}{h} \exp\left\{-\frac{\Delta G^f_{crit} + Q_{act}}{RT}\right\} \qquad (2-11)$$

(*i.e.*, equation 1-53) where N^f is the number density of grain surface nucleation sites, k_B and h are the Boltzmann and Planck constants respectively, R is the gas constant, ΔG^f_{crit} is the activation energy for

nucleation and Q_{act} is the activation energy for the transfer of atoms across the embryo/matrix phase boundary. As in Chapter 1 the latter is taken to be the activation energy for the self–diffusion of iron [Handbook of Chemistry and Physics; 1977], since the nucleus is likely to be coherent with the matrix. Thus, $Q_{act} = 2.5 \times 10^5\ \mathrm{J\,mol^{-1}}$.

The number density of sites is assumed to be

$$N^f = \frac{K_1^\alpha}{b^2} \qquad (2-12)$$

where $b = 0.25$ nm is the interatomic spacing in the boundary plane. If each atom is capable of nucleating ferrite then $K_1^\alpha = 1$, but this is unlikely. K_1^α is therefore treated as a non-dimensional adjustable parameter whose value is 5×10^{-7}.

The activation energy ΔG^f_{crit} should be a function of the chemical driving force for nucleation (ΔG_V) and the embryo/matrix interface energy per unit area (σ):

$$\Delta G^f_{crit} = \frac{\sigma^3}{\Delta G_V^2} K_2^\alpha \qquad (2-13)$$

where K_2^α is the second adjustable parameter whose value was obtained by fitting to experimental data on welds as 0.1 per atom for $\sigma = 0.05\ \mathrm{J\,m^{-2}}$.

As mentioned in Chapter 1, nucleation on the edges and corners can be ignored in the case of welds, so that $I_\alpha^B \approx I_\alpha^{Bf}$.

2.5 Ferrite Grain Size

The ferrite grain "diameter" $\bar{d}_\alpha$ is defined by the American Society for Testing and Materials (ASTM) [designation E 112-82] as the square root of the average areal grain–intercept on plane sections for equiaxed grains. It is related to the number density of ferrite grains per unit volume, N_B by the equation 1-66.

2.6 Cooling Curve

As discussed in Chapter 1, the cooling curve of the fusion zone of a weld, over the transformation temperature range of interest, can be represented empirically using a form of equation due to Weisman (equation 1-21) [Welding Handbook, 1981].

When the units of heat input, temperature and time are given by $\mathrm{J\,m^{-1}}$, °C and seconds respectively, the values of C_1, C_2 and η can be taken to be those given in Table 2-1 [Svensson *et al.*, 1986] for the manual metal arc and submerged arc welding processes.

Table 2-1 : Values of empirically determined heat–flow constants for the calculation of the cooling curve over the transformation temperature range [Svensson *et al.*, 1986].

Process	C_1	C_2	η
Manual metal arc	1325.0	1.60	0.775
Submerged arc	1.076	2.6798	0.9

2.7 Anisothermal Transformation

The kinetic theory presented above deals with isothermal transformation. The transformations occur during the continuous cooling of welds. It is therefore used the additivity approximation to deal with this [Christian, 1975]. The cooling curve is, over the transformation temperature range, divided into a series of discrete temperature steps which may be arbitrarily small. Suppose it takes a time period $\Delta\tau_1$ to achieve a fraction ξ_1 of transformation at a temperature T_1, where the subscript represents the first step in the cooling process below the paraequilibrium Ae_3 temperature. $\Delta\tau_1$ is the time spent at T_1 (Fig. 2-2).

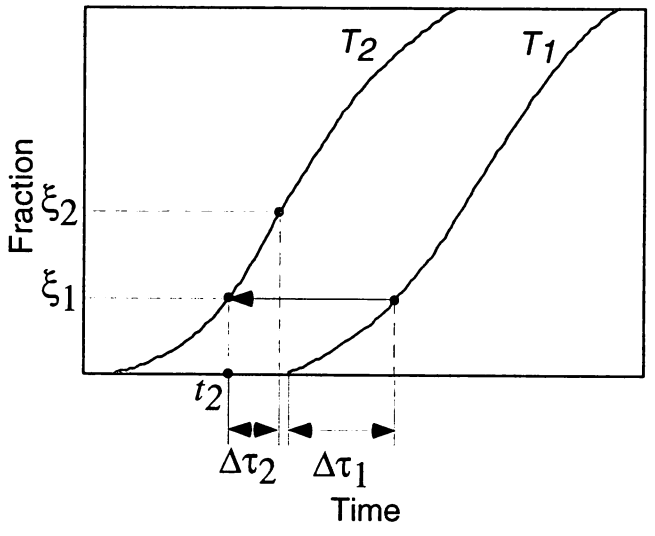

Fig. 2-2 : Schematic illustration of the isothermal and continuous cooling transformations.

At a lower temperature T_2, the time required to achieve a degree of transformation equal to ξ_1 is solved using the isothermal theory to be equal to say t_2. Thus, the total amount of transformation that is

assumed to occur during the interval Ae_3 and T_2 is ξ_2 which is obtained using the isothermal equation for a time interval $t_2 + \Delta\tau_2$. This process can be continued for further cooling until transformation is complete.

As explained in Chapter 1, the "additivity rule" can only be justified under the "isokinetic assumption". A reaction can only be "isokinetic" if nucleation and growth rates are proportional each other as a function of temperature [Avrami, 1940] or if all the nucleation sites have been covered with product phase (*i.e.*, "site saturation") [Cahn, 1956b]. Its application to allotriomorphic ferrite must therefore be regarded as an approximation.

2.8 Solidification–Induced Segregation

Welds generally solidify under conditions which are far from equilibrium. Consequently, the microstructure is rarely chemically homogeneous, the severity of any segregation depending both on the cooling conditions and the detailed average composition. The influence of this segregation on the formation of allotriomorphic ferrite is incorporated in the present work using the the Scheil [1942] equation for solidification.

It is assumed that there are no concentration gradients ahead of the solid/liquid interface, that the interface is flat, that there is local equilibrium at the interface, that the densities of the solid and liquid phases are identical and that there is no diffusion in the in the solid phase. This situation is described by Scheil's equation for solidification as the equation 1-25. We need to estimate the equilibrium partition coefficient k_0 of each alloying element to calculate c^{sol} by the equation 1-25. Values of k_0 are calculated using equation 1-27. $\Delta^\circ G$, Gibbs free energy change per mole in transforming the element concerned from the $\delta-$ferrite to the liquid state, is tabulated in Table 2-2 for a variety of solutes.

Table 2-2 : Gibbs free energy change per mole in transforming the element concerned from the $\delta-$ferrite to the liquid state [Kirkaldy *et al.*, 1978]. T is the absolute temperature.

$\Delta^\circ G_{Si}$	$16.33T - 34333$
$\Delta^\circ G_{Mn}$	$-9.66T + 12980$
$\Delta^\circ G_{Ni}$	$-1.591T - 8876$
$\Delta^\circ G_{Cr}$	$9.17T - 19260$
$\Delta^\circ G_{Mo}$	$9.59T - 27634$
$\Delta^\circ G_{V}$	$9.63T - 21354$

The partition coefficient is calculated at the melting temperature of the steel, which is estimated using an empirical equation due to Smrha [1983]:

$$T_m = 1537 - (88w_{\mathrm{C}} + 8w_{\mathrm{Si}} + 5w_{\mathrm{Mn}} + 5w_{\mathrm{Cu}} + 1.5w_{\mathrm{Cr}} + 4w_{\mathrm{Ni}} + 2w_{\mathrm{Mo}} + 2w_{\mathrm{V}} + 30w_{\mathrm{P}} + 25w_{\mathrm{S}}) \quad ^{\circ}\mathrm{C} \qquad (2-14)$$

The spatial distribution of all the elements can therefore be calculated and it is assumed that this distribution is not changed during cooling from the solidification to the transformation temperature. Carbon, however, is assumed to be distributed homogeneously since it diffuses very rapidly. To apply this model to weld metal, the fraction solidified is partitioned into a number n of segments as illustrated in Fig. 2-3.

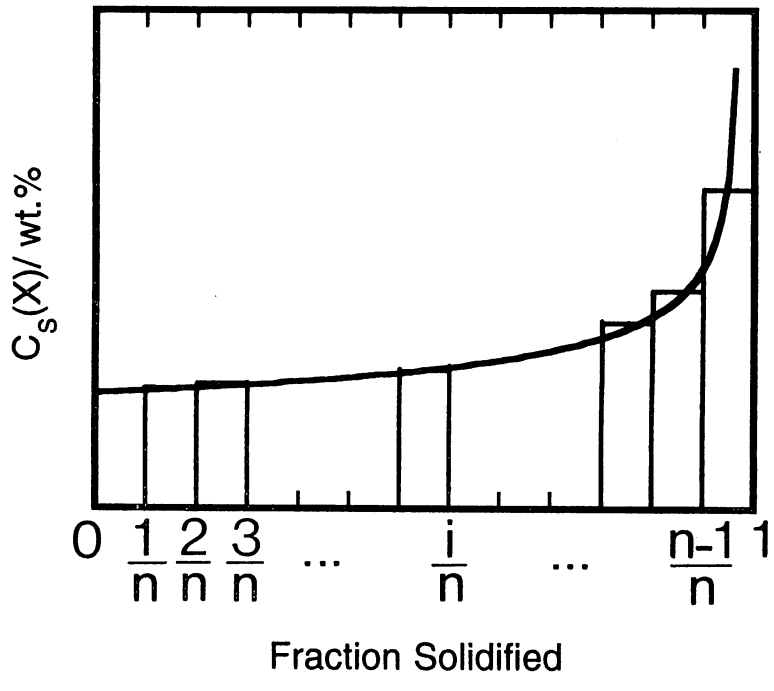

Fig. 2-3 : Schematic illustration of the concentration profile calculated using the Scheil equation and the partitioning of the profile into discrete segments.

The fraction solidified thus becomes

$$f_S = \frac{i}{n} - \frac{1}{2n} \qquad \text{where } i = 1, 2, 3, \ldots, n \qquad (2-15)$$

where i identifies the segment number. In this study, n is defined as 100. The value is supposed to be a reasonable value because of the following reasons. If n is too small, the model cannot represent

the solute distribution profiles properly. If that is too large, then the solute concentrations become very large at large i and exceed the ranges of a dilute solution which is an assumption of the model.

Transformation behaviour is then calculated separately for each segment and the mean amount of ferrite taken to be representative of a real weld. *i.e.*, If the volume fraction of ferrite in i-th segment is $V_\alpha(i)$, the total fraction in the weld as a whole, $\overline{V_\alpha}$, is given by:

$$\overline{V_\alpha} = \frac{1}{n}\sum_{i=1}^{n}\{V_\alpha(i)\} \qquad (2-16)$$

2.9 Application to Welds

The experimental data used to validate the model are listed in Table 2-3; the data are from the published literature [Bhadeshia *et al.*, 1986b; Evans, 1983; 1990; 1991, Gretoft *et al.*, 1985; Svensson and Gretoft, 1990; Surian *et al.*, 1994].

Table 2-3 : Chemical compositions of the weld metals.

Mark	Chemical compositions of the weld metals / wt.%										Ref.
	C	Si	Mn	P	S	Cu	Cr	Ni	Mo	V	
C1	0.045	0.30	0.65	0.008	0.006	-	-	-	-	-	(1)
C2	0.044	0.32	0.98	0.008	0.006	-	-	-	-	-	
C3	0.044	0.32	1.32	0.007	0.006	-	-	-	-	-	
C4	0.045	0.30	1.72	0.008	0.006	-	-	-	-	-	
C5	0.059	0.33	0.60	0.008	0.007	-	-	-	-	-	
C6	0.063	0.35	1.00	0.008	0.006	-	-	-	-	-	
C7	0.066	0.37	1.35	0.007	0.005	-	-	-	-	-	
C8	0.070	0.33	1.77	0.008	0.006	-	-	-	-	-	
C9	0.099	0.35	0.65	0.009	0.008	-	-	-	-	-	
C10	0.098	0.32	1.05	0.009	0.007	-	-	-	-	-	
C11	0.096	0.30	1.29	0.009	0.007	-	-	-	-	-	
C12	0.093	0.33	1.65	0.007	0.007	-	-	-	-	-	
C13	0.147	0.40	0.63	0.007	0.008	-	-	-	-	-	
C14	0.152	0.41	1.00	0.007	0.007	-	-	-	-	-	
C15	0.148	0.38	1.40	0.007	0.007	-	-	-	-	-	
C16	0.141	0.36	1.76	0.007	0.006	-	-	-	-	-	
CM1	0.030	0.45	0.78	0.010	0.013	-	-	-	-	-	(2)
CM2	0.032	0.45	1.27	0.010	0.008	-	-	-	-	-	
CM3	0.031	0.42	1.71	0.010	0.004	-	-	-	-	-	
CM4	0.032	0.45	2.05	0.010	0.020	-	-	-	-	-	
CM5	0.059	0.34	0.77	0.010	0.010	-	-	-	-	-	
CM6	0.059	0.33	1.09	0.010	0.008	-	-	-	-	-	
CM7	0.059	0.30	1.44	0.010	0.006	-	-	-	-	-	
CM8	0.065	0.33	1.83	0.010	0.003	-	-	-	-	-	
CM9	0.090	0.41	0.78	0.010	0.013	-	-	-	-	-	
CM10	0.089	0.35	1.18	0.010	0.011	-	-	-	-	-	
CM11	0.088	0.37	1.59	0.010	0.011	-	-	-	-	-	
CM12	0.098	0.39	2.25	0.014	0.008	-	-	-	-	-	
CM13	0.120	0.43	0.86	0.014	0.011	-	-	-	-	-	
CM14	0.120	0.44	1.35	0.014	0.010	-	-	-	-	-	
CM15	0.130	0.37	1.83	0.011	0.010	-	-	-	-	-	
CM16	0.110	0.36	2.18	0.011	0.008	-	-	-	-	-	
AL1	0.069	0.35	0.64	0.009	0.007	-	-	-	-	-	(3)
CR1	0.038	0.36	1.03	0.014	0.010	0.07	0.04	2.00	0.37	0.01	(4)
CR2	0.040	0.35	1.00	0.014	0.011	0.07	0.38	1.96	0.35	0.01	
CR3	0.041	0.35	1.03	0.014	0.010	0.07	0.78	1.96	0.37	0.01	
CR4	0.042	0.38	1.06	0.015	0.011	0.07	1.15	1.95	0.37	0.01	
CR5	0.042	0.40	1.07	0.014	0.011	0.07	1.50	1.98	0.35	0.01	
CR6	0.042	0.38	1.06	0.014	0.011	0.07	1.82	1.92	0.34	0.01	
CR7	0.042	0.33	1.46	0.013	0.010	0.065	0.04	1.98	0.37	0.01	
CR8	0.040	0.35	1.43	0.013	0.010	0.065	0.41	1.94	0.36	0.01	
CR9	0.048	0.34	1.37	0.013	0.010	0.065	0.75	1.86	0.34	0.01	
CR10	0.043	0.34	1.45	0.013	0.010	0.065	1.15	1.98	0.38	0.01	
CR11	0.044	0.33	1.39	0.014	0.011	0.065	1.43	1.88	0.36	0.01	
CR12	0.040	0.36	1.39	0.014	0.011	0.065	1.89	1.99	0.38	0.01	
NI1	0.07	0.38	1.20	-	-	-	-	0.94	-	-	(5)
MO1	0.14	0.29	1.44	0.029	0.006	-	0.05	0.06	0.01	-	(6)
MO2	0.14	0.24	1.54	0.027	0.029	-	0.03	0.03	0.19	-	
MO3	0.14	0.31	1.32	0.028	0.006	-	0.03	0.03	0.24	-	
MO4	0.13	0.27	1.60	0.025	0.027	-	0.04	0.04	0.39	-	
V1	0.073	0.35	0.64	0.004	0.005	-	-	-	-	0.0003	(7)
V2	0.071	0.36	0.63	0.006	0.007	-	-	-	-	0.0210	
V3	0.071	0.40	0.64	0.006	0.008	-	-	-	-	0.0435	
V4	0.074	0.36	0.63	0.005	0.008	-	-	-	-	0.0600	
V5	0.072	0.36	0.64	0.006	0.008	-	-	-	-	0.0815	
V6	0.077	0.31	1.33	0.005	0.007	-	-	-	-	0.0004	
V7	0.072	0.33	1.22	0.006	0.008	-	-	-	-	0.0190	
V8	0.077	0.26	1.36	0.007	0.007	-	-	-	-	0.0425	
V9	0.078	0.30	1.35	0.007	0.007	-	-	-	-	0.0595	
V10	0.076	0.26	1.36	0.006	0.007	-	-	-	-	0.1005	

Ref.:
(1) Evans, G. M., 1983
(2) Svensson, L-E. and Gretoft, B., 1990
(3) Evans, G. M., 1990
(4) Surian, E. *et al.*, 1994
(5) Gretoft, B. *et al.*, 1985
(6) Bhadeshia, H. K. D. H. *et al.*, 1986b
(7) Evans, G. M., 1991

Table 2-3 (continued) : Heat input and austenite parameters of the weld metals.

Mark	Heat input / kJ cm^{-1}	Austenite grain parameters	
		Average columnar grain width / μm	S_V / 10^4 m^{-1}
C1	10	104	1.67
C2		98	1.77
C3		102	1.70
C4		94	1.84
C5		94	1.84
C6		85	2.04
C7		91	1.90
C8		79	2.19
C9		69	2.51
C10		74	2.34
C11		65	2.66
C12		63	2.75
C13		67	2.59
C14		63	2.75
C15		63	2.75
C16		49	3.53
CM1	10.4	65	2.66
CM2		55	3.15
CM3		42	4.12
CM4		42	4.12
CM5		71	2.44
CM6		65	2.66
CM7		60	2.89
CM8		48	3.61
CM9		45	3.85
CM10		45	3.85
CM11		45	3.85
CM12		45	3.85
CM13		36	4.81
CM14		36	4.81
CM15		40	4.33
CM16		45	3.85
AL1	10	79	2.18
CR1	21	115	1.51
CR2		109	1.59
CR3		104	1.67
CR4		95	1.82
CR5		92	1.88
CR6		90	1.92
CR7		102	1.70
CR8		98	1.77
CR9		93	1.86
CR10		90	1.92
CR11		88	1.97
CR12		87	1.99
NI1	10.4	60	2.89
MO1	11.8	72	2.41
MO2		72	2.41
MO3		72	2.41
MO4		72	2.41
V1	10	118	1.46
V2		96	1.81
V3		106	1.64
V4		90	1.92
V5		96	1.81
V6		86	2.02
V7		95	1.83
V8		100	1.73
V9		83	2.09
V10		87	2.00

The nucleation equation (*i.e.*, equation 2-11) requires an estimation of two adjustable constants, which were determined by best fitting to the experimental data:

$$K_1^\alpha = 5 \times 10^{-7} \qquad K_2^\alpha = 10^{-1} \qquad \text{per atom}$$

It is reasonable for K_1^α to be very small because a large number of atoms in the boundary plane must participate in the formation of one ferrite grain. The value of K_2^α is difficult to properly justify since the detailed shape and interfacial energy of the nucleus are unknown.

Some calculations for specific weld metals are here first illustrated, without allowing for segregation, simply to show that the predicted trends are reasonable. Figs. 2-4, 2-5 and 2-6 show how the transformation start temperature, ferrite volume fraction and nominal ferrite grain boundary varies respectively with the heat input and chemistry with a constant austenite grain size.

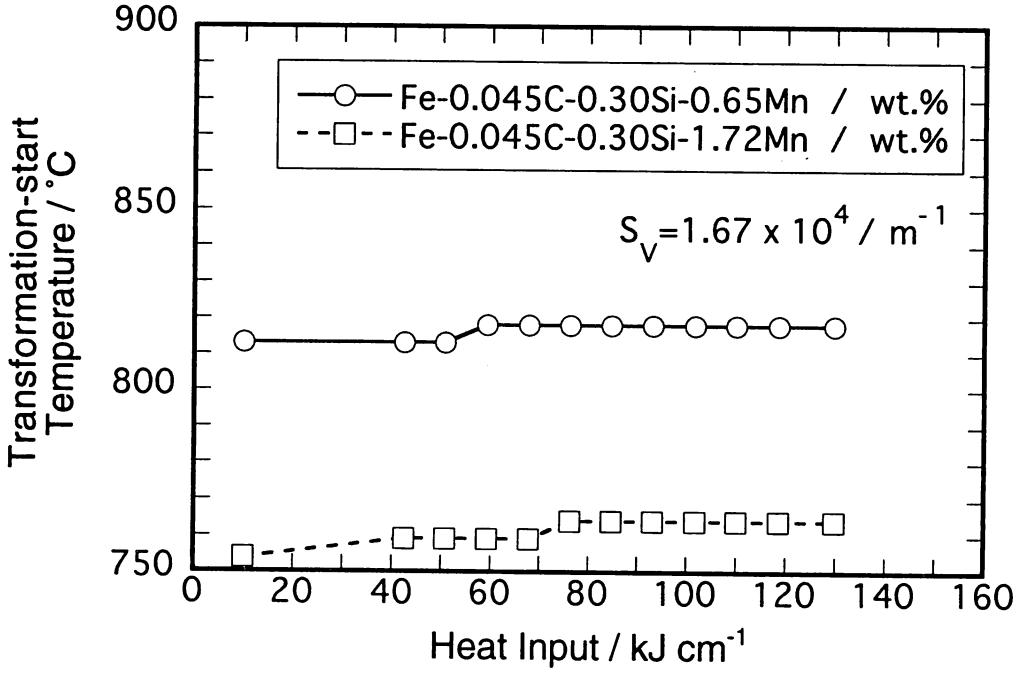

Fig. 2-4 : Variations in the transformation-start temperature for allotriomorphic ferrite with heat input and alloy chemistry.

Figs. 2-7 and 2-8 gives the variation in the nominal ferrite grain diameter and ferrite volume fraction with the austenite grain boundary surface per unit volume.

Based on general experience of the steel welds, the trends are all reasonable.

Figs. 2-9 to 2-15 show examples of the calculated concentration profiles of weld CR2 in Table 2-3.

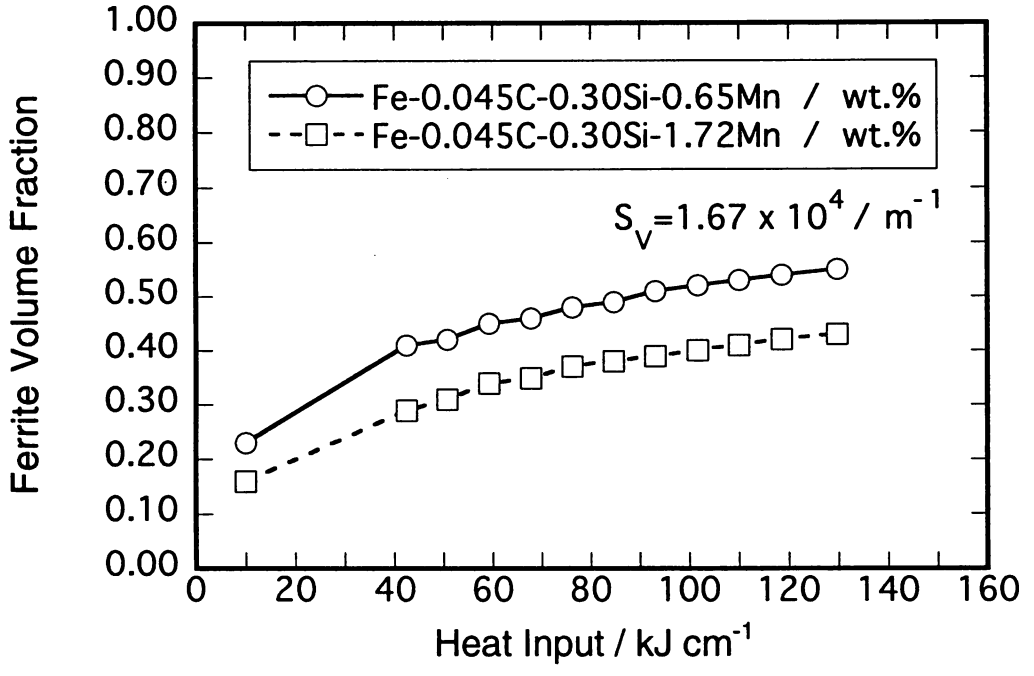

Fig. 2-5 : Variations in the ferrite volume fraction with heat input and alloy chemistry.

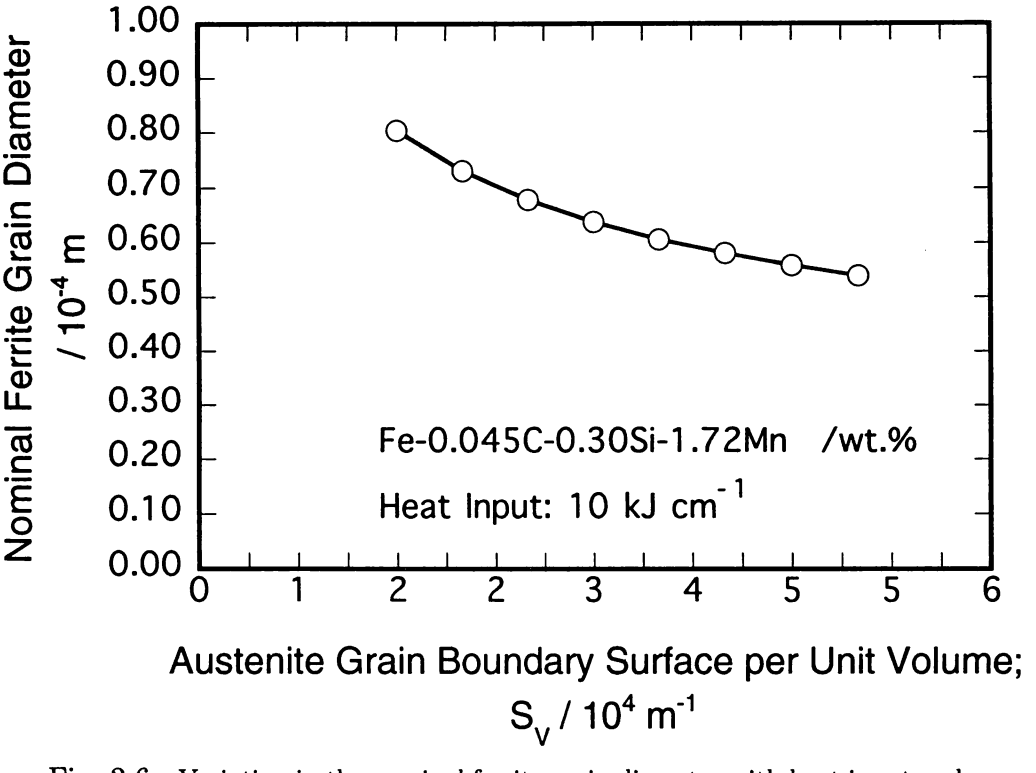

Fig. 2-6 : Variation in the nominal ferrite grain diameter with heat input and alloy chemistry.

As discussed previously the carbon concentration is assumed to be uniform everywhere (Fig. 2-9). All other substitutional alloying elements, silicon, manganese, chromium, nickel, molybdenum and

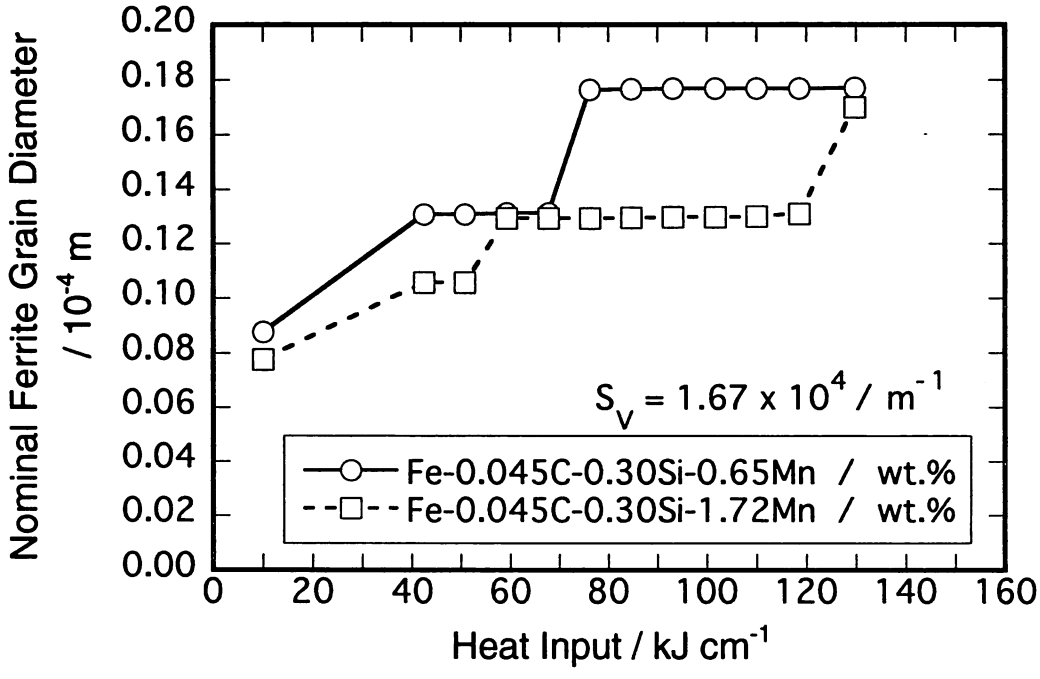

Fig. 2-7 : Variation in the nominal ferrite grain diameter with the austenite grain boundary surface per unit volume.

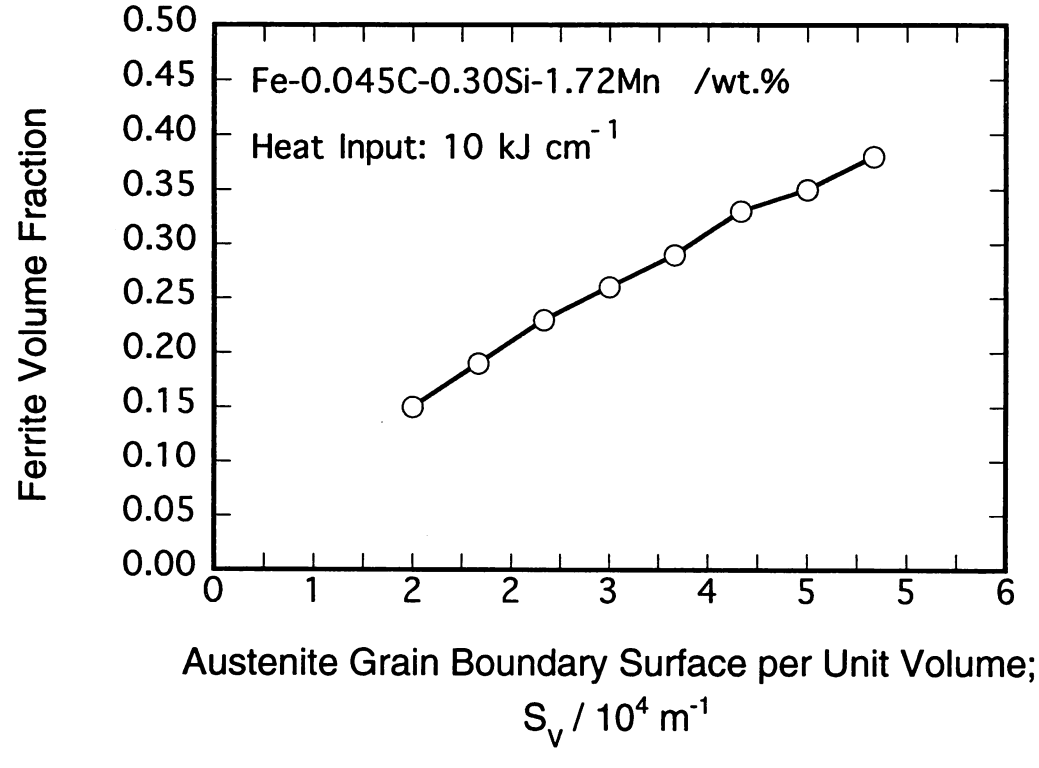

Fig. 2-8 : Variation in the ferrite volume fraction with the austenite grain boundary surface per unit volume.

vanadium show increasing concentration as a function of i (Figs. 2-10 to 2-15). As is often observed experimentally (Chapter 3), there is a steep increase in concentration at the final stages of the solidifi-

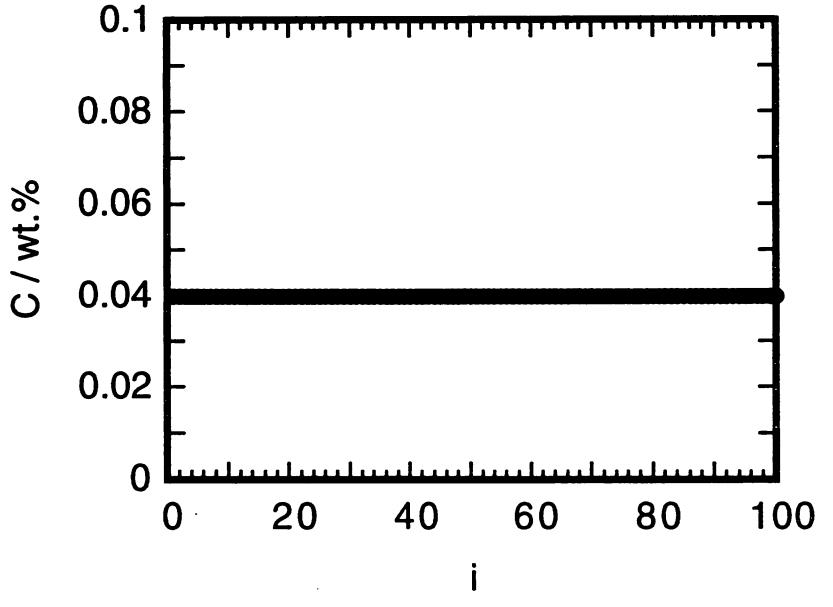

Fig. 2-9 : Uniform distribution of carbon (Weld CR2: Average carbon content 0.04, wt.%.).

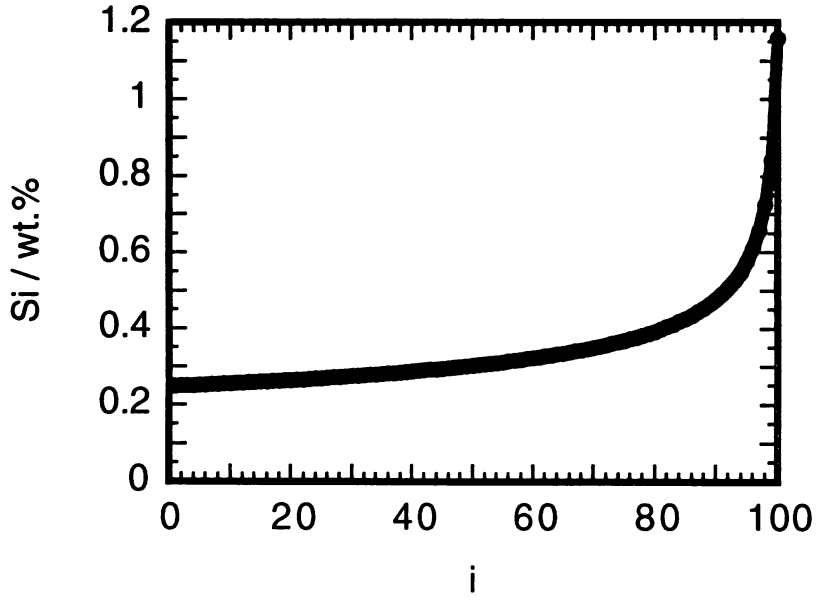

Fig. 2-10 : Calculated segregation profile of silicon concentration (Weld CR2: Average silicon content 0.35 wt.%.).

cation (*i.e.*, at large i's). The calculated variation is qualitatively satisfactory; quantitative measurement is an aim of the microanalytical work presented in Chapter 3.

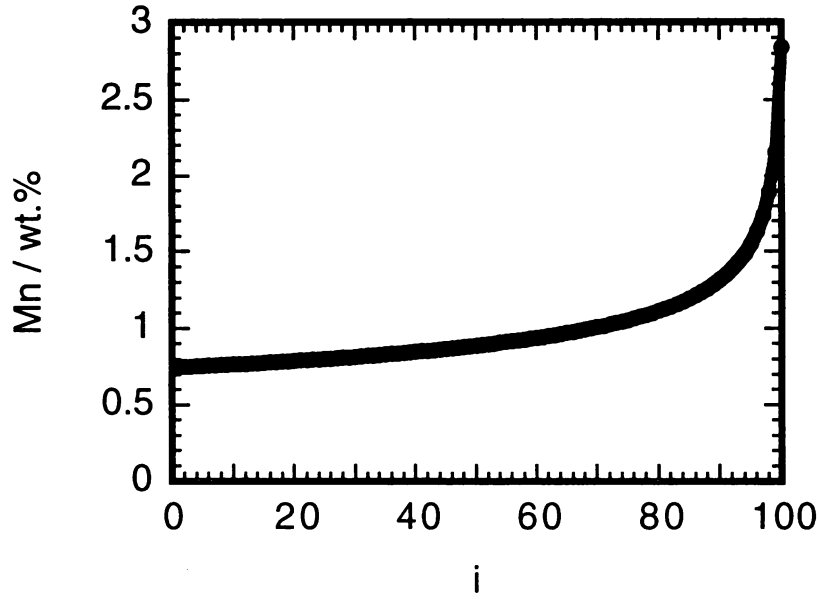

Fig. 2-11 : Calculated segregation profile of manganese concentration (Weld CR2: Average manganese content 1.00 wt.%.).

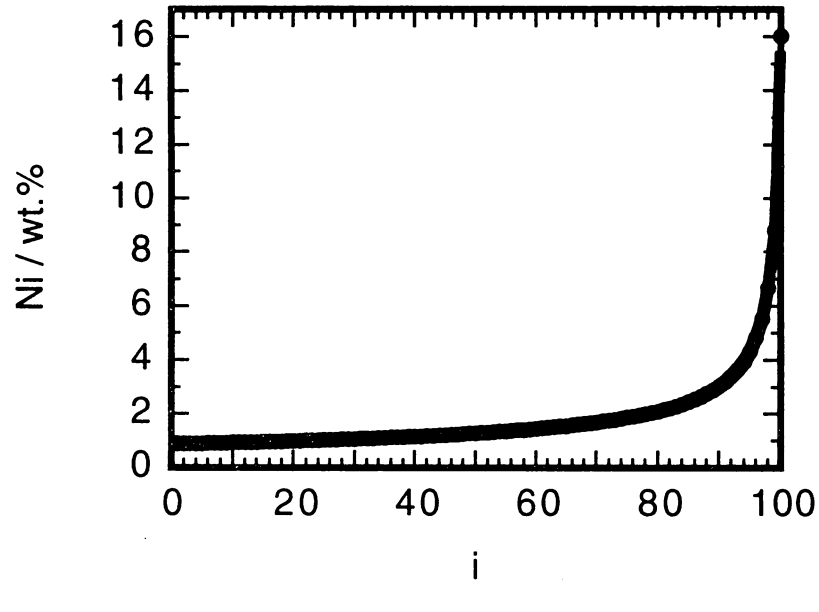

Fig. 2-12 : Calculated segregation profile of nickel concentration (Weld CR2: Average nickel content 1.96 wt.%.).

An example (CR2) of variation of ferrite due to chemical segregation is illustrated in Fig. 2-16.

This shows the calculated final ferrite content variation (at 600 °C) and that when site saturation

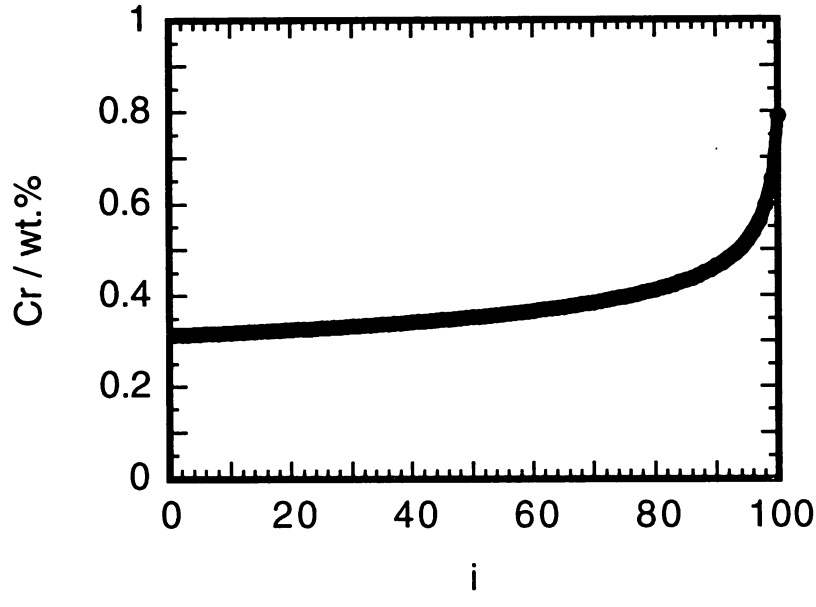

Fig. 2-13 : Calculated segregation profile of chromium concentration. (Weld CR2: Average chromium content 0.38 wt.%.).

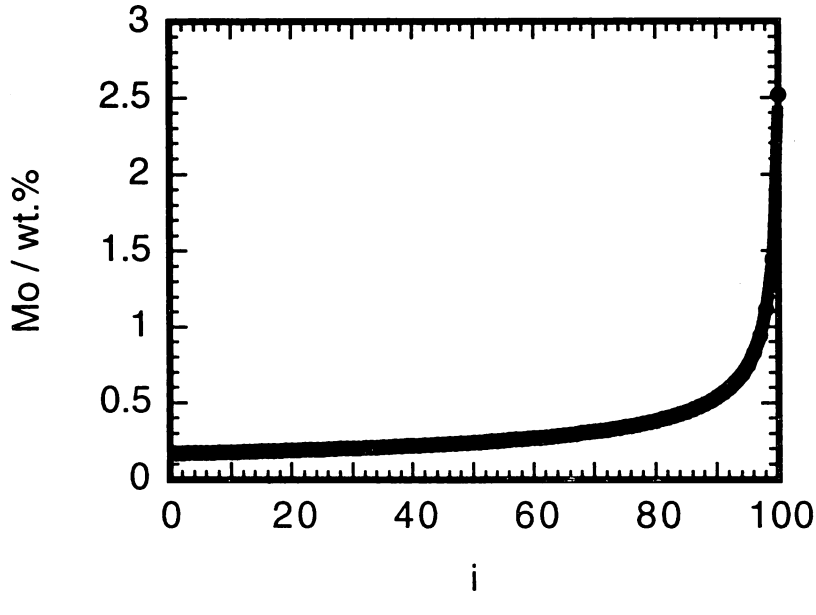

Fig. 2-14 : Calculated segregation profile of molybdenum concentration (Weld CR2: Average molybdenum content 0.35 wt.%.).

occurred. The final calculated amount of ferrite decreases and eventually becomes zero when i is equal to more than ninety-three. This result is in good agreement with real phenomena that the ferrite

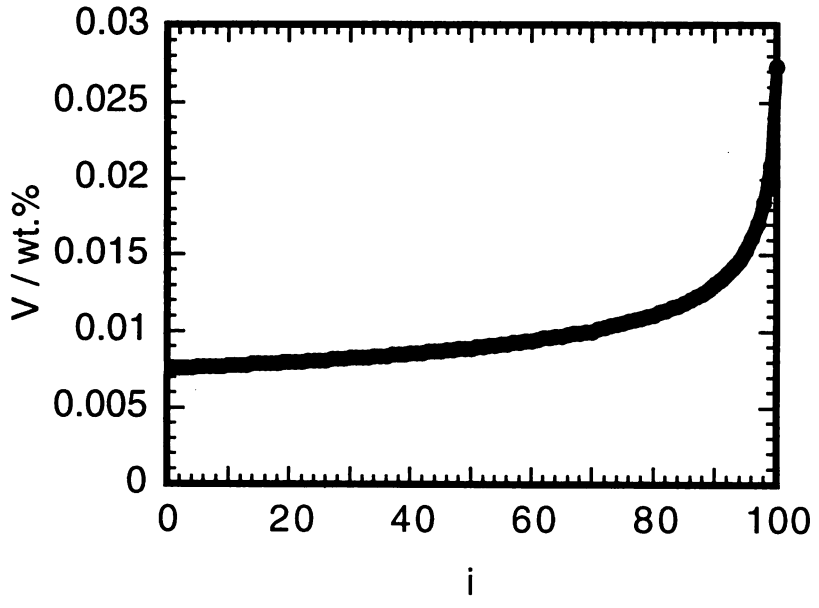

Fig. 2-15 : Calculated segregation profile of vanadium concentration. (Weld CR2: Average vanadium content 0.010 wt.%.).

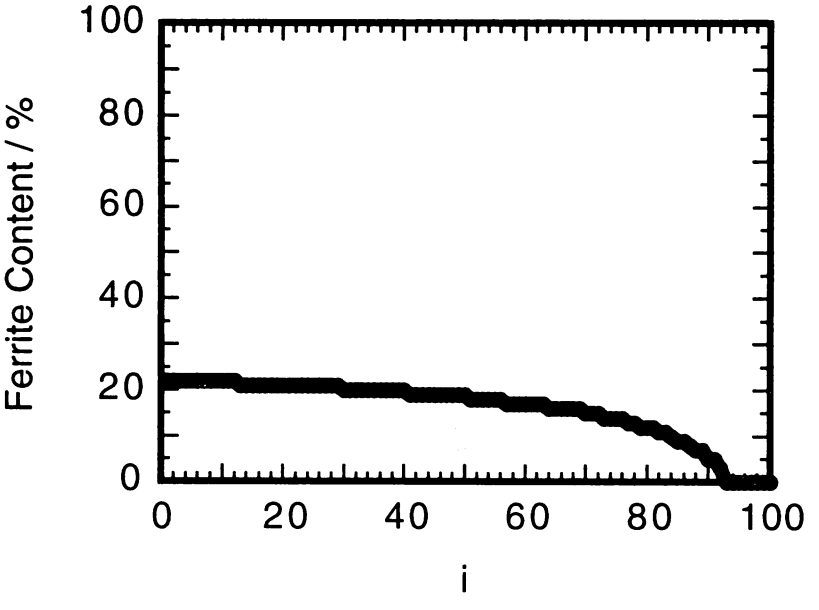

Fig. 2-16 : Calculated variation of ferrite due to segregation effect Weld CR2

transformation is impeded due to the high alloy concentrations in solute-enriched regions. The ferrite content at site saturation does not vary so much; however, the site saturation does not occur at i of more than ninety-one. This implies that there is a possibility of the existence of a small amount of

discontinuous allotriomorphic ferrite (in the segment of $i = 92$), which is schematically described in the second figure of Fig. 1-15b, even at the room temperature.

Some of the results (for C–Mn, Ni, Mo welds) are illustrated in Fig. 2-17.

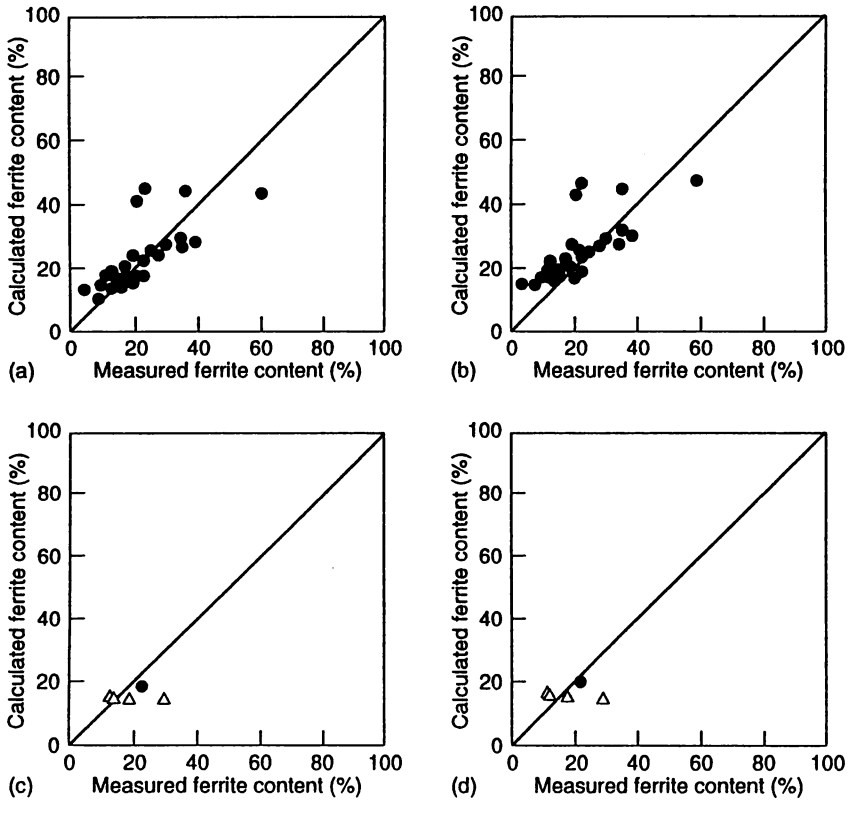

Fig. 2-17 : Comparison of the calculated volume fractions of allotriomorphic ferrite against data reported in the literature. (a) carbon–manganese welds; (b) carbon–manganese welds with segregation; (c) nickel or molybdenum containing weld; (d) nickel or molybdenum welds with segregation.

Taking into account that there are no "correction factors", and the fact that some of the reported experimental data for similar welds are inconsistent, the level of agreement achieved is reasonable. Note also that in the calculations it is arbitrarily assumed that allotriomorphic ferrite formation stops when a temperature of 600 °C is reached; this is probably a good approximation because reconstructive transformations become sluggish at low temperatures. The approximation is necessary because models for subsequent transformations such as Widmanstätten ferrite, acicular ferrite *etc.* are not yet ready. Chemical segregation modelled as discussed earlier does not seem to have much of an effect on the formation of allotriomorphic ferrite, but it may be found in future work that it influences the development of martensite and retained austenite (microphases).

Further calculations for the Cr or V containing welds are shown in Fig. 2-18.

For reasons which are not clear, the calculated data do not seem to be sensitive, within the concentration ranges given in Table 2-3, to the concentrations of these elements. The strange observation is that the discrepancies are largest when the concentration is small, *i.e.*, when the volume of allotriomorphic ferrite is large.

2.10 Conclusions

A model based on the detailed nucleation and growth functions for allotriomorphic ferrite has been found to give reasonable agreement with experimental data. This will in the future be developed further to enable the inclusion of transformations which occur as the weld cools to lower temperatures. The data for chromium and vanadium containing welds are not well reproduced by the model and require further investigation.

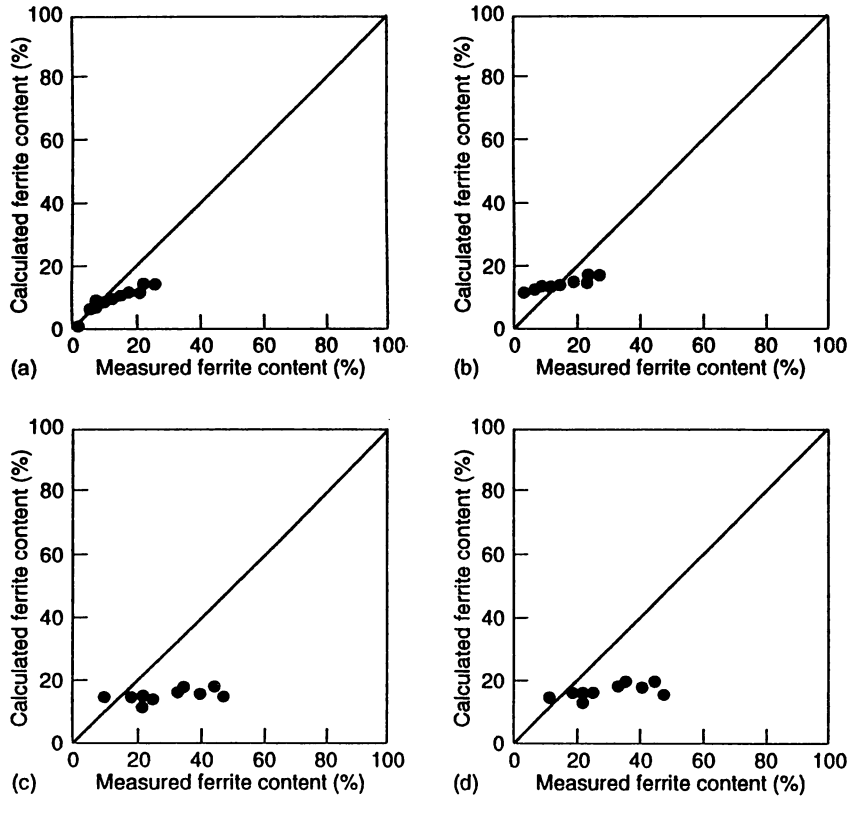

Fig. 2-18 : Comparison of the calculated volume fractions of allotriomorphic ferrite against data reported in the literature. (a) chromium containing welds; (b) chromium containing welds with segregation; (c) vanadium containing weld; (d) vanadium containing welds with segregation.

CHAPTER THREE

Application of the Ferrite Transformation Model to Large Heat-Input Welds

3.1 Introduction

In the previous chapter, published experimental data were used extensively to check the validity of the theory for allotriomorphic ferrite formation in welds. However, these data were obtained for welding processes which involve a small heat input about 10 kJ cm^{-1}. Larger heat input welding is frequently used in modern applications in order to achieve improved deposition rates. For example, heat inputs up to 200 kJ cm^{-1} or 700 kJ cm^{-1} for submerged arc welding (SAW) and electroslag welding (ESW) are now technologically important in industry [Sato *et al.*, 1981; Horii, 1989].

The control of allotriomorphic ferrite becomes a problem with large heat input welds because of the associated slower cooling of the weld. This is why materials for large heat input welding tend to be alloyed with minute quantities of titanium and boron. This promotes acicular ferrite by suppressing austenite grain boundary nucleated products [Mori *et al.*, 1981].

Therefore further data, including cooling characteristics, austenite grain size and the details of the microstructure, are needed to validate the models for large heat input welds. It shall be examined next that the cooling characteristics and microstructure of such welds in order to establish an experimental database. In addition, solidification-induced segregation was investigated experimentally here using computer aided X-ray microanalyser in order to examine the segregation model introduced previously.

3.2 Experimental Procedure

3.2.1 Welding and Materials

Alternating current tandem submerged arc welding with two different levels of heat input, without preheat (*i.e.*, T_i in equation 1-31 is 20 °C.) or post weld heat treatment, were fabricated at the Welding & Joining Research Centre, Nippon Steel Corporation. A schematic diagram of this welding process is illustrated in Fig. 3-1.

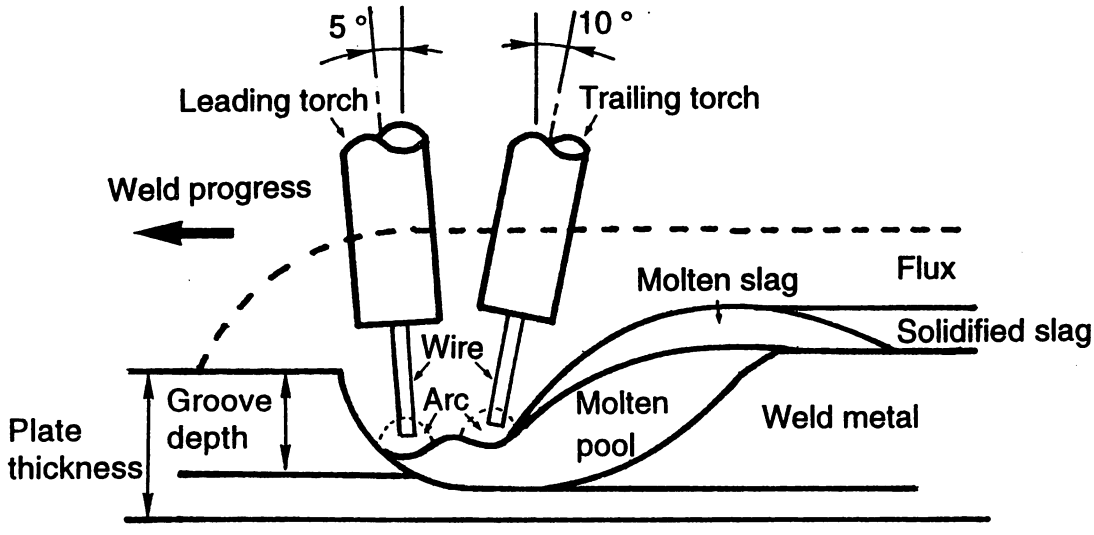

Fig. 3-1 : Schematic diagram of a tandem submerged arc welding process used in this study.

One of the welds was fabricated using a heat input of 75 kJ cm^{-1} and the other with 129 kJ cm^{-1}. These are much larger heat inputs than the published data utilised in Chapter 2. The details of the welding conditions are given in Table 3-1.

Table 3-1 : Submerged arc welding conditions.

Weld	Electrode position	Polarity	Welding current / A	Voltage / V	Welding speed / cm min^{-1}	***Heat input*** / kJ cm^{-1}	Extension / mm	Torch distance / mm	Torch angle / °
W1	Leading	AC	950	36	50	***75***	35	35	5[1]
	Trailing	AC	700	40			40		10[2]
W2	Leading	AC	1250	38	43	***129***	40	45	5[1]
	Trailing	AC	1000	45			45		10[2]

Torch angle (see Fig. 3-1):
[1] Backward to weld progress.
[2] Forward to weld progress.

Steel plates of thickness 40 mm were used; their chemical compositions is described in Table 3- 2. Grooves were machined on the plate with an angle of 60° and 10 mm depth for the weld with 75 kJ cm^{-1}

Table 3-2 : Chemical composition of the 40 mm thick steel plate / wt.%.

C	Si	Mn	P	S	Cr	Mo	V	Nb	Ti
0.11	0.25	1.15	0.012	0.002	0.03	0.53	-	0.024	0.01

heat input, and 50° and 16 mm for the 129 kJ cm^{-1} weld (Fig. 3-2). Both the leading and trailing SAW electrodes were 4.8 mm in diameter and are manufactured by Nippon Steel Welding Products & Engineering Co., Ltd.. Their chemical compositions are given in Table 3-3.

Table 3-3 : Chemical compositions of the 4.8 mm diameter welding electrode used / wt.%.

Position	C	Si	Mn	P	S
Leading	0.07	0.01	0.50	0.006	0.003
Trailing	0.02	0.01	0.50	0.006	0.003

Laboratory-manufactured agglomerated flux was used for all the welds. This flux is composed of silicon oxides, aluminium oxides, manganese oxides, calcium oxides, magnesium oxides, calcium fluoride and metallic elements including iron, silicon and manganese, the detailed chemical analysis is given in Table 3-4.

Table 3-4 : Chemical compositions of the submerged arc welding flux / wt.%.

SiO_2	$CaCO_3$	CaF_2	ZrO_2·CaO·SiO_2	Al_2O_3	MgO	Fe·Si	Mn
21.0	5.0	7.5	18.6	24.3	15.6	3.0	5.0

While boron significantly impedes the allotriomorphic transformation at the austenite boundaries, it was not intentionally added in order to simplify the studies. Titanium also was not alloyed from the welding materials, but a very small amount of titanium will naturally be expected from the base steel plates and may assist acicular ferrite transformation in the weld austenite grains.

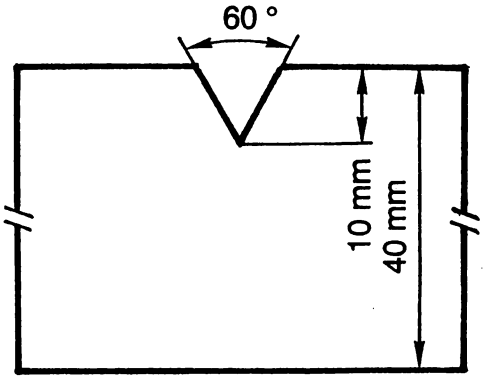

(a)

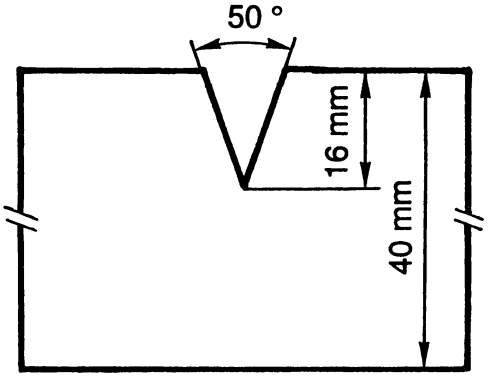

(b)

Fig. 3-2 : Groove geometries. (a) W1 (75 kJ cm^{-1}). (b) W2 (129 kJ cm^{-1}).

3.2.2 Thermal History

The cooling curves for the two welds were measured using 0.5 mm diameter Pt-Pt(13wt.%Rh) thermocouples harpooned into the molten pool during welding, immediately after the passage of the welding electrodes.

3.2.3 Analysis of the Welds

The chemical analyses was done on samples machined 5 mm under the top surface of the plates at the centre of weld bead. The concentrations of carbon, sulphur and oxygen were analysed using infrared absorption spectrometry. The nitrogen concentrations were analysed using a thermal conductivity method by fusing in active gas carrier. Extraction spectrophotometry with methylthionine chloride was used to measure the boron concentrations. All the other solutes were analysed using an inductively coupled plasma analysis. These are all standard method which are well-established.

Optical microscopy was carried out at the centre on transverse sections of the welds. The samples were etched using 2% nitric acid in alcohol. Microstructural measurements were then carried out on the weld metals. The austenite grain size was measured normal to the long axes of the columnar austenite grains visible in the sections prepared normal to the welding direction, and values of the mean average lineal intercept $\overline{L}_{tn}$ were deduced. Some six hundred and twenty-eight and three hundred twenty-four intercepts of grains were measured on welds W1 and W2 respectively. The quantitative assessment of the microstructural components was made using a "point counting technique" for each specimen. An ordered grid of points is superimposed on a random microstructure to deduce a fraction of each component of the specimen. Five thousand points were counted on each weld section. Vickers hardness measurements were also done on transverse sections of the each welds for 25 points with the applied force of 10 kgf.

The solidification-induced chemical segregation of silicon, manganese and molybdenum was investigated using computer-aided microanalysis on both weld W1 and W2 for the square having a side length of 1.5 mm. This microanalyser [Taguchi *et al.*, 1985] irradiates the sample with an electron beam in vacuum, measures generated characteristic X-rays after energy dispersive spectral analysis and determines the elements contained from the X-ray intensity of the sample calibrating with standard samples. This procedure is repeated at each of analysis spots on the sample surface. Image analysis is performed by a computer and the distributions of elements are output. Before the microanalysis, the solidification microstructures were investigated using optical microscopy and the regions were selected by marking with Vickers diamond hardness indents in order to correlate the microanalysis with microstructure. The etchant used was prepared as follows; 2 ml of 10 g solution dodecylbenzenesulfonic acid sodium salt+5g picric acid+5g oxalic acid+100 ml distilled water was solved into 100 ml distilled water. This solution was selected because it is effective in revealing the solidification microstructure. The etched surfaces were polished again taking care carefully to retain the Vickers hardness indents marks for for the micro analysis experiment. This polishing procedure is necessary in order to get smooth metallic

surface on the samples without contamination by the etchant.

3.3 Experimental Results

3.3.1 Chemical Compositions

Table 3-5 shows the chemical compositions of the two weld metals, which are virtually identical, so that the effect of heat input can be studied in isolation. Whilst very small amounts of boron were introduced into both welds in trace concentrations, most of the boron must be in oxide form and hence should not affect the phase transformation behaviour in the welds.

Table 3-5 : Chemical compositions of the welds / wt.%. The concentrations of Ti , B, N, and O are stated in parts per million by weight.

Weld	C	Si	Mn	P	S	Ni	Cr	Mo	Ti	B	N	O
W1	0.084	0.44	1.15	0.012	0.003	0.02	0.02	0.35	40	5	285	368
W2	0.084	0.48	1.20	0.014	0.003	0.02	0.03	0.33	40	6	284	309

3.3.2 Thermal History of the Welds

Fig. 3-3 shows macrostructures of the weldments. Due to the large heat input, the penetration is found to be larger in W2.

The cooling curves obtained from welds W1 and W2 are shown in Figs. 3-4 and 3-5 respectively. As expected, the cooling rate is lower for the larger heat input weld W2 at all temperatures. This difference in the cooling rate is consistent with the form of equation 1-21. Temperatures and times obtained from these weld cooling curves are given in Table 3-6.

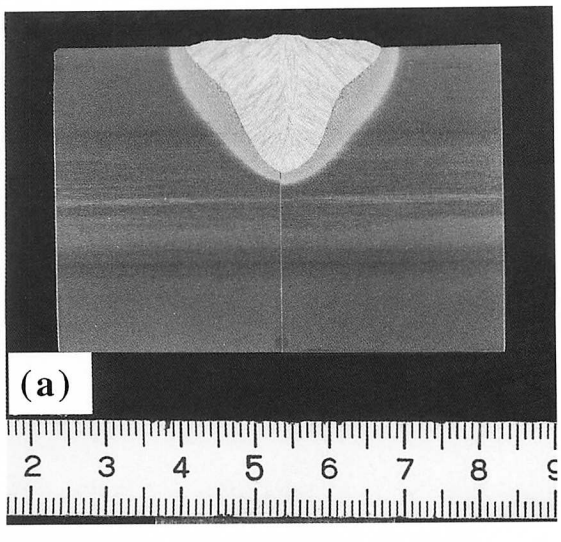

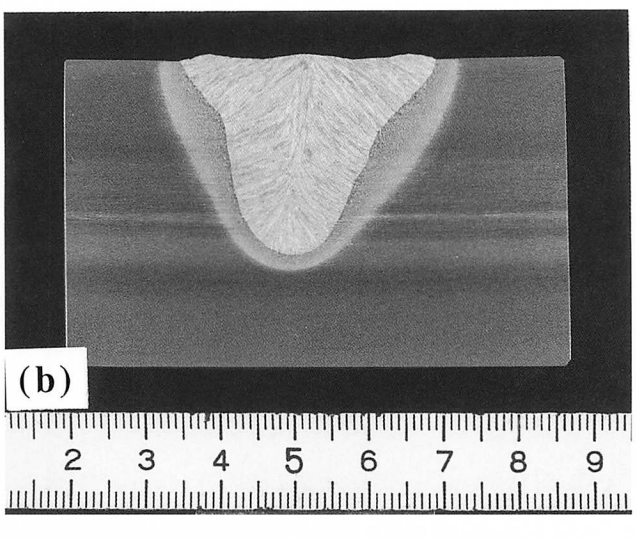

Fig. 3-3 : Macrostructures of the welds. (a) W1 (75 kJ cm^{-1}). (b) W2 (129 kJ cm^{-1})

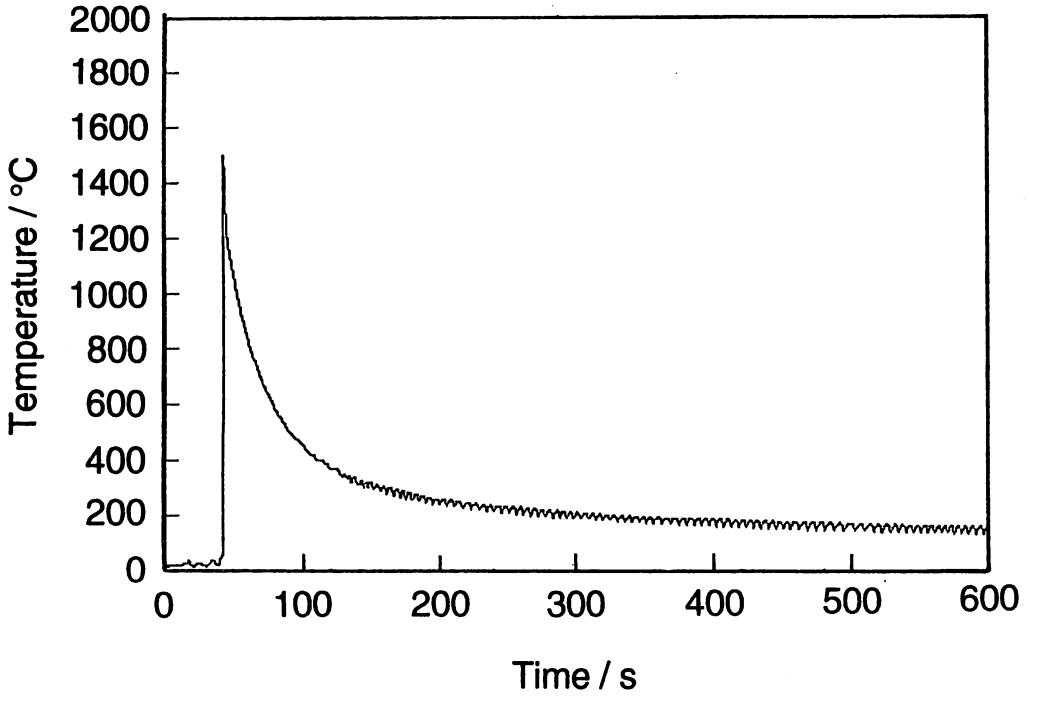

Fig. 3-4 : The cooling curve for the fusion zone of weld W1 (75 kJ cm^{-1}).

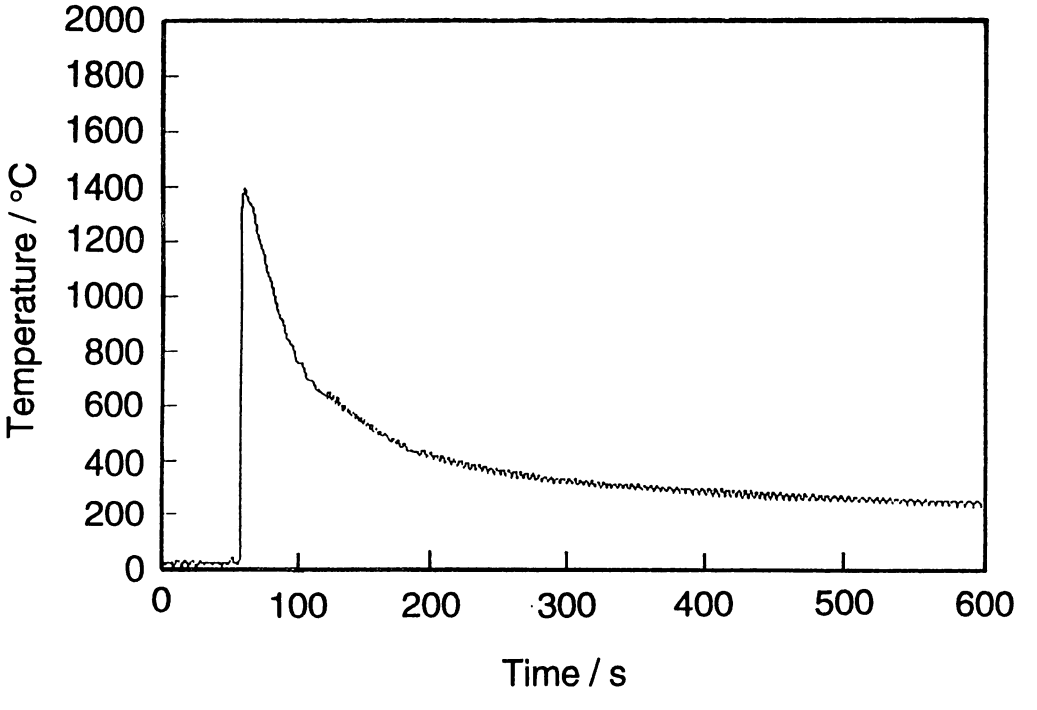

Fig. 3-5 : The cooling curve for the fusion zone of weld W2 (129 kJ cm^{-1}).

By fitting equation 1-21 to the experimental data over the temperature range 800 to 500 °C , the constants C_1 and C_2 were obtained (Table 3-7).

Table 3-6 : Temperatures and times obtained from weld cooling curves (Figs. 3-4 and 3-5).

Weld	Temperature T/ °C	Time t/ s
W1	800	58.3
	700	66.8
	600	76.2
	500	98.0
W2	800	93.6
	700	103.7
	600	127.4
	500	157.6

Table 3-7 : The values of fitting parameters for the weld cooling curves. The first standard error (SE) is for the regression constant (ln C_1) in a plot of $\ln(dT/dt)Q\eta$ versus $\ln(T-T_i)$ where η is arc efficiency and assumed to be 0.9. The second standard error is for the regression coefficient C_2. The values are with the units of Q, T and t being J m^{-1}, °C and second respectively.

Weld	C_1	*SE*	C_2	*SE*	Regression Coefficient
W1	**2.59 x 10^5**	0.179	**8.64 x 10^{-1}**	0.028	0.999
W2	**4.61 x 10^4**	0.446	**1.10**	0.069	0.996

3.3.3 Microstructures

Figs. 3-6 and 3-7 show the microstructures of welds W1 and W2 respectively. Prior austenite grain boundaries can be identified clearly by the allotriomorphic ferrite layers which decorate the boundaries.

As expected from the higher heat input, the austenite grain size is larger in W2 than in W1, confirmed by the quantitative measurements Table 3-8 with the statistical analysis. Where the 95 % confidence is the range in that the experimental measurement on samples (average measurement)$\pm 2SE$ where SE is the standard error. Detailed procedures of the statistical analysis are given in appendix one.

Table 3-8 : Austenite grain parameters of the welds.

Weld	Heat input/ kJ cm^{-1}	Austenite grain parameters		
		Measured columnar grain width / μm	95 % confidence	S_V/ 10^4 m^{-1}
W1	75	96	±0.02	1.81
W2	129	127	±0.02	1.36

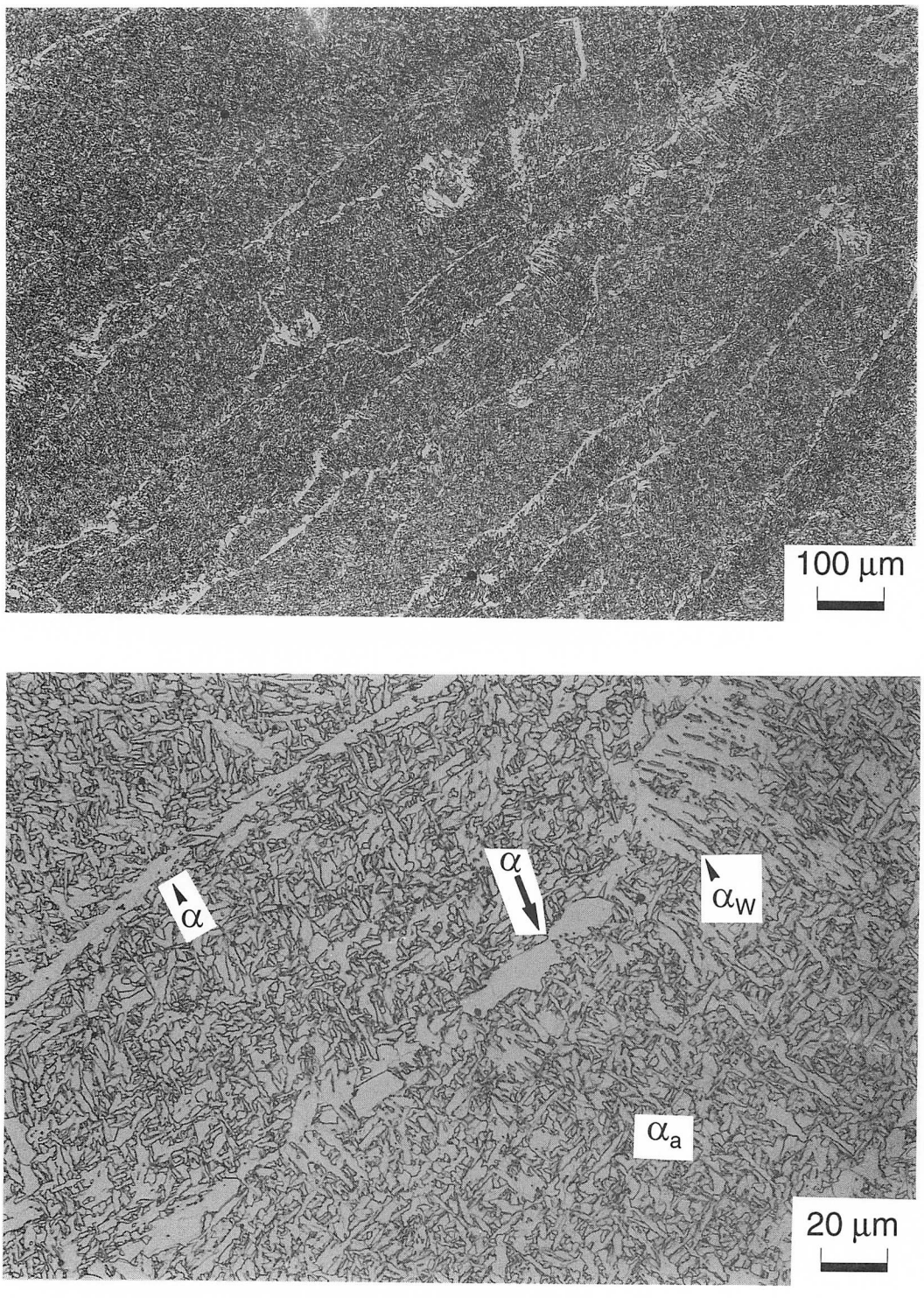

Fig. 3-6 : Optical microstructure of the weld W1 welded using a heat input of 75 kJ cm^{-1}, showing the allotriomorphic ferrite α, Widmanstätten ferrite α_W, acicular ferrite α_a. Discontinuous allotriomorphic ferrite (indicated by the arrow) also can be observed together with continuous layers.

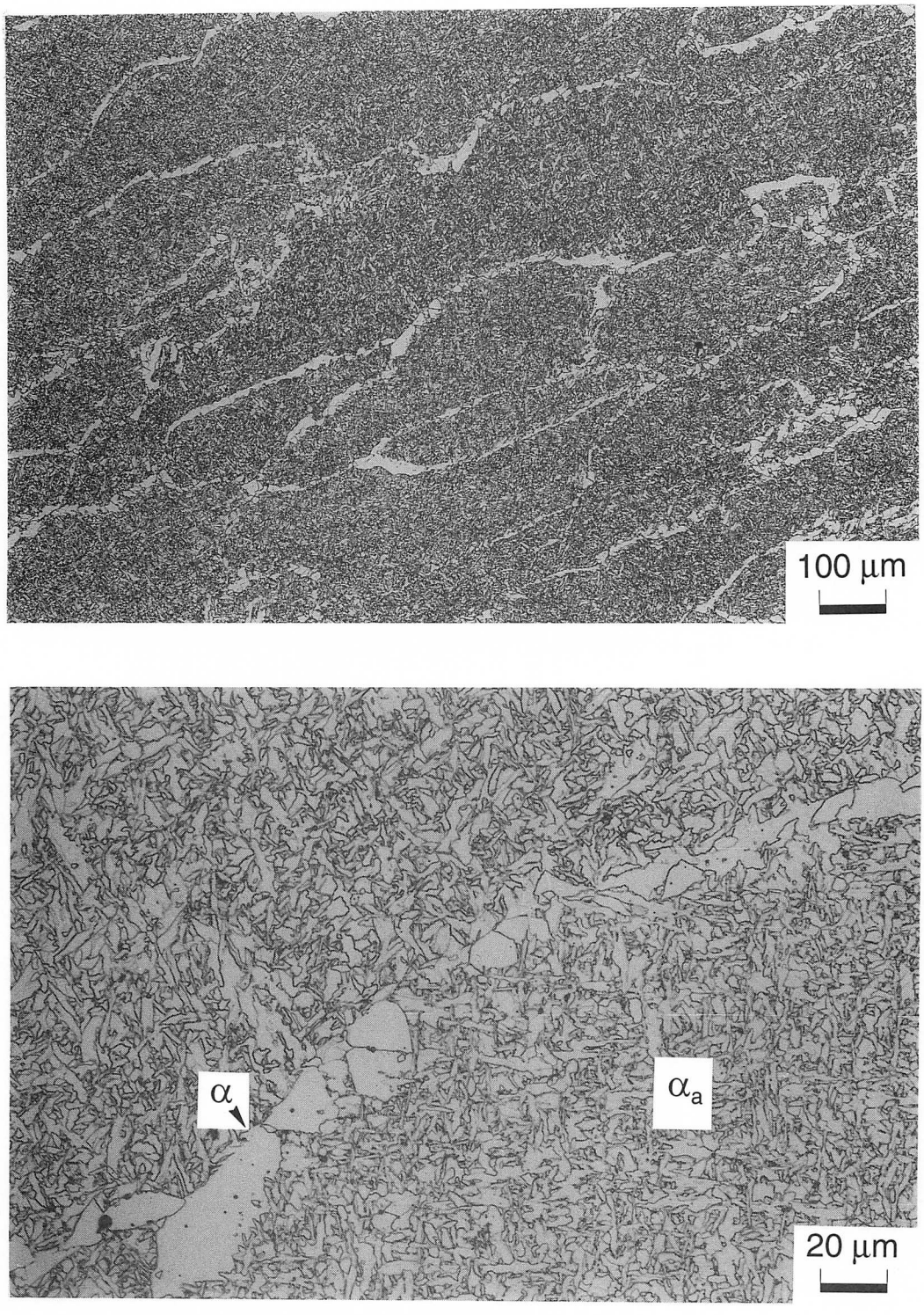

Fig. 3-7 : Optical microstructure of the weld W2 welded using a heat input of 129 kJ cm^{-1}, showing the allotriomorphic ferrite α, acicular ferrite α_a.

For the same reason, the allotriomorphic ferrite layers are thicker in W2 than in W1. It is interesting that the ferrite layers consist of many more individual ferrite grains per unit area in W1 with its faster cooling rate. This implies a larger nucleation rate which might be expected with faster cooling (as Bhadeshia *et al.*; 1987, Fig. 1-15b). W1 also shows a very small amount of Widmanstätten ferrite (Fig. 3-6b), which is absent from W2. The volume fractions of each microstructural component as measured using quantitative microscopy are given in Table 3-9 with the statistical analysis. Average values of Vickers hardness of W1 and W2 are 225 and 218 respectively. This slightly larger value in W1 might be due to the faster cooling rate associated with the lower heat input.

Table 3-9 : Measured and calculated ferrite fractions where α, α_W, α_a are allotriomorphic, Widmanstätten and acicular ferrite respectively.

Weld	Measured fraction, ( ): 95 % confidence			Calculated fraction
	α	α_w	α_a	α
W1	0.12 (±0.005)	0.01 (±0.001)	0.87 (±0.005)	0.24
W2	0.15 (±0.005)	0.00	0.85 (±0.005)	0.25

Figs. 3-8 and 3-9 show the solidification microstructure of weld W1 and W2 respectively.

Figs. 3-10 to 3-12 and 3-13 to 3-15 show the results of the microanalysis for silicon, manganese and molybdenum of weld W1 and W2 for the corresponding areas illustrated in Figs. 3-8 and 3-9 respectively. Corresponding to the solidification structures, which can be seen with the deep etched spots in the Figs. 3-8 and 3-9, segregations of substitutional alloying elements can be observed. Figs. 3-16 to 3-21 describe the comparison between calculated and experimental percentage occupied as a function of silicon, manganese, molybdenum concentration for weld W1 and W2. It can be seen that calculated area tends to underestimate the actual segregated area in higher concentrations, which may be responsible for the overestimation of the ferrite fraction.

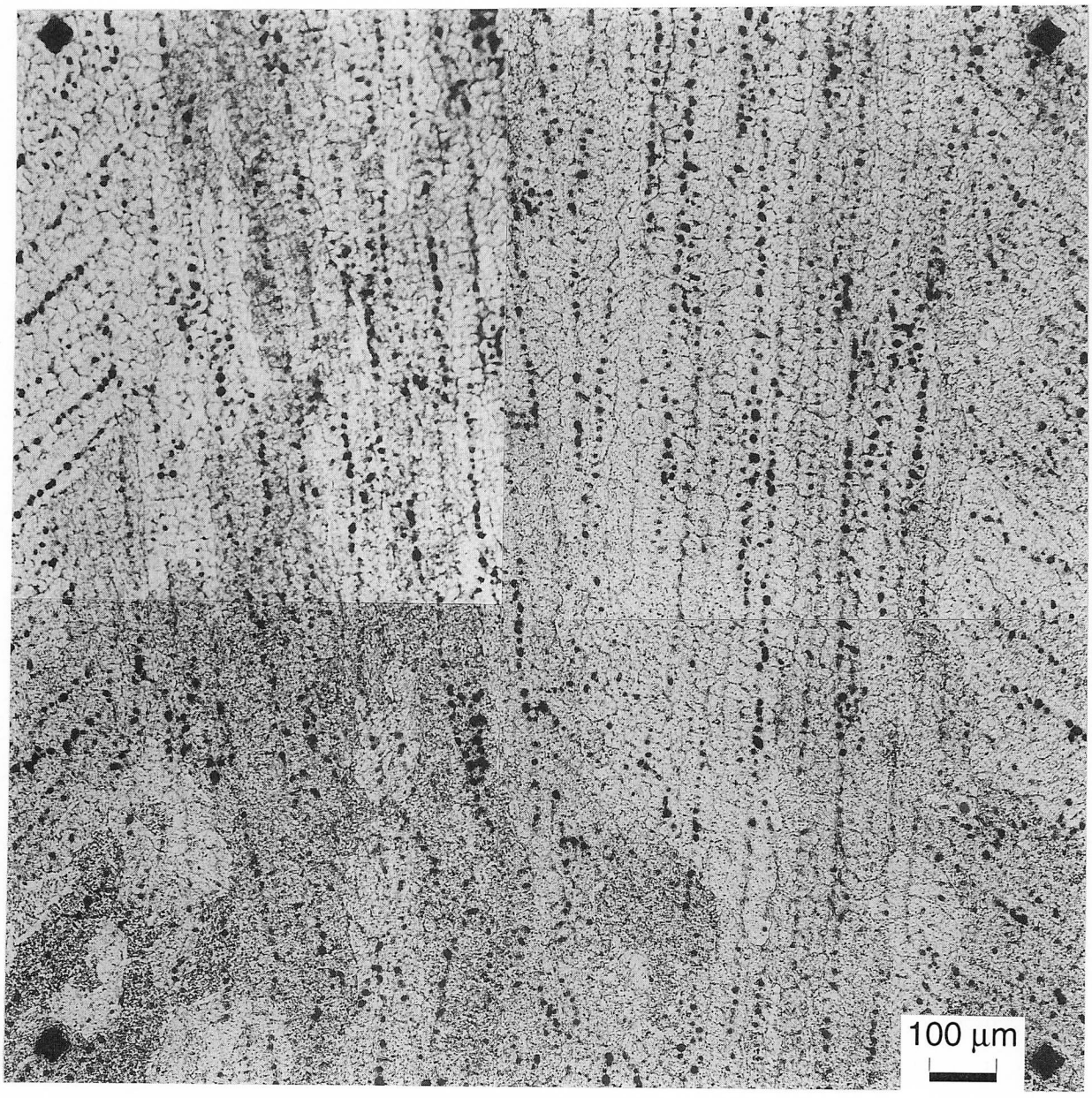

Fig. 3-8 : Solidification structure (seen with deep etched spots) of weld W1.

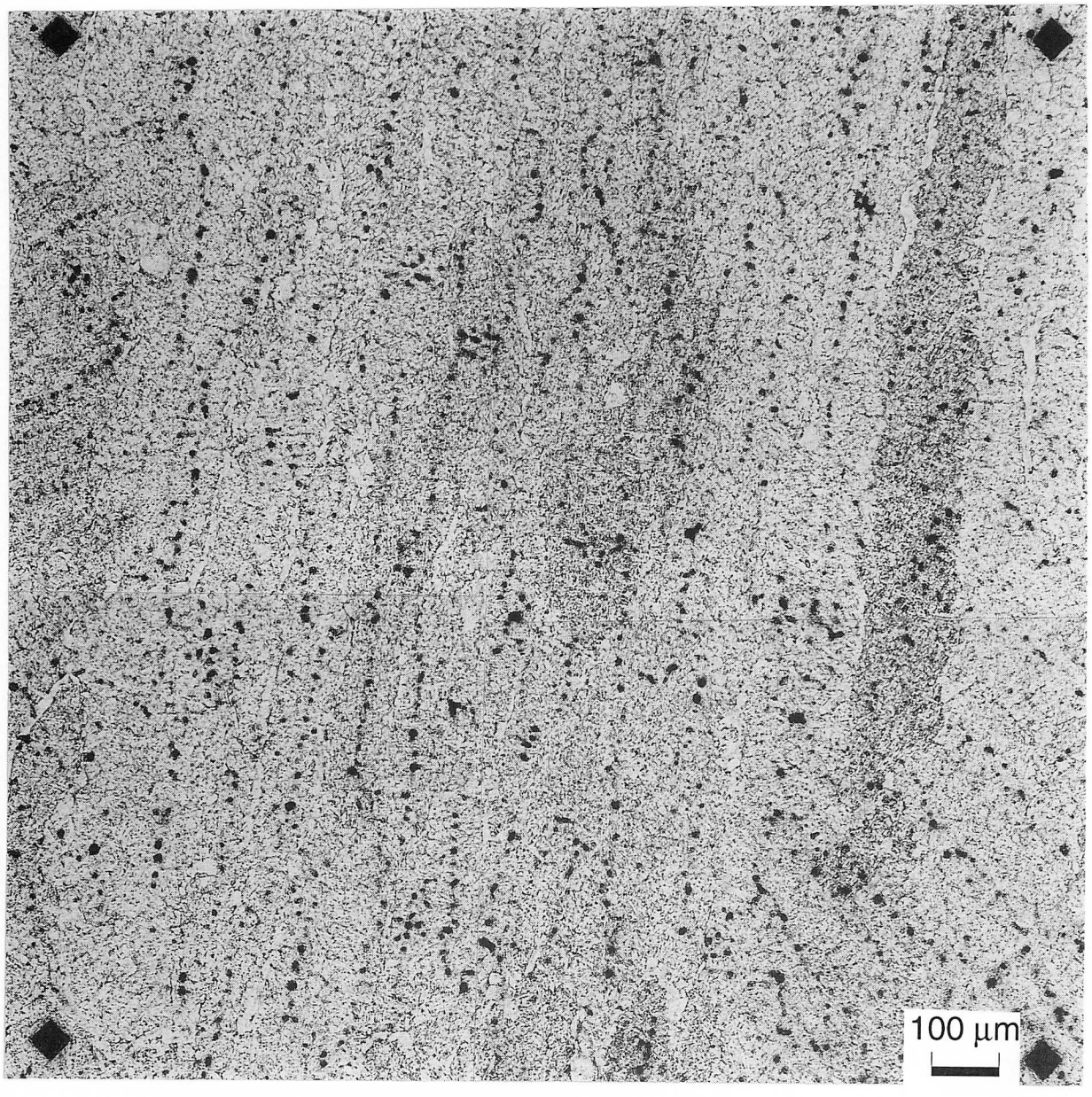

Fig. 3-9 : Solidification structure (seen with deep etched spots) of weld W2.

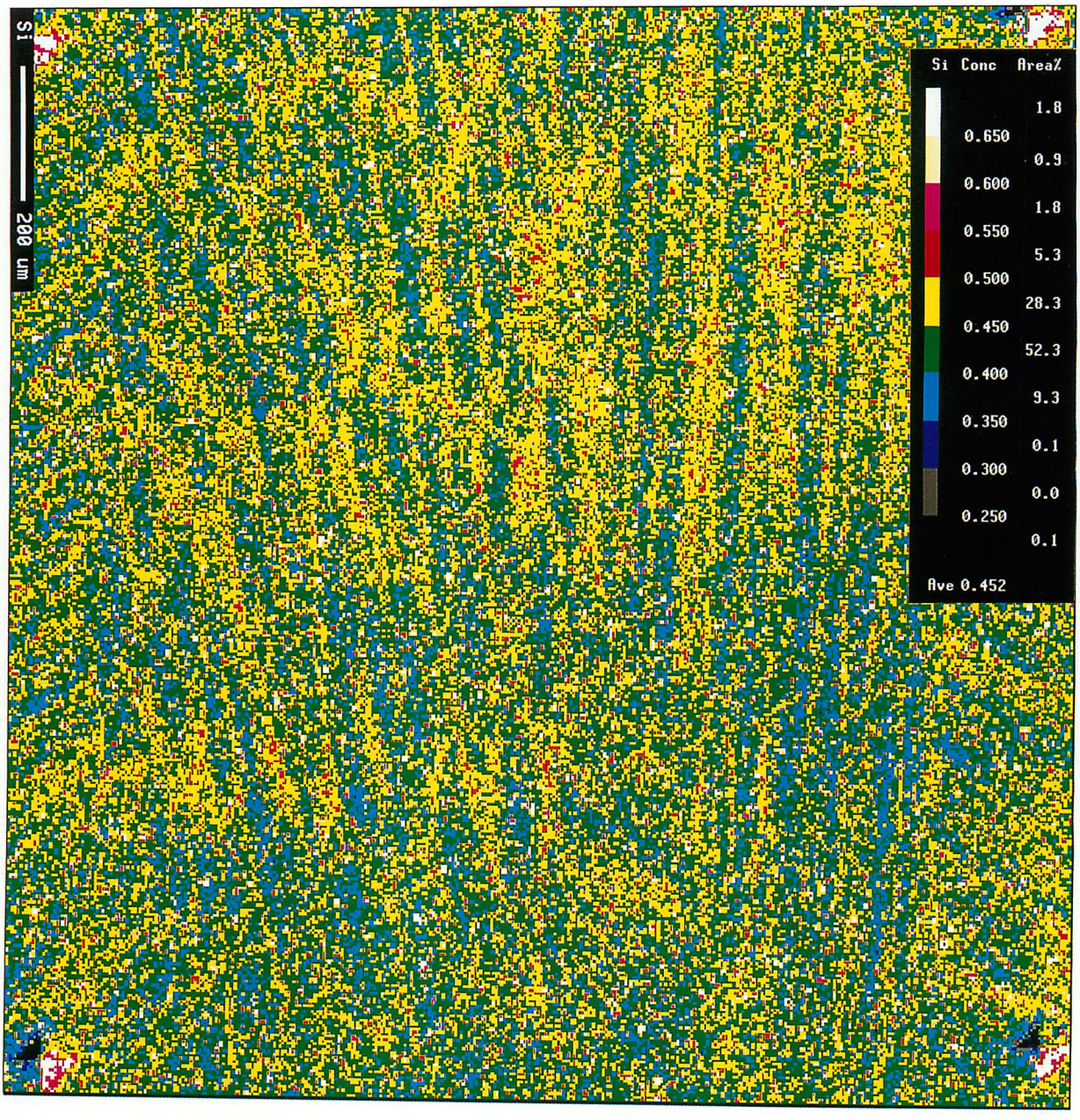

Fig. 3-10 : Microanalysis showing the solidification-induced segregation of silicon in weld W1.

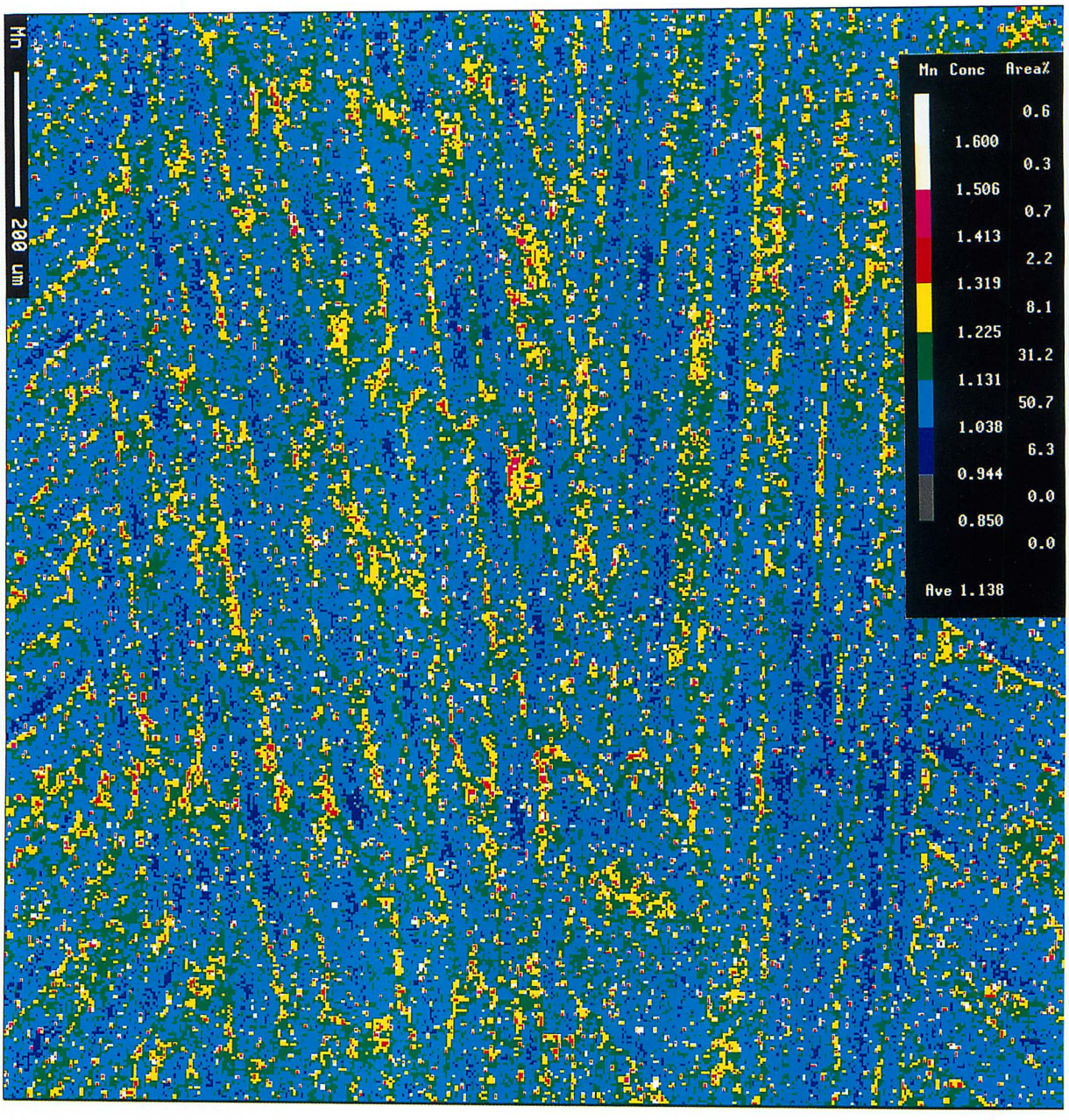

Fig. 3-11 : Microanalysis showing the solidification-induced segregation of manganese in weld W1.

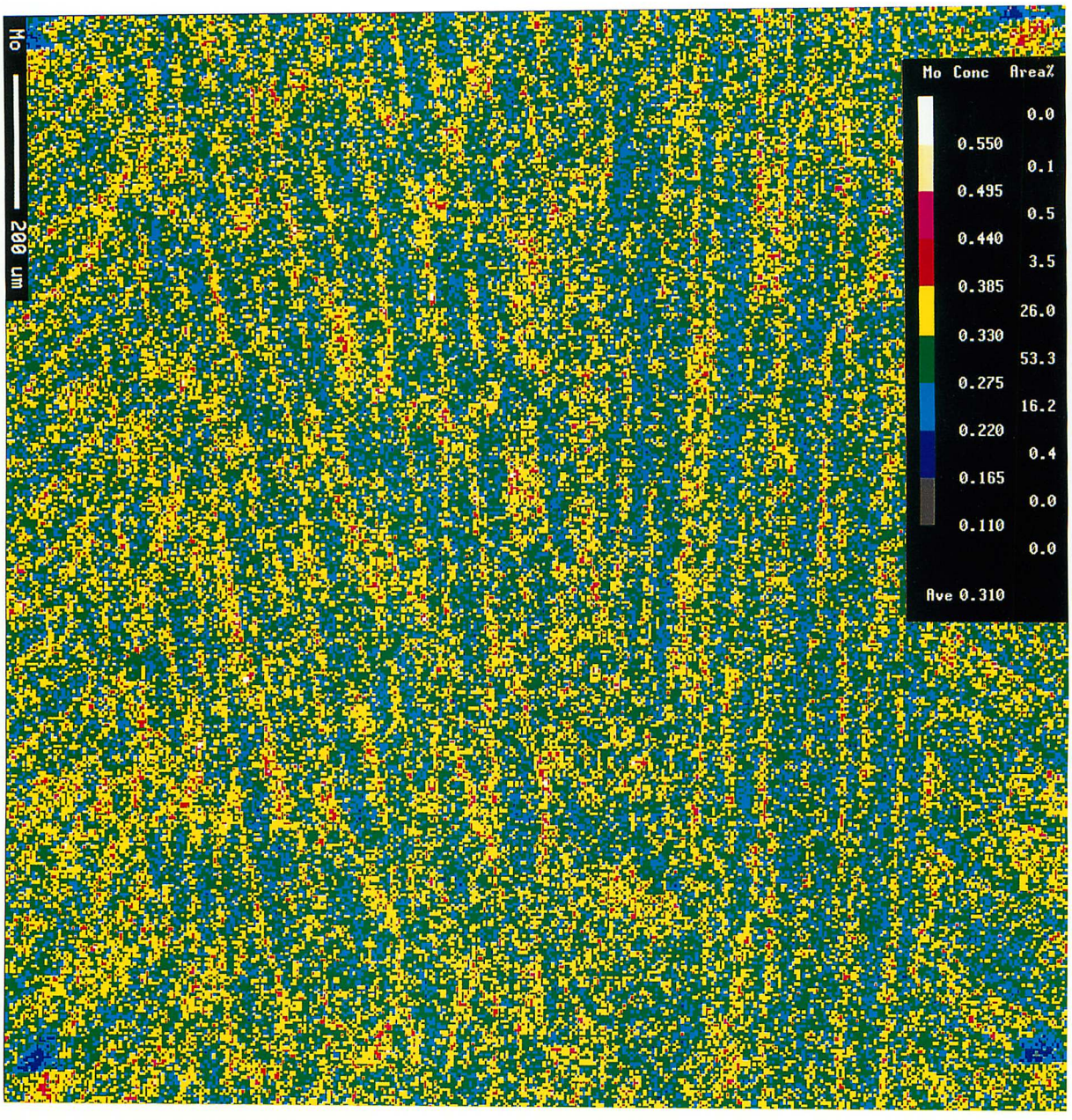

Fig. 3-12 : Microanalysis showing the solidification-induced segregation of molybdenum in weld W1.

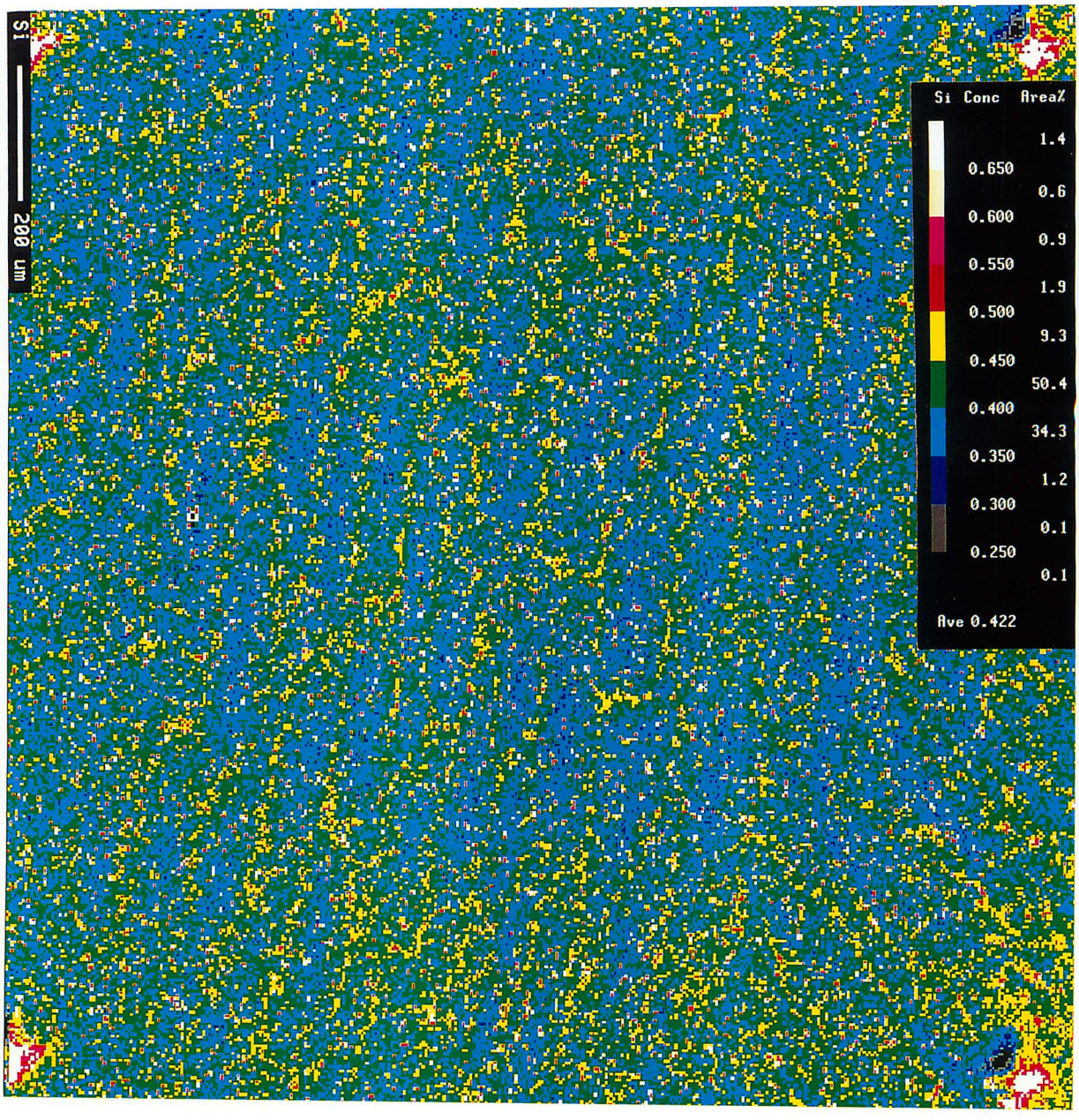

Fig. 3-13 : Microanalysis showing the solidification-induced segregation of silicon in weld W2.

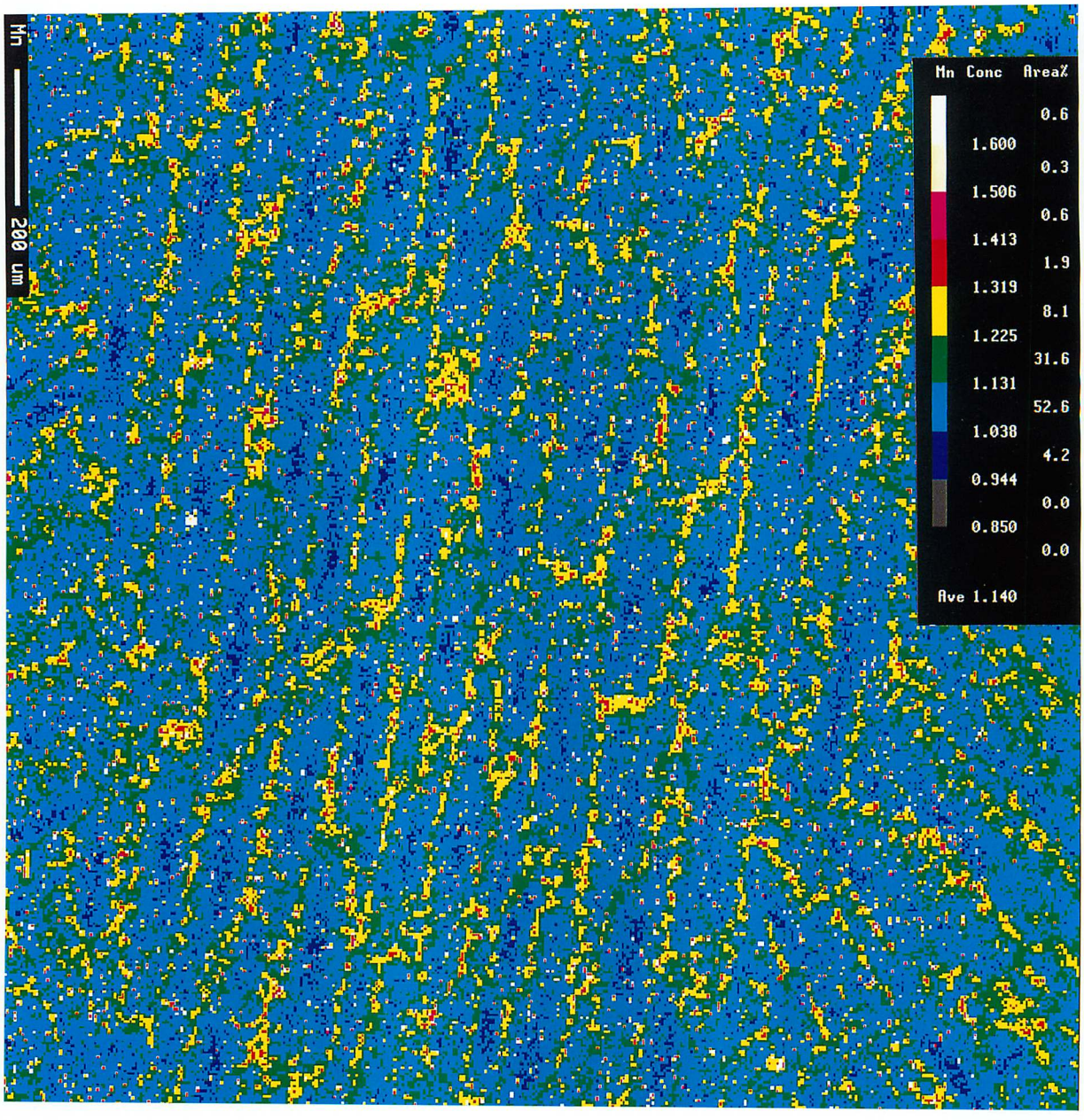

Fig. 3-14 : Microanalysis showing the solidification-induced segregation of manganese in weld W2.

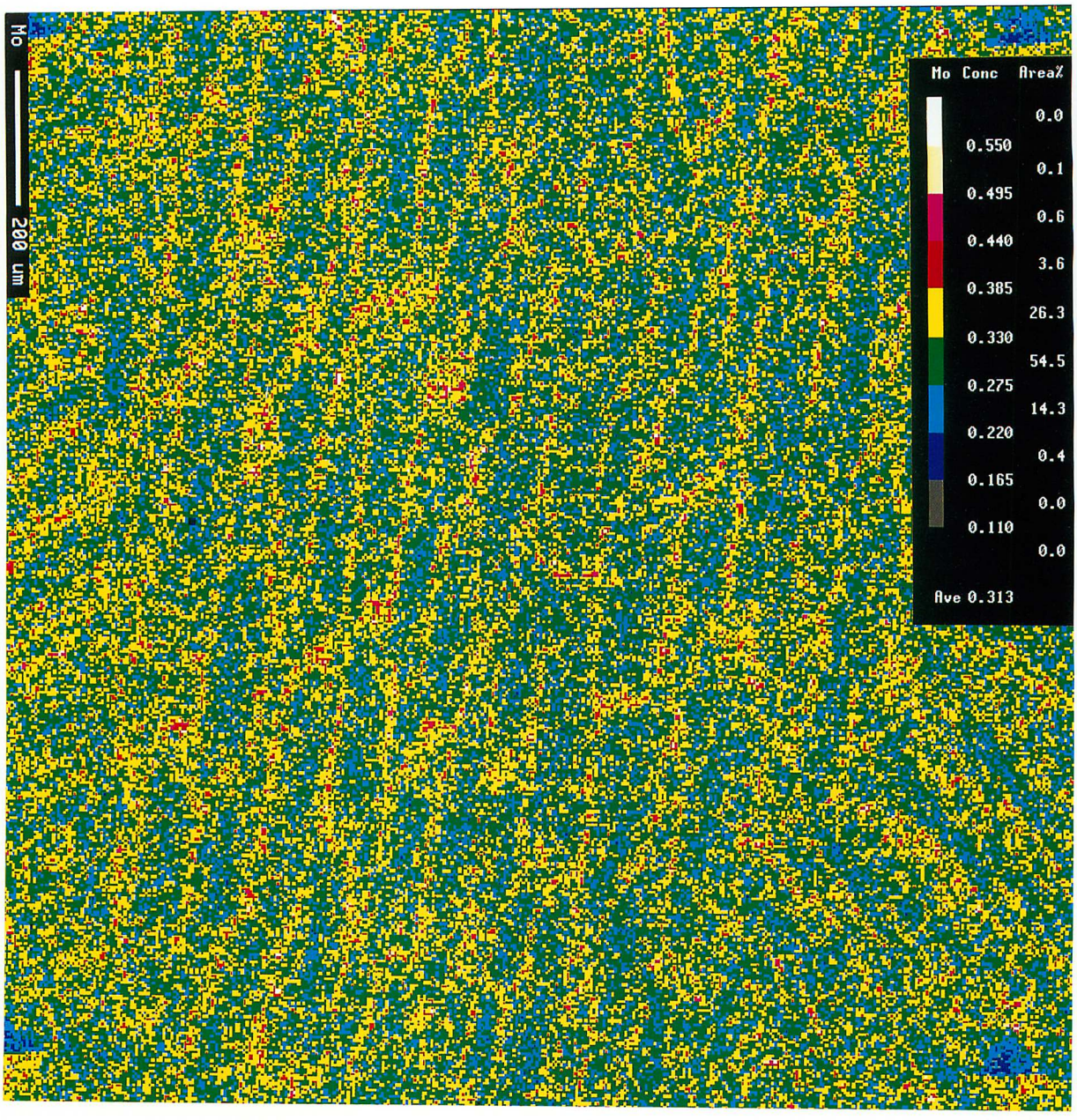

Fig. 3-15 : Microanalysis showing the solidification-induced segregation of molybdenum in weld W2.

3.4 Discussion

The volume fractions of allotriomorphic ferrite for welds W1 and W2 have been estimated using the segregation model described in chapter 2, the cooling curve data and S_V given in the Table 3-7. The results are listed in Table 3-8.

The calculated fraction of allotriomorphic ferrite is insensitive to the heat input. This is because there are two opposing effects of the heat input. Firstly, it increases the austenite grain size, which leads to a reduction in the allotriomorphic ferrite content. On the other hand, the slower cooling rate associated with the larger heat input provides a larger time period for allotriomorphic ferrite growth. In fact the experimental measurements show the reasonably small difference in allotriomorphic fraction between W1 and W2.

The inconsistency between the calculated and measured results is most likely due to the fact that the model is incomplete, *i.e.*, it is not yet possible to allow for the intervention of Widmanstätten ferrite or acicular ferrite. It could very well be the case that in W1, allotriomorphic ferrite formation is stifled by the onset of the Widmanstätten or acicular ferrite formation. However, it can be said that the degree of the inconsistency between the calculated and measured results in this chapter are rather acceptable considering the results shown in Figs. 2-17 and 2-18.

3.5 Conclusions

Data required for the application of the model developed previous chapter to large heat input welding, including cooling characteristics, austenite grain size and the ferrite fraction in welds have been obtained.

Same discrepancies have been noted which are probably due to the incomplete nature of the model, which does not as yet allow for the onset of Widmanstätten ferrite or acicular ferrite transformation.

CHAPTER FOUR

Simultaneous Transformation to Allotriomorphic and Widmanstätten Ferrite in Steel Welds

4.1 Introduction

It is well known that Widmanstätten ferrite can, in welding alloys, lead to a deterioration in mechanical properties [Savage and Aaronson, 1966; Dieter, 1976; Fick and Rogerson, 1977; Grong and Matlock, 1986; Spanos and Hall, 1996]. This is because the plates tend to grow in parallel formations called "packets", within which they are all in the same crystallographic orientation. Therefore, it is the packet which determines the size of cleavage facets rather than the individual plates. Both Widmanstätten and allotriomorphic ferrite have been extensively studied in the context of weld deposits, both experimentally and from a theoretical point of view [Bhadeshia *et al.*, 1985a; 1987; Ali and Bhadeshia, 1990; Rees and Bhadeshia,1992; Bhadeshia and Svensson, 1993; Spanos and Hall, 1996]. Although there appears to be an impression that the phases are well understood, there are some serious theoretical difficulties in dealing with transformations involving the *simultaneous* formation of more than one phase. As will be seen, another problem that has been identified here is that the published experimental data themselves have considerable unexplained variations.

Some of these problems arise because there are two kinds of Widmanstätten ferrite, primary and secondary. The former nucleates independently at the austenite grain boundaries whereas the latter develops from pre–existing allotriomorphic ferrite [Dubé, 1948; Dubé *et al.*, 1958]. It is secondary Widmanstätten ferrite which is predominant in welding alloys so that interactions with allotriomorphic ferrite are inevitable. Such interactions have never been taken into account when calculating the overall transformation kinetics. It has been normal practice instead, to arbitrarily stop a transformation in order to allow the next reaction in the sequence to proceed [Bhadeshia *et al.*, 1985a].

The purpose of the work presented in this Chapter was to develop and examine a model based on a new kinetic theory, which is capable of dealing with several transformations together. The theories of nucleation and growth for allotriomorphic and Widmanstätten ferrite are well known [Bhadeshia,

1985c; Ali and Bhadeshia, 1990; Van der Ven, and Delaey, 1996; Spanos and Hall, 1996] and so are introduced only briefly and in the context of the aim of the present chapter.

4.2 Simultaneous Transformations

A time–temperature–transformation diagram consists essentially of two C–curves (Fig. 4-1).

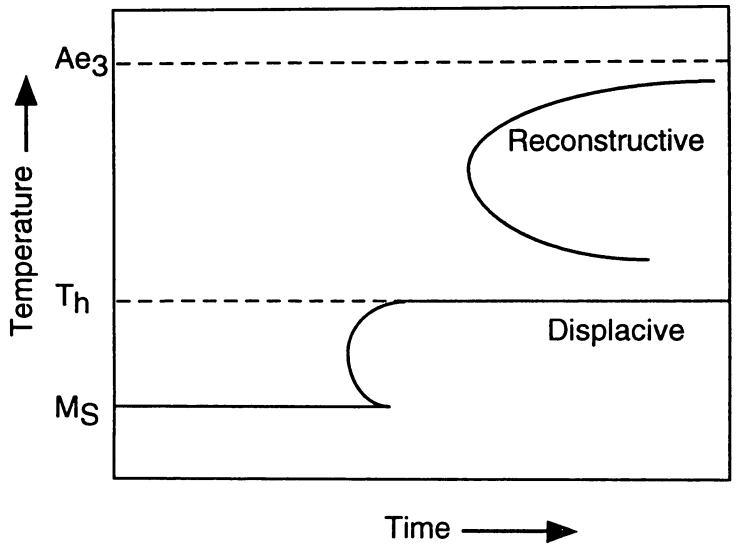

Fig. 4-1 : Schematic Time-Temperature-Transformation diagram illustrating the two C curves where T_h is the highest temperature at which ferrite can form by a displacive transformation.

The one at higher temperatures represents reconstructive transformations such as allotriomorphic ferrite and pearlite, whereas the lower C–curve is for displacive reactions such as Widmanstätten ferrite, acicular ferrite, and bainite. For many steels, the two C–curves intersect at a temperature which is about 600 °C, below which the overall rate of reaction is larger for displacive transformations. It is on this basis that previous work on the modelling of weld metal microstructures has assumed, that during continuous cooling transformation, the growth of allotriomorphic ferrite ceases at 600 °C to give way to Widmanstätten ferrite growth [Bhadeshia *et al.*, 1985a]. This approximation is patently unrealistic. Firstly, there is no dependence of this "transition temperature" on the cooling rate, and secondly, the point where the C–curves intersect should really be a function of the amount of austenite that is left untransformed. Furthermore, there is no evidence that the formation of Widmanstätten ferrite stops the continued growth of allotriomorphic ferrite; the reactions in reality occur simultaneously.

The reason why it has been necessary in the past to adopt such approximations is that the conventional

Johnson–Mehl–Avrami theory, which has been reviewed thoroughly by Christian [1975], deals with the kinetics of individual reactions occurring in isolation. The theory incorporates both nucleation and growth permitting the volume fraction to be calculated whilst accounting for hard impingement. The method can be introduced as follows.

Suppose that impingement effects are at first ignored and different particles are allowed to nucleate and grow in all regions, whether or not those regions are transformed. The transformed volume will obviously be overestimated. This volume is consequently called an *extended volume*. In Fig. 4-2, two particles have formed during the time interval t. A further short time interval Δt later, those particles increase in size but in addition, two new particles (a, b) nucleate and grow. Particle a nucleates in untransformed matrix whereas b does so in *extended* space. Particle b cannot therefore contribute to the change in real volume of the transformation product.

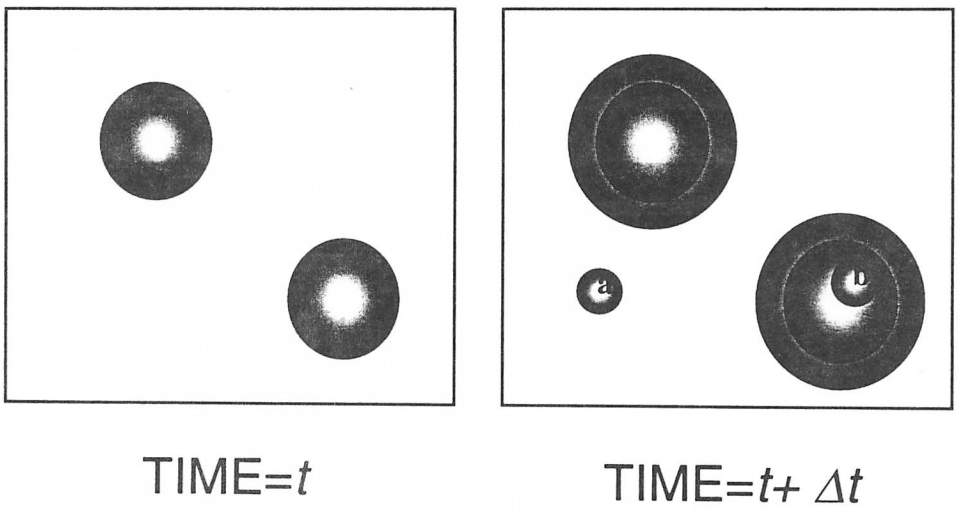

Fig. 4-2 : Schematic illustration of the extended volume concept. There are two particles that have formed during the time interval t. These particle grow with a further time increment Δt, and two other particles (a, b) precipitate.

Assuming random transformation on average, the relationship between the change in real and extended volumes of the product phase is governed by the probability that new regions form in untransformed matrix rather than in space which has already transformed. They are therefore related by the probability

of finding untransformed matrix, *i.e.*

$$dV_1 = \left(1 - \frac{V_1}{V_{total}}\right) dV_1^e \qquad (4-1)$$

where V_1 is the change in the actual volume of the product phase *1* and V_1^e is its extended volume. V is the total volume. This equation can, with appropriate nucleation and growth functions, be integrated so that the problem of calculating the fraction transformed as a function of time and temperature is solved. This theory has been used for decades to represent single precipitation reactions. It has been developed recently to deal with more than one reaction happening at a time [Robson and Bhadeshia, 1996; 1997a; b; Jones and Bhadeshia, 1997a; b].

If two different products *1* and *2* form at the same time then it is necessary to solve two equations simultaneously:

$$\left.\begin{aligned} dV_1 &= \left(1 - \frac{V_1 + V_2}{V_{total}}\right) dV_1^e \\ dV_2 &= \left(1 - \frac{V_1 + V_2}{V_{total}}\right) dV_2^e \end{aligned}\right\} \qquad (4-2)$$

where V_2 is the actual volume of transformed the second new product phase *2* and V_2^e is its extended volume. These equations cannot be integrated analytically except in special circumstances†, since the relationship between the two transformation products is not constant. For most circumstances the integration must be stepwise, but this has the advantage that the changes in the matrix chemical composition can easily be accounted for using the mean–field approximation. Complex heat–treatments can also be readily incorporated into the analysis [Jones and Bhadeshia, 1997a].

4.3 Allotriomorphic and Widmanstätten Ferrite

Both allotriomorphic and Widmanstätten ferrite are considered to initiate at the austenite grain surfaces (Fig. 4-3).

As described earlier, secondary Widmanstätten ferrite can form from the allotriomorphic ferrite/austenite phase boundaries. These two kinds of Widmanstätten ferrite nucleation events shall be treated identically, since the extended volume concept allows for any allotriomorphs which already exist. The only approximation therefore is that the two nucleation sites are considered to have identical kinetic parameters.

As is usual, each allotriomorph of ferrite is modelled as a disc parallel to the austenite grain boundary plane on which it nucleated [Bhadeshia *et al.*, 1987]. The allotriomorph has a half–thickness Z and

† Analytical solutions for these simultaneous equation describing simultaneous multiple transformations will be discussed in the Appendix for some special cases.

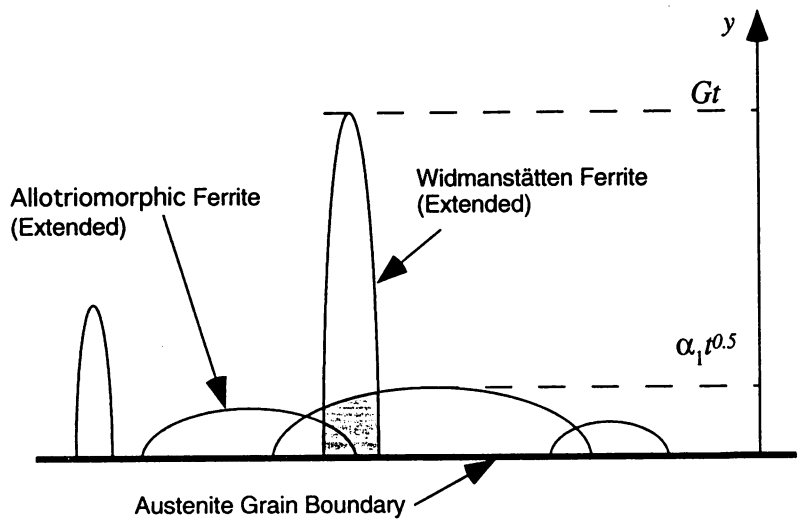

Fig. 4-3 : Schematic illustration showing the extended volumes of allotriomorphic and Widmanstätten ferrite nucleated from the austenite boundary. The hatched region is due to both transformations but is here allocated to allotriomorphic ferrite.

radius $\eta_\alpha Z$ as in Chapter 2. Each plate of Widmanstätten ferrite is approximated as a rectangular parallelepiped, the lengthening rate (G) of which in a direction normal to the austenite boundary, is estimated using the Trivedi theory for the diffusion–controlled growth of a particle in the shape of a parabolic cylinder [Trivedi, 1970]. The thickening rate of Widmanstätten ferrite is assumed to be βG^2 where the aspect ratio β is 0.045. This value was obtained by fitting to experimental data on welds. Nucleation at grain edges or corners is ignored, so that the analysis strictly only applies at the high supersaturations.

The thickness of an allotriomorph is related to the square root of time via the one–dimensional parabolic thickening rate constant α_1. The latter is calculated as a function of the alloy chemistry, diffusion coefficient *etc.* as described in Chapter 1 [Bhadeshia, 1985c]. The general theory of overall transformation kinetics has been reviewed by Christian [1975].

The method of Cahn [1956a] for grain boundary nucleated reactions was used in the derivation that follows. The simultaneous formation of allotriomorphic (α) and Widmanstätten ferrite (α_W) is illustrated in Fig. 4-3, where any overlap between the two transformation products is eliminated by converting extended volume into real volume.

Consider a plane test–surface of total area O, parallel to a particular boundary. The total extended area covered by the growth of α and α_W, $O^e_{\alpha+\alpha_W}$, is defined as the sum of the areas of intersection of the allotriomorphic ferrite discs (O^e_α) and Widmanstätten ferrite plates ($O^e_{\alpha W}$) with this test–plane. The

instant of time when a particular particle of ferrite nucleates is called the incubation time τ. It follows that the change $dO^e_{\alpha+\alpha w}$ in $O^e_{\alpha+\alpha w}$ due to ferrite nucleated in the time interval $t=\tau$ and $t=\tau+d\tau$ is:

$$\begin{aligned} O^e_{\alpha+\alpha w} &= O^e_{\alpha} + O^e_{\alpha W} \\ &= \int_0^{t-(y/\alpha_1)^2} (\eta\alpha_1)^2 \pi O_b I^B_\alpha (t-\tau) d\tau + \int_0^{t-(y/G)} (\beta G)^2 O_b I^B_{\alpha w} (t-\tau)^2 d\tau \end{aligned} \qquad (4-3)$$

where y is the distance between the boundary and an arbitrary plane parallel to the boundary. The nucleation rate of allotriomorphic and Widmanstätten ferrite is I^B_α and $I^B_{\alpha w}$ respectively.

It can be assumed that length of the Widmanstätten plate Gt is larger than the maximum thickness of any allotriomorph ($\alpha_1 t^{0.5}$), since the lengthening rate of α_W is much greater [Bhadeshia, 1985a]. It follows that:

$$O^e_{\alpha+\alpha w} = \begin{cases} \frac{1}{2}\pi O_b I^B_\alpha (\eta\alpha_1)^2 t^2 \left\{1 - \left(\frac{y}{\alpha_1 t^{0.5}}\right)^4\right\} \ldots & \\ \qquad \ldots + \frac{1}{3}\pi O_b I^B_W \beta G t^3 \left\{1 - \left(\frac{y}{Gt^3}\right)^3\right\}, & \text{for } 0 \leq y < \alpha_1 t^{0.5} \\ \frac{1}{3}\pi O_b I^B_W \beta G t^3 \left\{1 - \left(\frac{y}{Gt^3}\right)^3\right\}, & \text{for } \alpha_1 t^{0.5} \leq y < Gt \\ 0 & \text{for } Gt \geq y \end{cases} \qquad (4-4)$$

Given that the relationship between the extended area $O^e_{\alpha+\alpha w}$ and actual area $O_{\alpha+\alpha w}$ is [Christian, 1975; Cahn, 1956a]:

$$\frac{O^e_{\alpha+\alpha w}}{O} = -\ln\left(1 - \frac{O_{\alpha+\alpha w}}{O}\right) \qquad (4-5)$$

and assuming that there is no interference from other boundaries, the total volume of allotriomorphic and Widmanstätten ferrite $V^b_{\alpha+\alpha w}$ originating from this grain boundary is obtained by integrating for all y between negative and positive infinity:

$$\begin{aligned} V^b_{\alpha+\alpha w} &= \int_{-\infty}^{+\infty} O_{\alpha+\alpha w} dy \\ &= 2\int_0^{+\infty} O_{\alpha+\alpha w} dy \end{aligned} \qquad (4-6)$$

Thus,

$$\begin{aligned} V^b_{\alpha+\alpha w} &= 2O_b \int_0^{+\infty} \left\{1 - \exp\left(-\frac{O^e_{\alpha+\alpha w}}{O_b}\right)\right\} dy \\ &= 2O_b \left[\int_0^{\alpha_1 t^{0.5}} \left\{1 - \exp\left(-\frac{O^e_{\alpha+W}}{O_b}\right)\right\} dy + \int_{\alpha_1 t^{0.5}}^{Gt} \left\{1 - \exp\left(-\frac{O^e_{\alpha+\alpha w}}{O_b}\right)\right\} dy\right] \end{aligned} \qquad (4-7)$$

If the total grain boundary area is $O_B = \sum O_b$, then by substituting O_B for O_b in equation 4-7 the total extended volume $V^e_{\alpha+\alpha w}$ of allotriomorphic and Widmanstätten ferrite emanating from all boundaries

is found. This is a total *extended* volume because allowance was not made for impingement of particles originating from *different* boundaries. Thus,

$$V^e_{\alpha+\alpha_W} = 2O_B\left[\int_0^{\alpha_1 t^{0.5}}\left\{1-\exp\left(-\frac{O^e_{\alpha+\alpha_W}}{O_b}\right)\right\}dy + \int_{\alpha_1 t^{0.5}}^{Gt}\left\{1-\exp\left(-\frac{O^e_{\alpha+\alpha_W}}{O_b}\right)\right\}dy\right] \tag{4-8}$$

If V is total volume and S_V is the austenite grain surface per unit volume, then:

$$\frac{V^e_{\alpha+\alpha_W}}{V} = 2S_V\left[\int_0^{\alpha_1 t^{0.5}}\left\{1-\exp\left(-\frac{O^e_{\alpha+\alpha_W}}{O_b}\right)\right\}dy + \int_{\alpha_1 t^{0.5}}^{Gt}\left\{1-\exp\left(-\frac{O^e_{\alpha+\alpha_W}}{O_b}\right)\right\}dy\right] \tag{4-9}$$

Given that the relationship between extended volume $V^e_{\alpha+\alpha_W}$ and actual volume $V_{\alpha+\alpha_W}$ is

$$\frac{V_{\alpha+\alpha_W}}{V\phi} = 1-\exp\left(-\frac{V^e_{\alpha+\alpha_W}}{V\phi}\right) \tag{4-10}$$

where $\phi = (x^{\gamma\alpha} - \overline{x}) / (x^{\gamma\alpha} - x^{\alpha\gamma})$ and $x^{\gamma\alpha}$ is the mole fraction of carbon in the austenite which is in paraequilibrium [Hultgren, 1947] with ferrite, $x^{\alpha\gamma}$ is the corresponding concentration in ferrite in paraequilibrium with austenite, and $\overline{x}$ is the mean carbon concentration in the steel.

The actual fraction of ferrite, normalised by its equilibrium volume fraction, can then be obtained:

$$\zeta_{\alpha+\alpha_W} = \frac{V_{\alpha+\alpha_W}}{V\phi} \tag{4-11}$$

It is now necessary to estimate individual volume fractions of allotriomorphic ferrite and Widmanstätten ferrite. That of allotriomorphic ferrite originating from one grain boundary is:

$$V^b_\alpha \approx 2\int_0^{\alpha_1 t^{0.5}} O_{\alpha+\alpha_W}\,dy \tag{4-12}$$

The approximation arises because this calculation includes some Widmanstätten ferrite. This can be seen schematically in Fig. 4-2. The hatched region represents contributions from both allotriomorphic and Widmanstätten ferrite, but is here allocated to allotriomorphic ferrite alone. Since the amount of α_W within the region where α exists is small, the approximation is bound in general to be reasonable. Furthermore, experimental observations only classify as Widmanstätten ferrite, that region of the plates which extend beyond the α layers. It follows that

$$V^b_\alpha \approx 2O_b\int_0^{\alpha_1 t^{0.5}}\left\{1-\exp\left(\frac{O^e_{\alpha+W}}{O_b}\right)\right\}dy \tag{4-13}$$

and the extended volume V^e_α of allotriomorphic ferrite can be obtained by:

$$V^e_\alpha \approx 2O_B\int_0^{\alpha_1 t^{0.5}}\left\{1-\exp\left(\frac{O^e_{\alpha+W}}{O_b}\right)\right\}dy \tag{4-14}$$

The actual fraction of Widmanstätten ferrite normalised by the equilibrium volume of ferrite $\xi_{\alpha W}$ can now be obtained by substituting the ξ_{α} from the total ferrite fraction transformed $\xi_{\alpha+\alpha W}$:

$$\zeta_{\alpha W} = \zeta_{\alpha+\alpha W} - \zeta_{\alpha} \qquad (4-15)$$

Bainite and acicular ferrite also occur in steel welds at lower temperatures but possibly simultaneously with the allotriomorphic and Widmanstätten ferrite. For the present Chapter, the transformation to α and α_W is arbitrarily stopped at the calculated bainite–start (B_S) temperature [Bhadeshia, 1981a]. This may be a reasonable assumption if transformations below B_S occur rapidly. Bainite is assumed to occur when the current temperature becomes smaller that the calculated T_0' temperature* of untransformed austenite. The stored energy for the bainitic transformation has been taken to be 350 J mol^{-1} by best fitting to the published experimental data discussed later [Evans, 1983; Bhadeshia *et al.*, 1985a; Gretoft *et al.*, 1985; Bhadeshia *et al.*, 1986b; Svensson and Gretoft, 1990; Evans, 1990; Evans, 1991; Surian *et al.*, 1994; Vercesi and Surian, 1996]. This is slightly lower than 400 J mol^{-1} measured elsewhere [Bhadeshia, 1981a]. This was found to be necessary in order to get better agreement with experimental data on the steel welds to be discussed later. The flowchart illustrating the calculation scheme is shown in Fig. 4-4.

* Bainite forms by diffusionless transformation at a temperature just below T_0' where the austenite and ferrite of same composition have identical free energy accounting for the stored energy of ferrite [Bhadeshia, 1992]

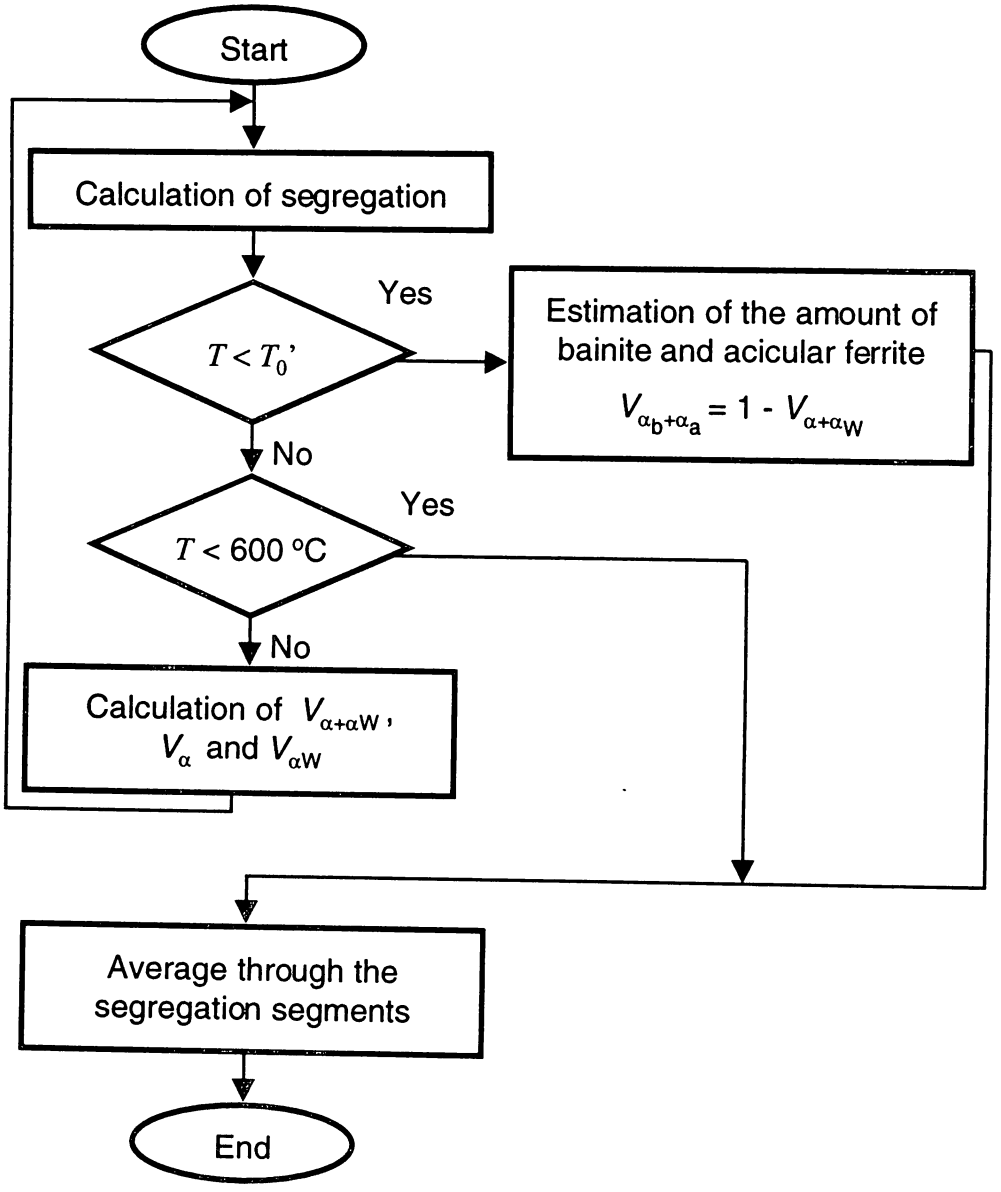

Fig. 4-4 : Flowchart showing the calculation procedure.Where $V_{\alpha+\alpha_W}$ is the total volume fraction of allotriomorphic and Widmanstätten ferrite, V_α is the volume fraction of allotriomorphic ferrite, V_α is the volume fraction of Widmanstätten ferrite and $V_{\alpha_b+\alpha_a}$ is the total volume fraction of bainite and acicular ferrite.

Many of the other theoretical details, including austenite grain structure of welds, anisothermal transformation, solidification–induced segregation in welds have been reviewed in Chapters 1 and 2 and are not reproduced here since Widmanstätten ferrite is the main focus of this Chapter.

4.4 Widmanstätten Ferrite Start

Ali and Bhadeshia [1990] have demonstrated that it is possible to explain the large variations in Widmanstätten ferrite-start temperatures using a theory due to Bhadeshia [1981a; 1982a]. This theory has been applied here to determine the Widmanstätten ferrite–start temperature. It is necessary to satisfy two conditions (equations 1-47 and 1-48) before α_W can nucleate.

4.5 Application and Assessment

The experimental data used to validate the model are listed in Tables 4-1 and 4-2, compiled from the published literature [Bhadeshia, 1982a; Evans, 1983; Bhadeshia *et al.*, 1985a; Gretoft *et al.*, 1985; Bhadeshia *et al.*, 1986b; Evans, 1990; Svensson and Gretoft, 1990; Evans, 1991; Surian *et al.*, 1994; Vercesi and Surian, 1996;].

Table 4-1 : Chemical compositions of the weld metals / wt.%.

Mark	Chemical compositions of the weld metals (wt.%)										Ref.
	C	Si	Mn	P	S	Cu	Cr	Ni	Mo	V	
C1	0.045	0.30	0.65	0.008	0.006	-	-	-	-	-	
C2	0.044	0.32	0.98	0.008	0.006	-	-	-	-	-	
C3	0.044	0.32	1.32	0.007	0.006	-	-	-	-	-	
C4	0.045	0.30	1.72	0.008	0.006	-	-	-	-	-	
C5	0.059	0.33	0.60	0.008	0.007	-	-	-	-	-	
C6	0.063	0.35	1.00	0.008	0.006	-	-	-	-	-	
C7	0.066	0.37	1.35	0.007	0.005	-	-	-	-	-	
C8	0.070	0.33	1.77	0.008	0.006	-	-	-	-	-	(1)
C9	0.099	0.35	0.65	0.009	0.008	-	-	-	-	-	
C10	0.098	0.32	1.05	0.009	0.007	-	-	-	-	-	
C11	0.096	0.30	1.29	0.009	0.007	-	-	-	-	-	
C12	0.093	0.33	1.65	0.007	0.007	-	-	-	-	-	
C13	0.147	0.40	0.63	0.007	0.008	-	-	-	-	-	
C14	0.152	0.41	1.00	0.007	0.007	-	-	-	-	-	
C15	0.148	0.38	1.40	0.007	0.007	-	-	-	-	-	
C16	0.141	0.36	1.76	0.007	0.006	-	-	-	-	-	
CM1	0.030	0.45	0.78	0.010	0.013	-	-	-	-	-	
CM2	0.032	0.45	1.27	0.010	0.008	-	-	-	-	-	
CM3	0.031	0.42	1.71	0.010	0.004	-	-	-	-	-	
CM4	0.032	0.45	2.05	0.010	0.020	-	-	-	-	-	
CM5	0.059	0.34	0.77	0.010	0.010	-	-	-	-	-	
CM6	0.059	0.33	1.09	0.010	0.008	-	-	-	-	-	
CM7	0.059	0.30	1.44	0.010	0.006	-	-	-	-	-	
CM8	0.065	0.33	1.83	0.010	0.003	-	-	-	-	-	(2)
CM9	0.090	0.41	0.78	0.010	0.013	-	-	-	-	-	
CM10	0.089	0.35	1.18	0.010	0.011	-	-	-	-	-	
CM11	0.088	0.37	1.59	0.010	0.011	-	-	-	-	-	
CM12	0.098	0.39	2.25	0.014	0.008	-	-	-	-	-	
CM13	0.120	0.43	0.86	0.014	0.011	-	-	-	-	-	
CM14	0.120	0.44	1.35	0.014	0.010	-	-	-	-	-	
CM15	0.130	0.37	1.83	0.011	0.010	-	-	-	-	-	
CM16	0.110	0.36	2.18	0.011	0.008	-	-	-	-	-	
AL1	0.069	0.35	0.64	0.009	0.007	-	-	-	-	-	(3)
CMT1	0.029	0.55	1.08	0.008	0.011	-	-	-	-	-	
CMT2	0.061	0.53	1.01	0.010	0.009	-	-	-	-	-	(4)
CMT3	0.080	0.58	1.15	0.010	0.010	-	-	-	-	-	
CMT4	0.100	0.55	1.02	0.010	0.010	-	-	-	-	-	
WP1	0.040	0.44	1.58	0.015	0.007	-	0.30	1.94	0.33	<0.010	
WP2	0.047	0.48	1.62	0.015	0.008	-	0.30	1.92	0.34	<0.010	(5)
WP3	0.045	0.54	1.69	0.016	0.008	-	0.31	1.98	0.34	<0.010	
CR1	0.038	0.36	1.03	0.014	0.010	0.07	0.04	2.00	0.37	0.01	
CR2	0.040	0.35	1.00	0.014	0.011	0.07	0.38	1.96	0.35	0.01	
CR3	0.041	0.35	1.03	0.014	0.010	0.07	0.78	1.96	0.37	0.01	
CR4	0.042	0.38	1.06	0.015	0.011	0.07	1.15	1.95	0.37	0.01	
CR5	0.042	0.40	1.07	0.014	0.011	0.07	1.50	1.98	0.35	0.01	
CR6	0.042	0.38	1.06	0.014	0.011	0.07	1.82	1.92	0.34	0.01	(6)
CR7	0.042	0.33	1.46	0.013	0.010	0.065	0.04	1.98	0.37	0.01	
CR8	0.040	0.35	1.43	0.013	0.010	0.065	0.41	1.94	0.36	0.01	
CR9	0.048	0.34	1.37	0.013	0.010	0.065	0.75	1.86	0.34	0.01	
CR10	0.043	0.34	1.45	0.013	0.010	0.065	1.15	1.98	0.38	0.01	
CR11	0.044	0.33	1.39	0.014	0.011	0.065	1.43	1.88	0.36	0.01	
CR12	0.040	0.36	1.39	0.014	0.011	0.065	1.89	1.99	0.38	0.01	
NI1	0.07	0.38	1.20	-	-	-	-	0.94	-	-	(7)
MO1	0.14	0.29	1.44	0.029	0.006	-	0.05	0.06	0.01	-	
MO2	0.14	0.24	1.54	0.027	0.029	-	0.03	0.03	0.19	-	(8)
MO3	0.14	0.31	1.32	0.028	0.006	-	0.03	0.03	0.24	-	
MO4	0.13	0.27	1.60	0.025	0.027	-	0.04	0.04	0.39	-	
V1	0.073	0.35	0.64	0.004	0.005	-	-	-	-	0.0003	
V2	0.071	0.36	0.63	0.006	0.007	-	-	-	-	0.0210	
V3	0.071	0.40	0.64	0.006	0.008	-	-	-	-	0.0435	
V4	0.074	0.36	0.63	0.005	0.008	-	-	-	-	0.0600	
V5	0.072	0.36	0.64	0.006	0.008	-	-	-	-	0.0815	(9)
V6	0.077	0.31	1.33	0.005	0.007	-	-	-	-	0.0004	
V7	0.072	0.33	1.22	0.006	0.008	-	-	-	-	0.0190	
V8	0.077	0.26	1.36	0.007	0.007	-	-	-	-	0.0425	
V9	0.078	0.30	1.35	0.007	0.007	-	-	-	-	0.0595	
V10	0.076	0.26	1.36	0.006	0.007	-	-	-	-	0.1005	

Ref.: (1): Evans, G. M., 1983
(2): Svensson, L-E. and Gretoft, B., 1990
(3): Evans, G. M., 1990
(4): Bhadeshia, H. K. D. H. *et al.*, 1985a
(5): Vercesi, J. and Surian, E., 1996
(6): Surian, E. *et al.*, 1994
(7): Gretoft, B. *et al.*, 1985
(8): Bhadeshia, H. K. D. H. *et al.*, 1986b
(9): Evans, G. M., 1991

Table 4-2 : Heat input and austenite parameters of the welds.

Mark	Heat input / kJ cm^{-1}	Austenite grain parameters		Ref.
		Average columnar grain width / μm	S_V / 10^4 m^{-1}	
C1	10	104	1.67	
C2		98	1.77	
C3		102	1.70	
C4		94	1.84	
C5		94	1.84	
C6		86	2.04	
C7		91	1.90	
C8		79	2.19	(1)
C9		69	2.51	
C10		74	2.34	
C11		65	2.66	
C12		63	2.75	
C13		67	2.59	
C14		63	2.75	
C15		63	2.75	
C16		49	3.53	
CM1	10.4	65	2.66	
CM2		55	3.15	
CM3		42	4.12	
CM4		42	4.12	
CM5		71	2.44	
CM6		65	2.66	
CM7		60	2.89	
CM8		48	3.61	(2)
CM9		45	3.85	
CM10		45	3.85	
CM11		45	3.85	
CM12		45	3.85	
CM13		36	4.81	
CM14		36	4.81	
CM15		40	4.33	
CM16		45	3.85	
AL1	10	79	2.18	(3)
CMT1	10	121	1.91	
CMT2		115	2.01	(4)
CMT3		118	1.96	
CMT4		95	2.43	
WP1	22.4	215.5	0.804	
WP2	20.0	188.7	0.918	(5)
WP3	16.4	159.4	1.09	
CR1	21	115	1.51	
CR2		109	1.59	
CR3		104	1.67	
CR4		95	1.82	
CR5		92	1.88	
CR6		90	1.92	(6)
CR7		102	1.70	
CR8		98	1.77	
CR9		93	1.86	
CR10		90	1.92	
CR11		88	1.97	
CR12		87	1.99	
NI1	10.4	60	2.89	(7)
MO1	11.8	72	2.41	
MO2		72	2.41	(8)
MO3		72	2.41	
MO4		72	2.41	
V1	10	118	1.46	
V2		96	1.81	
V3		106	1.64	
V4		90	1.92	
V5		96	1.81	(9)
V6		86	2.02	
V7		95	1.83	
V8		100	1.73	
V9		83	2.09	
V10		87	2.00	

The model includes chemical segregation effects as described in Chapter 1 and 2; the calculations subdivide the assembly into regions (segments) of different chemical composition according to the composition profile expected during solidification. The nucleation equation for Widmanstätten ferrite requires an estimation of two adjustable constants, which were determined by best fitting to the experimental data.

$$\frac{K'_{W1}}{u} = 5.0 \times 10^5 \, \mathrm{m^2 s}$$

where u is the volume of a Widmanstätten ferrite platelet and, in order to get best fit with the experimental data, is assumed to be:

$$u = \left(10.0 \times 10^{-6}\right) \times \left(10.0 \times 10^{-6}\right) \times \left(0.2 \times 10^{-6}\right) \, \mathrm{m^3}$$

$$K_{W2} = 1.5 \times 10^5 \, \mathrm{J \, mol^{-1}}$$

Fig. 4-5 shows an example calculation for allotriomorphic and Widmanstätten ferrite in weld C3 (Tables 4-1 and 4-2).

The influence of solidification induced segregation on the formation of Widmanstätten and allotriomorphic ferrite is incorporated in the present model using Scheil equation [Scheil, 1942] for solidification, as in the Chapters 1 and 2 in which the detailed procedure is described. For simplicity, three solidification segments 1, 2 and 3 are taken for the calculation here where the segment 1 has the largest depletion of substitutional elements whereas 3 is the most enriched by solidification induced segregation (Fig. 4-6).

Actual calculated compositions of the three segments are given in Fig. 4-7.

It can be seen from Fig. 4-5 that the growth of Widmanstätten ferrite in segment 3 is hindered by the formation of bainite and acicular ferrite at about 630 °C. This does not occur in segments 1 and 2 where Widmanstätten ferrite grows rapidly, the resulting carbon partitioning preventing the bainite from forming; the calculations were in these cases stopped when 600 °C was reached since the fraction of austenite left untransformed became very small.

Calculated results of allotriomorphic ferrite for all these welds are illustrated in Figs. 4-8 to 4-11. The degree of the agreement between experimental and calculated results is in general similar to Chapter 2. Calculation of Widmanstätten ferrite does not seem to affect the calculation of allotriomorphic ferrite.

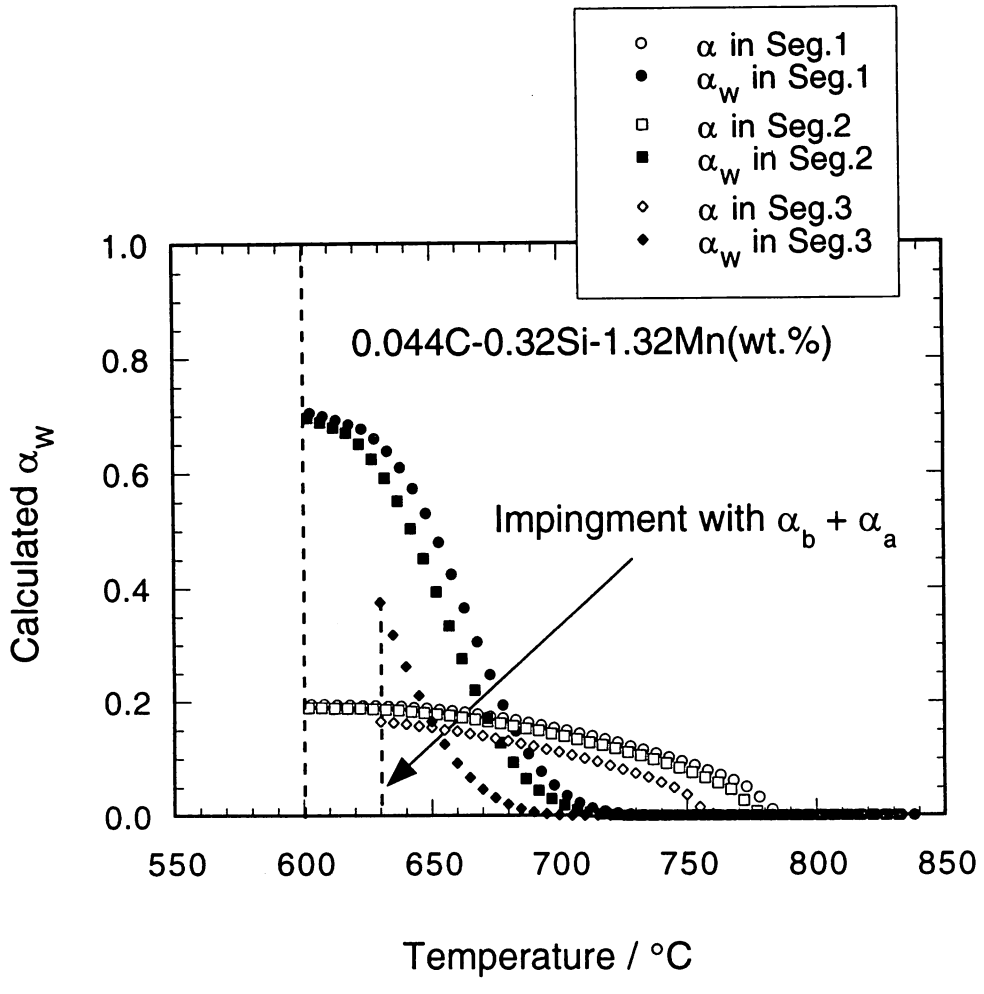

Fig. 4-5 : Example calculation of nucleation, growth and impingement of allotriomorphic and Widmanstätten ferrite in Weld C3.

Calculated results of Widmanstätten ferrite for the simple C–Si–Mn steels listed in Tables 4-1 and 4-2 are illustrated in Figs. 4-11 to 4-14. The calculations are based on the mean value from one hundred solidification segments per weld. The agreement is in general good given that all the calculations are based on a single set of parameters even though the data are from diverse sources. Note also that there are no arbitrary assumptions about the transition from allotriomorphic to Widmanstätten ferrite as in previous work.

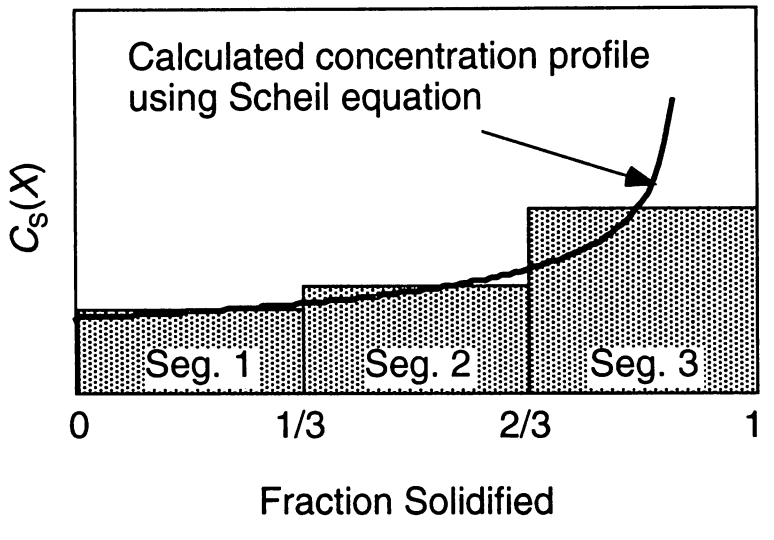

Fig. 4-6 : Schematic illustration of the concentration profile calculated using the Scheil equation and the partitioning of the profile into discrete segments where $C_S(X)$ is chemical concentration of the alloying element X.

Calculated results of Widmanstätten ferrite for the alloyed steels listed in the Tables 4-1 and 4-2 are illustrated in Fig. 4-15. One of the reasons for the discrepancies apparent in Fig. 4-11 is undoubtedly related with inaccuracies in the experimental data. There are large differences in the published data for quite similar two different C–Si–Mn–Ni–Cr–Mo alloyed welds series (See weld WP and CR series in the Tables 4-1 and 4-2.). These difficulties are natural given the problems associated with careful microstructural characterisation, especially in alloy welds.

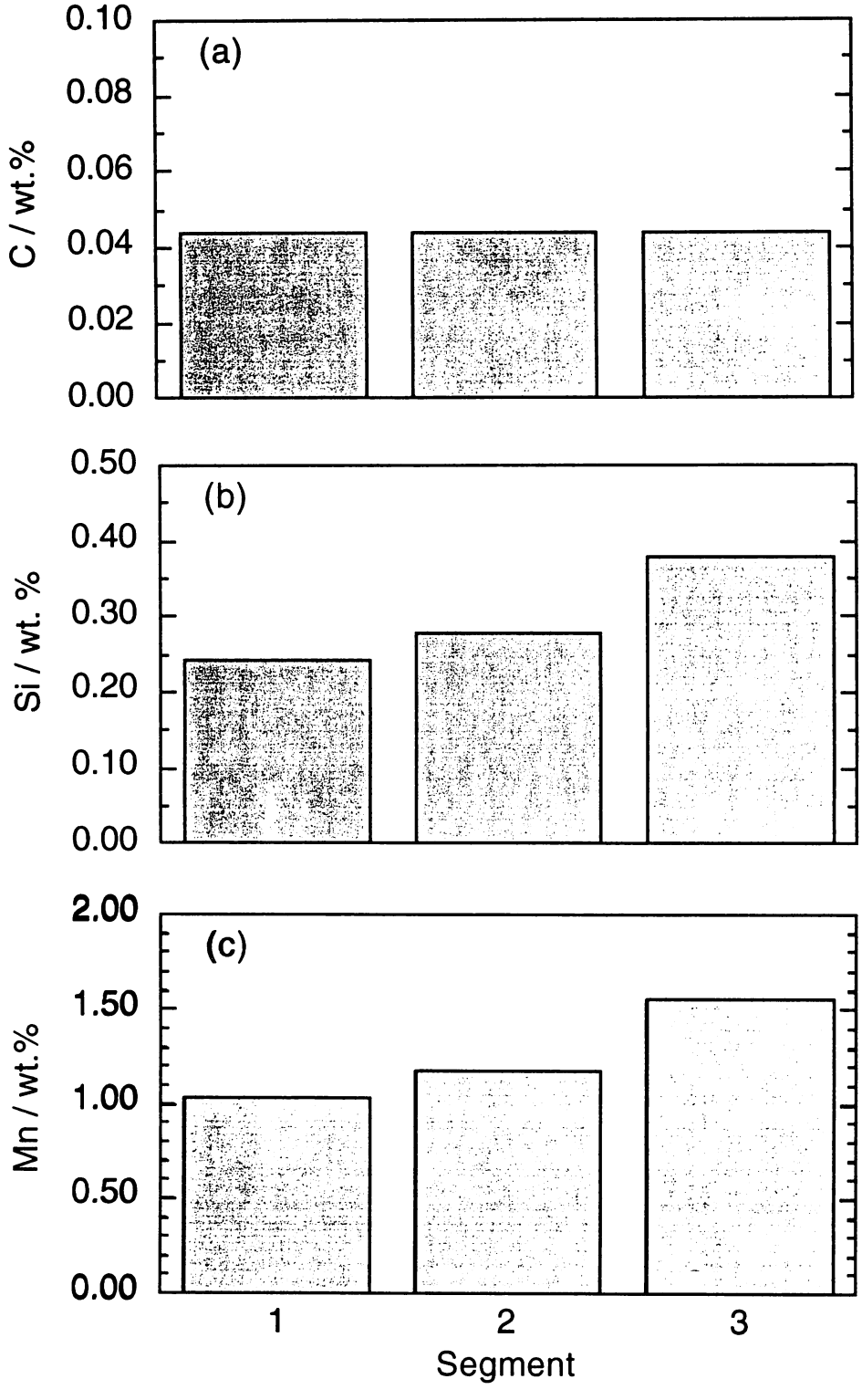

Fig. 4-7 : Calculated concentrations based on Scheil equation in each segment of weld C3 (0.044C–0.32Si–1.32Mn in wt.%).

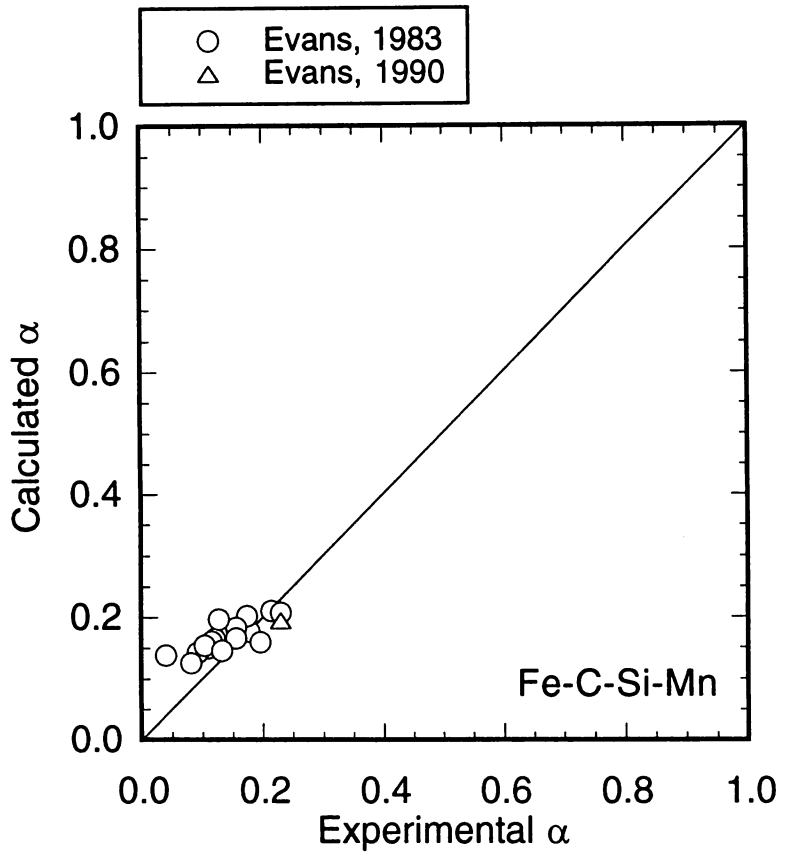

Fig. 4-8 : Plots of calculated volume fractions of allotriomorphic ferrite versus those measured for Fe–C–Si–Mn alloys. Experimental data are from Evans [1983; 1990].

4.6 Conclusions

A new simultaneous transformation model based on the detailed nucleation and growth functions for the allotriomorphic and Widmanstätten ferrite transformations in steel weld has been proposed. This includes a description of hard impingement with the formation of bainite and acicular ferrite.

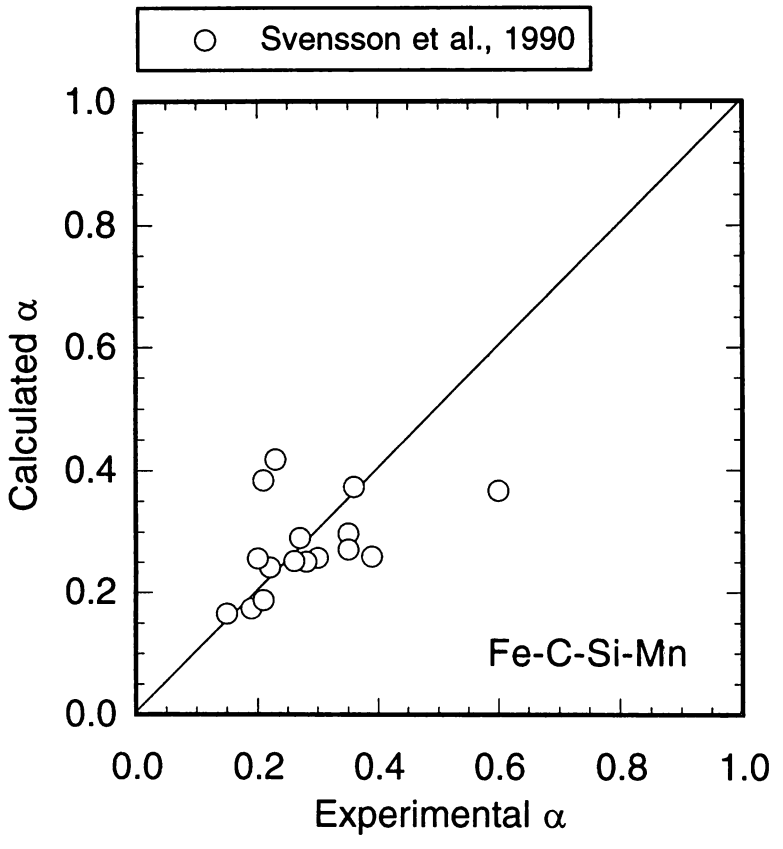

Fig. 4-9 : Plots of calculated volume fractions of allotriomorphic ferrite versus those measured for Fe–C–Si–Mn alloys. Experimental data are from Svensson and Gretoft [1990]

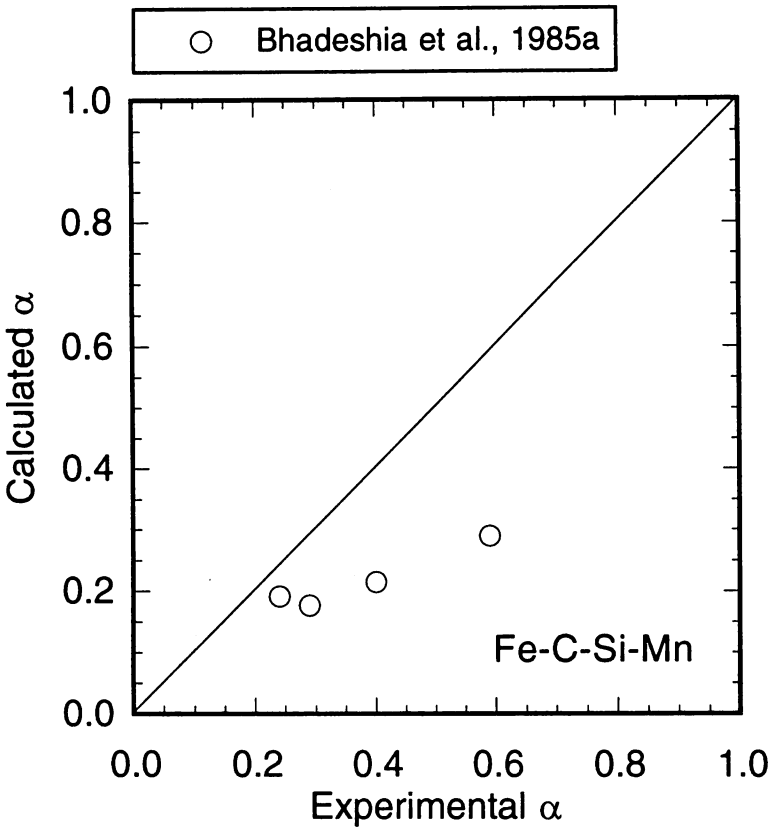

Fig. 4-10: Plots of calculated volume fractions of allotriomorphic ferrite versus those measured for Fe–C–Si–Mn alloys. Experimental data are from Bhadeshia *et al.* [1985a].

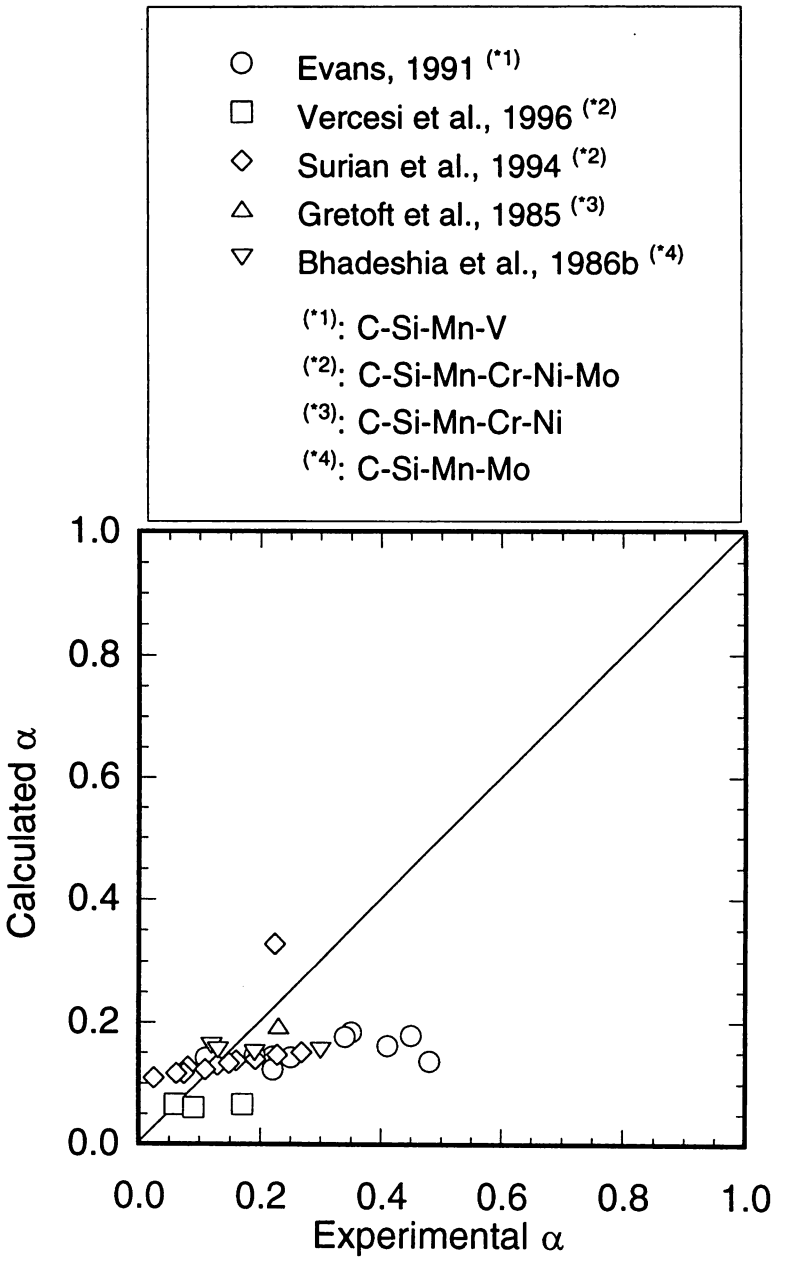

Fig. 4-11 : Plots of calculated volume fractions of allotriomorphic ferrite versus those measured for alloyed steel. Experimental data are from the published literature.

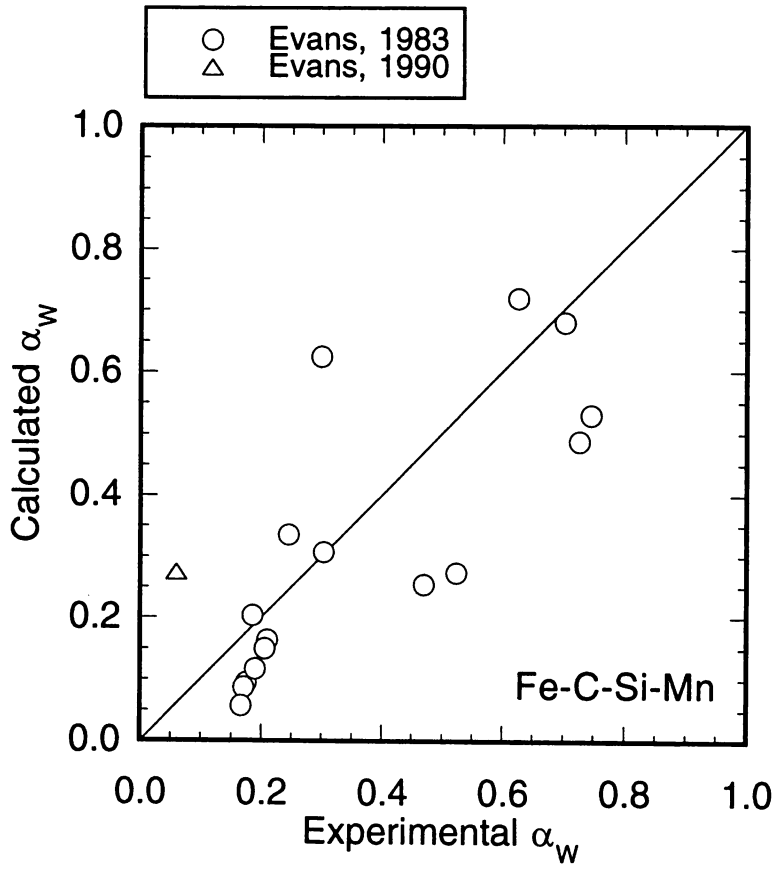

Fig. 4-12 : Plots of calculated volume fractions of Widmanstätten ferrite versus those measured for Fe–C–Si–Mn alloys. Experimental data are from Evans [1983; 1990].

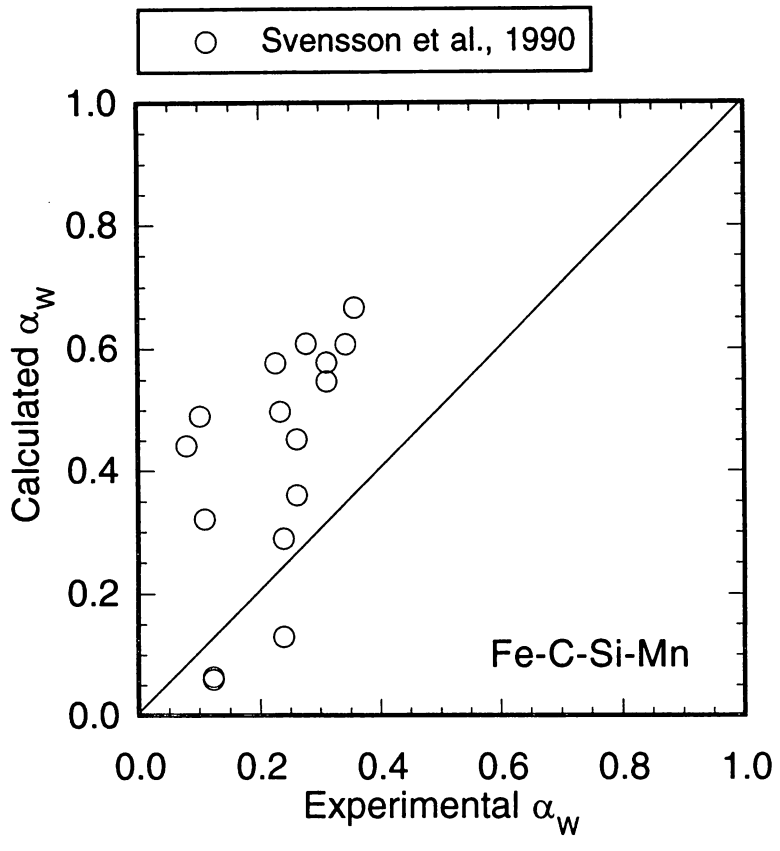

Fig. 4-13 : Plots of calculated volume fractions of Widmanstätten ferrite versus those measured for Fe–C–Si–Mn alloys. Experimental data are from Svensson and Gretoft [1990].

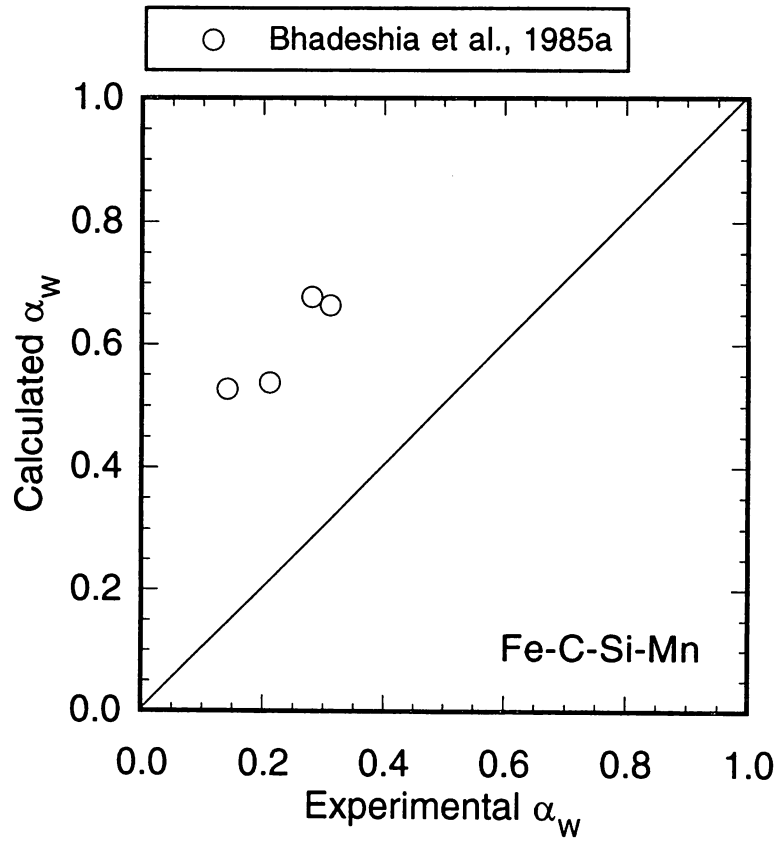

Fig. 4-14 : Plots of calculated volume fractions of Widmanstätten ferrite versus those measured for Fe–C–Si–Mn alloys. Experimental data are from Bhadeshia *et al.* [1985a].

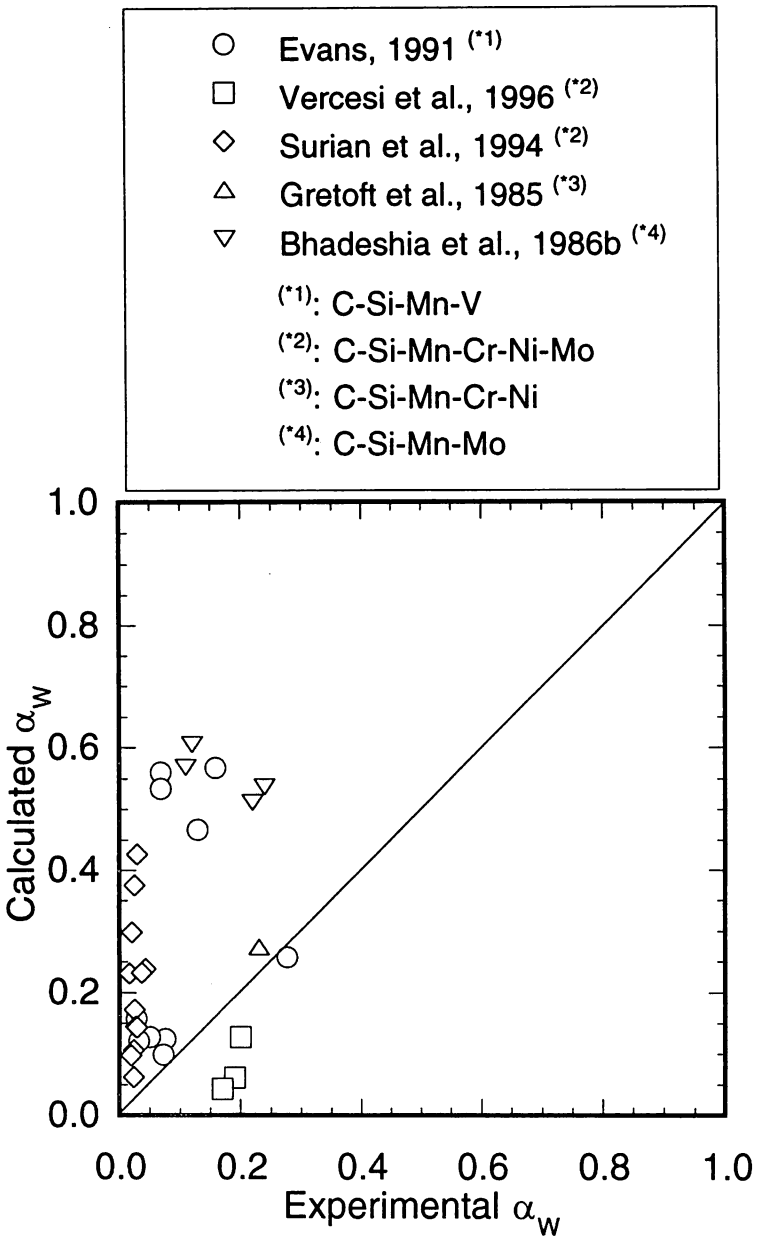

Fig. 4-15 : Plots of calculated volume fractions of Widmanstätten ferrite versus those measured for alloyed steel. Experimental data are from the published literature. Note that experimental volume fraction of Widmanstätten ferrite of two different C-Si-Mn-Cr-Ni-Mo series (by Vercesi and Surian [1996] and Surian *et al.* [1994]) show large discrepancies, while the chemical compositions are quite similar (See Table 4-1.).

CHAPTER FIVE

Thermodynamic Estimation of Inclusion Characteristics in Low-Alloy Steel Weld Metals

5.1 Introduction

Since sufficiently high toughness is required at low temperatures for weld metals used in the fabrication of pipelines and offshore oil-and-gas production platforms, many researchers have studied methods of optimising the mechanism of toughness. It is now widely accepted that this can be done in low-alloy steels by maximising the amount of acicular ferrite while reducing the amount of allotriomorphic ferrite in the as-welded regions. This fact has driven extensive studies on the transformation mechanism of acicular ferrite.

Acicular ferrite is known to nucleate on non-metallic substrates. Several kinds of inclusions have been reported to be effective acicular ferrite nucleation sites in weld metals. They are, for example, TiO [Mori *et al.*, 1981], titanium-oxides [Watanabe and Kojima, 1980], TiN [Ito and Nakanishi, 1975] and $MnO \cdot Al_2O_3$ [Dowling *et al.*, 1986; Horii *et al.*, 1995b]. The titanium content in the inclusions is a particularly important factor since it affects the crystal structure of the oxide [Horii *et al.*, 1995b]. Optimising the amount of deoxidising elements, including silicon, manganese, aluminium and titanium, in steel weld metals is thus necessary in order to maximise the amount of acicular ferrite. The number density of inclusions should also be important because it determines the number of sites for acicular ferrite nucleation.

Under these circumstances, the mathematical modelling of inclusion formation is now becoming an important issue [Babu *et al.*, 1995; Koseki *et al.*, 1997; Hsieh *et al.*, 1996]. Babu *et al.* introduced the principles of ladle deoxidisation and overall transformation kinetics to the modelling of inclusion formation in carbon-manganese steel welds [Babu *et al.*, 1995]. Koseki *et al.* employed Thermo-Calc^{TM} † to predict the stability of oxide inclusions in welds, and explained previous experimental results about

† Thermo-Calc^{TM} is a computer program, which when presented with thermodynamic data allows

the effect of weld alloy chemistry on acicular ferrite production [Koseki *et al.*, 1997]. If this method is confirmed to be applicable to wide range of steel welds, it would be a very potent and convenient tool for welding materials design.

The present study applies the method proposed by Koseki *et al.* [1997] to the prediction of the number density and chemical compositions of inclusions in low-alloy steel weld metals and examines whether equilibrium calculations are capable of predicting the inclusion characteristics over a wide range of weld compositions.

5.2 Computational Details

Calculations were performed for the Fe-Si-Mn-Ti-Al-N-O alloy system as in the previous work by Koseki *et al.* [1997]. Phases including liquid, bcc (body-centred cubic) iron, fcc (face-centred cubic) iron, slag, oxides and nitrides listed in the Table 5-1 were taken into account in the calculations.

Table 5-1 : Alloy system, phases, oxides and nitrides taken into account in the present work.

Alloy system:	Fe-Si-Mn-Al-Ti-N-O
Phases:	liquid (Fe, Si, Mn, Al, Ti, N, O)
	γ -fcc (Fe, Si, Mn, Al, Ti, N, O)
	δ -bcc (Fe, Si, Mn, Al, Ti, N, O)
	slag (Fe-Si-Mn-Al-Ti-N-O)
Oxides:	Al_2O_3, $Al_2O_3TiO_2$
	FeO, Fe_2O_3, $FeOAl_2O_3$, $2FeOSiO_2$
	MnO, $MnOAl_2O_3$, $MnOSiO_2$, $2MnOSiO_2$, $MnOTiO_2$, $2MnOTiO_2$
	SiO_2, $2SiO_2$-$3Al_2O_3$
	TiO, $Ti_2O_3(TiO_{1.5})$, $Ti_3O_5(TiO_{1.67})$, $Ti_4O_7(TiO_{1.75})$, TiO_2
Nitrides:	TiN, Ti_2N

The liquid, bcc (body-centred cubic) iron, fcc (face-centred cubic) iron and slag were assumed to be

assessment of phase stabilities [Sundman *et al.*, 1985].

the solutions containing all the elements considered, while the oxides and nitrides were assumed to be stoichiometric compounds as shown in Table 5-1. Thermodynamic data for the liquid, bcc and fcc were taken from the SSOL database in Thermo-Calc^{TM} [Sundman *et al.*, 1985] version J. Data for the slag were from the set assessed by Lehmann *et al.* [1990] which was extended to allow a larger number of components and phases including titanium oxides. Data for the stoichiometric compounds of oxides were taken from the SSUB database in Thermo-Calc^{TM} [Sundman *et al.*, 1985].

The calculations were conducted for the temperature 1800 K where the melt is assumed to be close to the liquidus temperature. The melt thus should have the same chemical composition as the weld metal of interest from which the composition was finally obtained by chemical analysis. As stated in the previous work by Koseki *et al.*, equilibrium was assumed between inclusions and the rest of the melt. Slag, oxides and nitrides predicted to exit were assumed to form the inclusions in the final weld metals. Deoxidisations in liquid+solid phase or solid phase were neglected in the present study. Using actual values of the mean three-dimensional inclusion diameter ($\bar{d}_V$) data for each weld reported in literature [Kluken and Grong, 1989; Fox *et al.*, 1996; Thewlis, 1989a; b; 1994; Dowling *et al.*, 1986], the number of particles per unit volume (N_V) was calculated as follows [Ashby and Ebeling, 1933; Underwood, 1970; Kluken and Grong, 1989];

$$N_V = \frac{6V_V}{\pi \bar{d}_V^3} \qquad (5-1)$$

where V_V is the volume fraction of inclusions. Since an equilibrium calculation by Thermo-Calc^{TM} gives the weights of slag, oxides and nitrides formed in a given mole of the system, V_V was approximated by;

$$V_V = \frac{\frac{W_{slag}}{\rho_{slag}} + \sum\left(\frac{W_{oxide,i}}{\rho_{oxide,i}}\right) + \sum\left(\frac{W_{nitride,j}}{\rho_{nitride,j}}\right)}{V_{total}} \qquad (5-2)$$

where W_{slag} and ρ_{slag} are the weight and density of the slag respectively, $W_{oxide,i}$ and $\rho_{oxide,i}$ are the weight and density of oxide i respectively, $W_{nitride,j}$ and $\rho_{nitride,j}$ are the weight and density of nitride j respectively and V_{total} is the total volume of the system approximated by:

$$V_{total} = \frac{W_{total}}{\rho_{Fe}} \qquad (5-3)$$

where W_{total} is the molar weight of the system considered and ρ_{Fe} is the density of iron. Density data used in the calculations are listed in Table 5-2 [American Institute of Physics Handbook, 1972; Touloukian *et al.*, 1970; Samsonova, 1969].

Table 5-2 : Density data used in the calculation of number densities and spacings of inclusion particles.

	Density (g cm^{-3})
Fe	7.86[†1]
Slag	2.2[†2]
Ti_3O_5	4.24[†3]
$2SiO_2Al_2O_3$ (Mullite)	3.97[†4]
Al_2O_3	3.97[†5]

Note: [†1]: Ref. [American Institute of Physics Handbook, 1972].
[†2]: Estimated using the density data of amorphous SiO_2 in Ref. [Touloukian *et al.*, 1970].
[†3]: Estimated using the density data of TiO_2 in Ref. [Samsonova, 1969].
[†4]: Estimated using the density data of Al_2O_3 in Ref. [Samsonova, 1969].
[†5]: Ref. [Samsonova, 1969].

Density data could not be found for some oxides, in which data of other similar oxides were used instead. Mean centre-to-centre [Kluken and Grong, 1989] and surface-to-surface [Thewlis, 1989a; b; 1994] spacing of inclusions (λ_V and L_V)can be computed using the following equations respectively;

$$\lambda_V = 0.554 \left(\frac{1}{N_V}\right)^{\frac{1}{3}} \qquad (5-4)$$

$$L_V = 1.36 N_a^{-1/2} \left(0.885 - V_V^{1/2}\right) \qquad (5-5)$$

where N_a is the number of particles per unit area, calculated using the following relationship [Ashby and Ebeling, 1933; Underwood, 1970; Kluken and Grong, 1989]:

$$N_a = N_V \bar{d}_V \qquad (5-6)$$

5.3 Experimental Data

The experimental data used to examine the model are listed in Tables 5-3, 5-4 and 5-5, being taken from published literature [Dowling *et al.*, 1986; Kluken and Grong, 1989; Thewlis, 1989a;

b; 1994; Fox *et al.*, 1996; Evans, 1995]. They are also available in digitalised form on http://www.msm.cam.ac.uk/map/data/materials/weldinc.html. Table 5-3 shows the chemical compositions of the welds. The geometrical characteristics of the inclusions are listed in Table 5-4.

Table 5-3 : Chemical compositions of welds studied†. / wt.%.

Mark	Si	Mn	Al	Ti	N	O	Ref.
K1	0.48	1.86	0.018	0.005	0.005	0.034	
K2	0.55	1.84	0.020	0.025	0.005	0.037	
K3	0.69	1.88	0.028	0.063	0.008	0.035	
K4	0.52	1.87	0.041	0.005	0.005	0.030	
K5	0.58	1.95	0.037	0.022	0.005	0.039	
K6	0.69	1.97	0.044	0.058	0.006	0.040	
K7	0.53	1.90	0.062	0.008	0.005	0.032	
K8	0.62	1.92	0.062	0.032	0.005	0.031	
K9	0.62	1.78	0.053	0.053	0.006	0.031	
K10	0.28	1.66	0.010	0.003	0.005	0.021	Kluken *et al.*, 1989
K11	0.28	1.40	0.014	0.026	0.009	0.029	
K12	0.64	1.42	0.003	0.002	0.008	0.042	
K13	0.49	1.79	0.029	0.006	0.005	0.019	
K14	0.69	1.82	0.057	0.061	0.005	0.018	
K15	0.39	1.55	0.020	0.005	0.004	0.057	
K16	0.38	1.51	0.019	0.005	0.004	0.058	
K17	0.54	1.64	0.058	0.065	0.006	0.049	
K18	0.70	1.89	0.028	0.058	0.006	0.022	
K19	0.77	1.96	0.023	0.043	0.006	0.030	
K20	0.75	1.91	0.026	0.046	0.007	0.029	
F1	0.38	1.45	0.013	0.006	0.007	0.030	
F2	0.46	1.49	0.020	0.008	0.006	0.027	
F3	0.42	1.28	0.011	0.004	0.006	0.034	Fox *et al.*, 1996
F4	0.28	1.51	0.011	0.005	0.009	0.035	
F5	0.34	1.54	0.014	0.006	0.006	0.032	
T1	0.20	1.27	0.008	0.007	0.0072	0.037	
T2	0.21	1.28	0.009	0.006	0.0064	0.030	
T3	0.19	1.31	0.015	0.008	0.0071	0.036	
T4	0.20	1.29	0.020	0.007	0.0066	0.037	
T5	0.24	1.34	0.027	0.013	0.0059	0.029	
T6	0.24	1.35	0.032	0.013	0.0081	0.028	
T7	0.26	1.37	0.032	0.012	0.0081	0.028	
T8	0.25	1.37	0.040	0.013	0.0074	0.029	
T9	0.25	1.27	0.021	0.008	0.0080	0.032	
T10	0.23	1.29	0.022	0.007	0.0088	0.033	
T11	0.23	1.29	0.020	0.007	0.0077	0.033	Thewlis, 1989a; b; 1994
T12	0.21	1.36	0.012	0.025	0.0070	0.028	
T13	0.21	1.42	0.015	0.026	0.0066	0.025	
T14	0.21	1.40	0.021	0.029	0.0069	0.029	
T15	0.24	1.39	0.023	0.026	0.0070	0.030	
T16	0.24	1.42	0.025	0.029	0.0068	0.023	
T17	0.21	1.35	0.027	0.026	0.0076	0.033	
T18	0.24	1.38	0.030	0.027	0.0082	0.030	
T19	0.24	1.38	0.039	0.026	0.0075	0.027	
T20	0.26	1.39	0.023	0.027	0.0076	0.029	
T21	0.25	1.39	0.025	0.025	0.0079	0.030	
T22	0.25	1.38	0.024	0.030	0.0078	0.028	
D1	0.34	1.69	0.010	0.005	0.0098	0.0454	
D2	0.34	1.71	0.005	0.033	0.0133	0.0303	
D3	0.52	1.80	0.010	0.200	0.0104	0.0523	
D4	0.26	1.38	0.009	0.020	0.0062	0.0357	Dowling *et al.*, 1986
D5	0.26	1.37	0.011	0.029	0.0066	0.0407	
D6	0.29	1.79	0.008	0.004	0.0062	0.0377	
D7	0.34	1.73	0.010	0.005	0.0072	0.0394	
E1	0.57	1.40	0.0500	0.0450	0.0060	0.0451	Evans, 1995

†Only compositions relevant to the calculations are listed.

Table 5-4 : Geometrical characteristics of inclusions†1. / wt.%.

Mark	$\overline{d_v}$ / μm	V_v /×10^{-3}	N_v /×10^7 mm^{-3}	λ_v / μm	L_v / μm	Ref.
K1	0.64	2.1	1.53	2.2	-	
K2	0.56	2.6	2.83	1.8	-	
K3	0.59	2.0	1.86	2.1	-	
K4	0.68	1.8	1.09	2.5	-	
K5	0.68	1.7	1.03	2.5	-	
K6	0.66	2.2	1.46	2.3	-	
K7	0.63	1.7	1.29	2.4	-	
K8	0.67	2.7	1.71	2.2	-	
K9	0.66	1.9	1.26	2.4	-	
K10	0.62	1.1	0.84	2.7	-	Kluken *et al.*, 1989
K11	0.65	1.6	1.12	2.5	-	
K12	0.66	2.4	1.60	2.2	-	
K13	0.59	1.2	1.12	2.5	-	
K14	0.57	1.1	1.13	2.5	-	
K15	0.61	3.2	2.69	1.8	-	
K16	0.60	3.3	2.92	1.8	-	
K17	0.64	2.9	2.11	2.0	-	
K18	0.70	1.6	0.86	2.7	-	
K19	0.49	1.6	2.60	1.9	-	
K20	0.33	1.6	8.50	1.3	-	
F1	0.503†2	1.8	10.49	-	-	
F2	0.594†2	2.2	7.78	-	-	
F3	0.506†2	9.7	55.49	-	-	Fox *et al.*, 1996
F4	0.507†2	1.9	10.77	-	-	
F5	0.664†2	1.7	4.29	-	-	
T1	0.445	3.78	3.605	-	8.84	
T2	0.445	3.72	3.337	-	9.20	
T3	0.446	3.57	3.506	-	8.97	
T4	0.447	3.61	3.178	-	9.41	
T5	0.453	2.94	2.770	-	10.09	
T6	0.453	2.98	2.608	-	10.39	
T7	0.465	3.42	2.475	-	10.48	
T8	0.469	3.34	2.239	-	10.99	
T9	0.467	4.13	2.748	-	9.85	
T10	0.456	3.33	3.083	-	9.49	
T11	0.468	4.38	2.651	-	9.99	Thewlis, 1989a; b; 1994
T12	0.441	2.97	2.751	-	10.25	
T13	0.450	2.79	2.624	-	10.41	
T14	0.443	2.26	2.727	-	10.36	
T15	0.450	2.43	2.431	-	10.87	
T16	0.460	2.76	2.239	-	11.16	
T17	0.461	3.23	2.274	-	11.00	
T18	0.459	3.07	2.266	-	11.07	
T19	0.473	2.70	1.999	-	11.65	
T20	0.456	3.09	2.373	-	10.85	
T21	0.468	2.99	2.247	-	11.01	
T22	0.460	3.29	2.330	-	10.86	
D1	0.5	-	-	-	-	
D2	0.6	-	-	-	-	
D3	0.5	-	-	-	-	
D4	0.4	-	-	-	-	Dowling *et al.*, 1986
D5	0.4	-	-	-	-	
D6	0.4	-	-	-	-	
D7	0.4	-	-	-	-	

†1 $\overline{d_v}$: Mean three-dimensional particle diameter.
V_v: Inclusion volume fraction.
N_v: Number of particles per unit volume.
λ_v: Mean particle centre to centre volume spacing.
L_v: Mean particle surface to surface volume spacing.

†2 Converted from two-dimensional particle diameter ($\overline{d_a}$) using;
$\overline{d_v}/\overline{d_a} = \pi/2$

It is noted that some of the data reported by Kluken and Grong [1989] are not experimentally obtained but estimated using the following equation [Franklin, 1969]:

$$V_V \approx 10^{-2}\,[5.0[\mathrm{O}]\,(\mathrm{wt.\%}) + 5.4\,\{[\mathrm{S}]\,(\mathrm{wt.\%}) - 0.003\}] \qquad (5-7)$$

As Fox *et al.*[1996] did not disclose their experimental data on the number of inclusions per unit volume, N_V was estimated by adapting their original experimental data of V_V and $\overline{d}_V$ to Equation 1 and the results are listed in Table 5-4. Since their experimental results on the particle diameter seems to be two-dimensional (*i.e.*, not stereologically corrected), according to their experimental procedure, the values of $\overline{d}_a$ were converted to the three-dimensional ones using the following equation [Kluken and Grong, 1989] and corrected values are listed in Table 5-4:

$$\frac{\overline{d}_V}{\overline{d}_a} = \frac{\pi}{2} \qquad (5-8)$$

The measured chemical compositions of the inclusions are shown in Table 5-5. Some conversions against the original published data were needed in order to make consistent comparisons between with the experimental and calculated results. This is because some of the published results contained elements, such as iron, sulphur and copper, which are not taken into account in the present study.

$$\begin{pmatrix} [\mathrm{Si}]' \\ [\mathrm{Mn}]' \\ [\mathrm{Al}]' \\ [\mathrm{Ti}]' \end{pmatrix} = \frac{100}{W_{total}} \begin{pmatrix} [\mathrm{Si}]_{original} \\ [\mathrm{Mn}]_{original} \\ [\mathrm{Al}]_{original} \\ [\mathrm{Ti}]_{original} \end{pmatrix} \qquad (5-9)$$

where $[\mathrm{Si}]_{original}$, $[\mathrm{Mn}]_{original}$, $[\mathrm{Al}]_{original}$ and $[\mathrm{Ti}]_{original}$ are the original concentrations of silicon, manganese, aluminium and titanium in wt.% respectively found in literature. W_{total} is the sum of these: $W_{total} = [\mathrm{Si}]_{original} + [\mathrm{Mn}]_{original} + [\mathrm{Al}]_{original} + [\mathrm{Ti}]_{original} \leq 100$; $[\mathrm{Si}]'$, $[\mathrm{Mn}]'$, $[\mathrm{Al}]'$ and $[\mathrm{Ti}]'$ are the converted values of silicon, manganese, aluminium and titanium concentrations in wt.% respectively: $[\mathrm{Si}]' + [\mathrm{Mn}]' + [\mathrm{Al}]' + [\mathrm{Ti}]' \approx 100$. Furthermore, the experimental composition of inclusions shown by Dowling *et al.* [1986] and Fox *et al.* [1996] are presented in at.%, and were thus converted to the concentrations in wt.% are listed in Table 5-5.

Table 5-5 : Chemical compositions of inclusions. / wt.%.

Mark	Si	Mn	Al	Ti	Ref.	Note
K1	29	31	32	8		†1
K2	13	27	34	26		†1
K3	5	12	36	48		†1
K4	10	23	61	6		†1
K5	9	21	51	19		†1
K6	4	15	56	26		†1
K7	4	10	83	4		†1
K8	4	13	71	12		†1
K9	4	11	57	28		†1
K10	31	38	26	6	Kluken *et al.*, 1989	†1
K11	6	25	26	43		†1
K12	43	49	4	4		†1
K13	4	13	80	4		†1
K14	5	12	70	14		†1
K15	14	54	27	5		†1
K16	38	38	21	3		†1
K17	6	15	45	34		†1
K18	6	14	44	36		†1
K19	-	-	-	-		
K20	-	-	-	-		
F1	9.77	25.05	50.87	12.16		†2
F2	23.08	38.40	28.69	8.410		†2
F3	21.90	38.42	29.77	7.960	Fox *et al.*, 1996	†2
F4	30.54	36.95	25.15	5.680		†2
F5	26.87	46.48	20.29	5.420		†2
D1	9	45±13	43±10	3±3		†3
D2	0	20±10	34±13	47±26		†3
D3	0	4±7	11±11	85±20		†3
D4	2±2	10±6	22±3	66±8	Dowling *et al.*, 1986	†3
D5	12±15	16±9	21±9	51±19		†3
D6	4±5	82±24	7±9	7±4		†3
D7	15±8	68±23	12±6	5±2		†3
E1	2.66 (0—12.96)	5.20 (0—9.49)	57.71 (21.71—81.35)	34.43 (10.69—65.38)	Evans, 1995	†4

†1 S and Cu are also included in the original data. Compositions shown in the table are normalised by Si, Mn, Al and Ti only.

†2 Zr is also included in the original data. Compositions shown in the table are converted from atom.% and normalised by Si, Mn, Al and Ti only.

†3 S and Cu are also included in the original data. Compositions shown in the table are converted from atom.% and normalised by Si, Mn, Al and Ti only.

†4 Semiquantitative analysis; Average (Minimum—Maximum). Fe is also included in the original data. Compositions shown in the table are normalised by Si, Mn, Al and Ti only.

5.4 Results and Discussion

Information on the number density of inclusions is important since it determines the number of sites for acicular ferrite nucleation. Fig. 5-1 shows a comparison of the calculated corresponding number density of inclusions with experimental data [Kluken and Grong, 1989; Thewlis, 1989a; b; 1994; Fox *et al.*, 1996]. There is good quantitative agreement between the calculated and measured data. This agreement thus demonstrates that the model can properly predict volume of inclusions formed in welds.

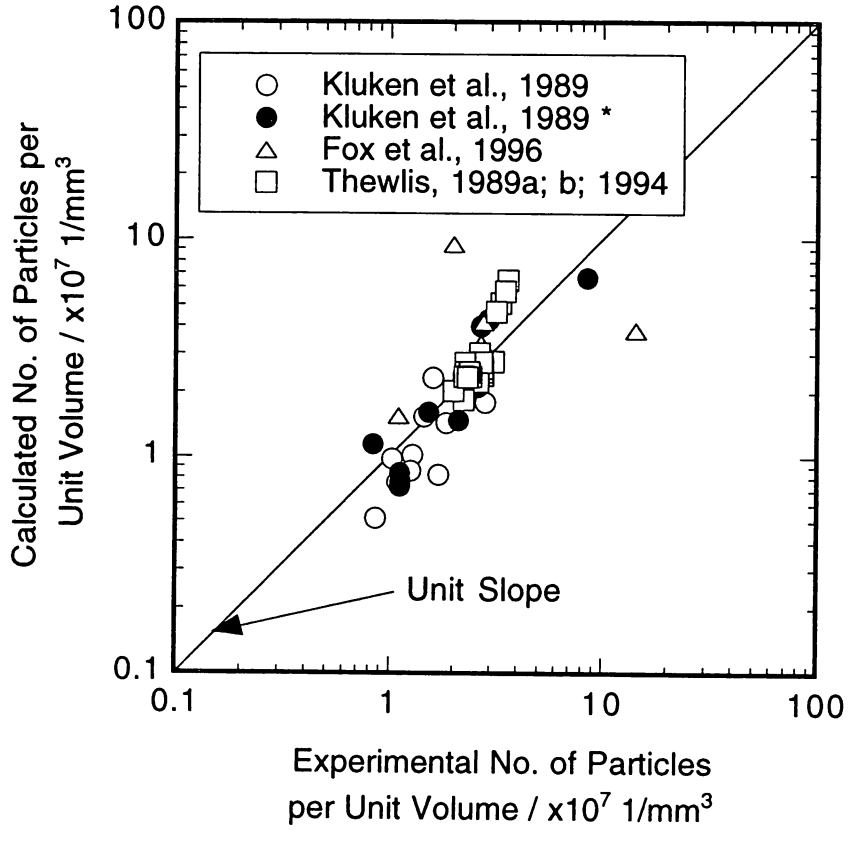

Fig. 5-1 : Comparison of experimental and calculated number density of inclusions in welds: Kluken *et al.* * obtained number of particles based on calculated inclusion volume fraction V_V using : $V_V \approx 10^{-2}[5.0[\mathrm{O}](\mathrm{wt.\%}) + 5.4[\mathrm{S}](\mathrm{wt.\%}) - 0.003]$ for these ten datapoints.

The comparison of mean particle spacing is shown in Fig. 5-2 and is again in good agreement between

theory and experiment [Kluken and Grong, 1989; Thewlis, 1989a; b; 1994]. These particle spacing calculations should be useful in any model for acicular ferrite.

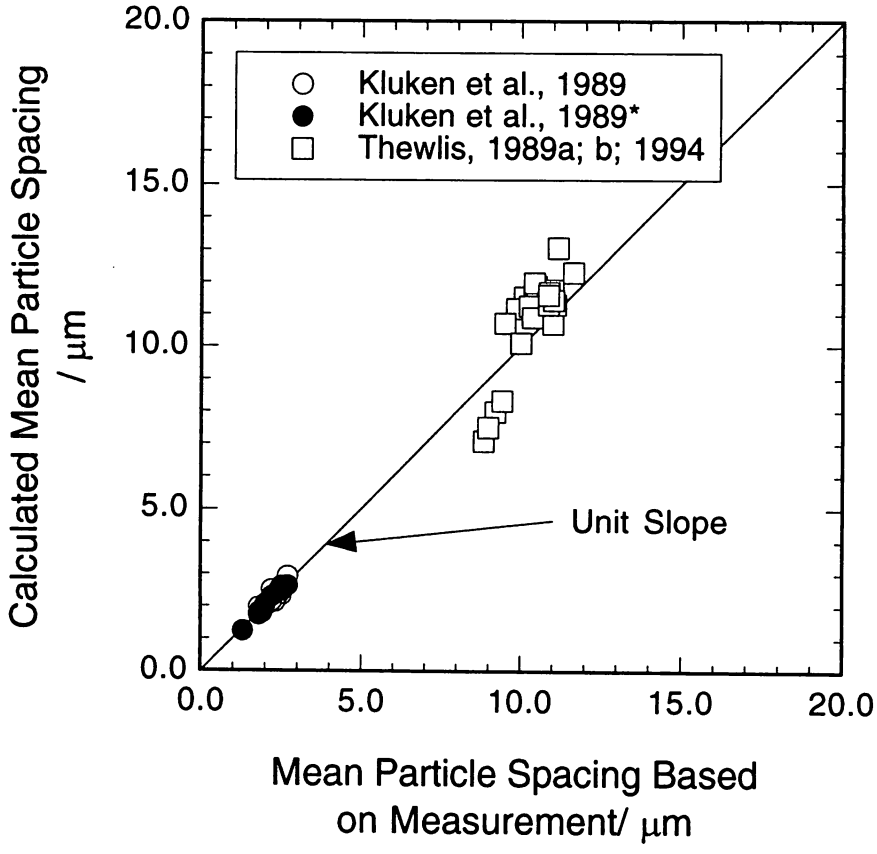

Fig. 5-2 : Comparison of experimental and calculated mean spacing of inclusions in welds: Kluken *et al.* * obtained number of particles based on calculated inclusion volume fraction V_V using : $V_V \approx 10^{-2}[5.0[O](wt.\%) + 5.4[S](wt.\%) - 0.003]$ for these ten datapoints.

The thermodynamic model presented here is not capable of giving any inclusion dimensions , since the calculations do not take the kinetics of inclusion formation into account. However, as shown in Fig. 5-3, most oxide inclusions in weld metals have a diameter around 0.5 μm regardless of weld chemical compositions. This fact may encourage the use of equilibrium calculations as a first approximation to estimate inclusion characteristics.

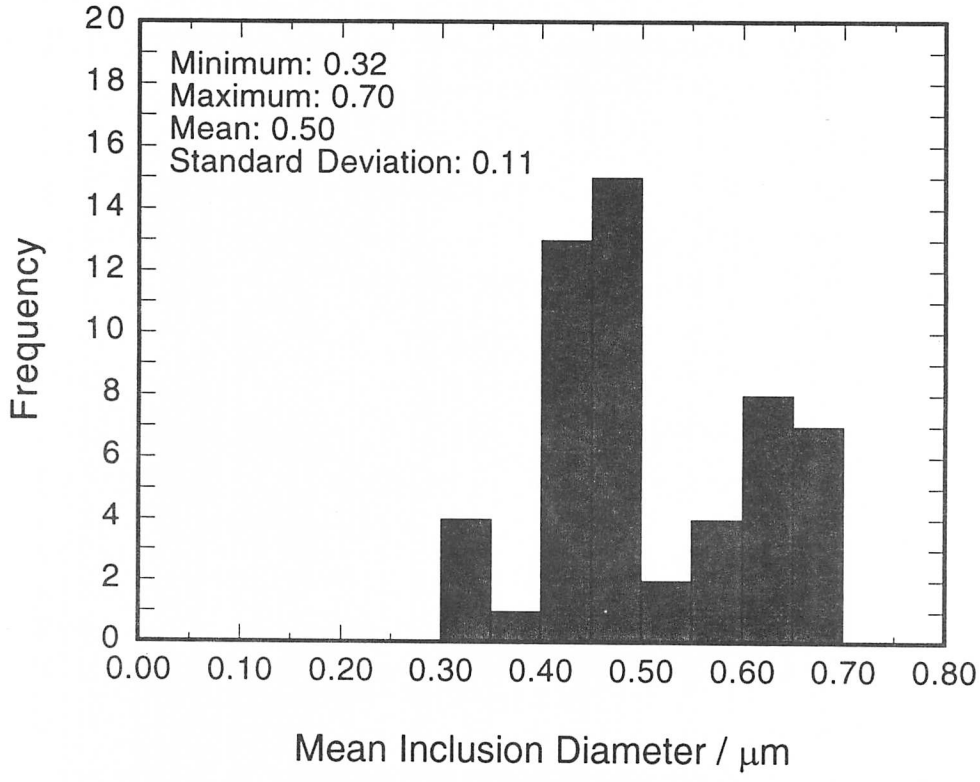

Fig. 5-3 : Mean oxide diameter distribution in the literature used for the calculation [Dowling *et al.*, 1986; Kluken and Grong, 1989; Thewlis, 1989a; b; 1994; Fox *et al.*, 1996].

The chemical composition of inclusions is also extremely important since it affects their crystalline structure. For example, Horii *et al.* [1995b] demonstrated that only small additions of titanium are sufficient to crystallise oxides in weld metal, as long as an appropriate balance of aluminium, titanium and oxygen included in the typical oxides is maintained in weld metal. Figs. 5-4 to 5-7 show comparisons of the chemical compositions of inclusions between experiment and calculations in terms of silicon, manganese, aluminium and titanium respectively. Some of the experimental data are plotted with error bars according to the original data in the published literature. Even though the experimental data are taken from the different sources, the degree of agreement is found to be reasonable for all the elements considered.

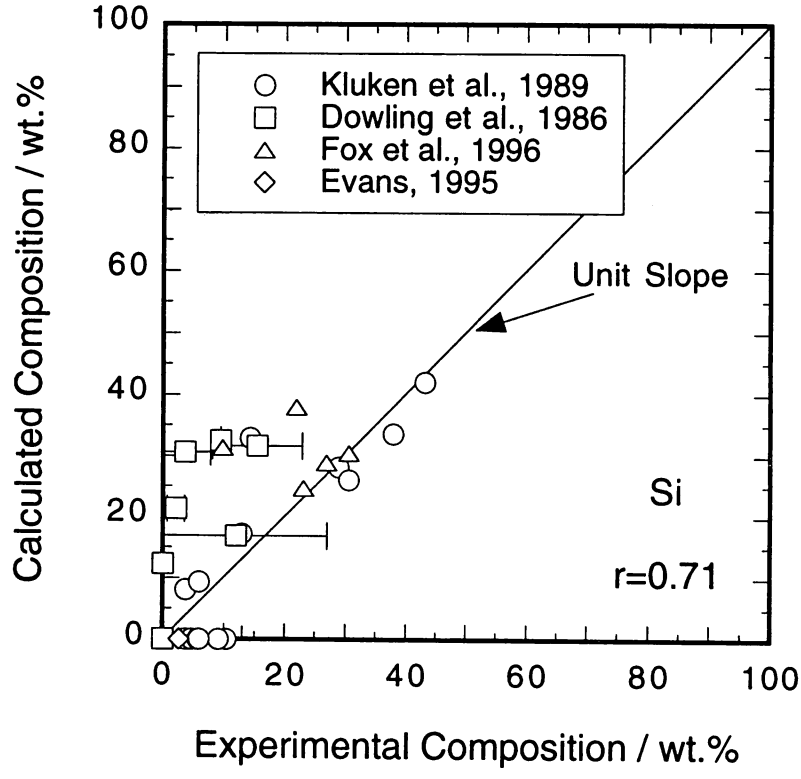

Fig. 5-4 : Comparison of experimental and calculated silicon concentration in inclusions.

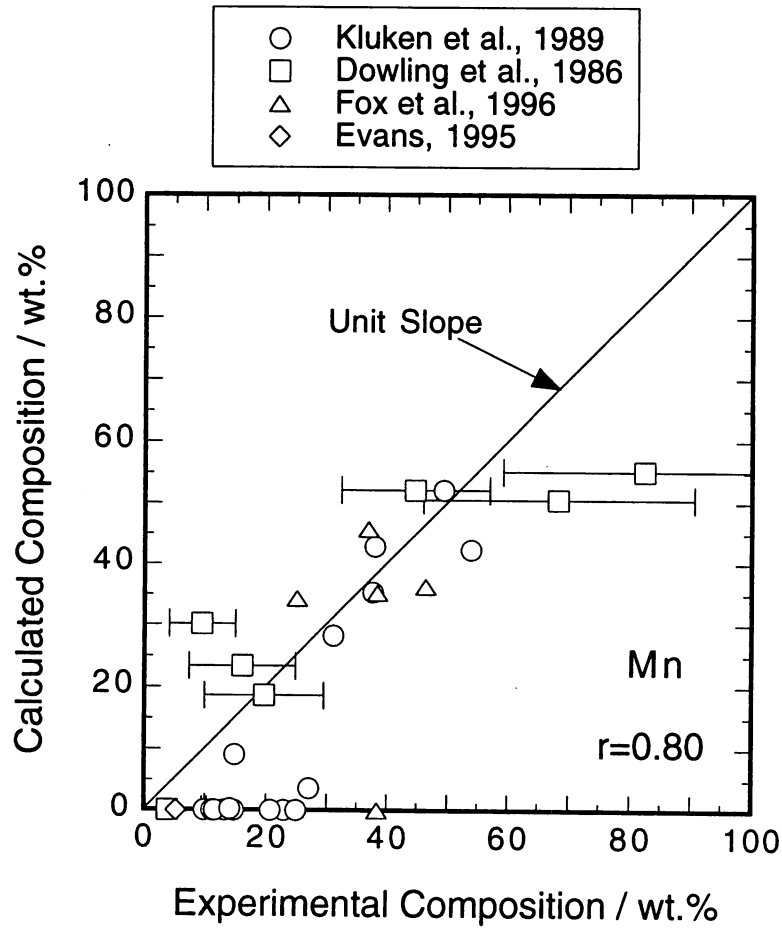

Fig. 5-5 : Comparison of experimental and calculated manganese concentration in inclusions.

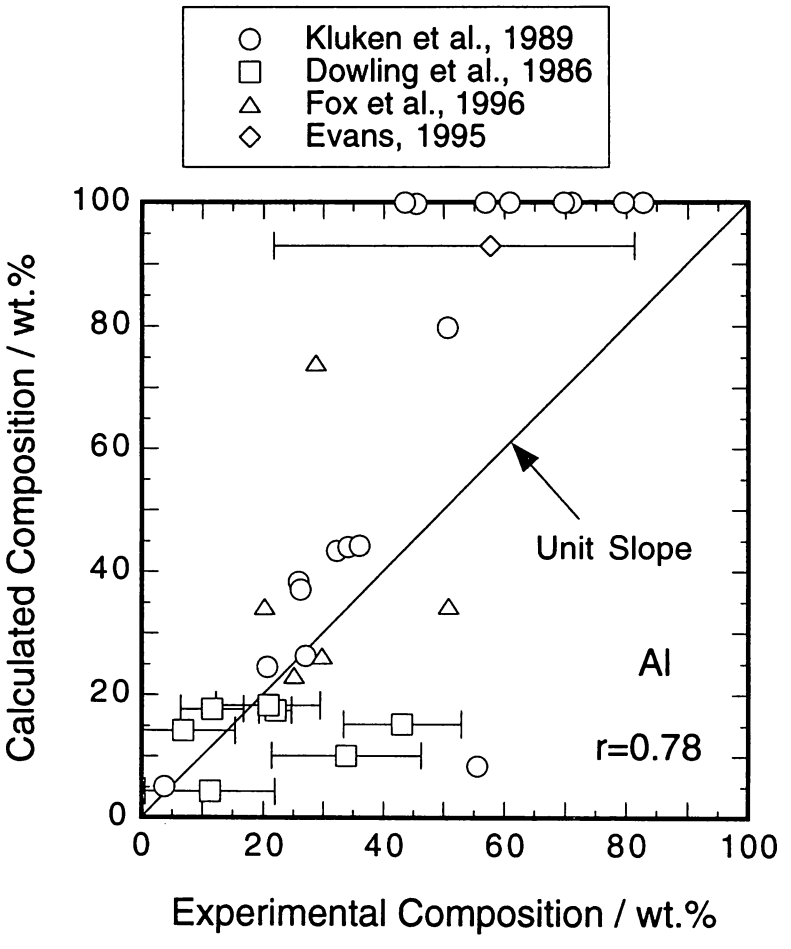

Fig. 5-6 : Comparison of experimental and calculated aluminium concentration in inclusions.

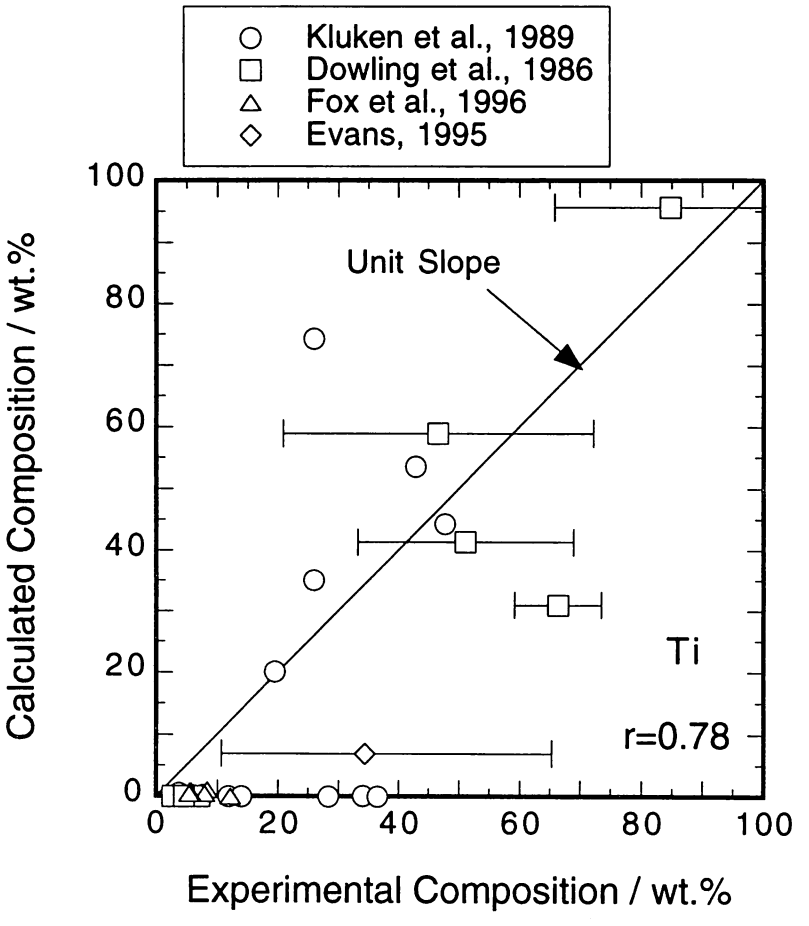

Fig. 5-7 : Comparison of experimental and calculated titanium concentration in inclusions.

In summary, it has been demonstrated that thermodynamic phase stability exerts a significant and perhaps an overriding influence on inclusion formation in low alloy steel weld metals. The model presented in this study has the potential for development of the theory for acicular ferrite.

5.5 Conclusions

Thermodynamic calculations were found to be effective in predicting the number density and chemical compositions of inclusions in steel welds as long as the mean inclusion diameter is known. Reasonable agreement was obtained between the calculated and experimental data. This approach may prove will be very useful in the design of welding materials, such as submerged arc welding flux and shielded

metal arc welding coatings which effectively control the inclusion characteristics in steel welds. It is suggested that thermodynamic phase stability exerts primary influence on the nature of inclusions in common low-alloy steel weld metals.

CHAPTER SIX

Model for Solidification Cracking in Low-Alloy Steel Weld Metals

6.1 Introduction

Solidification cracking occurs in welds during cooling from the liquidus temperature, if the density changes associated with solidification and thermal contraction cannot be accommodated by fluid flow or by the motion of the solid components which constitute the weld assembly. Fig. 6-1 shows the example of the solidification cracking found in submerged arc weld metal [Ichikawa, 1998].

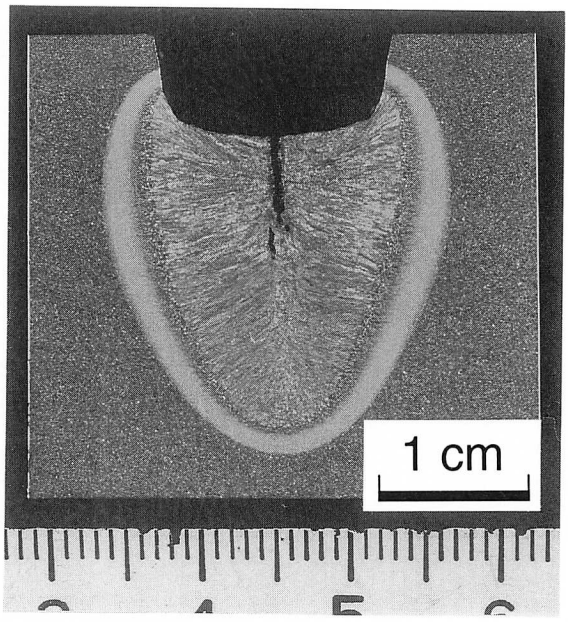

Fig. 6-1 : Example of the solidification cracking found in submerged arc weld metal [Ichikawa, 1998].

This kind of cracking depends partly on the chemical composition of the weld metal, since that in turn determines the solidification temperature range. However, the cooling rate and weld geometry (including the extent of constraint) also control the susceptibility to solidification cracking. Modern low-alloy steels for structural applications have compositions which are designed to avoid solidification cracking, for instance by minimising the sulphur concentration. Sulphur has a tendency to segregate

into the residual liquid; the resulting increases in the solidification temperature range increases the tendency for solidification cracking. Significant difficulties nevertheless remain with very high heat input welding of high tensile strength steels.

A great deal of excellent research has been reported in the published literature on the factors controlling solidification cracking in welds [Wilkinson *et al.*, 1958; Cottrell, 1962; Sekiguchi *et al.*, 1966; Masumoto and Imai, 1970; Kihara and Matsuda, 1973; Morgan-Warren and Jordan, 1974; Bailey, 1976; Garland and Bailey, 1976; Phillips and Jordan, 1977; Bailey and Jones, 1978; Dixon, 1981; Mori *et al.*, 1982b; Homma *et al.*, 1982; Ohshita *et al.*, 1983; Shinoda *et al.*, 1990; Komizo, 1994]. The essential phenomena are well characterised although difficulties remain with respect to the detailed mechanisms; the subject has been reviewed recently [Dixon, 1981; Komizo, 1994].

Appropriate model, which can predict the tendency of solidification cracking, has been required in industry in order to know the proper chemical composition and welding condition before proceeding the commercial welding processes. The physical models might be capable of predicting these cracking phenomena. These cracking problem are however not as yet amenable to mathematical treatment while the general concepts might be understood. Empiricism can in these circumstances be extremely useful in getting solutions [Bhadeshia, 1996].

The results of standard tests on the tendency of solidification cracking are actually usually expressed in terms of the chemical composition of the weld metal [Wilkinson *et al.*, 1958; Kihara and Matsuda, 1973; Morgan-Warren and Jordan, 1974; Bailey, 1976; Garland and Bailey, 1976; Phillips and Jordan, 1977; Bailey and Jones, 1978]. The following equations, for example, have been proposed to describe the chemical composition (in wt.%) effects on the tendency of solidification cracking in weld metal or liquation cracking in heat affected zone.

By Wilkinson *et al.*[1958] (for weld metal):

$$HCS = \frac{w_{\mathrm{C}}\{w_{\mathrm{S}} + w_{\mathrm{P}} + (w_{\mathrm{Si}}/25) + (w_{\mathrm{Ni}}/100)\} \times 10^3}{3w_{\mathrm{Mn}} + w_{\mathrm{Cr}} + w_{\mathrm{Mo}} + w_{\mathrm{V}}} \qquad (6-1)$$

for compositions $0.21 < w_{\mathrm{C}} < 0.38$, $0.15 < w_{\mathrm{Si}} < 1.55$, $0.35 < w_{\mathrm{Mn}} < 1.57$, $0.013 < w_{\mathrm{P}} < 0.034$, $0.007 < w_{\mathrm{S}} < 0.017$, $0.12 < w_{\mathrm{Ni}} < 1.90$, $0.11 < w_{\mathrm{Cr}} < 12.92$, $w_{\mathrm{Mo}} < 1.50$ and $w_{\mathrm{V}} < 0.54$ in wt.%.

By Kihara and Matsuda [1973] (for weld metal):

$$L_T = 91 \times \left(w_{\mathrm{C}} - \frac{w_{\mathrm{Si}}}{8} + \frac{w_{\mathrm{Mn}}}{15} + \frac{w_{\mathrm{S}}}{2} + \frac{w_{\mathrm{Ni}}}{26}\right) \qquad (6-2)$$

for compositions $0.041 < w_{\mathrm{C}} < 0.20$, $0.03 < w_{\mathrm{Si}} < 0.53$, $0.45 < w_{\mathrm{Mn}} < 1.76$, $0.001 < w_{\mathrm{P}} <$

$0.016, 0.002 < w_S < 0.036, w_{Cu} < 0.38, w_{Ni} < 3.44, w_{Cr} < 0.94, w_{Mo} < 0.84$ and $w_V < 0.06$ in wt.%.

By Bailey [1976] and Bailey and Jones [1978] (for weld metal):

$$UCS = 230C^* + 190w_S + 75w_P + 45w_{Nb} - 12.3w_{Si} - 5.4w_{Mn} - 1 \qquad (6-3)$$

where C^* is a function of carbon concentration in wt.%

$$\begin{cases} C^* = w_C & \text{for } w_C > 0.08 \\ C^* = 0.08 & \text{for } w_C \leq 0.08 \end{cases}$$

for compositions $0.03 < w_C < 0.18, 0.15 < w_{Si} < 0.65, 0.45 < w_{Mn} < 1.6, 0.010 < w_P < 0.045, 0.010 < w_S < 0.050, w_{Ni} < 1.18, 0.11 < w_{Cr} < 12.92$ and $w_{Mo} < 0.46$ in wt.%.

By Morgan-Warren and Jordan [1974] (for weld metal):

$$CSF = 42w_C + 847w_S + 265w_P - 10w_{Mo} - 3042w_O + 19 \qquad (6-4)$$

for compositions $0.08 < w_C < 0.59, 0.06 < w_{Si} < 1.85, 0.40 < w_{Mn} < 1.41, 0.002 < w_P < 0.049, 0.007 < w_S < 0.041, w_{Ni} < 1.54, 0.02 < w_{Cr} < 4.76, 0.18 < w_{Mo} < 2.10$ and $w_V < 0.60$ in wt.%.

By Garland and Bailey [1976] (for weld metal):

$$CS = 223w_C + 197w_S + 100w_P + 48w_{Nb} - 14.3w_{Si} - 6w_{Mn} - 16w_{Al} + 0.5 \qquad (6-5)$$

for compositions $0.06 < w_C < 0.19, 0.16 < w_{Si} < 0.63, 0.67 < w_{Mn} < 1.32, 0.009 < w_P < 0.042, 0.010 < w_S < 0.050, w_{Nb} < 0.065$ and $0.012 < w_{Al} < 0.04$ in wt.%.

By Phillips and Jordan [1977] (for heat affected zone):

$$CI = 5.47w_C + 27.27w_S + 75.29w_P + 2.79w_{Si} - 2.77 \qquad (6-6)$$

for compositions $0.11 < w_C < 0.46, 0.06 < w_{Si} < 0.58, 0.50 < w_{Mn} < 0.85, 0.001 < w_P < 0.049, 0.0016 < w_S < 0.040, 0.01 < w_{Ni} < 1.38, 0.88 < w_{Cr} < 1.14$ and $0.19 < w_{Mo} < 0.37$ in wt.%.

Relationships like these are very useful in that they help in the selection of weld metals. However, they are simple functions of the chemical composition and are unable to express certain known more complex effects. Unlike the proportional influence of carbon on the cold-cracking susceptibility of welded steels

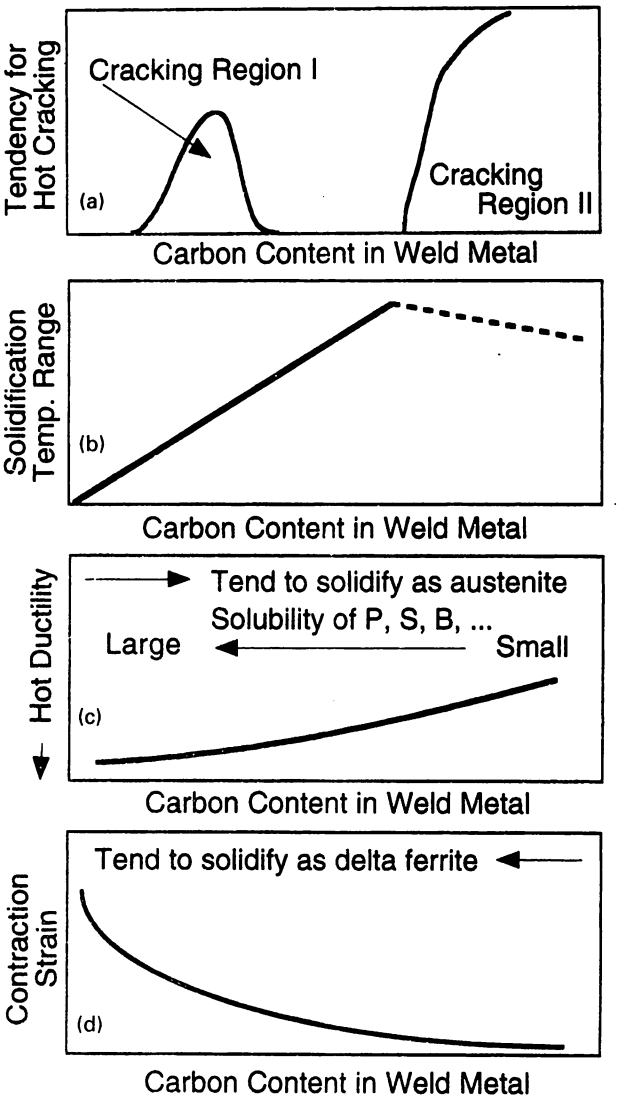

Fig. 6-2 : Schematic diagram of the effects of carbon on the solidification cracking susceptibility in low alloy steel welds ((a), (b) and (d) are after Homma *et al.* [1982]). (a) Comprehensive effect of carbon on solidification cracking susceptibility. (b) Effect of carbon on solidification temperature range. (c) Effect of carbon on hot ductility. (d) Effect of carbon on thermal contraction strain.

(as evident in the famous carbon-equivalent formulae), Fig. 6-2a shows a well-established non-linear effect of carbon on the solidification cracking susceptibility [Homma *et al.*, 1982].

The temperature range over which solidification to delta-ferrite occurs increases with the carbon concentration (Fig. 6-2b), but the density change on solidification decreases at the same time (Fig. 6-2c) [Homma *et al.*, 1982], giving rise to the first peak illustrated in Fig. 6-2a. At even larger concentrations, the mode of solidification switches from ferrite to austenite; impurities such as sulphur and phosphorus have a lower solubility in austenite so that segregation to the residual liquid is enhanced, thereby increasing the risk of solidification cracking (Fig. 6-2d) [Homma *et al.*, 1982]. As a further example of well-established non-linear effects, the ability of sulphur to induce solidification cracking is greatest when the nickel concentration is large, because nickel also promotes solidification to austenite [Sekiguchi *et al.*, 1966].

A more general method of regression analysis is neural network analysis [MacKay, 1997]. The input data x_j in the neural network analysis are multiplied by "weights" as in regression analysis, but sum of all these products forms the argument of a hyperbolic tangent. The output y is therefore a non-linear function of x_j; the function has been usually chosen being the hyperbolic tangent because of its flexibility. The exact shape of the hyperbolic tangent can be varied by altering the "weights". Further degrees of non-linearity can be introduced by combining several of these hyperbolictangent so that the neural network method is able to capture almost arbitrarily non-linear relationships.

A potential difficulty with the use of powerful regression methods, including *conventional* neural network technique, is the possibility of *overfitting* data by complicated model as shown by the curve drawn in Fig. 6-3.

A complicated model may fit the data, but in the case of Fig. 6-3, a linear relationship is all that is justified by the noise in the data [Bhadeshia, 1996] In order to avoid this overfitting problem, the experimental data can be divided into two sets, "training dataset" and "test dataset" [Bhadeshia, 1996]. The model is produced using only the training data. The "test dataset" are then used to check that the model behaves itself when presented with previously unseen data.

All of the issues in the solidification cracking problem mentioned above can be expected to be handled better using an artificial neural network, which has the capability of addressing complexity with relative ease. Ordinary regression analysis can not cope with such changes in the form of relationships. The aim of the present chapter was, therefore, to quantitatively model the tendency for solidification cracking using a neural network approach and to learn from the patterns that it recognises.

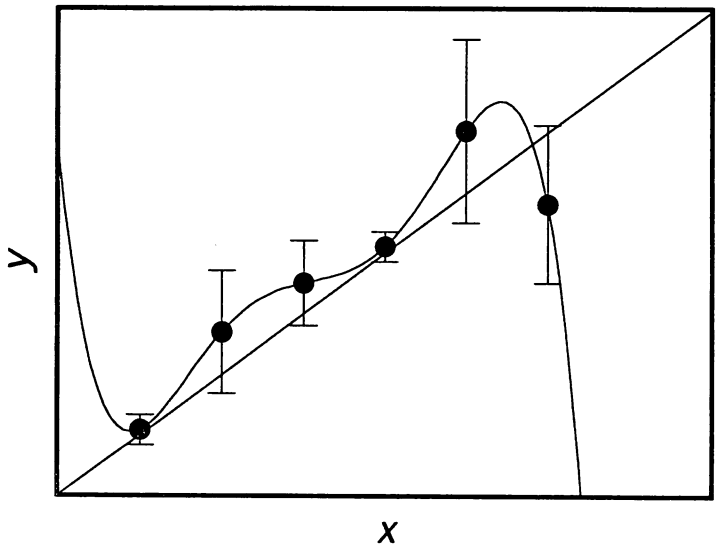

Fig. 6-3 : Schematic illustration showing the "over-fitting problem" in a regression analysis.

6.2 The Technique

Neural networks are parameterised non-linear models, used for empirical regression and classification modelling [MacKay, 1997]. Their flexibility makes them able to discover more complex relationships in data than traditional statistical models which assume a linear dependence of the predicted "output" variable on the given "input" variables [Bhadeshia *et al.*, 1995]. Neural networks are able to implement more general (and more complex) non-linear relationships. When the neural network is "trained" on empirical data, its parameters are adjusted so as to produce a non-linear interpolant which fits the data well.

The outcome of training is a set of coefficients (called "weights") and a specification of the functions which in combination with the weights relate the input to the output. The training process involves a search for the optimum non-linear relationship between the inputs and the outputs, and is computer intensive. Searching for the optimum non-linear relationship between the inputs and the outputs means minimising the total error function known as "objective function" for the classification problem [MacKay, 1995]. Once the network is trained, estimation of the outputs for any given inputs is very rapid.

Because the neural network is able to implement more complex relationships than linear regression, it

is also able to "overfit" the training data; there is therefore a potential problem of obtaining a model that fits the training data well, but generalises poorly to unseen data. To solve this problem, Bayesian regularisation theory can be used to control the complexity of the model [MacKay, 1992a; b; c; 1993; 1994; 1995; 1996; 1997]. It is then possible to identify automatically which of many possibly-relevant input variables are in fact important factors in the regression.

Neural networks are frequently used for regression problems in which continuous variables are modelled. In a recent example of this kind, the impact toughness of steel welds was expressed as a function of chemical compositions and temperature [Bhadeshia *et al.*, 1995]. There are many problems where the variables to be predicted adopt discrete values. For example, the solidification cracking tests used in the assessment of welds give a result which indicates whether the weld will crack (1) or not (0). Such a problem is known as a binary classification problem, and a neural network can be made to model the probability of a crack (1) as a function of the input variables. The neural network implements a parameterised function $y(\mathbf{x},\mathbf{w})$ where $\mathbf{x}$ are the input variables and $\mathbf{w}$ are the parameters; the output y is a real number between 0 and 1. Bayesian methods can also be applied to these neural network classifiers [MacKay, 1992c; 1995] and have two important consequences. First, it is possible automatically to control the complexity of a neural network, and, as in MacKay [1994] and Bhadeshia *et al.* [1995], to infer which input variables are most relevant in the non-linear regression. Second, Bayesian methods allow us to take into account the parameter uncertainty when making predictions by the process of marginalisation. In a classifier, the effect of marginalisation is to take the output of the best-fit neural network, which is over-confident prediction (MacKay [1995]), and move it closer to 0.5 by an amount depending on the parameters' uncertainty. The value 0.5 in the output indicates the highest level of uncertainty. This is the method of expressing an error bar in a classification problem.

This chapter deals with what is believed to be the first the first application of a classification neural network with a Bayesian framework to any practical problem here to the solidification cracking of welds.

6.3 Variables

It is possible to choose a set of variables which should affect the solidification cracking susceptibility in steel welds using metallurgical experience on welding. The input and output variables considered in this study are listed in Tables 6-1 and 6-2 respectively.

As suggested by previous work based on linear regression methods [Kihara and Matsuda, 1973; Morgan-Warren and Jordan, 1974; Bailey, 1976; Garland and Bailey, 1976; Phillips and Jordan, 1977; Bailey

Table 6-1 : The input variables used in this study.

Variables	Range	Mean	Standard Deviation
Carbon / wt.%	0.012-0.19	0.07492	0.009304
Silicon / wt.%	0.18-0.77	0.5225	0.02001
Manganese / wt.%	0.90-1.82	1.463	0.02885
Phosphorus / wt.%	0.01-0.10	0.01539	0.00684
Sulphur / wt.%	0.006-0.028	0.01176	0.001313
Nickel / wt.%	0.00-6.50	1.417	0.4117
Chromium / wt.%	0.00-0.08	0.04539	0.002798
Molybdenum / wt.%	0.00-0.22	0.07799	0.01148
Welding Current /A	422-800	580.7	17.73
Voltage / V	28.0-36.5	33.23	0.2646
Travel Speed / cm min^{-1}	30-55	41.65	1.079
Groove Angle / degree	0-90	43.05	3.796
Preheat Temperature / °C	20-150	22.53	10.31

Table 6-2 : The output variables used in this study.

Classification Label	Value	Number
No Cracks	0	95
Cracked	1	59

and Jones, 1978], alloying elements such as carbon, silicon, manganese, phosphorus, sulphur, nickel, chromium and molybdenum should all have an influence on the development of solidification cracks during welding; these elements were all included as input variables. Similarly, microalloying and impurity elements, such as niobium [Bailey, 1976; Bailey and Jones, 1978], vanadium [Wilkinson *et al.*, 1958], boron [Shinoda *et al.*, 1990], and oxygen [Morgan-Warren and Jordan, 1974] may influence cracking susceptibility, but were not included because of a lack of systematic data.

It is well known that the tendency for solidification cracking varies with the welding process parameters such as the welding conditions, joint configuration and preheat temperature because of their influence on the solidification structure, and stress and strain development as the weldment cools. Consequently, the welding current, voltage and travel speed were included as input variables. The joint configuration was represented by the groove angle which to a large extent controls the growth direction of the solidification microstructure.

There is a significant problem in determining a uniform representation of cracking susceptibility, the output variable, because of the variety of tests used in the welding industry. Thus, a binary index was

used, with values of 0 or 1 corresponding to a "no cracks" or "cracked" result respectively. In some literature, the cracking susceptibility was stated as a fractional cracking ratio rather than a binary index, in which case the outputs were defined as 1 if the ratio was greater than 0.05 and 0 if it was less than or equal to 0.05 in the neural network analysis.

6.4 Experimental Data

There were numerous difficulties in compiling a data set for analysis, primarily because many of the publications on the subject do not rigorously report the values of important variables. The exercise of data collection therefore had to be done pragmatically in order to collect a reasonable number of cases. Nevertheless, a positive aspect of this attempt at modelling is that it identifies for future work, the variables that must be controlled in order to do reliable research.

The database was composed using published results [Sekiguchi *et al.*, 1966; Masumoto and Imai, 1970; Garland and Bailey, 1976; Mori *et al.*, 1982b; Homma *et al.*, 1982]. Homma *et al.*[1982] have reported the complex effect of carbon for ultra-low carbon steels to a maximum concentration of about 0.15 wt.%. They did not disclose the exact chemical composition of the steel used for each test, but published the range of concentrations; we therefore specified the composition in terms of the average of the range quoted; the chromium concentration was assumed to be zero for their data. Masumoto and Imai [1970] published data on the effects of nickel and phosphorus on solidification cracking; the chromium and molybdenum compositions which they did not state, were again assumed to be zero. Sekiguchi *et al.*[1966] reported the complex effects of nickel and sulphur but only the sulphur and nickel concentrations of the welds were stated; the mean chemical composition of the welding electrodes they used in their study was therefore taken to represent the weld composition. In those cases where the published work did not report a preheat temperature, it was assumed that the base plate was not heated prior to welding so that the temperature was taken to be 20 °C .

The variety of approximations stated above should, if incorrect, reflect in the perceived uncertainty in the output. The entire dataset used in this study is presented in the Appendix. It is also available in digitalised form on: http://www. msm.cam.ac.uk/map/data/materials/weldhotmat-b.html.

6.5 Analysis

The input variables were normalised between -0.5 and $+0.5$, as follows:

$$x_N = \frac{x - x_{min}}{x_{max} - x_{min}} - 0.5 \qquad (6-6)$$

where x_N is the normalised value of x which has maximum and minimum values given by x_{max} and x_{min} respectively. This normalisation is not essential to the neural network modelling but enables convenient comparison of the influence of the individual input variables on an output [Bhadeshia *et al.*, 1995]. The neural network consisted of thirteen input units (one for each of the input variables), a number of hidden units and one output unit for the crack susceptibility (Fig. 6-4).

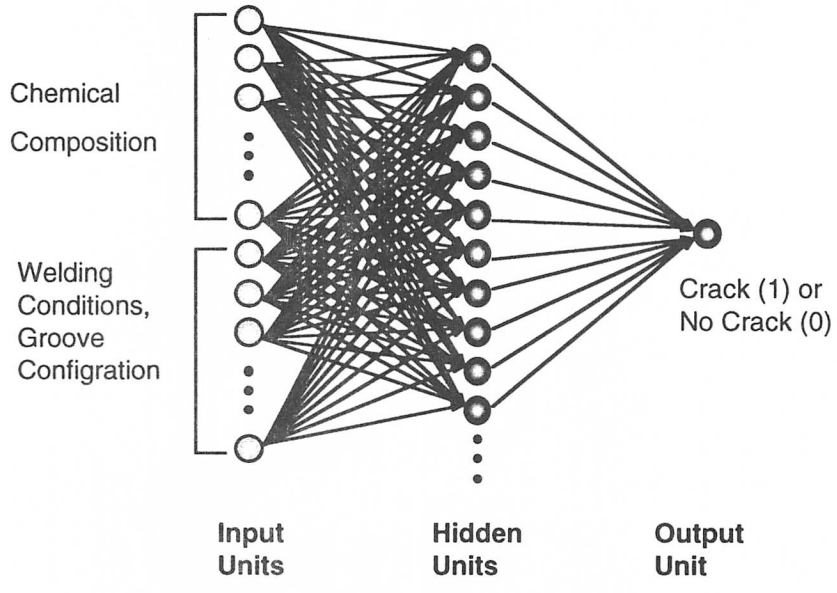

Fig. 6-4 : Schematic illustration of the neural network model used.

The network was trained using a randomly chosen seventy-seven of the samples from one hundred fifty-four available in the assembled dataset. The remaining seventy-seven data were used in order to test each model for its behaviour on unseen data.

Linear functions of the inputs x_j are operated on by a hyperbolic tangent transfer function:

$$h_i = \tanh\left(\sum_j w_{ij}^{(1)} x_j + \theta_i^{(1)}\right) \qquad (6-7)$$

so that each input contributes to every hidden unit. The bias of each hidden unit i is designated $\theta_i^{(1)}$ and is analogous to the constant that appears in linear regression. The strength of the transfer function is in each case determined by the weight $w_{ij}^{(1)}$. The transfer to the output y is:

$$y = \frac{1}{1 + \exp\left(-a_{out}\right)} \qquad (6-8)$$

where a_{out} is linear against h_i:

$$a_{out} = \sum_i w_i^{(2)} h_i + \theta^{(2)} \qquad (6-9)$$

This specification of the network structure, together with the set of weights is a complete description of the formula relating the inputs to the output. The weights are determined by training the neural network. The details are described elsewhere [MacKay, 1992a; b; c; 1993; 1994; 1995; 1996; 1997]. The targets (experimental outputs) are discrete binary classification labels; "cracked" or "no crack". The neural network's output y is bounded between 0 and 1 and corresponds to "cracked" and "no crack" respectively. The value of y indicates the probability that the test will result in a cracked sample. As stated earlier, $y = 0.5$ indicates the highest levels of uncertainty, where the tendency for cracking is the same as that for avoiding a crack.

The error function in a regression neural network model is then replaced by the logarithmic likelihood [MacKay, 1995]:

$$G = \sum_m t_m \ln y_m + (1 - t_m) \ln (1 - y_m) \qquad (6-10)$$

where y_m is the output for example m and t_m is the target (*i.e.*, experimental) value. Training involves minimisation of the following objective function M and a regulariser (the second term of the M) penalises over-complex models. The Bayesian probability theory has been used to optimise the parameter α_r which control the complexity of the model. [MacKay, 1995].

$$M = -G + \alpha_r \left(\frac{1}{2} \sum w^2 \right) \qquad (6-11)$$

where α_r is called "regularisation constant" and w is weights.

It is possible to have multiple classification models which are obtained by choosing different numbers of hidden units, initial values of weights and regularisation constants (σ_W). A single prediction can then be made by a committee (*i.e.*, by averaging the prediction of each model), *i.e.*:

$$\overline{y} = \frac{\sum_{k=1}^{N_{com}} y_k}{N_{com}} \qquad (6-12)$$

where N_{com} is the number of models in the committee and y_k is the estimate of a particular model k. The testing error is now obtained by replacing the y_m in Equation (6-10) by $\overline{y}$.

The complexity of the model is controlled by the number of hidden units, and the value of the fifteen σ_W, one associated with each input, one for biases and one for all weights connected to the output.

Four hundred and thirty-two different models were obtained by training on half the data by choosing different numbers of hidden units, different seeds and initial values of σ_W. The best one hundred and

twenty-six models (*i.e.*, models with the smallest values of marginalised test error) were then examined to construct a committee model [MacKay, 1994]. A "committee" is a collection of models. It is often found that the mean prediction from a committee is more reliable than from the best individual models.

Fig. 6-5 illustrates the marginalised test error calculated for the best twenty individual models. Fig. 6-6 shows clearly that a committee consisting of the four best models has the minimum test error. This committee consists in fact of three models with eleven hidden units and one with just two hidden units. The four models were then *retrained* individually on all the available data. This second training (*i.e.*, "retraining") begins with the values of weights already obtained by the first training on the training dataset.

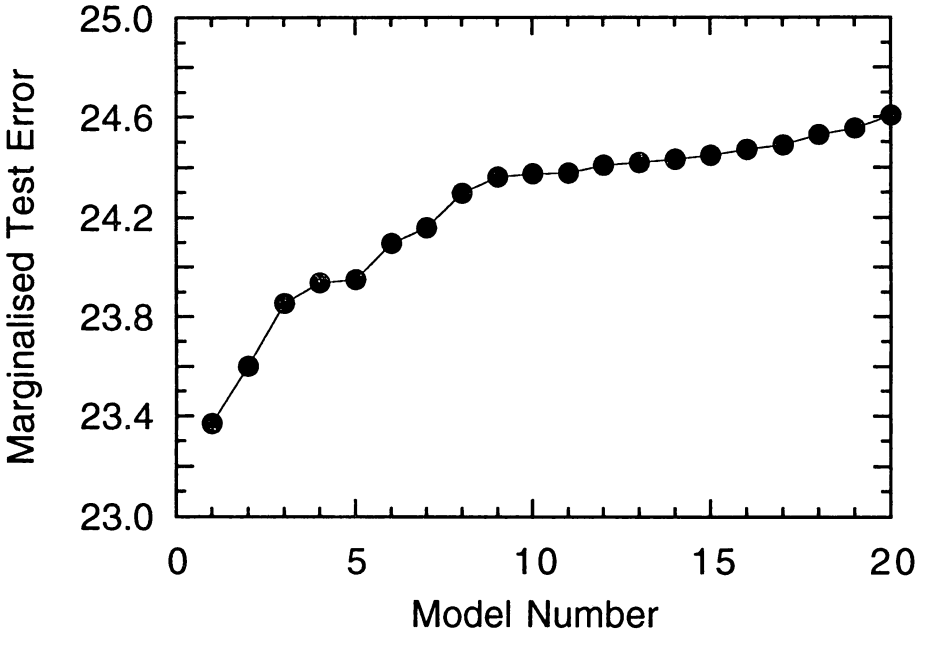

Fig. 6-5 : The marginalised test error for the best twenty individual models.

The committee model was then tested extensively to examine how well it represents metallurgical experience. Fig. 6-7 shows the model perceived role of each of the inputs in explaining the variations in the experimental data on the tendency for solidification cracking.

Carbon clearly has large effects on the tendency for solidification cracking as Fig. 6-2 shows and as Ohshita *et al.* suggested [1983] due to some complicated mechanism explained in the Introduction of this chapter. Sulphur has been reported to have detrimental influence on the tendency of solidification cracking [Sekiguchi *et al.*, 1966] through its segregation into the residual liquid during weld solidification process. Influence of the weld travel speed on the solidification cracking tendency also has been reported

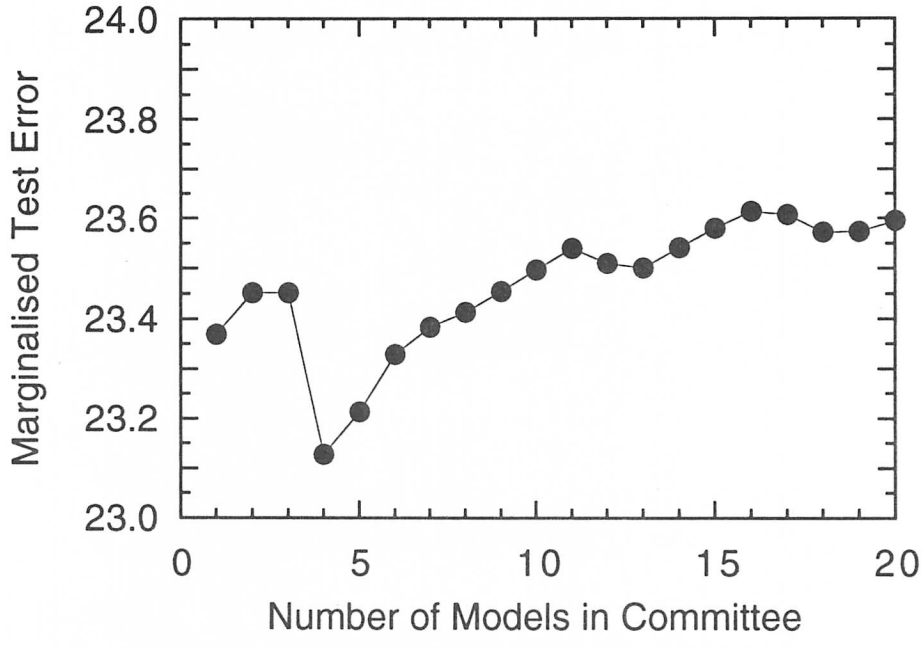

Fig. 6-6 : The marginalised test error as a function of the number of models in committee.

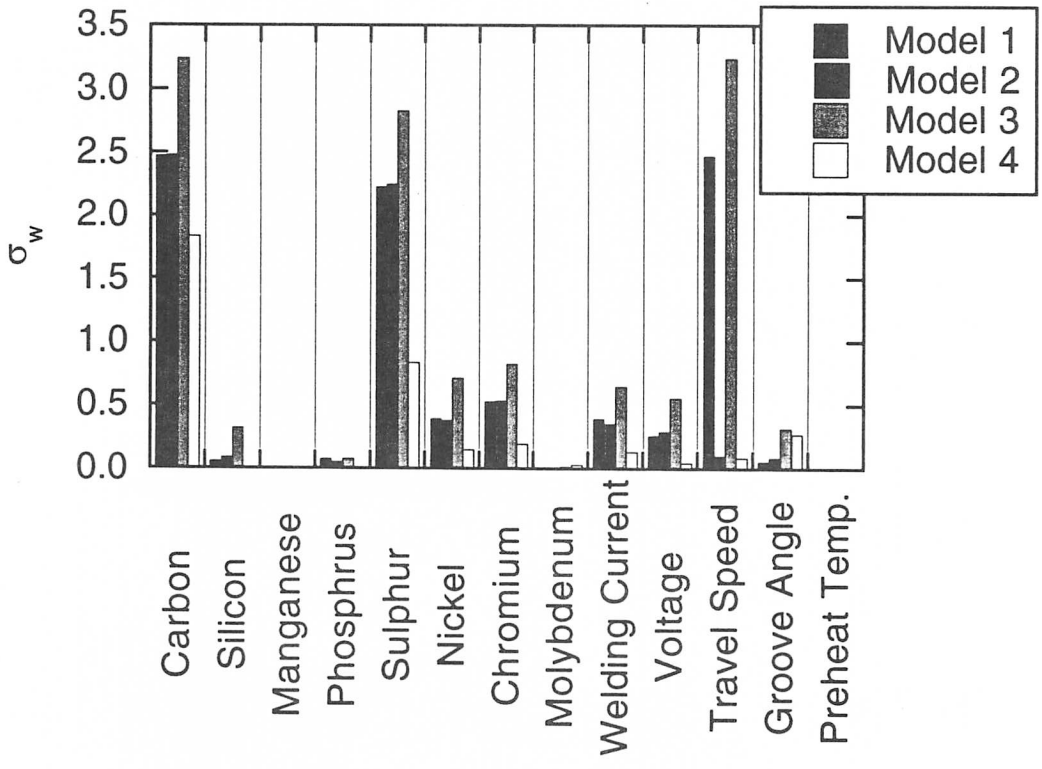

Fig. 6-7 : Chart showing a measure of the model-perceived significance of each input variable in affecting solidification cracking in steel welds.

by Ohshita *et al.*[1983]; solidification cracking never occurs when the travel speed is less than a critical level. These neural network models are therefore consistent with metallurgical experience.

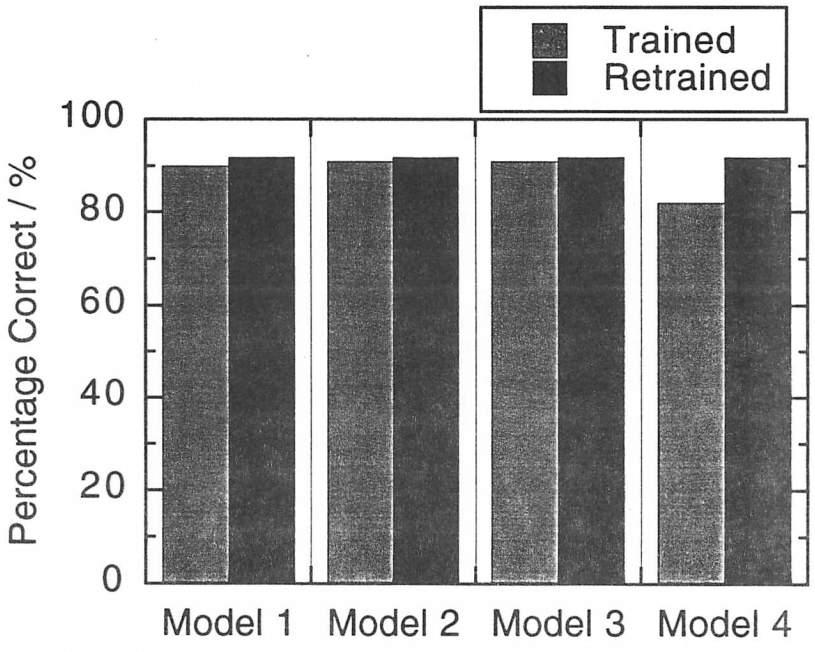

Fig. 6-8 : Percentage of correct answers on the test data set after training on the training data set then after retraining on all the data. *Retraining* is the second training, beginning with the values of weights already obtained by the first training on the training dataset, for the four individual models on all the available data.

Fig. 6-8 shows the reasonable accuracy obtained for the predictions for both the training and test data.

It was therefore decided to choose this committee consisting of four individual models, both because it gave reasonable statistical accuracy and because it reproduced metallurgical expectation rather well. The calculated influence of the carbon concentration on the tendency for solidification cracking represented by the marginalised probability for the data listed in Tables 6-3 and 6-4 using the retrained four models is illustrated in Fig. 6-9a.

Table 6-3 : Chemical compositions used to predict the effects of carbon.

C wt.%	Si wt.%	Mn wt.%	P wt.%	S wt.%	Ni wt.%	Cr wt.%	Mo wt.%
0.00 - 0.14	0.215	1.54	0.015	0.006	0.00	0.00	0.22

All the models, in this case, correctly reproduce the fact that solidification cracking does not occur at intermediate concentrations, as illustrated schematically in Fig. 6-2. Fig. 6-9b shows the best fit and marginalised predictions by the committee model. It can be found that marginalised prediction is moderated from the best fit one. Fig. 6-9a and b also show a significant possibility towards reduced

Table 6-4 : Process parameters used in the prediction of the carbon and molybdenum effects.

Welding Current A	Voltage V	Welding Speed cm min^{-1}	Groove Angle degrees	Preheat Temperature °C
650	31	40	60	20

cracking when the carbon concentration decreases towards zero (*c.f.*, Fig. 6-2).

Fig. 6-10 shows results of prediction of the effect of carbon and sulphur for the hypothetical input data listed in Tables 6-5 and 6-6 using the retrained model. The behaviour illustrated is expected since there should be a increase in the solidification cracking probability as a function of a sulphur particularly at higher carbon concentrations.

Table 6-5 : Chemical compositions used to predict the combined effects of carbon and sulphur.

C wt.%	Si wt.%	Mn wt.%	P wt.%	S wt.%	Ni wt.%	Cr wt.%	Mo wt.%
0.04 - 0.14	0.77	1.48	0.01	0.004 - 0.020	1.5	0.08	0.01

Table 6-6 : Process parameters used to predict the combined effects of carbon and sulphur.

Welding Current A	Voltage V	Welding Speed cm min^{-1}	Groove Angle degrees	Preheat Temperature °C
422	34	32.5	45	20

The final weights of all four models having been retrained on all data and organising the committee are presented in the Appendix. They are also available in digitalised form on http://www.msm.cam.ac.uk/map/data/materials/weldhot.html♯Two. This list, together with the minimum and maximum values in the input data and output values given in Tables 6-1 and 6-2, is sufficient to reproduce the necessary equations and predictions described in this study.

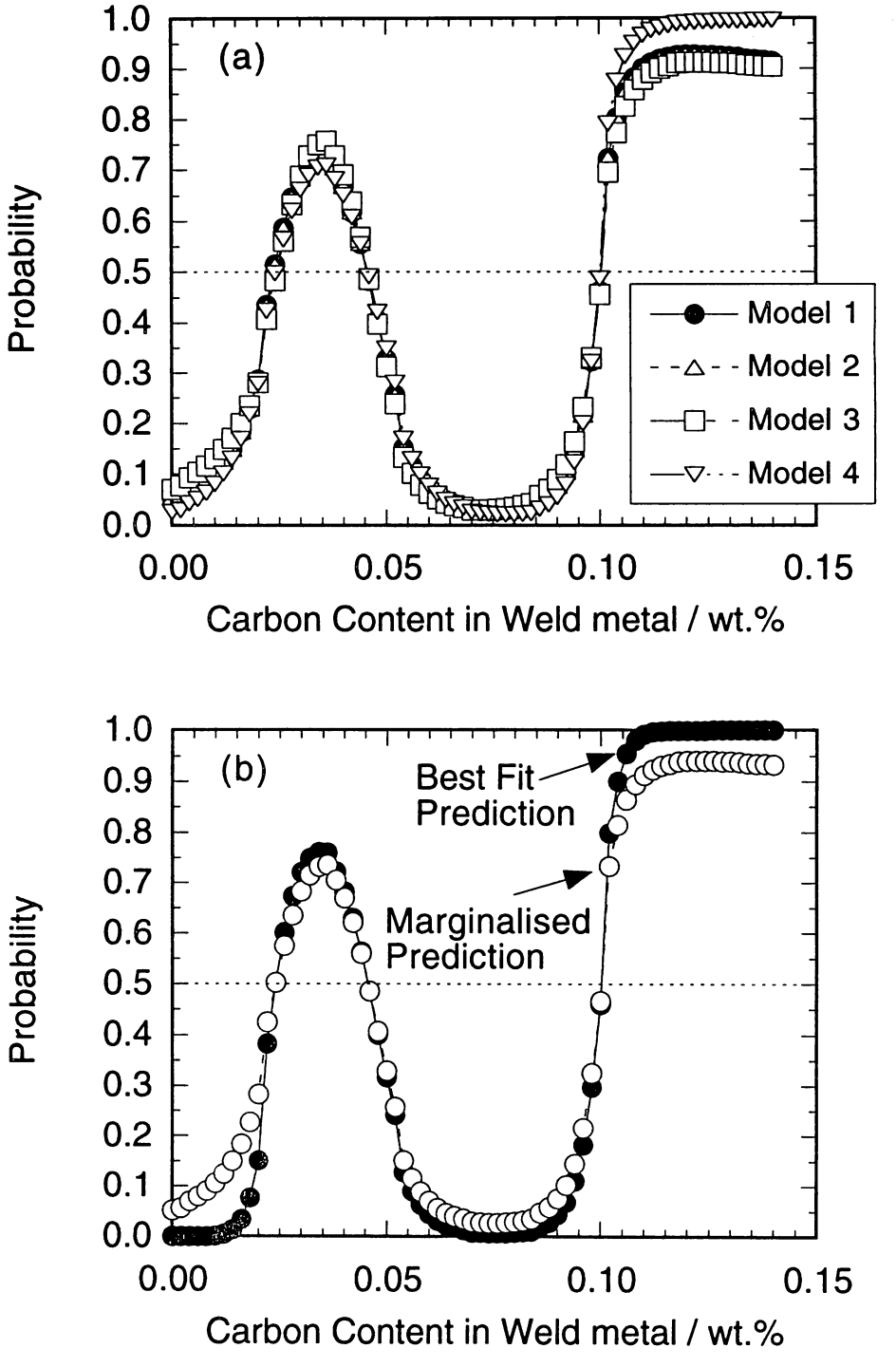

Fig. 6-9 : (a) Marginalised predictions of effect of carbon on solidification cracking probability in steel welds by the four individual retrained models. (b) Best fit and marginalised predictions of effect of carbon on solidification cracking probability in steel welds using the retrained committee model.

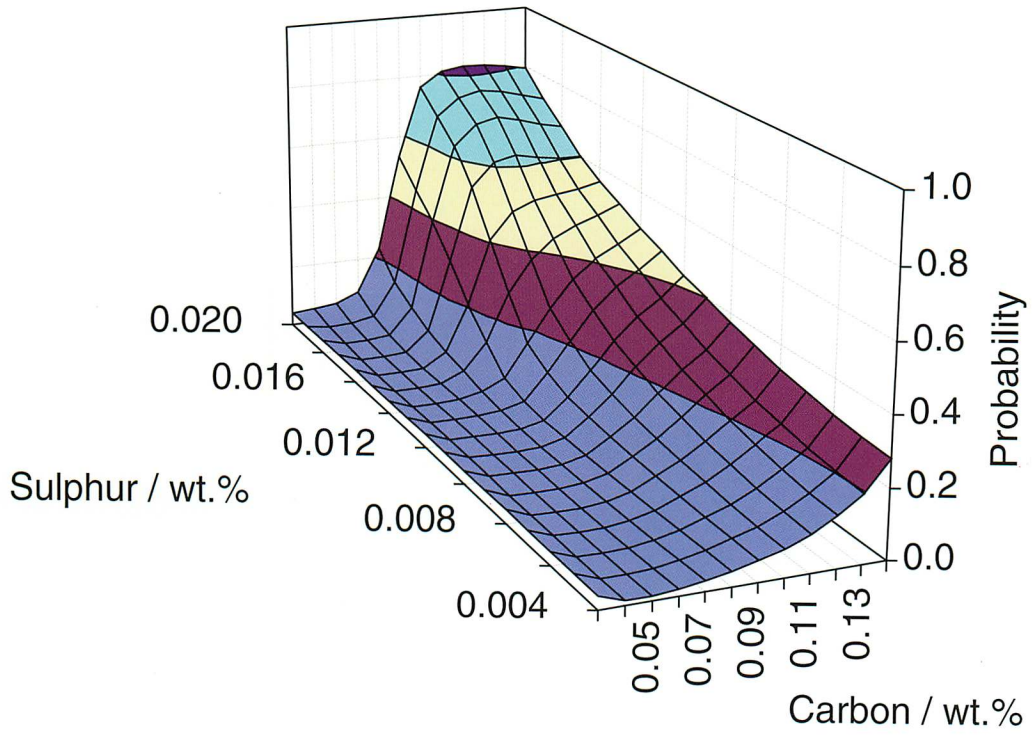

Fig. 6-10 : Predicted effect of sulphur and carbon on solidification cracking in steel welds.

6.6 Use of the Model

A number of further tests were carried out using the retrained model in order to ensure that the selected model predicts in a way consistent with metallurgical experience.

It is widely accepted that sulphur and phosphorus are harmful impurities with respect to the solidification cracking of steel welds. Sekiguchi *et al.* [1966] reported that the effect of sulphur is exacerbated by the presence of nickel as an alloying element. Calculations using the input data listed in Tables 6-7 and 6-8 were done to confirm this trend.

Table 6-7 : Chemical compositions used to predict the combined effects of sulphur and nickel.

C wt.%	Si wt.%	Mn wt.%	P wt.%	S wt.%	Ni wt.%	Cr wt.%	Mo wt.%
0.064	0.77	1.48	0.01	0.005-0.020	0.50-3.50	0.08	0.01

Table 6-8 : Process parameters used to predict the combined effects of sulphur and nickel.

Welding Current A	Voltage V	Welding Speed cm min^{-1}	Groove Angle degrees	Preheat Temperature °C
500	36	40	45	20

Any reduction in the sulphur concentration should increase the resistance to solidification cracking. An increase in the nickel concentration promotes austenitic solidification and therefore should promote solidification cracking, the effect being exaggerated when both the nickel and sulphur concentrations are large. The model reproduces this behaviour rather well, as illustrated in Fig. 6-11a and consistent with the published experimental data presented in Fig. 6-11b.

Molybdenum is a ferrite former and empirical data suggest that it reduces tendency for solidification cracking [Wilkinson *et al.*, 1958; Cottrell, 1962; Morgan-Warren and Jordan, 1974]. Calculations were carried out for the hypothetical input data listed in Tables 6-9 and 6-4 where the molybdenum concentration is varied in the range 0 to 0.6 wt.% which is typical for low-alloy steel welds.

Table 6-9 : Chemical compositions used to predict the effect of molybdenum.

C wt.%	Si wt.%	Mn wt.%	P wt.%	S wt.%	Ni wt.%	Cr wt.%	Mo wt.%
0.04 - 0.14	0.215	1.54	0.015	0.006	0.00	0.00	0.0-0.6

Fig. 6-12 shows that the addition of molybdenum decreases the risk of solidification cracking in general for the steel analysed here. This agrees with published regression equations [Wilkinson *et al.*, 1958; Cottrell, 1962; Morgan-Warren and Jordan, 1974].

As well as the chemical compositions of welds, welding conditions, such as the current, voltage and groove configuration, also influence the solidification cracking susceptibility. Figs. 6-13a and b show the predictions of effect of voltage on the solidification cracking probability for the data shown in Tables 6-10 and 6-11.

Table 6-10 : Chemical compositions used to study the effect of voltage.

C wt.%	Si wt.%	Mn wt.%	P wt.%	S wt.%	Ni wt.%	Cr wt.%	Mo wt.%
0.10	0.215	1.54	0.02	0.01	0.00	0.00	0.22

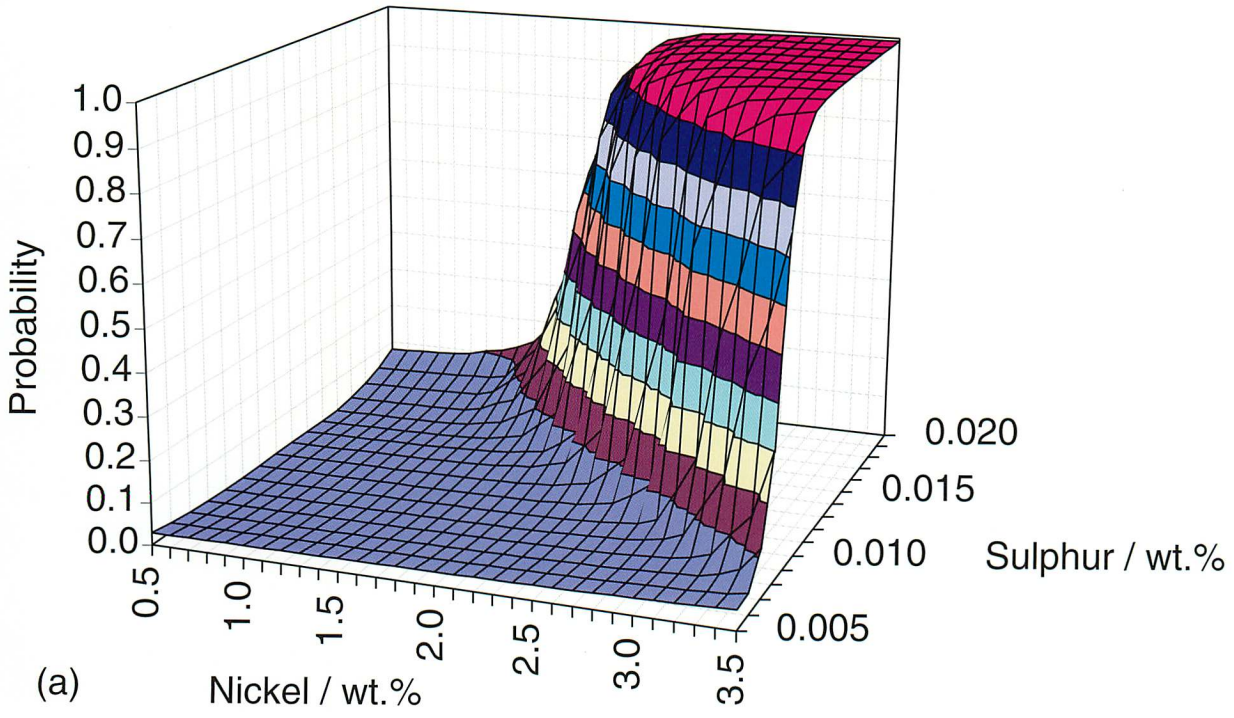

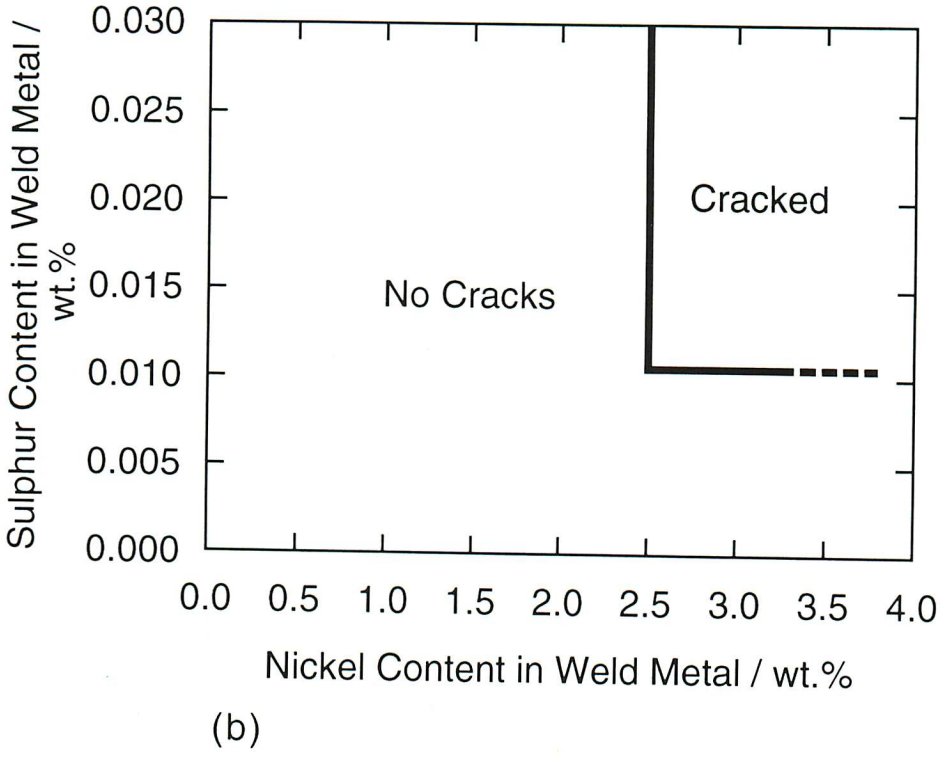

Fig. 6-11 : (a) Predicted effect of sulphur and nickel on solidification cracking in steel welds. (b) Effects of nickel and sulphur contents on solidification cracking in steel welds after Sekiguchi *et al.* [1966].

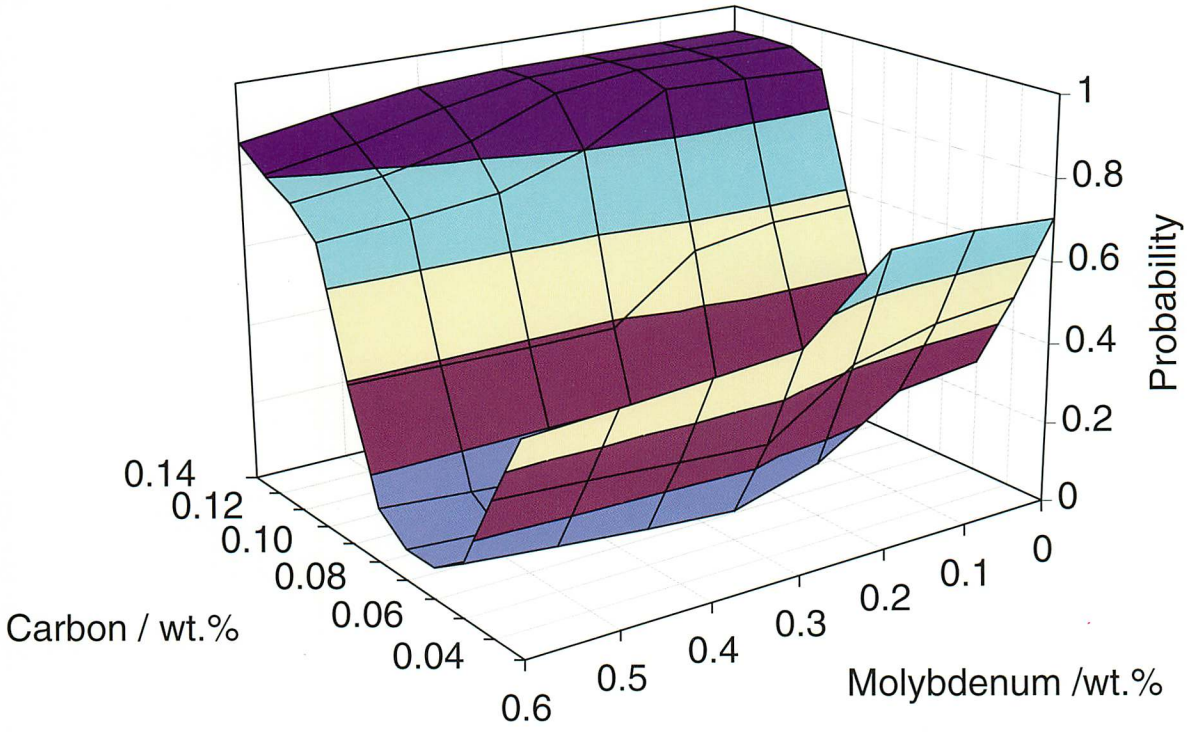

Fig. 6-12 : Predicted effect of molybdenum and carbon on solidification cracking in steel welds.

Table 6-11 : Process parameters used to study the effect of voltage.

Welding Current A	Voltage V	Welding Speed cm min^{-1}	Groove Angle degrees	Preheat Temperature °C
650	25-40	40	60	20

At the lower voltages, predictions by the two hidden unit model (MODEL 4) do not agree very well with those by the other three models and predictions are much uncertain. In fact, marginalised predictions are close to 0.5 there in the Fig. 6-13b.

Fig. 6-14a and b show the predicted effect of groove angle on the solidification cracking probability for the data listed in Tables 6-12 and 6-13.

Table 6-12 : Chemical compositions used to study the effect of groove angle.

C wt.%	Si wt.%	Mn wt.%	P wt.%	S wt.%	Ni wt.%	Cr wt.%	Mo wt.%
0.08	0.77	1.48	0.01	0.02	1.5	0.08	0.01

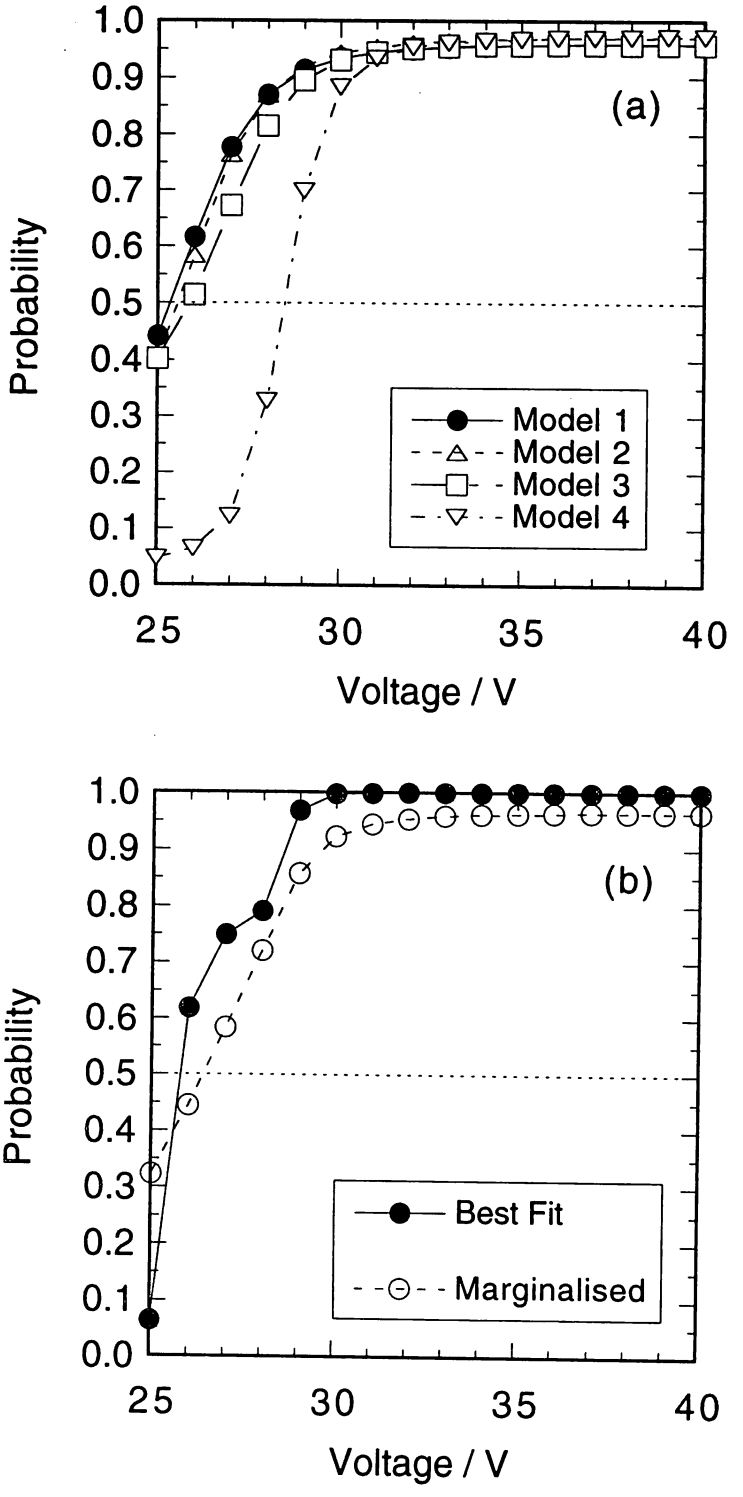

Fig. 6-13 : (a) Marginalised predictions of effect of voltage on solidification cracking in steel welds by the four individual retrained models. (b) Best fit and marginalised predictions of effect of voltage on solidification cracking in steel welds by the retrained committee model.

Table 6-13 : Process parameters used to study the effect of groove angle.

Welding Current A	Voltage V	Welding Speed cm min^{-1}	Groove Angle degrees	Preheat Temperature °C
422	34	32.5	0-90	20

For the effects of groove angle, predictions by each constituent of the committee model do not agree very well (Fig. 6-14a). And the committee model does not give very decisive predictions by the marginalised predictions (Fig. 6-14b). This is due to insufficient or noisy data on the effect of these welding conditions.

6.7 Conclusions

A classification neural network model has been successfully used to represent experimental data on the tendency for solidification cracking during the solidification of low-alloy steel welds. The model has been demonstrated to reproduce known metallurgical experience and will be updated as more data become available.

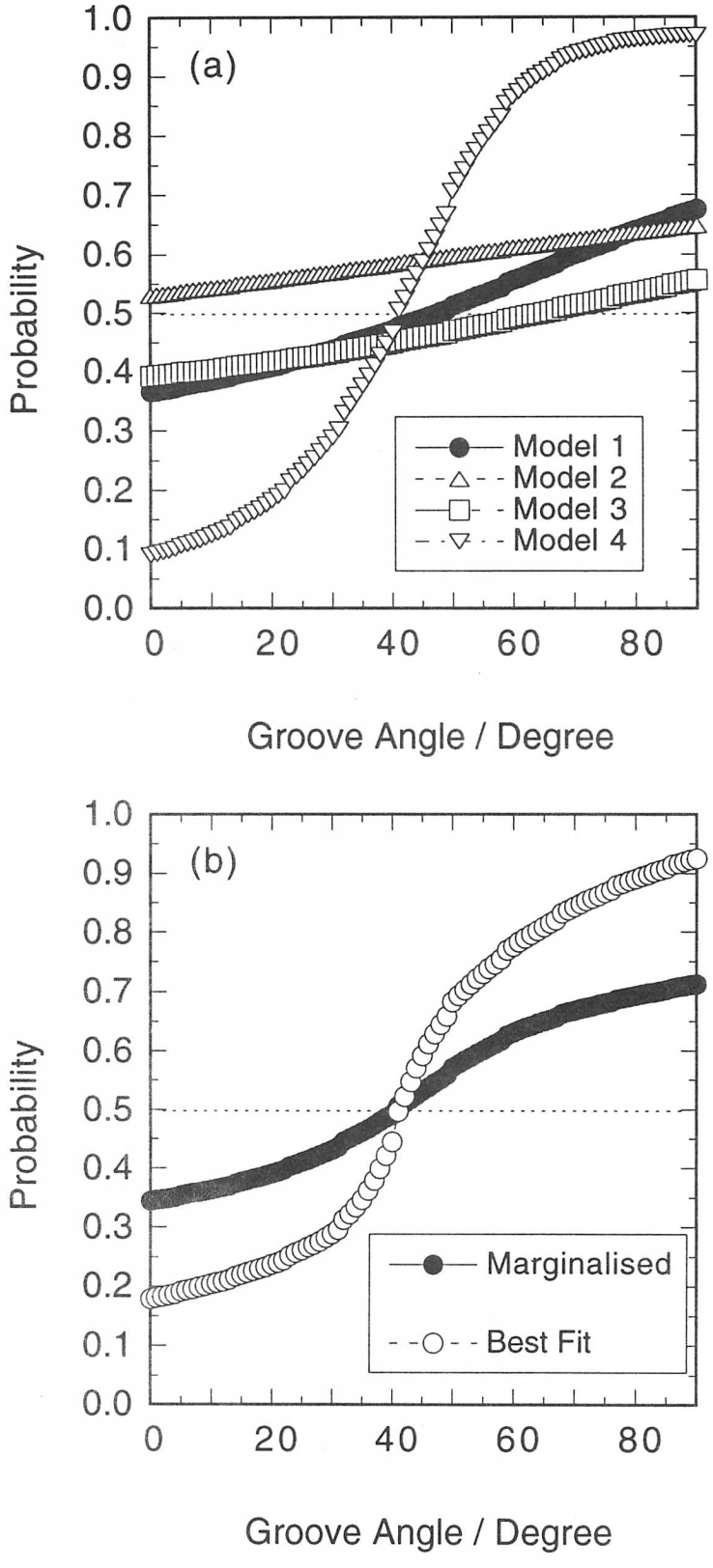

Fig. 6-14 : (a) Marginalised predictions of effect of groove angle on solidification cracking in steel welds by the four individual retrained models. (b) Best fit and marginalised predictions of effect of groove angle on solidification cracking in steel welds by the retrained committee model.

CHAPTER SEVEN

Future Work

A series of quantitative models have been developed and discussed in this thesis. The phase transformation models deal mainly with allotriomorphic and Widmanstätten ferrite in steel welds. However, acicular ferrite is also one of the most important microstructures in steel welds and needs to to be introduced into the scheme. According to the results revealed in Chapter 5, it is now possible to estimate number density of non-metallic inclusions in weld metal from the knowledge of the average inclusion diameter. This in turn gives an indication of the inclusion surface area and number density, parameters important in the development of kinetic theory of acicular ferrite, which is essentially intragranularly nucleated bainite bainite. The segregation model introduced in this work enables the estimation of the local solute-enriched zone in which martensite and/or retained austenite may be observed. This provides a lead into the modelling of those microphases, which are very important local brittle zone.

Morphological parameters, such as unit volumes of Widmanstätten ferrite, bainite and acicular ferrite and aspect ratio, are important since they affect the mechanical properties of the welds. Appropriate models capable of predicting such parameter would be very useful. A start has recently been made by Singh and Bhadeshia [1998] on the bainite and acicular ferrite plate thickness.

Stochastic models, such as Monte Carlo simulation, may provide different information from the deterministic models described Chapter 2 to 4. Three dimensional Monte Carlo simulation with the combination of the finite difference method (FDM) could reveal anisotropic weld solidification and simultaneous heterogeneous grain growth in the adjusted heat affected zone. Such a method can automatically deal with soft and hard impingement and morphology, the most difficult parts of deterministic models. The drawback is that important elements of the microstructure are assumed before the calculations begin. The models can nevertheless be useful in, for example, predicting the cellular/equiaxed transition in weld metal solidification. This is important since it affects subsequent phase transformations.

A solidification cracking model was proposed in Chapter 6. The experimental dataset on which it was based on is not sufficient to evaluate the effect of welding conditions and we need further accumulation of experimental data. Cold cracking in the weld metal is now one of the growing subjects because of the

trends towards higher tensile strengths. We thus need to be able to estimate cold cracking susceptibility for a wide range of weld metals.

APPENDIX ONE

Statistical Analysis of Stereological Measurements

95 % confidence limits in lineal intercept measurements are given by following equations [DeHoff and Rhines, 1968]:

for mean linear intercept:

$$95\%\text{confidence} = \pm 2\sqrt{\frac{1}{N}\left(\frac{\sigma_L}{\overline{L}_{tn}}\right)^2} \qquad (A1-1)$$

where

N: number of measurements,

σ_L: standard deviation in the size distribution of L_{tn},

L_{tn}:a lineal intercept measured in the transverse section in a direction normal to the major axes of grains.

$\overline{L}_{tn}$:a mean lineal intercept measured in the transverse section in a direction normal to the major axes of grains.

The corresponding limits for point counting are:

$$95\%\text{confidence} = \pm 2\sqrt{\frac{1-V_x}{N}} \qquad (A1-2)$$

where V_x is a volume fraction of microstructural component x.

Reference

DeHoff, R. T. and Rhines, F. N.: *Quantitative Microscopy,* McGraw Hill, New York (1968).

APPENDIX TWO

Real and Extended Volumes in Simultaneous Transformations

A2.1 Introduction

In a modelling for a single transformation, an estimation of the volume fraction requires impingement between particles transformed to be taken into account. This is generally done using the *extended volume* concept and has been reviewed thoroughly by Christian [1975]. Total volume of the products *1* transformed (V_1) can be related with its extended volume V_1^e by:

$$dV_1 = \left(1 - \frac{V_1}{V_{total}}\right) dV_1^e \qquad \text{and} \qquad \frac{V_1}{V_{total}} = 1 - \exp\left(-\frac{V_1^e}{V_{total}}\right) \qquad (A2-1)$$

where V_{total} is a total volume of the system.

In practice, there are many cases where several transformations occur together. The different reactions interfere with each other in a way which is seminal to the development of power plant microstructures. Therefore, considerable effort has recently been devoted to the development of an Avrami model for simultaneous reactions [Robson and Bhadeshia, 1996; 1997a; b; Jones and Bhadeshia, 1997a; b]. The solutions in these simultaneous transformation models are numerical except for the special case where the two phases form with a fixed ratio of fractions.

The purpose of the present work was to see whether other more complex analytical solutions exist.

A2.2 Method

First redefine the variables for n phases as follows:

$$\begin{aligned} z_n &= (V_1 + V_2 + V_3 + \cdots + V_n)/V_{total} \\ z_n^e &= (V_1^e + V_2^e + V_3^e + \cdots + V_n^e)/V_{total} \end{aligned} \qquad (A2-2)$$

where V_i and V_i^e $(i = 1, 2, 3, \cdots, n)$ are total real and extended volumes of the products i respectively.

and hence

$$dz_n = (1 - z_n)dz_n^e \qquad \text{and} \qquad z_n = 1 - \exp\{-z_n^e\} \qquad (A2-3)$$

It follows that in general for phase i in a system transforming to n phases,

$$\begin{aligned} dV_i &= (1 - z_n)dV_i^e \\ &= \{1 - (1 - \frac{dz_n}{dz_n^e})\}dV_i^e \\ &= \frac{dz_n}{dz_n^e}dV_i^e \\ &= (1 - z_n)dV_i^e \\ &= [1 - \{1 - \exp(-z_n^e)\}]dV_i^e \\ &= \exp\{-z_n^e\}dV_i^e \\ V_i &= \int \exp\{-z_n^e\}dV_i^e \end{aligned} \qquad (A2-4)$$

Hence

$$V_i = \int \exp\{-z_n^e\}dV_i^e \qquad (A2-5)$$

A2.3 **Solutions**

Analytical solutions exist for cases where the extended volumes of the different phases can be related. Thus, for two simultaneous reactions, the extended volume of phase 2 may be written as a general, differentiable function f of phase 1,

$$\begin{aligned} V_2^e &= f\{V_1^e\} \\ z_2^e &= (V_1^e + f\{V_1^e\})/V_{total} \\ dz_2^e &= (dV_1^e + df\{V_1^e\})/V_{total} \end{aligned} \qquad (A2-6)$$

where df is the derivative of f. Substitution into equation (A2-5) gives:

$$\begin{aligned} v_2 &= \int \exp\left\{-\frac{V_1^e + f\{V_1^e\}}{V_{total}}\right\} \frac{df\{V_1^e\}}{V_{total}} \\ v_1 &= \int \exp\left\{-\frac{V_1^e + f\{V_1^e\}}{V_{total}}\right\} \frac{dV_1^e}{V_{total}} \end{aligned} \qquad (A2-7)$$

where $v_i = V_i/V_{total}$ gives the volume fraction of phase i.

A2.4 **Examples**

A2.4.1 *Linear Case*

Suppose that the extended volumes are related linearly:

$$V_2^e = BV_1^e + C \qquad \text{with} \qquad B \geq 0 \qquad \text{and} \qquad C \geq 0 \qquad (A2-8)$$

then $df\{V_1^e\} = BdV_1^e$ and from equation (A2-7):

$$v_2 = \int \exp\left\{-\frac{(1+B)V_1^e + C}{V_{total}}\right\} \frac{BdV_1^e}{V_{total}}$$
$$v_1 = \int \exp\left\{-\frac{(1+B)V_1^e + C}{V_{total}}\right\} \frac{dV_1^e}{V_{total}} \qquad (A2-9)$$

If the isotropic growth rate of phase 1 is G_r and if all particles of phase 1 start growth at time $t = 0$ from a fixed number of sites n_V per unit volume then

$$V_1^e = n_V \frac{4\pi}{3} G_r^3 t^3 \qquad (A2-10)$$

It is emphasised that the specific assumptions made to express V_1^e can be selected at will, for example to include a nucleation rate (details can be found in Christian [1975]. Substitution of the extended volume in equations (A2-9) gives

$$v_2 = \frac{B}{1+B} \exp\{-\frac{C}{V_{total}}\}\left[1 - \exp\left\{-\frac{(1+B)n_V \frac{4\pi}{3} G_r^3 t^3}{V_{total}}\right\}\right]$$
$$v_1 = \frac{1}{1+B} \exp\{-\frac{C}{V_{total}}\}\left[1 - \exp\left\{-\frac{(1+B)n_V \frac{4\pi}{3} G_r^3 t^3}{V_{total}}\right\}\right] \qquad (A2-11)$$

Notice that *both* equations contain the term $n_V \frac{4\pi}{3} G_r^3 t^3$ which has the growth rate of phase 1. This is because the extended volume of phase 2 is not independent of that of phase 1. The term $\exp\{-C/V_{total}\}$ is the fraction of parent phase available for transformation at $t = 0$; it arises because $1 - \exp\{-C/V_{total}\}$ of phase 2 exists prior to commencement of the simultaneous reaction at $t = 0$. Thus, v_2 is the additional fraction of phase 2 that forms during simultaneous reaction. When $C = 0$, equations (A2-8) reduce to the cases considered by Robson and Bhadeshia [1996; 1997a; b]. It is emphasised that $C \geq 0$. A negative value simply implies that a fraction of phase 1 exists prior to $t = 0$ and would require a rearrangement of equation (A2-9) with corresponding changes to the subsequent derivations.

A2.4.2 *Parabolic Case*

Suppose that the extended volumes are related parabolically:

$$V_2^e = A(V_1^e)^2 + BV_1^e + C \quad \text{with} \quad A \geq 0 \quad \text{and} \quad B \geq 0 \quad \text{and} \quad C \geq 0 \quad (A2-12)$$

then $df\{V_1^e\} = 2AV_1^e + BdV_1^e$ and from equation (A2-7):

$$v_2 = \int \exp\left\{-\frac{A(V_1^e)^2 + (1+B)V_1^e + C}{V_{total}}\right\} \frac{(2AV_1^e + B)dV_1^e}{V_{total}}$$
$$v_1 = \int \exp\left\{-\frac{A(V_1^e)^2 + (1+B)V_1^e + C}{V_{total}}\right\} \frac{dV_1^e}{V_{total}} \qquad (A2-13)$$

It follows that †

$$v_2 = \exp\left\{-\frac{C}{V_{total}}\right\}\left[\sqrt{\frac{\pi}{4A}}\exp\left\{\frac{(1+B)^2}{4A}\right\}\left(\mathrm{erf}\left\{\frac{1+B}{\sqrt{4A}}\right\} - \mathrm{erf}\left\{\frac{1+B}{\sqrt{4A}} + \sqrt{A}V_1^e\right\}\right)\right]$$
$$- \exp\left\{-\frac{C}{V_{total}}\right\}\left[\exp\left\{-\frac{A(V_1^e)^2 + (1+B)V_1^e}{V_{total}}\right\}\right]$$
$$v_1 = \exp\left\{-\frac{C}{V_{total}}\right\}\left[\sqrt{\frac{\pi}{4A}}\exp\left\{\frac{(1+B)^2}{4A}\right\}\left(\mathrm{erf}\left\{\frac{1+B}{\sqrt{4A}}\right\} - \mathrm{erf}\left\{\frac{1+B}{\sqrt{4A}} + \sqrt{A}V_1^e\right\}\right)\right] \quad (A2-14)$$

The volume fractions v_i again refer to the phases that form *simultaneously* and hence there is a scaling factor $\exp\{-C/V_{total}\}$ which is the fraction of parent phase available for coupled transformation to phases 1 and 2.

Reference

Christian, J. W.: *The Theory of Transformations in Metals and Alloys, Part 1 Equilibrium and General Kinetic Theory, 2nd ed.*,Pergamon Press Ltd, Oxford (1975).

Jones, S. J. and Bhadeshia, H. K. D. H.: *Acta Materialia* **45** (1997a) 2911–2920.

Jones, S. J. and Bhadeshia, H. K. D. H.: *Metallurgical and Materials Transactions A* **28A** (1997b) 2005–2013.

Robson, J. D. and Bhadeshia, H. K. D. H.: *Calphad* **20** (1996) 447–460.

Robson, J. D. and Bhadeshia, H. K. D. H.: *Materials Science and Technology* **13** (1997a) 631–639.

Robson, J. D. and Bhadeshia, H. K. D. H.: *Materials Science and Technology* **13** (1997b) 640–644.

† erf(z) is the *error function* defined as:

$$\mathrm{erf}(z) = \int_0^z \exp(-t^2)dt$$

APPENDIX THREE

The Experimental and Neural Network Datasets for Solidification Cracking Modelling

The entire dataset used for training of the neural network in Chapter 6 is listed in Table A3-1.

The values for the weights obtained by the training with all the data listed in Tables 6-1 and 6-2 in Chapter 6 are shown in Table A3-2a–d. Best fit predictions of solidification cracking in steel welds can be made using these data and the data in Tables 6-1 and 6-2 together with equations (6-6) to (6-9) and (6-12).

Table A3-1 : The entire experimental dataset used for training of the neural network in Chapter 6.

C	Si	Mn	P	S	Ni	Cr	Mo	Reference
0.085	0.260	1.330	0.1000	0.0070	0.030	0.000	0.000	Masumoto and Imai, 1970
0.077	0.190	1.180	0.0490	0.0070	0.550	0.000	0.000	
0.083	0.220	1.300	0.0480	0.0070	2.310	0.000	0.000	
0.083	0.220	1.300	0.0480	0.0090	3.020	0.000	0.000	
0.063	0.210	1.000	0.0220	0.0090	3.420	0.000	0.000	
0.074	0.210	1.070	0.1000	0.0080	4.360	0.000	0.000	
0.059	0.200	1.000	0.0220	0.0070	5.210	0.000	0.000	
0.059	0.190	0.900	0.0250	0.0080	6.510	0.000	0.000	
0.150	0.180	1.280	0.0245	0.0255	0.045	0.045	0.020	Garland and Bailey, 1976
0.150	0.180	1.195	0.0250	0.0240	0.050	0.035	0.015	
0.175	0.485	1.820	0.0135	0.0230	0.045	0.040	0.020	
0.150	0.180	1.280	0.0490	0.0255	0.045	0.045	0.020	
0.150	0.180	1.195	0.0250	0.0240	0.050	0.035	0.015	
0.175	0.485	1.820	0.0135	0.0230	0.045	0.040	0.020	
0.160	0.290	0.980	0.0310	0.0280	0.040	0.030	0.010	
0.160	0.290	0.980	0.0310	0.0280	0.040	0.030	0.010	
0.160	0.290	0.980	0.0310	0.0280	0.040	0.030	0.010	
0.160	0.290	0.990	0.0300	0.0270	0.040	0.030	0.010	
0.160	0.290	0.990	0.0300	0.0270	0.040	0.030	0.010	
0.160	0.290	0.990	0.0300	0.0270	0.040	0.030	0.010	
0.190	0.740	1.620	0.0210	0.0200	0.040	0.030	0.010	
0.190	0.740	1.620	0.0210	0.0200	0.040	0.030	0.010	
0.190	0.740	1.620	0.0210	0.0200	0.040	0.030	0.010	

Table A3-1 : (Continued.)

C	Si	Mn	P	S	Ni	Cr	Mo	Reference
0.012	0.215	1.540	0.0150	0.0060	0.000	0.000	0.220	Homma *et al.*, 1982
0.013	0.215	1.540	0.0150	0.0060	0.000	0.000	0.220	
0.014	0.215	1.540	0.0150	0.0060	0.000	0.000	0.220	
0.016	0.215	1.540	0.0150	0.0060	0.000	0.000	0.220	
0.033	0.215	1.540	0.0150	0.0060	0.000	0.000	0.220	
0.076	0.215	1.540	0.0150	0.0060	0.000	0.000	0.220	
0.086	0.215	1.540	0.0150	0.0060	0.000	0.000	0.220	
0.091	0.215	1.540	0.0150	0.0060	0.000	0.000	0.220	
0.093	0.215	1.540	0.0150	0.0060	0.000	0.000	0.220	
0.096	0.215	1.540	0.0150	0.0060	0.000	0.000	0.220	
0.044	0.215	1.540	0.0150	0.0060	0.000	0.000	0.220	
0.045	0.215	1.540	0.0150	0.0060	0.000	0.000	0.220	
0.048	0.215	1.540	0.0150	0.0060	0.000	0.000	0.220	
0.051	0.215	1.540	0.0150	0.0060	0.000	0.000	0.220	
0.052	0.215	1.540	0.0150	0.0060	0.000	0.000	0.220	
0.053	0.215	1.540	0.0150	0.0060	0.000	0.000	0.220	
0.054	0.215	1.540	0.0150	0.0060	0.000	0.000	0.220	
0.056	0.215	1.540	0.0150	0.0060	0.000	0.000	0.220	
0.057	0.215	1.540	0.0150	0.0060	0.000	0.000	0.220	
0.058	0.215	1.540	0.0150	0.0060	0.000	0.000	0.220	
0.060	0.215	1.540	0.0150	0.0060	0.000	0.000	0.220	
0.064	0.215	1.540	0.0150	0.0060	0.000	0.000	0.220	
0.066	0.215	1.540	0.0150	0.0060	0.000	0.000	0.220	
0.067	0.215	1.540	0.0150	0.0060	0.000	0.000	0.220	
0.068	0.215	1.540	0.0150	0.0060	0.000	0.000	0.220	
0.071	0.215	1.540	0.0150	0.0060	0.000	0.000	0.220	
0.071	0.215	1.540	0.0150	0.0060	0.000	0.000	0.220	
0.073	0.215	1.540	0.0150	0.0060	0.000	0.000	0.220	
0.073	0.215	1.540	0.0150	0.0060	0.000	0.000	0.220	
0.075	0.215	1.540	0.0150	0.0060	0.000	0.000	0.220	
0.078	0.215	1.540	0.0150	0.0060	0.000	0.000	0.220	
0.081	0.215	1.540	0.0150	0.0060	0.000	0.000	0.220	
0.088	0.215	1.540	0.0150	0.0060	0.000	0.000	0.220	
0.088	0.215	1.540	0.0150	0.0060	0.000	0.000	0.220	
0.103	0.215	1.540	0.0150	0.0060	0.000	0.000	0.220	
0.096	0.215	1.540	0.0150	0.0060	0.000	0.000	0.220	
0.128	0.215	1.540	0.0150	0.0060	0.000	0.000	0.220	
0.106	0.215	1.540	0.0150	0.0060	0.000	0.000	0.220	
0.130	0.215	1.540	0.0150	0.0060	0.000	0.000	0.220	
0.134	0.215	1.540	0.0150	0.0060	0.000	0.000	0.220	
0.095	0.215	1.540	0.0150	0.0060	0.000	0.000	0.220	
0.097	0.215	1.540	0.0150	0.0060	0.000	0.000	0.220	
0.053	0.215	1.540	0.0150	0.0060	0.000	0.000	0.220	
0.046	0.215	1.540	0.0150	0.0060	0.000	0.000	0.220	
0.041	0.215	1.540	0.0150	0.0060	0.000	0.000	0.220	
0.039	0.215	1.540	0.0150	0.0060	0.000	0.000	0.220	
0.045	0.215	1.540	0.0150	0.0060	0.000	0.000	0.220	
0.035	0.215	1.540	0.0150	0.0060	0.000	0.000	0.220	
0.029	0.215	1.540	0.0150	0.0060	0.000	0.000	0.220	
0.042	0.215	1.540	0.0150	0.0060	0.000	0.000	0.220	

Table A3-1 : (Continued.)

C	Si	Mn	P	S	Ni	Cr	Mo	Reference
0.064	0.77	1.480	0.0100	0.015	0.434	0.080	0.010	Sekiguchi *et al.*, 1966
0.064	0.77	1.480	0.0100	0.013	0.332	0.080	0.010	
0.064	0.77	1.480	0.0100	0.012	0.880	0.080	0.010	
0.064	0.77	1.480	0.0100	0.010	0.829	0.080	0.010	
0.064	0.77	1.480	0.0100	0.009	0.957	0.080	0.010	
0.064	0.77	1.480	0.0100	0.009	0.995	0.080	0.010	
0.064	0.77	1.480	0.0100	0.010	1.072	0.080	0.010	
0.064	0.77	1.480	0.0100	0.013	1.327	0.080	0.010	
0.064	0.77	1.480	0.0100	0.015	1.697	0.080	0.010	
0.064	0.77	1.480	0.0100	0.013	1.812	0.080	0.010	
0.064	0.77	1.480	0.0100	0.013	1.977	0.080	0.010	
0.064	0.77	1.480	0.0100	0.016	2.258	0.080	0.010	
0.064	0.77	1.480	0.0100	0.016	2.373	0.080	0.010	
0.064	0.77	1.480	0.0100	0.017	2.513	0.080	0.010	
0.064	0.77	1.480	0.0100	0.016	2.513	0.080	0.010	
0.064	0.77	1.480	0.0100	0.014	2.424	0.080	0.010	
0.064	0.77	1.480	0.0100	0.013	2.500	0.080	0.010	
0.064	0.77	1.480	0.0100	0.016	2.615	0.080	0.010	
0.064	0.77	1.480	0.0100	0.014	2.602	0.080	0.010	
0.064	0.77	1.480	0.0100	0.013	2.692	0.080	0.010	
0.064	0.77	1.480	0.0100	0.013	2.845	0.080	0.010	
0.064	0.77	1.480	0.0100	0.009	2.309	0.080	0.010	
0.064	0.77	1.480	0.0100	0.009	2.373	0.080	0.010	
0.064	0.77	1.480	0.0100	0.008	2.271	0.080	0.010	
0.064	0.77	1.480	0.0100	0.010	2.921	0.080	0.010	
0.064	0.77	1.480	0.0100	0.010	3.189	0.080	0.010	
0.064	0.77	1.480	0.0100	0.009	3.126	0.080	0.010	
0.064	0.77	1.480	0.0100	0.009	3.177	0.080	0.010	
0.064	0.77	1.480	0.0100	0.008	3.189	0.080	0.010	
0.064	0.77	1.480	0.0100	0.020	3.610	0.080	0.010	
0.064	0.77	1.480	0.0100	0.017	3.610	0.080	0.010	
0.064	0.77	1.480	0.0100	0.016	3.649	0.080	0.010	
0.064	0.77	1.480	0.0100	0.013	3.508	0.080	0.010	
0.064	0.77	1.480	0.0100	0.013	3.521	0.080	0.010	
0.064	0.77	1.480	0.0100	0.017	3.240	0.080	0.010	
0.064	0.77	1.480	0.0100	0.016	3.279	0.080	0.010	
0.064	0.77	1.480	0.0100	0.013	3.164	0.080	0.010	
0.064	0.77	1.480	0.0100	0.013	2.998	0.080	0.010	
0.064	0.77	1.480	0.0100	0.014	2.807	0.080	0.010	
0.064	0.77	1.480	0.0100	0.014	2.832	0.080	0.010	
0.064	0.77	1.480	0.0100	0.015	2.896	0.080	0.010	
0.064	0.77	1.480	0.0100	0.013	0.332	0.080	0.010	
0.064	0.77	1.480	0.0100	0.013	1.135	0.080	0.010	
0.064	0.77	1.480	0.0100	0.016	1.442	0.080	0.010	
0.064	0.77	1.480	0.0100	0.014	1.569	0.080	0.010	
0.064	0.77	1.480	0.0100	0.011	1.709	0.080	0.010	
0.064	0.77	1.480	0.0100	0.014	1.837	0.080	0.010	
0.064	0.77	1.480	0.0100	0.017	2.143	0.080	0.010	
0.064	0.77	1.480	0.0100	0.013	2.424	0.080	0.010	
0.064	0.77	1.480	0.0100	0.013	2.424	0.080	0.010	
0.064	0.77	1.480	0.0100	0.011	2.488	0.080	0.010	
0.064	0.77	1.480	0.0100	0.010	2.590	0.080	0.010	
0.064	0.77	1.480	0.0100	0.010	3.036	0.080	0.010	
0.064	0.77	1.480	0.0100	0.011	2.934	0.080	0.010	
0.064	0.77	1.480	0.0100	0.011	3.062	0.080	0.010	
0.064	0.77	1.480	0.0100	0.019	3.585	0.080	0.010	
0.064	0.77	1.480	0.0100	0.015	3.572	0.080	0.010	
0.064	0.77	1.480	0.0100	0.012	3.559	0.080	0.010	
0.064	0.77	1.480	0.0100	0.017	3.049	0.080	0.010	
0.064	0.77	1.480	0.0100	0.016	2.985	0.080	0.010	
0.064	0.77	1.480	0.0100	0.015	2.551	0.080	0.010	

Table A3-1 : (Continued.)

C	Si	Mn	P	S	Ni	Cr	Mo	Reference
0.064	0.77	1.480	0.0100	0.013	0.549	0.080	0.010	Sekiguchi *et al.*, 1966
0.064	0.77	1.480	0.0100	0.012	0.804	0.080	0.010	
0.064	0.77	1.480	0.0100	0.009	0.765	0.080	0.010	
0.064	0.77	1.480	0.0100	0.007	0.714	0.080	0.010	
0.064	0.77	1.480	0.0100	0.014	2.003	0.080	0.010	
0.064	0.77	1.480	0.0100	0.009	2.437	0.080	0.010	
0.064	0.77	1.480	0.0100	0.007	2.284	0.080	0.010	
0.064	0.77	1.480	0.0100	0.008	2.972	0.080	0.010	
0.064	0.77	1.480	0.0100	0.010	2.998	0.080	0.010	
0.064	0.77	1.480	0.0100	0.012	2.539	0.080	0.010	
0.064	0.77	1.480	0.0100	0.012	2.641	0.080	0.010	
0.064	0.77	1.480	0.0100	0.012	2.870	0.080	0.010	
0.064	0.77	1.480	0.0100	0.011	3.189	0.080	0.010	
0.064	0.77	1.480	0.0100	0.013	3.572	0.080	0.010	
0.064	0.77	1.480	0.0100	0.018	0.651	0.080	0.010	
0.064	0.77	1.480	0.0100	0.015	2.641	0.080	0.010	
0.064	0.77	1.480	0.0100	0.014	2.679	0.080	0.010	
0.064	0.77	1.480	0.0100	0.027	2.781	0.080	0.010	
0.064	0.77	1.480	0.0100	0.026	2.679	0.080	0.010	
0.064	0.77	1.480	0.0100	0.026	2.717	0.080	0.010	

Table A3-1 : (Continued.)

Welding Current/ A	Voltage/ V	Welding Speed/ cm min^{-1}	Groove Angle/ degree	Preheat Temperature/ ℃	Cracking Ratio	Classified Output	Reference
800	30	30	60	20	0.0000	0	Masumoto and Imai, 1970
800	30	30	60	20	0.0000	0	
800	30	30	60	20	0.0000	0	
800	30	30	60	20	1.0000	1	
800	30	30	60	20	1.0000	1	
800	30	30	60	20	1.0000	1	
800	30	30	60	20	1.0000	1	
800	30	30	60	20	1.0000	1	
800	28	55	75	20	0.2300	1	Garland and Bailey, 1976
800	28	55	75	20	0.4300	1	
800	28	55	75	20	0.5500	1	
800	28	55	75	150	0.0500	0	
800	28	55	75	150	0.1500	1	
800	28	55	75	150	0.1400	1	
550	31	53	90	20	1.0000	1	
550	31	53	90	20	1.0000	1	
550	31	53	90	20	1.0000	1	
550	31	53	90	20	1.0000	1	
550	31	53	90	20	1.0000	1	
550	31	53	90	20	1.0000	1	
550	31	53	90	20	1.0000	1	
550	31	53	90	20	1.0000	1	

Table A3-1 : (Continued.)

Welding Current/ A	Voltage/ V	Welding Speed/ cm min^{-1}	Groove Angle/ degree	Preheat Temperature/ ℃	Cracking Ratio	Classified Output	Reference
650	31	40	60	20	0.0000	0	Homma *et al.*, 1982
650	31	40	60	20	0.0000	0	
650	31	40	60	20	0.0000	0	
650	31	40	60	20	0.0000	0	
650	31	40	60	20	0.0000	0	
650	31	40	60	20	0.0000	0	
650	31	40	60	20	0.0000	0	
650	31	40	60	20	0.0000	0	
650	31	40	60	20	0.0000	0	
650	31	40	60	20	0.0000	0	
650	31	40	60	20	0.0000	0	
650	31	40	60	20	0.0000	0	
650	31	40	60	20	0.0000	0	
650	31	40	60	20	0.0000	0	
650	31	40	60	20	0.0000	0	
650	31	40	60	20	0.0000	0	
650	31	40	60	20	0.0000	0	
650	31	40	60	20	0.0000	0	
650	31	40	60	20	0.0000	0	
650	31	40	60	20	0.0000	0	
650	31	40	60	20	0.0000	0	
650	31	40	60	20	0.0000	0	
650	31	40	60	20	0.0000	0	
650	31	40	60	20	0.0000	0	
650	31	40	60	20	0.0000	0	
650	31	40	60	20	0.0000	0	
650	31	40	60	20	0.0000	0	
650	31	40	60	20	0.0000	0	
650	31	40	60	20	0.0000	0	
650	31	40	60	20	0.0000	0	
650	31	40	60	20	0.0000	0	
650	31	40	60	20	0.0000	0	
650	31	40	60	20	0.0000	0	
650	31	40	60	20	0.0000	0	
650	31	40	60	20	0.0000	0	
650	31	40	60	20	0.0000	0	
650	31	40	60	20	0.9957	1	
650	31	40	60	20	0.7043	1	
650	31	40	60	20	0.3348	1	
650	31	40	60	20	0.0739	1	
650	31	40	60	20	0.0478	0	
650	31	40	60	20	0.0217	0	
650	31	40	60	20	0.0304	0	
650	31	40	60	20	0.0217	0	
650	31	40	60	20	0.0522	1	
650	31	40	60	20	0.0217	0	
650	31	40	60	20	0.1957	1	
650	31	40	60	20	0.0783	1	
650	31	40	60	20	0.0565	1	
650	31	40	60	20	0.5522	1	

Table A3-1 : (Continued.)

Welding Current/ A	Voltage/ V	Welding Speed/ cm min^{-1}	Groove Angle/ degree	Preheat Temperature/ ℃	Cracking Ratio	Classified Output	Reference
545	36	47.5	0	20	0.0000	0	Sekiguchi *et al.*, 1966
545	36	47.5	0	20	0.0000	0	
545	36	47.5	0	20	0.0000	0	
545	36	47.5	0	20	0.0000	0	
545	36	47.5	0	20	0.0000	0	
545	36	47.5	0	20	0.0000	0	
545	36	47.5	0	20	0.0000	0	
545	36	47.5	0	20	0.0000	0	
545	36	47.5	0	20	0.0000	0	
545	36	47.5	0	20	0.0000	0	
545	36	47.5	0	20	0.0000	0	
545	36	47.5	0	20	0.0000	0	
545	36	47.5	0	20	0.0000	0	
545	36	47.5	0	20	0.0000	0	
545	36	47.5	0	20	0.0000	0	
545	36	47.5	0	20	0.0000	0	
545	36	47.5	0	20	0.0000	0	
545	36	47.5	0	20	0.0000	0	
545	36	47.5	0	20	0.0000	0	
545	36	47.5	0	20	0.0000	0	
545	36	47.5	0	20	0.0000	0	
545	36	47.5	0	20	0.0000	0	
545	36	47.5	0	20	0.0000	0	
545	36	47.5	0	20	0.0000	0	
545	36	47.5	0	20	0.0000	0	
545	36	47.5	0	20	0.0000	0	
545	36	47.5	0	20	0.0000	0	
545	36	47.5	0	20	0.0000	0	
545	36	47.5	0	20	0.0000	0	
545	36	47.5	0	20	1.0000	1	
545	36	47.5	0	20	1.0000	1	
545	36	47.5	0	20	1.0000	1	
545	36	47.5	0	20	1.0000	1	
545	36	47.5	0	20	1.0000	1	
545	36	47.5	0	20	1.0000	1	
545	36	47.5	0	20	1.0000	1	
545	36	47.5	0	20	1.0000	1	
545	36	47.5	0	20	1.0000	1	
545	36	47.5	0	20	1.0000	1	
545	36	47.5	0	20	1.0000	1	
545	36	47.5	0	20	1.0000	1	
422	34	32.5	45	20	0.0000	0	
422	34	32.5	45	20	0.0000	0	
422	34	32.5	45	20	0.0000	0	
422	34	32.5	45	20	0.0000	0	
422	34	32.5	45	20	0.0000	0	
422	34	32.5	45	20	0.0000	0	
422	34	32.5	45	20	0.0000	0	
422	34	32.5	45	20	0.0000	0	
422	34	32.5	45	20	0.0000	0	
422	34	32.5	45	20	0.0000	0	
422	34	32.5	45	20	0.0000	0	
422	34	32.5	45	20	0.0000	0	
422	34	32.5	45	20	0.0000	0	
422	34	32.5	45	20	0.0000	0	
422	34	32.5	45	20	1.0000	1	
422	34	32.5	45	20	1.0000	1	
422	34	32.5	45	20	1.0000	1	
422	34	32.5	45	20	1.0000	1	
422	34	32.5	45	20	1.0000	1	
422	34	32.5	45	20	1.0000	1	

Table A3-1 : (Continued.)

Welding Current/ A	Voltage/ V	Welding Speed/ cm min^{-1}	Groove Angle/ degree	Preheat Temperature/ ℃	Cracking Ratio	Classified Output	Reference
500	36.5	40	45	20	0.0000	0	Sekiguchi *et al.*, 1966
500	36.5	40	45	20	0.0000	0	
500	36.5	40	45	20	0.0000	0	
500	36.5	40	45	20	0.0000	0	
500	36.5	40	45	20	0.0000	0	
500	36.5	40	45	20	0.0000	0	
500	36.5	40	45	20	0.0000	0	
500	36.5	40	45	20	0.0000	0	
500	36.5	40	45	20	0.0000	0	
500	36.5	40	45	20	1.0000	1	
500	36.5	40	45	20	1.0000	1	
500	36.5	40	45	20	1.0000	1	
500	36.5	40	45	20	1.0000	1	
500	36.5	40	45	20	1.0000	1	
500	35.5	35	60	20	0.0000	0	
500	35.5	35	60	20	0.0000	0	
500	35.5	35	60	20	0.0000	0	
500	35.5	35	60	20	1.0000	1	
500	35.5	35	60	20	1.0000	1	
500	35.5	35	60	20	1.0000	1	

Table A3-2 : The weights and biases describing the trained network with all the data in the Tables 6-1 and 6-2. a: MODEL 1, b: MODEL 2, c: MODEL 3, d: MODEL 4. The data are arranged in a continuous horizontal sequence in the following order in a, b and c and d.

a, b and c:

$$\theta_1^{(1)}, \theta_2^{(1)}, \theta_3^{(1)}, \cdots, \theta_{11}^{(1)}, \theta^{(2)}$$
$$w_{1,1}^{(1)}, w_{2,1}^{(1)}, w_{3,1}^{(1)}, \cdots, w_{11,1}^{(1)}, w_1^{(2)}$$
$$w_{1,2}^{(1)}, w_{2,2}^{(1)}, w_{3,2}^{(1)}, \cdots, w_{11,2}^{(1)}, w_2^{(2)}$$
$$w_{1,3}^{(1)}, w_{2,3}^{(1)}, w_{3,3}^{(1)}, \cdots, w_{11,3}^{(1)}, w_3^{(2)}$$
$$\cdots\cdots\cdots\cdots\cdots\cdots\cdots\cdots$$
$$w_{1,11}^{(1)}, w_{2,11}^{(1)}, w_{3,11}^{(1)}, \cdots, w_{11,11}^{(1)}, w_{11}^{(2)}$$
$$w_{1,12}^{(1)}, w_{2,12}^{(1)}, w_{3,12}^{(1)}, \cdots, w_{11,12}^{(1)}$$
$$w_{1,13}^{(1)}, w_{2,13}^{(1)}, w_{3,13}^{(1)}, \cdots, w_{11,13}^{(1)}$$

d:

$$\theta_1^{(1)}, \theta_2^{(1)}, \theta^{(2)}$$
$$w_{1,1}^{(1)}, w_{2,1}^{(1)}, w_1^{(2)}$$
$$w_{1,2}^{(1)}, w_{2,2}^{(1)}, w_2^{(2)}$$
$$w_{1,3}^{(1)}, w_{2,3}^{(1)}$$
$$\cdots\cdots\cdots\cdots$$
$$w_{1,11}^{(1)}, w_{2,11}^{(1)}$$
$$w_{1,12}^{(1)}, w_{2,12}^{(1)}$$
$$w_{1,13}^{(1)}, w_{2,13}^{(1)}$$

a:

-0.0091755	-0.032463	-0.0118383	0.0115176	0.0113844	-0.0120624	-0.0096163	0.0117545	0.0118417	0.0102982	-0.163997	252432
-0.300981	3.10162	-0.326395	0.324679	0.322941	-0.327151	-0.308952	0.325809	0.325247	0.314011	-1.75412	-473938
0.00628468	0.00825333	0.00729347	-0.0071909	-0.0071334	0.00737016	0.00646907	-0.0072556	-0.0072844	-0.0067456	0.00915692	-107251
-1.66E-07	-4.36E-07	-1.97E-07	1.94E-07	1.92E-07	-1.99E-07	-1.72E-07	1.96E-07	1.96E-07	1.80E-07	-3.61E-07	-56377
0.00017104	0.00318338	0.0003746	-0.0003499	-0.0003347	0.00039636	0.00020422	-0.0003785	-0.0003776	-0.0002524	0.0028133	554186
-0.330114	-2.06618	-0.366941	0.362103	0.361927	-0.36796	-0.336933	0.36543	0.365136	0.349784	2.42364	54.9796
-0.0925052	-0.126957	-0.109805	0.108029	0.107012	-0.110793	-0.0955258	0.109492	0.109417	0.100491	-0.26091	-57.0025
0.165749	0.237317	0.192124	-0.189206	-0.188032	0.193882	0.170564	-0.191526	-0.191833	-0.17773	0.150095	-49.0127
-2.67E-05	5.73E-05	-2.41E-05	2.41E-05	2.41E-05	-2.43E-05	-2.60E-05	2.42E-05	2.43E-05	2.54E-05	0.00049564	56.1529
0.0521927	0.0696646	0.0639139	-0.0626563	-0.0620562	0.0646223	0.054363	-0.0636657	-0.0637269	-0.0571845	0.394019	56.3075
-0.0423861	-0.198352	-0.0500808	0.0492641	0.0488666	-0.0506314	-0.0437876	0.0498961	0.0500524	0.0457985	-0.077941	51.444
-0.0277938	-0.0652673	-0.0327468	0.0322355	0.0319719	-0.0331034	-0.0286819	0.0326367	0.0327241	0.0300388	-0.0634171	-143.533
-0.0088969	-0.0249612	-0.0103767	0.0102292	0.010145	-0.0104839	-0.0091655	0.010347	0.0103724	0.0095975	-0.0089575	
3.58E-07	-9.30E-07	3.84E-07	-3.74E-07	-3.74E-07	3.79E-07	3.57E-07	-3.92E-07	-3.82E-07	-3.40E-07	-4.94E-06	

b:

-0.0090004	0.00617678	0.00877136	0.00863844	0.184887	0.0402363	-0.00817765	-0.0061651	-0.0053069	-0.0115699	-0.0055476	24.7564
-0.356377	0.325229	0.362858	0.355222	1.80467	-3.06376	-0.351002	-0.324581	-0.303266	-0.366394	-0.312952	-56.6623
0.0140394	-0.0117172	-0.0139178	-0.0137666	-0.0178269	-0.0179145	0.0134352	0.011702	0.0108112	0.0157022	0.0110862	45.9764
-0.000000819	0.000000639	0.000000775	0.000000768	0.00000139	8.97E-08	-0.000000713	-0.000000635	-0.000000564	-0.000000893	-0.000000574	56.6576
0.00112773	-0.000812899	-0.00110744	-0.00107834	-0.0151737	-0.00397738	0.00104386	0.000815645	0.000713608	0.00139916	0.000741754	55.521
-0.393145	0.346069	0.402855	0.390146	-2.41619	2.10254	-0.38129	-0.34789	-0.324169	-0.422017	-0.332688	148.247
-0.103355	0.0844031	0.104179	0.101621	0.287631	0.117755	-0.0984584	-0.0843467	-0.0767118	-0.117276	-0.0791895	112.293
0.193774	-0.162089	-0.192242	-0.190151	-0.17493	-0.259129	0.185573	0.161964	0.149956	0.216687	0.153508	-53.8364
-0.000192473	0.000162455	0.00019001	0.000188612	-0.0000931	0.000240469	-0.00018487	-0.000162162	-0.000150562	-0.000213954	-0.000154061	-45.9284
0.0700287	-0.055426	-0.0703533	-0.0685392	-0.342131	-0.0794593	0.0661423	0.0553817	0.0498341	0.0812124	0.0516128	-41.8194
-0.0513906	0.0422722	0.0511463	0.0502935	0.0855933	0.257741	-0.0488858	-0.0422982	-0.0388706	-0.0581306	-0.0398962	-64.6475
-0.0228677	0.0187681	0.0228206	0.0224111	0.0436994	0.0448799	-0.0217668	-0.0187397	-0.0171478	-0.025903	-0.0176374	-43.1312
-0.00810795	0.00259333	0.00309036	0.00305014	0.00234654	0.00804485	-0.00297395	-0.00258974	-0.00239019	-0.0034883	-0.00245281	
-0.0000012	0.000000103	0.000000122	0.0000012	-0.000000104	0.000000109	-0.000000115	-0.000000102	-0.000000948	-0.000000133	-0.000000974	

c:

-0.0366355	-0.0408499	-0.0366495	-0.0478686	0.0365939	-0.0362014	-0.0389165	-0.037685	-0.0364905	0.0315459	-0.0371582	13.7861
-0.401509	-0.413823	-0.401356	-0.419616	0.40187	-0.403579	-0.404594	-2.56738	-0.402909	-4.04579	-0.402573	-262.749
0.0660502	0.0696079	0.0660532	0.0751955	-0.066153	0.0657007	0.068149	0.0898807	0.065916	-0.122676	0.0665135	-28.3433
6.29E-05	6.87E-05	6.19E-05	7.61E-05	-6.21E-06	6.29E-05	6.53E-05	2.33E-05	6.20E-05	1.12E-05	6.31E-06	-262.532
0.00121267	0.00138408	0.0012207	0.00165626	-0.00122446	0.00120181	0.00130108	0.0152952	0.00121113	-0.00068153	0.00124838	-31.318
-0.496351	-0.522203	-0.495236	-0.540368	0.494636	-0.497117	-0.510639	2.88564	-0.496137	2.83769	-0.499956	26.257
-0.154126	-0.165814	-0.15385	-0.181503	0.153531	-0.153085	-0.160948	-0.635247	-0.15348	0.211747	-0.156065	-26.1325
0.244261	0.25837	0.244282	0.280659	-0.244515	0.243085	0.252519	0.304551	0.243857	-0.4681	0.246234	-27.4385
-0.000385868	-0.000381	-0.000383045	-0.000391237	0.000387091	-0.000381704	-0.000383641	0.00285792	-0.000383118	0.00126307	-0.000386375	-86.369
0.103083	0.113065	0.103063	0.127233	-0.103234	0.102385	0.108716	0.641671	0.102787	-0.201603	0.104611	-262.088
-0.0761329	-0.0823799	-0.0761963	-0.092475	0.0762573	-0.0754275	-0.0799931	-0.107512	-0.0758937	0.551131	-0.076754	62.2323
-0.0407485	-0.0437674	-0.0407583	-0.048306	0.0407679	-0.0405102	-0.0425097	-0.139306	-0.0406661	0.0583099	-0.0411967	-26.5851
-0.012626	-0.0133556	-0.0126237	-0.014539	0.0126158	-0.0125237	-0.0130491	0.0111055	-0.0125839	0.0553371	-0.0127187	
0.0010305	0.00111287	0.00102917	0.00125266	-0.00102891	0.00102458	0.00107889	0.0034734	0.00102782	-0.002274	0.00104134	

d:

-0.0826657	-0.0282645	-18.5827
-0.751424	2.30129	-690.159
-0.000418127	-0.000216636	-241.413
-1.17E-05	-2.64E-06	
-0.000131672	-3.38E-05	
0.240573	-1.07271	
-0.146145	0.00899508	
0.20154	-0.0300502	
0.0248627	0.00924685	
0.117378	0.0629832	
-0.037813	-0.0192351	
-0.0762119	-0.041357	
-0.131658	0.314876	
0.00288703	0.000938893	

APPENDIX FOUR

FORTRAN Program to Calculate Allotriomorphic Ferrite in Steel Welds

Introduction

The program described in this appendix was used to calculate the allotriomorphic ferrite fraction in the model discussed in Chapter Two and Three.

It is presented using documentation defined in the MAP format [Bhadeshia, H. K. D. H., 1995, http:/www.msm.cam.ac.uk/map/mapmain.html].

MAP FORTRAN LIBRARY

Program MAP_WELDALLOT

0. Provenance of Source Code

Kazutoshi Ichikawa, Phase Transformation Group, Department of Materials Science and Metallurgy, University of Cambridge, Cambridge, UK.

1. Purpose

To calculate the allotriomorphic ferrite in the heterogeneous weld metal with explicit nucleation theory.

2. Specification

The program is self-contained.

3. Description

4. References

1. K. Ichikawa and H.K.D.H. Bhadeshia, *Mathematical modelling of weld phenomena 3*, ed. Cerjak, The Institute of Materials (1997) 181–198.

5. Parameters

Input parameters

CARBON - real

Concentration of carbon in wt.%.

SI - real

Concentration of silicon in wt.%.

MN - real

Concentration of manganese in wt.%

NI - real

Concentration of nickel in wt.%.

MO - real

Concentration of molybdenum in wt.%.

CR - real

Concentration of chromium in wt.%.

V - real

Concentration of vanadium in wt.%.

SV - real

Austenite grain surface per unit volume in m^{-1}.

DUMM - real

Fitting constant for nucleation (K_2^{α} in Chapter Two).

SITE - real

Fitting constant for nucleation (K_1^{α} in Chapter Two).

LOWT - real

Lowest temperature at which the calculation is stopped arbitrary.

J - integer

Flag identifies welding method (See the comments in the subroutine HFLOW for detail.).

CURR - real

Welding current in A.

VOLT - real

Voltage in V.

SPEED - real

Welding speed in m s^{-1}.

TINT - real

Interpass temperature in °C.

Output parameters

FVF - real

Average volume fraction of allotriomorphic ferrite 100 segregation segments.

6. Program data

None.

7. Program text

```
C Copyright, Dr. H. K. D. H. Bhadeshia
C and Kazutoshi Ichikawa (Nippon Steel Corporation)
C Department of Materials Science and Metallurgy,
C University of Cambridge Cambridge
C Pembroke Street, CB2 3QZ, England. Telephone 01223 334301.
C
C TYPICAL DATA SET FOLLOW
C 0.003 8392
C 760 610   2D04 0.217 0.05 1.0
C
C AB1 is set between 0,1,saturation value for grain boundary coverage
C AB2 sets the temperature interval between successive calculations
C   of parabolic rate constant
C CARBON, SI, MN, NI, MO, CR, V in wt.%
C SITE allows the number of sites for nucleation to be multiplied by a f
C SIGMA is the interface energy per unit area
C SIGMA2 is an effective interface energy which takes into account the
C   effect of DUMM
C LINEAL is the mean lineal intercept in micrometers for equiaxed grains
C SV is the austenite grain surface per unit volume (1/m)
C TIME2 is the time to achieve the same fraction at a lower temperature
C TIME3 is the net time spent at any given temperature to achieve
C    the total amount of transformation that has occurred
C TIME(I) is defined to be zero at the Ae3 temp,
C    and it is the TOTAL amount of time between Ae3 and the temperature
C    of interest. It is incremented in regular steps determined by the
C    cooling curve.
C XBAR mole fraction carbon in alloy as a whole
C XBARN mole fraction carbon in enriched austenite
C
C Sheil equation was introduced to provide segregation profiles for
C each element.
C*****************************************************************
      IMPLICIT REAL*8(A-H,K,M,O-Z,N,L), INTEGER(I,J)
      DOUBLE PRECISION CTEMP(100),
     &                 C(8),
     &                 CTEMPS(200,100)
     &                 ,VF(100),VFS(200,100),A(200,3)
     &                 ,CTEMPE(200),VFE(200)

C
        FIDDLE=1.0D+00
        SIGMA=0.05D+00
        AB1=0.90D+00
        AB2=5.0
        ICI=0
```

```
C ICI is a indicater which indicates the incorrect convergent of
C calculation of XEQ, GMAX. IF ICI=0, no such probrem was occured in
C the calculation. IF ICI=2 convergent could NOT completed in the
C calculation in SUBROUTINE AG and/or HIGH.
C
      READ(5,*) CARBON,SI,MN,NI,MO,CR,V
      READ(5,*) SV, DUMM, SITE, LOWT
C
C Read welding parameters
C J defines the welding process (see subroutine HFLOW)
C CURR is the welding current, amps
C VOLT is the welding voltage, Volts
C SPEED is the welding speed, m/s
C TINT is the interpass temperature, Centigrade
      READ(5,*) J, CURR, VOLT, SPEED, TINT
      WRITE(6,7) CURR,VOLT,SPEED,J,TINT
C
      C(1)=CARBON
      C(2)=SI
      C(3)=MN
      C(4)=NI
      C(5)=MO
      C(6)=CR
      C(7)=V

      CALL INITCC(C,CARBON,SI,MN,NI,MO,CR,V)

C Display of Average Chemical Composition as a reference
      WRITE(*,446)
      WRITE(*,445)
      WRITE(*,261) (C(J5),J5=1,7)
      CALL OMEGA(C,W,XBAR,T10,T20,0)
      XBARN=XBAR
      WRITE(*,262) (C(J5),J5=1,7)
      CALL INITCC(C,CARBON,SI,MN,NI,MO,CR,V)
C
C     Explanation of the Process of Calculation:
C
     CALL DETN(C,SV,DUMM,SITE,
    &LOWT,J,CURR,VOLT,SPEED,TINT,CTEMP,VF,J2,HIGHT,J10)
C
     DO 80 I=1,J10
     CTEMPE(I)=0.0
     VFE(I)=0.0
80   CONTINUE
      DO 50 I=1,J10,1
      WRITE (*,570)
      CALL INITCC(C,CARBON,SI,MN,NI,MO,CR,V)
      WRITE(*,560) I, J10, 1.0*I/J10
      CALL SCHEIL(CARBON,SI,MN,NI,MO,CR,V,C,I,J10)
      CALL MAINCONP(C,SV, DUMM,SITE,
```

```
     & LOWT,J,CURR,VOLT,SPEED,TINT,CTEMP,VF,J2,HIGHT,ICI)
C
       DO 60 J7=1,J2
        CTEMPS(I,J7)=CTEMP(J7)
        VFS(I,J7)=VF(J7)
60    CONTINUE
C
C      CALL CURVE(J2,CTEMPS,VFS,A,I)
        A(1,1)=A(1,1)
        CTEMPE(I)=CTEMPS(I,J2)
        VFE(I)=VFS(I,J2)

50     CONTINUE

        CALL SUMF(CTEMPE,VFE,J10)
        IF (ICI .EQ. 2) WRITE(*,580)

580    FORMAT(5X,'*** Calculations of XEQ and/or GMAX could not be'/
     &         10X,' conpleted correctly for some "i" ***'//)
       STOP
C
7      FORMAT(//20X,'Welding Current (amps) =',F5.0/
     &20X,'Voltage (V) =',F3.0/
     &20X,'Welding Speed (m/s) =',D10.3/
     &20X,'Welding Technique (SMAW:1, Tandem SAW:4, Single SAW:5)=',I5/
     &20X,'Interpass Temperature (Centigrade) =',F5.0)
C
446    FORMAT('----------------------------------------',
     &'------------------------',
     &'----------------------------------')
445    FORMAT (4H      )
261    FORMAT (6H      C=,F8.4,6H    SI=,F8.4,6H    MN=,F8.4,
     &6H    NI=,F8.4,6H    MO=,F8.4,6H    CR=,F8.4,6H      V=,F8.4
     &,5X,'wt.%')
262    FORMAT (6H      C=,F8.4,6H    SI=,F8.4,6H    MN=,F8.4,
     &6H    NI=,F8.4,6H    MO=,F8.4,6H    CR=,F8.4,6H      V=,F8.4
     &,5X,'mole fraction')
550    FORMAT (/'Coefficients A(1), A(2) and A(3) of quadaratic'
     &' polynomial y=A(1)+A(2)x+A(3)x**2 for Segregated Region.'/)
510    FORMAT (/'Coefficients A(1), A(2) and A(3) of quadaratic'
     &' polynomial y=A(1)+A(2)x+A(3)x**2 for Depleted Region.'/)
520    FORMAT ('Where y is VF and x is CTEMP.')
560    FORMAT(//20X,'i =',I5/
     &20X,'n =',I5/
     &20X,'i/n =',F8.4)
570    FORMAT('========================================
     =========',
     &'============================',
     &'==========================================')
       END
C*****************************************************************
```

```
      SUBROUTINE MAINCONP(C,SV,DUMM,SITE,
     &LOWT,J,CURR,VOLT,SPEED,TINT,CTEMP,MVF,J3,HIGHT,ICI)
C
      IMPLICIT REAL*8(A-H,K-Z), INTEGER(I,J)
      DOUBLE PRECISION TIME(2000), VOLF(2000), CTEMP(2000), GV(2000),
     &                 XAGA(2000),XGAG(2000),ALP(2000),C(8),
     &                 MVF(2000)
C
         FIDDLE=1.0D+00
         SIGMA=0.05D+00
         AB1=0.90D+00
         AB2=5.0
C
      WRITE(*,446)
      WRITE(*,445)
      WRITE(*,261) (C(J5),J5=1,7)
      CALL OMEGA(C,W,XBAR,T10,T20,0)
      XBARN=XBAR
      WRITE(*,262) (C(J5),J5=1,7)
      WRITE (*,28) T10,T20,W
      CALL HIGH(C,W,T10,T20,HIGHT,ICI)

      IF (HIGHT .LE. LOWT) GOTO 2
C
      SIGMA2=SIGMA*(DUMM**0.33)
      LINEAL=(2.0D+00/SV)*1.0d+06
      WRITE(6,7) SIGMA,SIGMA2, HIGHT,LOWT,SITE,SV,LINEAL,FIDDLE,AB1
      WRITE(*,446)
         J3=((HIGHT-LOWT)/AB2)+1
         HIT=HIGHT+AB2
C
C Reset matrix
                        DO 4 I=1,J3
                          TIME(I)=0.0
                          VOLF(I)=0.0
4                       CONTINUE
C Reset parameters
                        WRITE(6,6)
                        DUMMY=DUMM
                        IF(DUMMY .LT. 0.0D+00) GOTO 2
                        TIME2=0.0D+00
                        TIME3=0.0D+00
                        JTEST=0
                        AV=0.0
C
C                           ***** Calculations for each cooling rate
      DO 1 I=1,J3
C
C calculate grain boundary nucleation rate
C
         CTEMP(I)=HIT-AB2*I
```

```
      KTEMP=CTEMP(I)+273.15D+00
      CALL AG(C,W,XBARN,T10,T20,KTEMP,XGAG(I),GMAX)
      XAGA(I)=XALPH(CTEMP(I))
      CALL ALP11(W,XBARN,CTEMP(I),XAGA(I),XGAG(I),ALP(I))
      ALP(I)=ALP(I)/1.0D+02
      GV(I)=GMAX/7.2D-06
C
      CALL TIM(CULRAT1,TIMEI,AB2,CTEMP(I),CURR,VOLT,SPEED,TINT,J)
      IF(I .EQ. 1) THEN
      TIME(I)=TIMEI
      ELSE
      TIME(I)=TIMEI+TIME(I-1)
      ENDIF
C
      CALL NUC(SITE,GSTAR,CTEMP(I),GV(I),BI,DUMMY,FIDDLE,SIGMA)
C
C calculate fraction of ferrite, for aniosthermal transformation
C using the Scheil rule, beginning with the highest temperature (I=1)
C
      IF    (I .EQ. 1)THEN
            CALL AVOLF(AREA,ANS,VF,SV,BI,TIME(I),ALP(I),
     &       VOLF(I),XBAR,XAGA(I),XGAG(I))
      ELSE
C           allow for carbon enrichment in austenite
            XBARN=(XBAR - XAGA(I)*VF)/(1.0-VF)
C
3           AV=VOLF(I-1)
            IF(AV .EQ. 1.0D+00)GOTO 2
            TIME2=TIME(I-1)
            CALL ATIM(SV,BI,TIME2,ALP(I),AV,XBARN,XAGA(I),XGAG(I))
            TIME3=TIME(I)+TIME2-TIME(I-1)
            CALL AVOLF(AREA,ANS,VF,SV,BI,TIME3,ALP(I),
     &       VOLF(I),XBARN,XAGA(I),XGAG(I))
      ENDIF
C
      MVF(I)=VF
      IF    (AREA .GE. 0.005)THEN

            WRITE(6,5)CTEMP(I),VOLF(I),MVF(I),
     &       AREA,ANS,GV(I),GSTAR,XAGA(I),XGAG(I),
     &       TIME(I),TIME3,TIME2,ALP(I),BI,CULRAT1
            IF (VOLF(I) .GE. 0.99) GOTO 2

      ENDIF
C
C     check for site saturation
C     jtest ensures grain size calculation at site saturation
C     jtest set to unity at site saturation
C
      IF    (AREA .GT. AB1 .AND. JTEST .EQ. 0) THEN
            CALL ISONUC(TIME3,SV,BI,ALP(I),XBARN,XAGA(I),XGAG(I),AB1)
```

```
                JTEST=1
            ENDIF
C
1       CONTINUE
C
2       RETURN
C
5       FORMAT(F5.0,4F7.2,2D10.2,D10.2,F10.4,3F8.2,2D9.2,D10.3,D10.2)
6       FORMAT(//' CTEMP    VOL     VF    AREA      ANS     GV      GSTAR      ',
     &' XAGA       ',
     &' XGAG    TIME(I)   TIME3    TIME2 ',
     &'    ALP(I)     BI      K/s '/)
7       FORMAT(//20X,'Interface energy,                J/m**2= ',F10.3/
     &20X,          'Effective interface energy, J/m**2= ',F10.3//
     &20X,'Paraequilibrium Ae3 (Centigrade)',F5.0/
     &20X,'Temperature transformation stopped (Centigrade)',F5.0/
     &20X,'Fraction of boundary atoms forming nucleation sites',D10.3//
     &20X,'Austenite grain surface per unit volume      SV (1/m)',D10.3/
     &20X,'Lineal intercept, equiaxed austenite grains (microns)',F10.0//
     &20X,'Fiddle (1 means no fiddle factor) =',D12.4/
     &20X,'Nucleation stopped at fractional coverage = ',F8.3//)
28      FORMAT (/'      T10=',F10.6,
     &'      T20=',F10.6,'      WGAMMA=',F7.0,'  J/mol')
446     FORMAT('-----------------------------------',
     &'----------',
     &'-----------------------------')
445     FORMAT (4H     )
261     FORMAT (6H     C=,F8.4,6H    SI=,F8.4,6H    MN=,F8.4,
     &6H    NI=,F8.4,6H    MO=,F8.4,6H    CR=,F8.4,6H     V=,F8.4
     &,5X,'wt.%')
262     FORMAT (6H     C=,F8.4,6H    SI=,F8.4,6H    MN=,F8.4,
     &6H    NI=,F8.4,6H    MO=,F8.4,6H    CR=,F8.4,6H     V=,F8.4
     &,5X,'mole fraction')
        END
C*********************************************************************
      SUBROUTINE AAARG(ARG)
C
      DOUBLE PRECISION ARG
C
       IF(DABS(ARG) .LT. 1.0D-04) GOTO 1
       GOTO 2
1      ARG=0.0D+00
2      RETURN
      END
C*********************************************************************
      SUBROUTINE AARG(ARG)
C
C HELPS AVOID UNDERFLOW ERRORS IN EXPONENTIALS
C
      DOUBLE PRECISION ARG
C
```

```
      IF(ARG .GT. 173.0D+00) GOTO 1
      GOTO 2
1     ARG=179.0D+00
2     RETURN
      END
C*****************************************************************
       DOUBLE PRECISION FUNCTION AFEG(XEQ,AJ)
C
C C AFEG AFEG LN ACTIVITY OF IRON IN GAMMA
C
      DOUBLE PRECISION XEQ,AJ,DEQ,TEQ
C
      DEQ=DSQRT(1-2*(1+2*AJ)*XEQ+(1+8*AJ)*XEQ*XEQ)
      TEQ=5*DLOG((1-XEQ)/(1-2*XEQ))
      TEQ=TEQ+DLOG(((1-2*AJ+(4*AJ-1)*XEQ-DEQ)/(2*AJ*(2*XEQ-1)))**6)
      AFEG=TEQ
      RETURN
      END
C*****************************************************************
      SUBROUTINE AG(C,W,XBAR,T10,T20,KTEMP,XEQ,GMAX)
C
      IMPLICIT REAL*8 (A-H,K-Z), INTEGER (I,J)
C
      DOUBLE PRECISION C(8)
C
      X1=C(1)
      XA=0.001D+00
      R=8.31432D+00
      W1=48570.0D+00
      H=38575.0D+00
      S=13.48D+00
      XEQ=0.1D+00
      IC=0
C
      T=KTEMP
      CTEMP=T-273.00D+00
C
      IF (T .LE. 1000.0) GOTO 20
      H1=105525.0D+00
      S1=45.34521D+00
      GOTO 19
20    H1=111918.0D+00
      S1=51.44D+00
C
19    F=ENERGY(T,T10,T20)
      AJ=1.0D+00-DEXP(-W/(R*T))
      AJ1=1.0D+00-DEXP(-W1/(R*T))
51    TEQ=R*T*AFEG(XEQ,AJ)-F
      IF (DABS(TEQ) .LT. 1.0) GOTO 52
      ETEQ=DAFEG(XEQ,AJ)*R*T
      XEQ=XEQ-TEQ/ETEQ
```

```
C Modified by K. Ichikawa Until ****
      IC=IC+1
      IF (IC .GE. 1000000) GOTO 55
C ****
      GOTO 51
52    AEQ=CG(XEQ,T,W,R)
      AFEQ=AFEG(XEQ,AJ)
      A=CG(X1,T,W,R)
      AFE=AFEG(X1,AJ)
C
      CALL GMAAX(A1,A,W1,F,R,T,X,AFE,H1,S1)
      GMAX=R*T*(A1-A)
C
60    RETURN

55    WRITE(*,56)
56    FORMAT(5X,'*** Calculations of XEQ and GMAX could not'/
     &       10X,' conpleted correctly  ***'//)

      GOTO 60
      END
C*************************************************************
      SUBROUTINE AL(XGAG,XBAR,XAGA,DIFF,CTEMP,ALPHA)
C
      IMPLICIT REAL*8(A-H,K-Z), INTEGER(I,J)
      DOUBLE PRECISION X2(22),Y2(22),X(60),Y(60),X1(3),Y1(3)
C
      GES=0.51466
C     GES IS A GUESS VALUE OF ALPHA1/(2*SQRT(D))
      I3=0
      J=0
      OMEGA=(XGAG-XBAR)/(XGAG-XAGA)
3     I3=I3+1
      DUM1=GES*DEXP(GES*GES)*(1.0D+00-DERF(GES))-(OMEGA
     &/DSQRT(3.14159D+00))
      X2(I3)=GES
      Y2(I3)=DUM1
C       WRITE(4,5)GES,DUM1
      DER=(DEXP(GES*GES)*(1.0D+00 + 2.0D+00*GES*GES))*
     &(1.0D+00-DERF(GES))-GES*2.0D+00/(DSQRT(3.14159D+00))
      I1=DINT(GES*1000000)
      GES=GES-DUM1/DER
      IF(GES .GT. 12.0) GOTO 1
      I2=DINT(GES*1000000)
      IF(I1 .EQ. I2)GOTO 2
      IF(I3 .GT. 20)GOTO 1
      GOTO 3
1     GES=0.51466
7     J=J+1
      DUM1=GES*DEXP(GES*GES)*(1.0D+00-DERF(GES))-(OMEGA
     &/DSQRT(3.14159D+00))
```

```
      DER=(DEXP(GES*GES)*(1.0D+00 + 2.0D+00*GES*GES))*
     &(1.0D+00-DERF(GES))-GES*2.0D+00/(DSQRT(3.14159D+00))
      X(J)=GES
      Y(J)=DUM1
      IF(J .EQ. 1) GOTO 7
      IF(DABS(Y(J)) .GT. DABS(Y(J-1)))GOTO 6
      GES=GES-0.5*DUM1/DER
      GOTO 7
6     X1(3)=X(J-1)
      X1(2)=X(J-2)
      X1(1)=X(J-3)
      Y1(3)=Y(J-1)
      Y1(2)=Y(J-2)
      Y1(1)=Y(J-3)
      CALL ANAL(3,0,CONST,SLOPE,CORR,X1,Y1)
      GES=-1.0D+00*CONST/SLOPE
      DUM1=GES*DEXP(GES*GES)*(1.0D+00-DERF(GES))-(OMEGA
     &/DSQRT(3.14159D+00))
      DO 10 J1=1,I3
      IF(DABS(DUM1) .GT. DABS(Y2(J1)))GOTO 9
      GOTO 10
9     GES=X2(J1)
      DUM1=Y2(J1)
10    CONTINUE
2     ALPHA=GES*2.0D+00*DSQRT(DIFF)
C       WRITE(4,4)CTEMP,ALPHA,DUM1
4     FORMAT(' CTEMP=', F8.0,10X,' ALPHA1, (cm/(sec)**.5)=',
     &D12.5,    10X,' DUM1=',D12.5/
     &/'******** ********** ********** ********** **********')
5     FORMAT(2D12.4)
      RETURN
      END
C*********************************************************************
      SUBROUTINE ALP11(W,XBAR,CTEMP,XAGA,XGAG,ALPHA)
C
C Modified allow easier low T calculations and provide iteration error messages
C TYPICAL DATASET
C 780 0.0100
C 740 0.0176
C 700 0.0266
C 660 0.0389
C 600 0.0552
C Modified 24-6-85 to include XINCR
C - this limits no. of Diff coeffs calculated for T¡700C
C PROGRAM TO CALCULATE PARABOLIC RATE CONSTANT, 4-1-84
C PROGRAM MODIFIED, 30-8-83, FOR ACCURATE XAPLPHA
C PROGRAM TO CALCULATE THE EFFECTIVE DIFFUSIVITY OF CARBON IN
C AUSTENITE, TAKING ACCOUNT OF THE FACT THAT THIS DIFFUSIVITY
C IS CONCENTRATION DEPENDENT.  USES SILLER AND MCLELLAN
C THEORY
C TO EXPRESS THE CONCENTRATION DEPENDENCE, AND LACHER ET AL
```

```
C THEORY TO ALLOW FOR THE EFFECT OF SUBSTITUTIONAL ALLOYING
C ELEMENTS
C ON THE ACTIVITY AND W OF CARBON IN AUSTENITE.
C TEMPERATURE IS READ IN IN DEGREES CENTIGRADE
C CARBON CONTENT READ IN AS MOL FRAC, EXCEPT FOR THE
C SUBROUTINE OMEGA,
C WHERE THE CARBON CONTENT AND ALLOYING CONTENT IS READ IN
C AS WT PCT IN
C THE FIRST LINE OF THE DATASET.
C HH=PLANCKS CONST.JOULES/SEC,KK=BOLTZMANNS
C CONST.JOULES/DEGREE KELVIN
C       D=DIFFUSIVITY OF CARBON IN AUSTENITE
C       Z=COORDINATION OF INTERSTIAL SITE
C       PSI=COMPOSITION DEPENDENCE OF DIFFUSION COEFFICIENT
C       THETA=NO. C ATOMS/ NO. FE ATOMS
C       ACTIV=ACTIVITY OF CARBON IN AUSTENITE
C       R=GAS CONSTANT
C       X=MOLE FRACTION OF CARBON
C       T=ABSOLUTE TEMPERATURE
C       SIGMA=SITE EXCLUSION PROBABLITY
C       W=CARBON CARBON INTERACTION ENERGY IN AUSTENITE
C
        IMPLICIT REAL*8(A-H,K-Y), INTEGER(I,J,Z)
        DOUBLE PRECISION DIFF(500), CARB(500)
C
        HH=6.6262D-34
        KK=1.38062D-23
        Z=12
        A5=1.0D+00
        R=8.31432D+00
        T=CTEMP+273.00D+00
        II2=0
C       WRITE(4,7)T,CTEMP,XBAR,XGAG,XAGA
        DASH=(KK*T/HH)*DEXP(-(21230.0D+00/T))*DEXP(-31.84D+00)
        DO 9    II=1,1000
        CARB(1)=XBAR
        IF (II .GT. 1)GOTO 1
        GOTO 8
1       IF((XGAG-XBAR) .LT. 0.005)GOTO 2
        GOTO 3
2       XINCR=0.0001D+00
        GOTO 4
3       XINCR=0.001D+00
4       CARB(II)=CARB(II-1)+XINCR
        IF (CARB(II) .GT. XGAG) GOTO 5
8       X=CARB(II)
        II2=II2+1
        THETA=X/(A5-X)
        ACTIV=CG(X,T,W,R)
        ACTIV=DEXP(ACTIV)
        DACTIV=DCG(X,T,W,R)
```

```
      DACTIV=DACTIV*ACTIV
      DACTIV=DACTIV*A5/((A5+THETA)**2)
      SIGMA=A5-DEXP((-(W))/(R*T))
      PSI=ACTIV*(A5+Z*((A5+THETA)/(A5-(A5+Z/2)*THETA+(Z/2)*(A5+Z/2)*
     &(A5-SIGMA)*THETA*THETA)))+(A5+THETA)*DACTIV
      DIFF(II)=DASH*PSI
9     CONTINUE
5     II3=0
C       CALL D01GAF(CARB,DIFF,II2,ANS,ERROR,II3)
      CALL TRAPE(CARB,DIFF,ANS,II2)
      ANS=ANS/(XGAG-XBAR)
C       WRITE(4,6)ANS,ERROR
      CALL AL(XGAG,XBAR,XAGA,ANS,CTEMP,ALPHA)
7     FORMAT(' ABSOLUTE TEMPERATURE, DEGREES KELVIN =',F8.1/
     &'              TEMPERATURE IN DEGREES CENTIGRADE =',F8.1/
     &' MOL FRAC CARBON IN ALLOY = ',F8.4/
     &' EQUILIBRIUM MOL FRAC CARBON IN AUSTENITE =',F8.4/
     &' EQUILIBRIUM MOL FRAC OF C IN FERRITE=',D12.4)
6     FORMAT(' INTEGRAL, XGAG-XBAR = ',D12.4, '   CM**2/SEC   ',
     &8HERROR = , D12.4)
      RETURN
      END
C*********************************************************************
      SUBROUTINE ANAL(J7,J9,CONST,SLOPE,CORR,X,Y)
C
      DOUBLE PRECISION AX,AX2,AY,AY2,AXY,CONST,CORR,SLOPE,
     &X(60),Y(60)
      INTEGER I,J8,J9,J7
C
      J8=J7-J9
      AX=0.0D+00
      AY=0.0D+00
      AX2=0.0D+00
      AY2=0.0D+00
      AXY=0.0D+00
      DO 1 I=1,J8
      AX=AX+X(I)
      AY=AY+Y(I)
      AXY=AXY+X(I)*Y(I)
      AX2=AX2+X(I)*X(I)
      AY2=AY2+Y(I)*Y(I)
1     CONTINUE
      CONST=(AY*AX2-AX*AXY)/(J8*AX2-AX*AX)
      SLOPE=((J8*AXY-AX*AY)/(J8*AX2-AX*AX))
      CORR=(J8*AXY-AX*AY)/(DSQRT((J8*AX2-AX*AX)*
     &(J8*AY2-AY*AY)))
      WRITE(6,2)CONST,SLOPE,CORR
2     FORMAT('    INTERCEPT=',D12.4,'     SLOPE=',D10.3,
     &'     CORRELATION=',F8.4)
      RETURN
      END
```

```
C*****************************************************************
      SUBROUTINE ATIM(SV,BI,TIME,ALP,VOL,XBAR,XAGA,XGAG)
C
C Calculates time required to transform to a given volume fraction
      IMPLICIT REAL*8(A-H,K-Z), INTEGER(I,J)
C
      DOUBLE PRECISION D(70),E(70)
C
          ADUM=1.0D-8
C
C This statement determines the entire accuracy at high cooling rates
          IF(VOL .LE. 1.0D-08) GOTO 4
C
          DTIME=TIME
          J=0
          I=0
3         CALL AVOLF(AREA,ANS,VF,SV,BI,DTIME,ALP,
     &                          DVOL,XBAR,XAGA,XGAG)
          I=I+1
          D(I)=DVOL/VOL
          E(I)=DABS(D(I)-1.0D+00)
          E1=DABS(1.0/D(I)-1.0D+00)
          IF(DABS(D(I)) .GT. (1.0D+00+1.0D-10) ) GOTO 13
          IF(DABS(D(I)) .LT. (1.0D+00-1.0D-10) ) GOTO 13
          TIME=DTIME
          GOTO 2
13        IF(I .GT. 1 .AND. J .LT. 1)GOTO 10
          GOTO 11
10        IF(E(I) .GT. E(I-1))GOTO 12
          IF(E1 .GT. E(I-1)) GOTO 12
          GOTO 11
12        DTIME=DTIME*0.9D+00
          CALL AVOLF(AREA,ANS,VF,SV,BI,DTIME,ALP,
     &                          DVOL,XBAR,XAGA,XGAG)
          IF((DVOL-VOL) .GT. 0.0D+00) GOTO 12
          J=J+1
          GOTO 3
C
C Newton's Iteritive method
C
11        DTIM1=DTIME-ADUM
          DTIM2=DTIME+ADUM
          CALL AVOLF(AREA,ANS,VF,SV,BI,DTIM1,ALP,
     &                         DVOL1,XBAR,XAGA,XGAG)
          CALL AVOLF(AREA,ANS,VF,SV,BI,DTIM2,ALP,
     &                          DVOL2,XBAR,XAGA,XGAG)
          ADUM2=((DVOL-VOL)*(-2.0D+00*ADUM))/(DVOL1-DVOL2)
          IF(DABS(ADUM2) .GT. DTIME)GOTO 14
          DTIME=DTIME-ADUM2
          GOTO 3
14        DTIME=1.5D+00*DTIME
```

```
            GOTO 3
C
C VOL = volume fraction / equilibrium volume fraction
4           TIME=0.0D+00
C
2       RETURN
        END
C*********************************************************************
        SUBROUTINE AVOLF(AREA,ANS,VF,SV,BI,TIME,ALP,
       &VOL,XBAR,XAGA,XGAG)
C
C AREA is the fraction of boundary covered
C TIME is in seconds
C VOl is volume fraction of ferrite/equilibrium vol. frac.
C VF is the actual volume fraction
C ALP is the one-dimensional parabolic thickening rate constant
C ALP1 is the one-dimensional parabolic lengthening rate constant
C BI is the grain boundary face nucleation rate per unit area per unit t
C XGAG, XAGA = equilibrium mol frac of carbon in gamma and alpha respect
C XBAR = average mol frac of carbon in alloy
C SV = austenite grain boundary area per unit volume (1/m)
C
        IMPLICIT REAL*8(A-H,K-Z), INTEGER(I,J)
        DOUBLE PRECISION THETA(1000),FUN(1000)
C
            ILOOP=51
            AILOOP=ILOOP*1.0d+00
            ALP1=3.0D+00*ALP
            OMEGA=(XGAG-XBAR)/(XGAG-XAGA)
C
C Numerical integration using ILOOP-1 slices
C
        DO 1 I=1,ILOOP
            IDUM=I-1
            THETA(I)=IDUM/(AILOOP-1.0D+00)
            ARG=0.5D+00*3.14159D+00*BI*ALP1**2.0D+00*TIME**2.0D+00*
       &        (1.0D+00-THETA(I)**4.0D+00)
            CALL AARG(ARG)
            FUN(I)=1.0D+00-DEXP(-ARG)
1       CONTINUE
C
            CALL TRAPE(THETA,FUN,ANS,ILOOP)
            ARG=2.0D+00*SV*ANS*ALP*TIME**0.5D+00/OMEGA
            CALL AARG(ARG)
            VOL=1.0D+00-DEXP(-ARG)
            VF=VOL*OMEGA
            AREA=FUN(1)
C
        RETURN
        END
C*********************************************************************
```

```
      DOUBLE PRECISION FUNCTION CG(X,T,W,R)
C
C FUNCTION GIVING LFG   LN(ACTIVITY) OF CARBON IN AUSTENITE
C
      DOUBLE PRECISION J,DG,DUMMY,T,R,W,X
C
      J=1-DEXP(-W/(R*T))
      DG=DSQRT(1-2*(1+2*J)*X+(1+8*J)*X*X)
      DUMMY=5*DLOG((1-2*X)/X)+6*W/(R*T)+((38575.0)-(
     &13.48)*T)/(R*T)
      CG=DUMMY+DLOG(((DG-1+3*X)/(DG+1-3*X))**6)
      RETURN
      END
C*********************************************************************
      DOUBLE PRECISION FUNCTION DCG(X,T,W,R)
C
C FUNCTION GIVING DIFFERENTIAL OF LN(ACTIVITY) OF CARBON IN
C AUSTENITE, L
C DIFFERENTIAL IS WITH RESPECT TO X
C
      DOUBLE PRECISION J,DG,DDG,X,T,W,R
C
      J=1-DEXP(-W/(R*T))
      DG=DSQRT(1-2*(1+2*J)*X+(1+8*J)*X*X)
      DDG=(0.5/DG)*(-2-4*J+2*X+16*J*X)
      DCG=-((10/(1-2*X))+(5/X))+6*((DDG+3)/(DG-1+3*X
     &)-(DDG-3)/(DG+1-3*X))
      RETURN
      END
C*********************************************************************
      DOUBLE PRECISION FUNCTION DAFEG(XEQ,AJ)
C
C DAFEG DAFEG DIFFERENTIAL OF LN ACTIVITY OF IRON IN GAMMA
C
      DOUBLE PRECISION ETEQ,ETEQ2,DEQ,XEQ,AJ
C
      DEQ=DSQRT(1-2*(1+2*AJ)*XEQ+(1+8*AJ)*XEQ*XEQ)
      ETEQ=5*((1/(XEQ-1))+2/(1-2*XEQ))
      ETEQ2=6*((4*AJ-1-(0.5/DEQ)*(-2-4*AJ+2*XEQ+16*XEQ*AJ))
     &/(1-2*AJ+(4*AJ-1)*XEQ-DEQ))+6*(4*AJ/(2*AJ*(2*XEQ-1)))
      DAFEG=ETEQ+ETEQ2
      RETURN
      END
C*********************************************************************
      DOUBLE PRECISION FUNCTION ENERGY(T,T10,T20)
C
C     ENERGY
C
      DOUBLE PRECISION T,T10,T20,F,T7
C
      T7=T-100*T20
```

```
      IF (T7 .LT. 300) GOTO 1
      IF (T7 .LT. 700) GOTO 2
      IF (T7 .LT. 940) GOTO 3
      F=-8.88909+0.26557*(T7-1140)-1.04923D-3*((T7-1140)**2)
      F=F+2.70013D-6*((T7-1140)**3)-3.58434D-9*((T7-1140)**4)
      GOTO 4
1     F=1.38*T7-1499
      GOTO 4
2     F=1.65786*T7-1581
      GOTO 4
3     F=1.30089*T7-1331
4     ENERGY=(141.0*T10 + F)*4.187
      RETURN
      END
C*********************************************************************
      SUBROUTINE HIGH(C,W,T10,T20,HIGHT,ICI)
C
C Finds approximate temperature at which paraequilibrium ferrite
C formation first becomes possible
C
      IMPLICIT REAL*8(A-H,K-Z), INTEGER(I,J)
      DOUBLE PRECISION C(8)
C
       X1=C(1)
       XA=0.001D+00
       R=8.31432D+00
       W1=48570.0D+00
       H=38575.0D+00
       S=13.48D+00
       XEQ=0.05D+00
       IC=0
C
C      Modified following line from "DO 1 I=1183,973,-1" to
C      "DO 1 I=1183,893,-1", by K. Ichikawa
C      and modified again to "DO 1 I=1183,879,-1".

      DO 1 I=1183,473,-1
C
       KTEMP=I
C
       T=KTEMP
C
        IF (T .LE. 1000.0) GOTO 20
          H1=105525.0D+00
          S1=45.34521D+00
        GOTO 19
20        H1=111918.0D+00
          S1=51.44D+00
C
19    F=ENERGY(T,T10,T20)
      AJ=1.0D+00-DEXP(-W/(R*T))
```

```
      AJ1=1.0D+00-DEXP(-W1/(R*T))
51    TEQ=R*T*AFEG(XEQ,AJ)-F
      IF (DABS(TEQ) .LT. 1.0) GOTO 52
      ETEQ=DAFEG(XEQ,AJ)*R*T
      XEQ=XEQ-TEQ/ETEQ
C Modified by K.Ichikawa until ***
      IC=IC+1
      IF (IC .GE. 1000000) GOTO 220
C ***
      GOTO 51
52      IF(XEQ .GE. X1) THEN
          HIGHT=KTEMP-273.15D+00
          GOTO 222
        ENDIF
1     CONTINUE
C
        IF(XEQ .LT. X1) THEN
            WRITE(*,53)
53          FORMAT(5X,'*** Alloy cannot transform to ferrite'/
     &           10X,' at temperature as low as 473 K   ***'//)
            HIGHT=0.0D+00
        ENDIF
C
222     RETURN
220   WRITE(*,221)
221   FORMAT(5X,'*** Calculation of XEQ could not be'/
     &       10X,' conpleted correctly   ***'//)
      ICI=2
      GOTO 222
      END
C*****************************************************************
      SUBROUTINE ISONUC(TIME3,SV,BI,ALP,XBAR,XAGA,XGAG,A1)
C
      IMPLICIT REAL*8(A-H,K-Z), INTEGER(I,J)
      DOUBLE PRECISION A(200)
C
      J2=50
      TINC=TIME3/J2
      TIME=0.0D+00
      SUM=0.0D+00
C
C Write statement is interesting but not necessary (1994)
C       WRITE(6,6)
C 6     FORMAT(9X,'  A(I)        TIME        AREA        VF')
C
      DO 1 I=1,J2
12        TIME=TIME+TINC
          CALL AVOLF(AREA,ANS,VF,SV,BI,TIME,ALP,VOL,XBAR,XAGA,XGAG)
          IF(I .EQ. 1 .AND. AREA .GT. A1)GOTO 10
          IF(TIME .GT. TIME3)GOTO 2
          IF(AREA .GT. A1)GOTO 2
```

```
          GOTO 11
10        TINC=TINC/2000.0
          TIME=0.0D+00
          AREA=0.0
          GOTO 12
11        A(I)=(1.0D+00-AREA)*TINC*BI
          SUM=SUM+A(I)
C
C         Write statement is interesting but not necessary (1994)
C         WRITE(6,4)A(I),TIME,AREA,VF
C 4       FORMAT(' ISONUC ',5D10.2)
1       CONTINUE
C
2         WRITE(6,3)SUM
          IF(SUM .EQ. 0.0)GOTO 9
3         FORMAT(20X,' Number of particles per unit area =',D12.4)
          DALPHA=(2.0D+00/(3.0D+00*SV*SUM))**0.333333
          DGAMMA=2.0D+00/(SV)
          WRITE(6,8)DALPHA,DGAMMA
8         FORMAT(20X,' DALPHA =',D12.4,' m    DGAMMA = ',D12.4,' m')
C
9       RETURN
        END
C*********************************************************************
        SUBROUTINE NUC(SITE,GSTAR,CTEMP,GV,BI,DUMMY,FIDDLE,SIGMA)
C
C KELVIN = temperature in kelvin
C H, K = Planck constant, Boltzmann constant respectively
C Q = activation energy for self-diffusion of iron
C GSTAR = activation energy for grain boundary nucleation
C NS is the number of nucleation sites per unit area of boundary
C BI is the Grain boundary nucleation rate per second, per square meter
C SV is deleted from the equation of BI=(NS*K*KELVINE/H)*DEXP(-ARG),
C because Sally found the mistake of that on9 Jan. 1995. By K. Ichikawa.
C CTEMP is temperature in centigrade
C GV is gibbs free energy change per unit volume, for nucleation, J/m**3
C SIGMA is an interfacial energy per square meter
C
        IMPLICIT REAL*8(A-H,K-Z), INTEGER(I,J)
C
        KELVIN=CTEMP+273.15D+00
        K=1.38062D-23
        H=6.6262D-34
        GSTAR=SIGMA**3.0D+00*DUMMY/(GV*GV)
C calculate number of sites pers unit area by dividing by the area
C   of an atom, taking width as 2.5d-10 metres. SITE is a fiddle factor
        NS=SITE/((2.5D-10)**2)
        Q=FIDDLE*2.4D+05/6.02217D+23
        ARG=(GSTAR+Q)/(K*KELVIN)
        CALL AARG(ARG)
        BI=(NS*K*KELVIN/H)*DEXP(-ARG)
```

```
2       RETURN
        END
C*****************************************************************
        SUBROUTINE NUCC(SITE,GSTAR,CTEMP,GV,BI,SV,DUMMY,SIGMA)
C
C KELVIN = temperature in kelvin
C H, K = Planck constant, Boltzmann constant respectively
C Q = activation energy for self-diffusion of iron
C GSTAR = activation energy for grain boundary nucleation
C NS is the number of nucleation sites per unit area of boundary
C BI is the Grain boundary nucleation rate per second, per square meter
C CTEMP is temperature in centigrade
C GV is gibbs free energy change per unit volume, for nucleation, J/m**3
C SIGMA is an interfacial energy per square meter
C
        IMPLICIT REAL*8(A-H,K-Z), INTEGER(I,J)
C
        IF(CTEMP .GT. 721) GOTO 1
        IF(CTEMP .GT. 701) GOTO 2
        IF(CTEMP .GT. 681) GOTO 3
        IF(CTEMP .GT. 661) GOTO 4
        IF(CTEMP .GT. 641) GOTO 5
        IF(CTEMP .GT. 621) GOTO 6
        IF(CTEMP .GT. 601) GOTO 7
        IF(CTEMP .GT. 581) GOTO 8
        IF(CTEMP .GT. 561) GOTO 9
        IF(CTEMP .GT. 541) GOTO 10
1       BI=0.0D+00
        GOTO 11
2       BI=2.8D+05
        GOTO 11
3       BI=4.7D+06
        GOTO 11
4       BI=1.42D+07
        GOTO 11
5       BI=2.0D+07
        GOTO 11
6       BI=2.4D+07
        GOTO 11
7       BI=2.1D+07
        GOTO 11
8       BI=1.7D+07
        GOTO 11
9       BI=1.3D+07
        GOTO 11
10      BI=8.5D+06
11      RETURN
          END
C*****************************************************************
        SUBROUTINE OMEGA(C,W,XBAR,T10,T20,J)
C
```

```
C SUBROUTINE TO CALCULATE THE CARBON CARBON INTERACTION
C ENERGY IN
C AUSTENITE, AS A FUNCTION OF ALLOY COMPOSITION.  BASED ON
C .MUCG18
C THE ANSWER IS IN JOULES PER MOL.    **7 OCTOBER 1981**
C
      DOUBLE PRECISION C(8),W,P(8),B1,B2,Y(8),T10,T20,B3,XBAR
      INTEGER U,J
C
      B3=0.0D+00
      IF(J .EQ. 1) GOTO 2
      C(8)=C(1)+C(2)+C(3)+C(4)+C(5)+C(6)+C(7)
      C(8)=100.0D+00-C(8)
      C(8)=C(8)/55.84D+00
      C(1)=C(1)/12.0115D+00
      C(2)=C(2)/28.09D+00
      C(3)=C(3)/54.94D+00
      C(4)=C(4)/58.71D+00
      C(5)=C(5)/95.94D+00
      C(6)=C(6)/52.0D+00
      C(7)=C(7)/50.94D+00
2     B1=C(1)+C(2)+C(3)+C(4)+C(5)+C(6)+C(7)+C(8)
      DO 107 U=2,7
      Y(U)=C(U)/C(8)
107   CONTINUE
      DO 106 U=1,8
      C(U)=C(U)/B1
106   CONTINUE
      XBAR=C(1)
      XBAR=DINT(10000.0D+00*XBAR)
      XBAR=XBAR/10000
      B2=0.0D+00
      T10=Y(2)*(-3)+Y(3)*2+Y(4)*12+Y(5)*(-9)+Y(6)*(-1)+Y(7)*(-12)
      T20=-3*Y(2)-37.5*Y(3)-6*Y(4)-26*Y(5)-19*Y(6)-44*Y(7)
      P(2)=2013.0341+763.8167*C(2)+45802.87*C(2)**2-280061.63*C(2)**3
     &+3.864D+06*C(2)**4-2.4233D+07*C(2)**5+6.9547D+07*C(2)**6
      P(3)=2012.067-1764.095*C(3)+6287.52*C(3)**2-21647.96*C(3)**3-
     &2.0119D+06*C(3)**4+3.1716D+07*C(3)**5-1.3885D+08*C(3)**6
      P(4)=2006.8017+2330.2424*C(4)-54915.32*C(4)**2+1.6216D+06*C(4)**3
     &-2.4968D+07*C(4)**4+1.8838D+08*C(4)**5-5.5531D+08*C(4)**6
      P(5)=2006.834-2997.314*C(5)-37906.61*C(5)**2+1.0328D+06*C(5)**3
     &-1.3306D+07*C(5)**4+8.411D+07*C(5)**5-2.0826D+08*C(5)**6
      P(6)=2012.367-9224.2655*C(6)+33657.8*C(6)**2-566827.83*C(6)**3
     &+8.5676D+06*C(6)**4-6.7482D+07*C(6)**5 +2.0837D+08*C(6)**6
      P(7)=2011.9996-6247.9118*C(7)+5411.7566*C(7)**2
     &+250118.1085*C(7)**3-4.1676D+06*C(7)**4
      DO 108 U=2,7
      B3=B3+P(U)*Y(U)
      B2=B2+Y(U)
108   CONTINUE
      IF (B2 .EQ. 0.0D+00) GOTO 455
```

```
      W=(B3/B2)*4.187
      GOTO 456
455   W=8054.0
456   CONTINUE
      RETURN
      END
C*********************************************************************
      SUBROUTINE TIM(CULRAT1,TIME,AB2,LOWT,CURR,VOLT,
     &SPEED,TINT,J)
C
C Find constants for particular welding process
C
      IMPLICIT REAL*8(A-H,K-Z),INTEGER(I,J)

C
      CALL HFLOW(J,C1,C2,EFF)
C
C Find cooling rate at intermediate temperature T=(HIGHT-LOWT)/2
C Units of cooling rate in K/s
C
        T= LOWT
        CULRAT1= CULRAT(T,TINT,C1,C2,CURR,VOLT,EFF,SPEED)
C
C Find time to cool between HIGHT and LOWT (units of time = s)
C
       TIME=(AB2)/CULRAT1
C
      RETURN
      END
C*********************************************************************
      SUBROUTINE TRAPE(X,Y,ANS,NDIM)
C
C         PURPOSE
C            TO COMPUTE THE VECTOR OF INTEGRAL VALUES FOR A GIVEN
C            GENERAL TABLE OF ARGUMENT AND FUNCTION VALUES.
C
C         USAGE
C               CALL TRAPE (X,Y,Z,NDIM)
C
C         DESCRIPTION OF PARAMETERS
C            X       - DOUBLE PRECISION INPUT VECTOR OF ARGUMENT
C                        VALUES.
C            Y       - DOUBLE PRECISION INPUT VECTOR OF FUNCTION VALUES.
C            Z       - THE RESULTING DP. VECTOR OF INTEGRAL VALUES. Z MAY C
BE IDENTICAL WITH X OR Y.
C
C            NDIM    - THE DIMENSION OF VECTORS X,Y,Z. NDIM MAX. 1000
C
C         REMARKS
C            NO ACTION IN CASE NDIM LESS THAN 1.
C
```

```
C          SUBROUTINES AND FUNCTION SUBPROGRAMS REQUIRED
C             NONE
C
C          METHOD
C             BEGINNING WITH Z(1)=0, EVALUATION OF VECTOR Z IS DONE BY
C             MEANS OF TRAPEZOIDAL RULE (SECOND ORDER FORMULA).
C             FOR REFERENCE, SEE
C             F.B.HILDEBRAND, INTRODUCTION TO NUMERICAL ANALYSIS,
C             MCGRAW-HILL, NEW YORK/TORONTO/LONDON, 1956, PP.75.
C
      DOUBLE PRECISION X(1000),Y(1000),AZ(1000)
      DOUBLE PRECISION SUM1,SUM2,ANS
C
      SUM2=0.D+00
      IF(NDIM-1)4,3,1
C
C     INTEGRATION LOOP
1     DO 2 I=2,NDIM
      SUM1=SUM2
      SUM2=SUM2+.5D+00*(X(I)-X(I-1))*(Y(I)+Y(I-1))
2     AZ(I-1)=SUM1
3     AZ(NDIM)=SUM2
      ANS=SUM2
4    RETURN
      END
C*********************************************************************
      SUBROUTINE GMAAX(A1,A,W1,F,R,T,X,AFE,H1,S1)
C
C CALCULATION OF THE OPTIMUM NUCLEUS C CONTENT AND ACTIVITY C OF C IN
FERRITE NUCLEUS
C
C Estimate a value for X
C
      IMPLICIT REAL*8(A-H,K-Z)
C
      X=6.3998D-07*T-3.027D-04
       IF(X .LT. 0.1D-07)X=1.0D-08
       IF(X .GT. 0.32D-03)X=0.32D-03
C Estimation complete
C
      AJ1=1.0D+00-DEXP(-W1/(R*T))
1     D1=DSQRT(9.0D+00-6.0D+00*X*(2.0D+00*AJ1+3.0D+00)
     &+(9.0D+00+16.0D+00*AJ1)*X*X)
      B1=((D1-3.0D+00+5.0D+00*X)/(D1+3.0D+00-5.0D+00*X))
      B2=((3.0D+00-4.0D+00*X)/X)
      B3=(H1 - S1*T + 4.0D+00*W1)/(R*T)

      A1=DLOG(B1*B1*B1*B1*B2*B2*B2)+B3
C
      IF(X .GT. 1.0D-08)THEN
        A1FE=DLOG(1.0D+00-X)
```

```
      ELSE
        A1FE=X
      ENDIF
C
      TEST=F+R*T*(A1FE-AFE) - R*T*(A1-A)
C
C Newton iteration
C
      IF (DABS(TEST) .GT. 10.0) THEN
        DA1=(3.0D+00*X/(3.0D+00-4.0D+00*X))*(
     &   (4.0D+00*X-3.0D+00)/(X*X)-4.0D+00/X)
        DA2=(0.5D+00/D1)*(-12.0D+00*AJ1-18.0D+00+
     &   18.0D+00*X+32.0D+00*AJ1*X)
        DA2=4.0D+00*(((DA2+5.0D+00)/(D1-3.0D+00+5.0D+00*X))
     &   -((DA2-5.0D+00)/(D1+3.0D+00-5.0D+00*X)))
        DA1=DA1+DA2
        DA1FE=1.0D+00/(X-1.0D+00)
        ERROR=TEST/(R*T*(DA1FE-DA1))
        IF (ERROR .GT. X) ERROR = 0.3D+00*X
        X=DABS(X-ERROR)
        GOTO 1
      ENDIF
C End of iteration
      RETURN
      END
C*********************************************************************
    DOUBLE PRECISION FUNCTION XALPH(T)
C
C FUNCTION GIVING THE EQUILIBRIUM MOL.FRAC. CARBON IN ALPHA
C TEMP READ IN AS CENTIGRADE
C BASED ON MY PAPER ON FIRST ORDER QUASICHEMICAL
C THEROY,METSCI
C
      DOUBLE PRECISION T,CTEMP
C
      CTEMP=T/900.0D+00
      XALPH=0.1528D-02-0.8816D-02*CTEMP+0.2450D-01*CTEMP*CTEMP
     &-0.2417D-01*CTEMP*CTEMP*CTEMP+
     &0.6966D-02*CTEMP*CTEMP*CTEMP*CTEMP
      RETURN
      END
C*********************************************************************
      SUBROUTINE HFLOW(J,C1,C2,EFF)
C
      DOUBLE PRECISION C1,C2,EFF
      INTEGER J
C
      IF(J .EQ. 2) GOTO 2
      IF(J .EQ. 3) GOTO 3
      IF(J .EQ. 4) GOTO 4
      IF(J .EQ. 5) GOTO 5
```

```
      IF(J .EQ. 6) GOTO 6
      IF(J .EQ. 7) GOTO 7
      IF(J .EQ. 8) GOTO 8
      IF(J .EQ. 9) GOTO 9
      IF(J .EQ. 10) GOTO 10
      IF(J .EQ. 11) GOTO 11
      IF(J .EQ. 12) GOTO 12
      IF(J .EQ. 13) GOTO 13
      IF(J .EQ. 14) GOTO 14
      IF(J .EQ. 15) GOTO 15
      IF(J .EQ. 16) GOTO 16
C     Manual Metal Arc
      C1=1325.0
      C2=1.60
      EFF=0.775
      GOTO 22
C     Metal Cored Wire, CO2 shielding; SUSAN PARK
2     C1=4.452
      C2=2.411
      EFF=0.9
      GOTO 22
C     Metal Cored Wire, Fogon 20 shielding; SUSAN PARK
3     C1=28.535
      C2=2.064
      EFF=0.9
      GOTO 22
C     Tandem submerged arc
4     C1= 1.076
      C2= 2.6798
      EFF=0.9
      GOTO 22
C     Submerged Arc
5     C1=4359.0
      C2=1.51
      EFF=0.9
      GOTO 22
C     Vertical-Up MMA
6     C1=1125.0
      C2=1.7
      EFF=0.775
      GOTO 22
C     Bead on Plate FCAW Chakravati et al. Metal Const. 1985 p.178R
7     C1=206.1
      C2=2.0
      EFF=0.700
      GOTO 22
C     Bead on Plate Self-Sheilded Chakravati et al. Metal Const. 1985 p.178R
8     C1=173.4
      C2=2.0
      EFF=0.700
      GOTO 22
```

```
C  Bead on Plate SAW Chakravati et al. Metal Const. 1985 p.178R
9    C1=150.2
       C2=2.0
       EFF=0.950
       GOTO 22
C  Measured time-temperature Horizontal GMAW data EB, DTRC, NRL
C  Interpass temperature 150 C  Ed Metzbower
10   C1=24.013
       C2=2.2619
       EFF=0.755
       GOTO 22
C  Measured time-temperature Flat GMAW data EB, DTRC, NRL
C  Interpass temperature 150 C  Ed Metzbower
11   C1=23.172
       C2=2.2845
       EFF=0.755
       GOTO 22
C  Measured time-temperature Vertical GMAW data EB, DTRC, NRL
C  Interpass temperature 150 C Ed Metzbower
12   C1=8.3292
       C2=2.3884
       EFF=0.755
       GOTO 22
C  Measured time-temperature Vertical GMAW data EB, DTRC, NRL
C  Interpass temperature 93 C Ed Metzbower
C  At To=93 C1 values are 46.540, 41.806, and 36.104
C  At To=93 C2 values are 2.1996, 2.2217, and 2.1888 for
C  horizontal, flat, and vertical welds. There is only a small difference
C  in dT/dt for low To values.
13   C1=41.483
       C2=2.2030
       EFF=0.755
       GOTO 22
C  Computed time-temperature for laser weld 117000 W 5 mm/s EFF=0.50
C   Philips  data, modified laser.for program, centre of weldment
14   C1=498.42
       C2=2.0500
       EFF=0.50
       GOTO 22
C  Large heat input tandem submerged arc welding (130kJ/cm)
C  Data obtained by K. Ichikawa, Nippon Steel
15   C1= 46130.0
       C2= 1.10
       EFF=0.9
       GOTO 22
C  Large heat input tandem submerged arc welding (70kJ/cm)
C  Data obtained by K. Ichikawa, Nippon Steel
16   C1= 258600.0
       C2= 0.864
       EFF=0.9
       GOTO 22
```

```
22      RETURN
        END
C*********************************************************************
        DOUBLE PRECISION FUNCTION CULRAT
       &(T,TINT,C1,C2,CURR,VOLT,EFF,SPEED)
C
C     FUNCTION TO GET COOLING RATE AT TEMPERATURE T
C
        IMPLICIT REAL*8 (A-H,O-Z)
C
        CULRAT=(T-TINT)**C2
        CULRAT=CULRAT*C1*SPEED/(CURR*VOLT*EFF)
        RETURN
        END
C*********************************************************************
        SUBROUTINE INITCC(C,CARBON,SI,MN,NI,MO,CR,V)
C
C This SUROUTINE stores the average chemical compositions.
C The function of this program is INITiarizing the Chemical
C Compositions to the average compositions.
C K. Ichikawa on 5 January, 1995
C
        IMPLICIT REAL*8(A-H,K-Z), INTEGER(I,J)
        DOUBLE PRECISION C(8)
C
          C(1)=CARBON
          C(2)=SI
          C(3)=MN
          C(4)=NI
          C(5)=MO
          C(6)=CR
          C(7)=V
C
          RETURN
          END
C*********************************************************************
        SUBROUTINE SCHEIL(CCARBON,CSI,CMN,CNI,CMO,CCR,CV
       &,C,I,N)
C
C       Sheil equation is applied in this subroutine by K. Ichikawa.
C       on 12 Jan. 1995.
C       However, g in original Sheil equation is substituted
C       to i/n-1/(2*n).
C       n is a number of division.
C       i means 'i'th   from the g=0.
C
        IMPLICIT REAL*8(A-H,K-M,O-Z), INTEGER(J,I,N)
        DOUBLE PRECISION C(7)
C
        CALLEDC(CCARBON,CSI,CMN,CNI,CMO,CCR,CV,
       &KC,KSI,KMN,KNI,KMO,KCR,KV)
```

```
      CSC =KC *C(1)*((1.00-((1.0*I/N)-(1.00/(2.00*N))))**(KC -1.00))
      CSSI=KSI*C(2)*((1.00-((1.0*I/N)-(1.00/(2.00*N))))**(KSI-1.00))
      CSMN=KMN*C(3)*((1.00-((1.0*I/N)-(1.00/(2.00*N))))**(KMN-1.00))
      CSNI=KNI*C(4)*((1.00-((1.0*I/N)-(1.00/(2.00*N))))**(KNI-1.00))
      CSMO=KMO*C(5)*((1.00-((1.0*I/N)-(1.00/(2.00*N))))**(KMO-1.00))
      CSCR=KCR*C(6)*((1.00-((1.0*I/N)-(1.00/(2.00*N))))**(KCR-1.00))
      CSV =KV *C(7)*((1.00-((1.0*I/N)-(1.00/(2.00*N))))**(KV -1.00))
C
      C(1)=C(1)
      C(2)=CSSI
      C(3)=CSMN
      C(4)=CSNI
      C(5)=CSMO
      C(6)=CSCR
      C(7)=CSV
      RETURN
      END
C*********************************************************************
      SUBROUTINE EDC(CARBON,SI,MN,NI,MO,CR,V,
     &KC,KSI,KMN,KNI,KMO,KCR,KV)
C
C PROGRAM TO CALCULATE Equivalent Distribution Coefficient
C M=MELTING POINT IN KELVIN, LIQUIDUS TEMPERATURE
C CARBON PARTITIONING IGNORED
C THERMODYNAMIC DATA FROM KIRKALDY AND BAGANIS
C SOLIDIFICATION AS DELTA FERRITE
C NOTICE: Originaly, the name of this subroutine is "HETRO"
C         which is made by Dr. H.K.D.H.Bhadeshia.
C
C     Modified by K. ICHIKAWA on 12 Jan. 1995.
C     Sinple empirical calculations of Liquidus Temperature.
C
C     LIQUID(Centigrade) is a liquidus temperature and is calculated
C     by very simple empilical approximation (L. SMRHA: Solidification and
C     crystallization of steel ingots, SNTL, Prague, 1983 (in Czech)).
C
      IMPLICIT REAL*8(A-H,K-Z)
C
      LIQUID=1537.0-
     &(88.0*CARBON+8.0*SI+5.0*MN+4.0*NI+2.0*MO+1.5*CR+2.0*V)
C
      M=LIQUID+273.0
      WRITE(*,2) M
      A=4.187D+00
      R=8.3143D+00
      PC =1.0
      PSI=DEXP((3.9*M-8200.0)*A/(R*M))
      PMN=DEXP((3100.0-2.308*M)*A/(R*M))
      PNI=DEXP((-2120.0-0.38*M)*A/(R*M))
      PCR=DEXP((2.19*M-4600.0)*A/(R*M))
      PMO=DEXP((2.29*M-6600.0)*A/(R*M))
```

```
      PV =DEXP((-5100.0+2.3*M)*A/(R*M))
C
      KC =PC
      KSI=PSI
      KMN=PMN
      KNI=PNI
      KMO=PMO
      KCR=PCR
      KV =PV

2     FORMAT('    '/
     & ' Assumed Melting Point of Delta Ferrite=',F8.0,' K')
      RETURN
      END
C*********************************************************************
      SUBROUTINE DETN(C,SV,DUMM,SITE,
     &LOWT,J,CURR,VOLT,SPEED,TINT,CTEMP,VF,J2,HIGHT,J10)
C
C Calculate the Chemical compositions in the most depleted region.
C
      IMPLICIT REAL*8(A-H,K-Z), INTEGER(I,J)
      DOUBLE PRECISION CTEMP(2000),C(8),
     &                 VF(200)
C
      WRITE(*,446)
      WRITE(*,500)
      CARBON=C(1)
      CALL EDC(CARBON,SI,MN,NI,MO,CR,V,
     &KC,KSI,KMN,KNI,KMO,KCR,KV)
      CC0 =KC* C(1)
      CSI0=KSI*C(2)
      CMN0=KMN*C(3)
      CNI0=KNI*C(4)
      CCR0=KCR*C(5)
      CMO0=KMO*C(6)
      CV0 =KV* C(7)
      C(1)=CC0
      C(2)=CSI0
      C(3)=CMN0
      C(4)=CNI0
      C(5)=CCR0
      C(6)=CMO0
      C(7)=CV0
C Calculate the VF in the most depleted region.
      CALL MAINCONP(C,SV, DUMM,SITE,
     &LOWT,J,CURR,VOLT,SPEED,TINT,CTEMP,VF,J2,HIGHT)
C Determin the "n". J10, in the following procedure, means the "n".
      J10=100
      WRITE(*,560) J10
      WRITE(*,446)
446   FORMAT('----------------------------------------',
```

```
     &'----------',
     &'----------')
560   FORMAT('    '/
     & ' Determination of n.              n =',I5/)
500   FORMAT(//20X,'Calculations for determination of the value of "n".'/
     &20X,'(Calculation in the most depleted region.)')
      RETURN
      END
C*********************************************************************
      SUBROUTINE SUMF(CTEMPE,VFE,J10)
C
C This SUBROUTINE can calculate the sum of VF which are divided by n.
C by K. Ichikawa on 12 Jan., 1995.
C JN(I) is a number of calculation for the 'T'th divided segment.
C
      IMPLICIT REAL*8(A-H,K-M,O-Z), INTEGER(I,J,N)
      DOUBLE PRECISION CTEMPE(200),
     &VFE(200)
C
      DO 10 I=2,J10
       VFE(I)=VFE(I-1)+VFE(I)
10    CONTINUE
      FVF=VFE(J10)/J10
C Print the final results.
      WRITE(6,90) FVF
90    FORMAT(F7.2)
100   CONTINUE
      RETURN
      END
C*********************************************************************
```

APPENDIX FIVE

FORTRAN Program to Calculate Allotriomorphic and Widmanstätten Ferrite in Steel Welds

Introduction

The program described in this appendix was used to calculate the simultaneous transformation of allotriomorphic and Widmanstätten ferrite in the model discussed in Chapter Four.

It is presented using documentation defined in the MAP format [Bhadeshia, H. K. D. H.,1995, http:/www.msm.cam.ac.uk/map/mapmain.html].

MAP FORTRAN LIBRARY

Program MAP_WELDAW

0. Provenance of Source Code

Kazutoshi Ichikawa, Phase Transformation Group, Department of Materials Science and Metallurgy, University of Cambridge, Cambridge, UK.

1. Purpose

To calculate the simultaneous formation allotriomorphic and Widmanstätten ferrite in the heterogeneous weld metal.

2. Specification

The program is self-contained.

[illegible] Program to Determine Multidimensional and Vibrational Energy Levels [illegible]

[illegible]

3. Description

4. References

1. K. Ichikawa and H. K. D. H. Bhadeshia, *Mathematical modelling of weld phenomena 4*, Ed. H. Cerjak, The Institute of Materials, pp. 302–320.

5. Parameters

Input parameters

CARBON - real

Concentration of carbon in wt.%.

SI - real

Concentration of silicon in wt.%.

MN - real

Concentration of manganese in wt.%

NI - real

Concentration of nickel in wt.%.

MO - real

Concentration of molybdenum in wt.%.

CR - real

Concentration of chromium in wt.%.

V - real

Concentration of vanadium in wt.%.

SV - real

Austenite grain surface per unit volume in m^{-1}.

DUMM - real

Fitting constant for nucleation (K_2^{α} in Chapter Two).

SITE - real

Fitting constant for nucleation (K_1^{α} in Chapter Two).

LOWT - real

Lowest temperature at which the calculation is stopped arbitrary.

J - integer

Flag identifies welding method (See the comments in the subroutine HFLOW for detail.).

CURR - real

Welding current in A.

VOLT - real

Voltage in V.

SPEED - real

Welding speed in m s^{-1}.

TINT - real

Interpass temperature in °C.

Output parameters

FVFAW - real

Total average volume fraction of allotriomorphic and Widmanstätten ferrite of 100 segregation segments.

FVFA - real

Average volume fraction of allotriomorphic ferrite of 100 segregation segments.

FVFW - real

Average volume fraction of Widmanstätten ferrite of 100 segregation segments.

FVFBAF - real

Total average volume fraction of bainite and acicular ferrite of 100 segregation segments.

FVFRGM - real

Average volume fraction of retained austenite and martensite of 100 segregation segments.

6. Program data

None.

7. Program text

```
C Copyright, Dr. H. K. D. H. Bhadeshia, University of Cambridge
C   and Kazutoshi Ichikawa, Nippon Steel
C Department of Materials Science and Metallurgy, Pembroke St.
C Cambridge CB2 3QZ, England. Telephone Cambridge 334301.
C
C Major modifications March 1994
C Major modifications 5th July 1994
C Modification to include variable cooling rate, 19 October 1994
C Description of input data about welding parameters were also added to be
C appeared on the screen by K. Ichikawa on 19 October 1994
C Version 1.2
C
C Major modifications
C Modified to take acount the segregation effect by K. Ichikawa on
C 1 Nov., 1994
C
C This program is based on a rectangular segregation model.
C Adding up of VF is not possible by this program for each calculating Temp.
C 5 JAN 1995.
C
C SUBROUTINEs "SUM" and "OUTPUT" do not work in this program.
C K. ICHIKAWA on 5 JAN 1995.
C
C Interpolation method is adapted for adding up the VF.
C K. ICHIKAWA on 5 JAN 1995.
C
C Allows carbon enrichment in austenite to affect the kinetics of
C   ferrite formation via soft impingement effects
C
C Program on overall transformation kinetics (non-isothermal).
C
```

```
C Subroutine NUC designed from their nucleation function.
C
C needs to ensure that ANS, AREA increase as T decreases.
C this is a problem associated with the treatment of anisothermal
C transformation.
C There should never be a decrease in the fraction of boundary covered
C as the temperature drops.
C
C TYPICAL DATA SET FOLLOW
C 0.003 8392
C 760 610   2D04 0.217 0.05 1.0
C C MOL FRAC, carbon-carbon interaction energy, J/mol,
C   approx Ae3 centigrade,
C Approx allot. ferrite finish temp centigrade,
C surface per unit volume
C DUMM, FIDDLE and SITE are required for subroutine NUC
C 0.0139   -112.0
C Equilibrium C content of austenite
C Maximum driving force for diffusional nucleation, J/mol
C End of dataset
C
C AB1 is set between 0,1,saturation value for grain boundary coverage
C AB2 sets the temperature interval between successive calculations
C     of parabolic rate constant
C CARBON, SI, MN, NI, MO, CR, V in wt.%
C
C SITE allows the number of sites for nucleation to be multiplied by a f
C SIGMA is the interface energy per unit area
C SIGMA2 is an effective interface energy which takes into account the
C     effect of DUMM
C LINEAL is the mean lineal intercept in micrometers for equiaxed grains
C SV is the austenite grain surface per unit volume (1/m)
C
C TIME2 is the time to achieve the same fraction at a lower temperature
C TIME3 is the net time spent at any given temperature to achieve
C     the total amount of transformation that has occurred
```

```
C TIME(I) is defined to be zero at the Ae3 temp,
C     and it is the TOTAL amount of time between Ae3 and the temperature
C     of interest. It is incremented in regular steps determined by the
C     cooling curve.
C
C XBAR mole fraction carbon in alloy as a whole
C XBARN mole fraction carbon in enriched austenite
C
C Sructure of the program has completely revised on 21 Dec., 1994
C by K.Ichikawa. That is into as followings.
C (1) Mainprogram only manages the datainput, output for each region
C       (i.e., Enriched region, Depleted region, ...(Number of Region
C       can be increased as any Segregation profile model)), calculations
C       of adding up the VF for all regions and their output.
C (2) "Main" calculations of transformation are conducted in a Sub-
C       routine "MAINCONP", which is almost same as original program by
C       Dr. Bhadeshia.
C
C Sheil equation was introduced to provide segregation profiles for
C each element on 12 Jan. 1995 by K.Ichikawa.
C
C Adding up of VF for each divided segment regarding to the
C segregations is still imposibble on 12 Jan. by K. Ichikawa.
C
C The number of division "n" into the independed segment should be
C as following.
C                                   (1/n) ¡ Maximum VF
C
C Therefore (1/n) ¡ VF in the most depleted region.
C Subroutine DETN calculate the "n" according to the above principle.
C K. Ichiokawa on 20 Jan., 1995.
C
C
C New cooling rate data on (very) large heat input were instolled
C by K. Ichikawa on 2 May, 1995 in SUBROUTINE HFLOW
C
```

```
C In this program, hard impingement effect was introduced in the
C calculation of Widmanstatten ferrite of ferrp48.for
C by K. Ichikawa on 19 July 1995.
C
C Trying to find Widmanstatten Ferrite Transformation Start Temp. in
C more regorous way. By K. Ichikawa on 12 Oct 1995.
C
C Harry's new concept on simalteneous kinetics is beeing adapted in this
C program.
C
C Hard inpingement effects are temporarily killed in this program
C (6 Feb. 1996).
C
C SIBROUTINE PROGC were replace to the original version by Harry
C on 15 Feb. 1996. (previously ferrp54.for)
C
C Allow simultanious transformation of allotriomorphic ferrite and
C Widmanstatten ferrite. K. Ichikawa 11 April 1996.
C
##################################################################
##############
C This program is completed version on 22th July 1996.
C
##################################################################
##############
C
C*****************************************************************
      IMPLICIT REAL*8(A-H,K,M,O-Z,N,L), INTEGER(I,J)
      DOUBLE PRECISION CTEMP(100),
     &                 C(8),
     &                 CTEMPS(200,200)
     &                 ,VFAW(200),VFA(200),VFW(200),VFBAF(200),
     &                  VFRGM(200)
     &                 ,VFSAW(200,200),VFSA(200,200),VFSW(200,200)
     &                 ,VFSBAF(200,200),VFSRGM(200,200)
     &                 ,CTEMPE(200),CTEMPW(1000)
```

```
     &                ,CTEMPWS(200,200),VW(1000),VWS(200,200)
     &                ,CTEMPWSE(200)
     &                ,VWSE(200)
     &                ,VFEAW(200),VFEA(200),VFEW(200),
     &                 VFEBAF(200),VFERGM(200)

C
          FIDDLE=1.0D+00
          SIGMA=0.05D+00
          AB1=0.90D+00
          AB2=5.0
          ICI=0
          IIMP=0

C ICI is a indicater which indicates the incorrect convergent of
C calculation of XEQ, GMAX. IF ICI=0, no such probrem was occured in
C the calculation. IF ICI=2 convergent could NOT completed in the
C calculation in SUBROUTINE AG and/or HIGH.
C
          READ(5,*) CARBON,SI,MN,NI,MO,CR,V
          READ(5,*) SV, DUMM, SITE, LOWT
C
C Read welding parameters
C J defines the welding process (see subroutine HFLOW)
C CURR is the welding current, amps
C VOLT is the welding voltage, Volts
C SPEED is the welding speed, m/s
C TINT is the interpass temperature, Centigrade
          READ(5,*) J, CURR, VOLT, SPEED, TINT
C          WRITE(6,7) CURR,VOLT,SPEED,J,TINT
C
          C(1)=CARBON
          C(2)=SI
          C(3)=MN
          C(4)=NI
          C(5)=MO
```

```
      C(6)=CR
      C(7)=V

      CALL INITCC(C,CARBON,SI,MN,NI,MO,CR,V)

C Display of Average Chemical Composition as a reference
C       WRITE(*,446)
C       WRITE(*,445)
C       WRITE(*,261) (C(J5),J5=1,7)
      CALL OMEGA(C,W,XBAR,T10,T20,0)
      XBARN=XBAR
C       WRITE(*,262) (C(J5),J5=1,7)
      CALL INITCC(C,CARBON,SI,MN,NI,MO,CR,V)
C
C       Explanation of the Process of Calculation:
C
C*****************************************************************
C Modificated using Sheil equiation by K. Ichikawa
C on 9 Jan. ,1995.

      CALL DETN(C,SV,DUMM,SITE,
     &LOWT,J,CURR,VOLT,SPEED,TINT,CTEMP,
     &VFAW,VFA,VFW,VFBAF,VFRGM,
     &J2,HIGHT,J10,CTEMPW,IIMP,ISTOP)

      DO 80 I=1,J10
       CTEMPE(I)=0.0
       VFEAW(I)=0.0
       VFEA(I)=0.0
       VFEW(I)=0.0
       VFEBAF(I)=0.0
       VFERGM(I)=0.0

80    CONTINUE

C %%%%%%%%%%%%%%%%%%%v
```

```
      DO 50 I=1,J10,1
C
C IIMP is 1, if the transformation was never occured because of too
C low WS Temp.
C Once IIMP becomes 1, calculations of transformations for
C following segments are not done. So, the following MAINCONP is
C being skipped.
C
C       IF (IIMP .EQ. 1) THEN
C        J2=1
C        CTEMP(1)=0.0
C        VF(1)=0.0
C        GOTO 51
C       ENDIF
C %%%%%%%%%%%%%%%%%%%%

C       WRITE (*,570)
      CALL INITCC(C,CARBON,SI,MN,NI,MO,CR,V)
C       WRITE(*,560) I, J10, 1.0*I/J10
      CALL SCHEIL(CARBON,SI,MN,NI,MO,CR,V,C,I,J10)

      CALL MAINCONP(C,SV, DUMM,SITE,
     & LOWT,J,CURR,VOLT,SPEED,TINT,CTEMP,
     & VFAW,VFA,VFW,VFBAF,VFRGM,J2,HIGHT,ICI
     & ,CARBON,SI,MN,NI,MO,CR,V,VW,CTEMPW,IIMP,ISTOP)
C

51    CONTINUE

C %%%%%%%%%%%% Memory Over Flow? %%%%%%%%%%%% v
C       DO 60 J7=1,J2
C        CTEMPS(I,J7)=CTEMP(J7)
C        VFSAW(I,J7)=VFAW(J7)
C        VFSA(I,J7)=VFA(J7)
C        VFSW(I,J7)=VFW(J7)
C        VFSBAF(I,J7)=VFBAF(J7)
```

```
C          VFSRGM(I,J7)=VFRGM(J7)
C60      CONTINUE
C
C        CALL INITCC(C,CARBON,SI,MN,NI,MO,CR,V)
C
C          CTEMPE(I)=CTEMPS(I,ISTOP)
C          VFEAW(I)=VFSAW(I,ISTOP)
C          VFEA(I)=VFSA(I,ISTOP)
C          VFEW(I)=VFSW(I,ISTOP)
C          VFEBAF(I)=VFSBAF(I,ISTOP)
C          VFERGM(I)=VFSRGM(I,ISTOP)
C %%%%%%%%%%%%%%%%%%%%%%%%%%%%%%%%%%%%%%%%%%%

        CALL INITCC(C,CARBON,SI,MN,NI,MO,CR,V)


          CTEMPE(I)=CTEMP(ISTOP)
          VFEAW(I)=VFAW(ISTOP)
          VFEA(I)=VFA(ISTOP)
          VFEW(I)=VFW(ISTOP)
          VFEBAF(I)=VFBAF(ISTOP)
          VFERGM(I)=VFRGM(ISTOP)


          CTEMPWSE(I)=CTEMPWS(I,J9)
          VWSE(I)=VWS(I,J9)

50      CONTINUE
C51       CONTINUE
C       CALL SUMN(HIGHTD,LOWT,AB2,A,AD,HIGHT)

        CALL SUMF(CTEMPE,VFEAW,VFEA,VFEW,VFEBAF,VFERGM,J10,1)
C         CALL SUMF(CTEMPWSE,VWSE,J10,2)
```

```
C       IF (ICI .EQ. 2) WRITE(*,580)

580   FORMAT(5X,'*** Calculations of XEQ and/or GMAX could not be'/
     &        10X,' conpleted correctly for some "i" ***'//)
C*************************************************************
      STOP
C
7     FORMAT(//20X,'Welding Current (amps) =',F5.0/
     &20X,'Voltage (V) =',F3.0/
     &20X,'Welding Speed (m/s) =',D10.3/
     &20X,'Welding Technique (SMAW:1, Tandem SAW:4, Single SAW:5)=',I5/
     &20X,'Interpass Temperature (Centigrade) =',F5.0)
C
446   FORMAT('-----------------------------------',
     &'----------',
     &'----------')
445   FORMAT (4H     )
261   FORMAT (6H     C=,F8.4,6H    SI=,F8.4,6H    MN=,F8.4,
     &6H    NI=,F8.4,6H    MO=,F8.4,6H    CR=,F8.4,6H     V=,F8.4
     &,5X,'wt.%')
262   FORMAT (6H     C=,F8.4,6H    SI=,F8.4,6H    MN=,F8.4,
     &6H    NI=,F8.4,6H    MO=,F8.4,6H    CR=,F8.4,6H     V=,F8.4
     &,5X,'mole fraction')
550   FORMAT (/'Coefficients A(1), A(2) and A(3) of quadaratic'
     &' polynomial y=A(1)+A(2)x+A(3)x**2 for Segregated Region.'/)
510   FORMAT (/'Coefficients A(1), A(2) and A(3) of quadaratic'
     &' polynomial y=A(1)+A(2)x+A(3)x**2 for Depleted Region.'/)
520   FORMAT ('Where y is VF and x is CTEMP.')
560   FORMAT(//20X,'i =',I5/
     &20X,'n =',I5/
     &20X,'i/n =',F8.4)
570   FORMAT('==========================================
     ==========',
     &'==========',
     &'==========')
```

```
      END
C*********************************************************************
      SUBROUTINE MAINCONP(C,SV,DUMM,SITE,
     &LOWT,J,CURR,VOLT,SPEED,TINT,CTEMP,
     &MVF,MVFA,MVFW,MVFBAF,MVFRGM,
     &J3,HIGHT,ICI
     &,CARBON,SI,MN,NI,MO,CR,V,VW,CTEMPW,IIMP,ISTOP)
      IMPLICIT REAL*8(A-H,K-Z), INTEGER(I,J)
      DOUBLE PRECISION TIME(2000), VOLF(2000), CTEMP(2000), GV(2000),
     &                 XAGA(2000),XGAG(2000),ALP(2000),C(8),
     &                 MVF(2000),VFW(2000),TIMED(1000),TTIME(1000),
     &                 G(1000),TSTIME(1000),
     &                 TIMEII(1000),VOLFA(2000),MVFA(2000),TIMEA(2000)
     &                 ,MVFW(2000),TIMEWS(2000)
     &                 ,MVFBAF(2000),MVFRGM(2000)
C
C Arranged by K. Ichikawa, University of Cambridge based on the Harry's
C main program; "ferrp".
C
          FIDDLE=1.0D+00
          SIGMA=0.05D+00
          AB1=0.90D+00
          AB2=5.0D+00
          IMPING=0
          ISTOPIMP=0
          IEND=0
C
C       WRITE(*,446)
C       WRITE(*,445)
C       WRITE(*,261) (C(J5),J5=1,7)
      CALL OMEGA(C,W,XBAR,T10,T20,0)
      XBARN=XBAR
C       WRITE(*,262) (C(J5),J5=1,7)
C       WRITE (*,28) T10,T20,W
      CALL HIGH(C,W,T10,T20,HIGHT,ICI)
```

```
      IF (HIGHT .LE. LOWT) GOTO 2
C
      SIGMA2=SIGMA*(DUMM**0.33)
      LINEAL=(2.0D+00/SV)*1.0d+06

C       WRITE(6,7) SIGMA,SIGMA2, HIGHT,LOWT, SITE,SV,LINEAL,FIDDLE,AB1
C       WRITE(*,446)
        J3=((HIGHT-LOWT)/AB2)+1
        HIT=HIGHT+AB2
C
C Reset matrix
                      DO 4 I=1,J3
                        TIME(I)=0.0
                        TIMEA(I)=0.0
                        VOLF(I)=0.0
                        VOLFA(I)=0.0
                        VFW(I)=0.0
                        G(I)=0.0
                        CTEMP(I)=0.0
                        MVF(I)=0.0
                        MVFA(I)=0.0
                        MVFW(I)=0.0
                        MVFBAF(I)=0.0
                        MVFRGM(I)=0.0
                        TIMEWS(I)=0.0
4                     CONTINUE
C Reset parameters
C                      WRITE(6,6)
                      DUMMY=DUMM
                      IF(DUMMY .LT. 0.0D+00) GOTO 2
                      TIME2=0.0D+00
                      TIME3=0.0D+00
                      TIME2A=0.0D+00
                      TIME3A=0.0D+00
```

```
                    JTEST=0
                    AV=0.0
                    AVA=0.0
C
C                       ***** Calculations for each cooling rate

          IWC=1
          IWS=1
          ILC=1
C############################v
          WSI=0.0D+00
          VMAX=0.0+00
C############################^
          DO 1 I=1,J3
          ISTOP=J3
C
C calculate grain boundary nucleation rate
C
          CTEMP(I)=HIT-AB2*I
          KTEMP=CTEMP(I)+273.15D+00
          CALL AG(C,W,XBARN,T10,T20,KTEMP,XGAG(I),GMAX,FPRO,
     &              H,S,H1,S1,W1,F,AJ,AJ1)
C
C Following "CALL AGX" was put for the calculation of AXTO.
C This "AGX is almost same as "SUBROUTINE AG".
C 25 June 1996.
C
C         CALL AG(C,WX,XBARN,T10X,T20X,KTEMP,XGAGX(I),GMAXX,FPROX,
C      &              HX,SX,H1X,S1X,W1X,FX,AJX,AJ1X)

          XAGA(I)=XALPH(CTEMP(I))
          CALL ALP11(W,XBARN,CTEMP(I),XAGA(I),XGAG(I),ALP(I))
          ALP(I)=ALP(I)/1.0D+02
          GV(I)=GMAX/7.2D-06
          XAGA1=XAGA(1)
          XGAG1=XGAG(1)
```

```
C
      CALL TIM(CULRAT1,TIMEI,AB2,CTEMP(I),CURR,VOLT,SPEED,TINT,J)
C ############################v
      TIMEII(I)=TIMEI
C ############################^
      IF(I .EQ. 1) THEN
      TIME(I)=TIMEI
      TIMEA(I)=TIMEI
      ELSE
      TIME(I)=TIMEI+TIME(I-1)
      TIMEA(I)=TIMEI+TIMEA(I-1)
      ENDIF
C
      CALL NUC(SITE,GSTAR,CTEMP(I),GV(I),BI,DUMMY,FIDDLE,SIGMA)
C
C calculate fraction of ferrite, for aniosthermal transformation
C using the Scheil rule, beginning with the highest temperature (I=1)
C
      IF    (I .EQ. 1)THEN
C              CALL AVOLF(AREA,ANS,VF,SV,BI,TIME(I),ALP(I),
C     &        VOLF(I),XBAR,XAGA(I),XGAG(I))
C############################v
C Under modification
              CALL AVOLFW2(AREA,ANS,VF,SV,BI,TIME(I),ALP(I),
     &        VOLF(I),XBAR,XAGA(I),XGAG(I),WSI,VMAX,XBAR
     &        ,XAGA1,XGAG1)

              CALL AVOLFW1(AREAA,ANSA,VFA,SV,BI,TIMEA(I),ALP(I),
     &        VOLFA(I),XBAR,XAGA(I),XGAG(I),WSI,VMAX,XBAR
     &        ,XAGA1,XGAG1)

C############################^
      ELSE
C allow for carbon enrichment in austenite by
C allotriomorphic and Widmanstatten ferrite transformations
```

```
C
```

```
C
C VFW is not necessary any more so that following 4 lines are
C killed here.
C                IF(I .EQ. 1) THEN
C                XBARN=(XBAR - XAGA(I)*(VF              ))/(1.0-VF            )
C                ELSE
C                XBARN=(XBAR - XAGA(I)*(VF+VFW(I-1)))/(1.0-VF-VFW(I-1))
C                ENDIF
C Following new line is installed.
          XBARN=(XBAR - XAGA(I)*VF)/(1.0D+00-VF)
C
C ##############################v
C Inpingiment effect.
C Condition: If The Temp. ¡ T'0,
C then all the transformation stop.
C
C 6 June 1996
C
C Modefied 25 June 1996
C
C


        CALL AXTO(H,S,H1,S1,XTO,KTEMP,W,W1,F,AJ,AJ1,
      &STORE,XBARN,XBAR)

        IF (IWC .GE. 2) THEN
         TIMEWS(I)=TIME(I)-TIME(IWS)
        ENDIF



C         WRITE(*,*)'############################## Begining of the next temp.
C       &step ##############################'
C         WRITE(*,*)'X'T'zero (mole fraction) =',XTO
C         WRITE(*,*)'C in Austenite (mole fraction) =',XBARN
C         WRITE(*,*)'Time from alpha'W start /sec =',TIMEWS(I)
C         WRITE(*,*)'OMEGAO=',(XGAG(I)-XBAR)/(XGAG(I)-XAGA(I))
```

```
C   %%%%%%%%%%%%%%%%%%%%%%%%%%%%%%%%%%%%%%%%%%%%%%%%%
%%%%%%v
C

      IF (XBARN .LE. XTO) THEN
C       WRITE(*,*)
C     &'!!alpha & alpha'W were impinged at the following carbon
C     & concentrations.!!'

C IIMP is a"flag". It becomes 1 when the Widmanstatten Ferrite
C Transformation Starting Temp. is too low and the transformation
C is never occured.

        IF (WS .LT. CTEMP(I)) THEN
         IIMP=1
        ENDIF

C ISTOPIMP is 1 when the impingement occured with the acicular
C ferrite.

C ISTOP is value of I at which final VF can be seen
C for the segregation segment.
C
C If ISTOPIMP=1, ISTOP=I-1. Because at this I here, VF=0.0,
C because the VF calculation were skipped. But the other case
C ISTOP should be I.
C
C Modified after running the runallcw on 18 June 1996.

          ISTOP=I-1

        ISTOPIMP=1
      GOTO 700
C Getting out from the do-loop. (DO-loop of "DO 1 I=... .")
```

```
      ENDIF
C  %%%%%%%%%%%%%%%%%%%%%%%%%%%%%%%%%%%%%%%%%%%%%%%%%%%%%%%%%%%%%%%%%%%%%%
%%%%%%^

C
C #############################^
C
C
C
3              AV=VOLF(I-1)
               AVA=VOLFA(I-1)

               IF(AV .EQ. 1.0D+00)GOTO 2
               TIME2=TIME(I-1)
               TIME2A=TIMEA(I-1)
               CALL ATIM(SV,BI,TIME2,ALP(I),AV,XBARN,XAGA(I),XGAG(I),
     &VMAX,WSI,XBAR,XAGA1,XGAG1)
               CALL ATIMA(SV,BI,TIME2A,ALP(I),AVA,XBARN,XAGA(I),XGAG(I),
     &VMAX,WSI,XBAR,XAGA1,XGAG1)

               TIME3=TIME(I)+TIME2-TIME(I-1)
               TIME3A=TIMEA(I)+TIME2A-TIMEA(I-1)
C                CALL AVOLF(AREA,ANS,VF,SV,BI,TIME3,ALP(I),
C    &           VOLF(I),XBARN,XAGA(I),XGAG(I))
C###########################
C Under modification
C
               CALL AVOLFW2(AREA,ANS,VF,SV,BI,TIME3,ALP(I),
     &         VOLF(I),XBARN,XAGA(I),XGAG(I),WSI,VMAX,XBAR
     &         ,XAGA1,XGAG1)

               CALL AVOLFW1(AREAA,ANSA,VFA,SV,BI,TIME3A,ALP(I),
     &         VOLFA(I),XBARN,XAGA(I),XGAG(I),WSI,VMAX,XBAR
     &         ,XAGA1,XGAG1)

C###########################
```

```
      ENDIF
C
      MVF(I)=VF
      MVFA(I)=VFA
      IF    (AREA .GE. 0.005)THEN

C           WRITE(6,5)CTEMP(I),VOLF(I),MVF(I),
C     &       AREA,ANS,GV(I),GSTAR,XAGA(I),XGAG(I),
C     &       TIME(I),TIME3,TIME2,ALP(I),BI,CULRAT1
C           WRITE(*,*)VOLFA(I),'    ',MVFA(I)
            IF (VOLF(I) .GE. 0.99) GOTO 2

      ENDIF
C
C     check for site saturation
C     jtest ensures grain size calculation at site saturation
C     jtest set to unity at site saturation
C
      IF    (AREA .GT. AB1 .AND. JTEST .EQ. 0) THEN
            CALL ISONUC(TIME3,SV,BI,ALP(I),XBARN,XAGA(I),XGAG(I),AB1
     &                  ,WSI,VMAX,XBAR,XAGA1,XGAG1)
            CALL ISONUCA(TIME3A,SV,BI,ALP(I),XBARN,XAGA(I),XGAG(I),AB1
     &                  ,WSI,VMAX,XBAR,XAGA1,XGAG1)
            JTEST=1
      ENDIF
C
C ???????????  Under Modification, beeing installed the Widmanstatten
C Ferrite Transformation.

      CALL MOLTOWT(XBARN,C,CARBON,SI,MN,NI,MO,CR,V)

C     WRITE(*,261) (C(J5),J5=1,7)

      IF (IWC .LE. 1) THEN
       CALL WSTEMP(C,W,GAX,GAAF,WS,HIGHT)
       WS=WS-273.15D+00
```

```
C WS is Widmanstatten Ferrite Transformation Starting Temperature
C in degree C.
C          WRITE(*,1005)WS
         ENDIF

         IF (IWC .GE. 2) THEN
          CALL OMEGA(C,W,XBARN,T10W,T20W,0)
         ENDIF


1005   FORMAT(' Widmanstatten Ferrite starts at, (degree C) ',F8.1)

         CTEMPW=CTEMP(I)

         IF (CTEMP(I) .LE. WS) THEN
          IWC=IWC+1


         IF (IWC .EQ. 2) THEN
          IWS=I
         ENDIF

           IF (IMPING .EQ. 1) THEN
C

C%%%%%%%%%%%%%%%%%%%%%%%%%%%%%%%%%%%%%v
C This part is killed. Because here "IIMP" is used differently
C as it is defined differently before.
C
C Set the remained values of VFW(I).

C
C            DO 630 IRS=IIMP+1,J3
C             VFW(IRS)=VFW(IIMP)
C630         CONTINUE
C%%%%%%%%%%%%%%%%%%%%%%%%%%%%%%%%%%%%%^
```

```
          GOTO 610
          ENDIF

          CALL VWMAINCOMP(SV,CURR,VOLT,EFF,SPEED,TINT,
     &   T,XMAX,WDIFF,W,XBARN,AB2,VF,J2,CTEMP,J,C,T10,T20,J3,VFW
     &   ,CTEMPW,HIGHT,I,WS,JW,TIMED,TTIME,G,VMAX,WSI)

C############################
       IF (CTEMP(I) .GT. WS) THEN
        WSI=0.0D+00
        VMAX=0.0D+00
       ENDIF
C############################

          IF (I .EQ. 1) THEN
           TTIME(I)=TIMED(I)
          ELSE
           TTIME(I)=TTIME(I-1)+TIMED(I)
          ENDIF

          IF (IWC .EQ. 2) THEN
           TSTIME(I)=0.0
          ENDIF

          IF (IWC .GE. 3) THEN
           TSTIME(I)=TSTIME(I-1)+TIMEII(I)
          ENDIF

C
C ############################v
C Impingement Effect ****************************************
C
C
C            AI=2.0/((3.0)**(1/2))/SV
C            L=2.0*AI
C
```

```
C          IF (I .EQ. 1) THEN
C           LW=G(I)*TIMEII(I)
C          ELSE
C           LW=LW+G(I)*(TIMEII(I))
C          ENDIF
C
C
C
C Q is half-thickness of allotriomorphic ferrite
C
C VFTEMPO is tentative value of VF for testing purpose.
C
C           VFTEMPO=0.2
C
C           Q=((3.0**(1/2))/2.0)*(1.0-(1.0-VFTEMPO)**(1/2))
C
C          LC=L*(3.0**(1/2))-2.0*Q
C
C          IF (LW .GT. LC) THEN
C           IIMP=I
C           IMPING=1
C           WRITE(6,60)
C          ENDIF
C
C          IF (TSTIME(I) .GT. 0.21) THEN
C            IIMP=I
C            IMPING=1
C            WRITE(6,80)
C            ISTOP=I
C            GOTO 700
C           ENDIF
60         FORMAT(//'Widmanstatten Ferrite was impinged with
     &Allotriomorphic Ferrite'/)

80         FORMAT(//'Widmanstatten Ferrite was impinged with
     &Acicular Ferrite'/)
```

```
81        FORMAT(//'All the transformations were impinged'/)
82        FORMAT(F5.0)

C Until here, Impingement Effect ******************************
C ##########################^
C
C TIMEW(I) is Times in the SUBROUTINE VWMAINCOMP. This times are
C introduced here to store all the values of TIME(I) (for I=1, 2.
C 3, ...) in the SUBROUTINE VWMAINCONP.
C
          ENDIF
C
          ILC=ILC+1


610       CONTINUE
620       CONTINUE
C %%%%%%%%%%%%%%%%%%%%%%%%v

          IF (I .EQ. J3) THEN
           IEND=1
          ENDIF
C %%%%%%%%%%%%%%%%%%%%%%%%^




1         CONTINUE
700       CONTINUE
C %%%%%%%%%%%%%%%%%%%%%%%%
C Display again the carbon concentration when the impingement
C with the acicular ferrite occured.
C           WRITE(*,*)'X'T'zero (mole fraction) =',XTO
C           WRITE(*,*)'C in Austenite (mole fraction) =',XBARN
```

```
C          WRITE(*,*)'Time from alpha W start /sec =',TIMEWS(I)
C %%%%%%%%%%%%%%%%%%%%%%%%%
C Display the amount of Widmanstatten ferrite transformed.
C by K. Ichikawa on 4 Dec., 1995.


C############################

C          WRITE(6,600)
C############################


C Display again only Temp. and Wid. ferrite fraction

C############################


C2         OPEN(10,FILE='widtip')

2          DO 1000 I=1,J3

           IF (CTEMP(I) .EQ. 0) THEN
            GOTO 1020
           ENDIF


C            WRITE(10,601)CTEMP(I),MVF(I)


1000       CONTINUE
1020       CONTINUE
C            WRITE(10,*)'0','      ','0'
C            WRITE(10,1010)
```

```
          DO 500 I=1, J3

C   %%%%%%%%%%%%%%%%%%%%%%%%%%%%%%%%%%%%%%%%%%%%%%%%%%%%%%%
%%%%%%%%%%
C Following two lines were modified for the case of that calculation
C is stopped because of VOLF( )=1.0
C on 25 July 1996.

         IF (CTEMP(I) .EQ. 0.0) THEN
           ISTOP=I-1
         ENDIF

C   %%%%%%%%%%%%%%%%%%%%%%%%%%%%%%%%%%%%%%%%%%%%%%%%%%%%%%%
%%%%%%%%%%

          MVFW(I)=MVF(I)-MVFA(I)

C           WRITE(6,601)CTEMP(I),MVF(I),MVFA(I),MVFW(I),TIMEWS(I)

C Following two lines were modified for the case of that calculation
C is stopped because of VOLF( )=1.0
C on 25 July 1996.

          IF (I .GE. ISTOP) THEN
           J4=ISTOP
           GOTO 510
          ENDIF

601       FORMAT(' ',F5.0,'   ',F7.5,'     ',F7.5,'     ',F7.5,'     ',F7.5)
600       FORMAT(//' CTEMP VF'alpha+W VF'alpha   VF'W         TIME'W'/)

500      CONTINUE
         GOTO 520
510      CONTINUE

C          WRITE(6,*)' '
```

```
            IF (ISTOPIMP .EQ. 1) THEN
C             WRITE(6,*)'Fraction of bainite+AF=',1.00D+00-MVF(J4)
C             WRITE(6,*)'Retained Austenite+M= 0.00000'
             MVFBAF(ISTOP)=1.00D+00-MVF(J4)
             MVFRGM(ISTOP)=0.0
            ELSE
C             WRITE(6,*)'Fraction of bainite+AF= 0.00000'
C             WRITE(6,*)'Retained Austenite+M=',1.00D+00-MVF(J4)
             MVFBAF(ISTOP)=0.0
             MVFRGM(ISTOP)=1.00D+00-MVF(J4)

            ENDIF
            GOTO 530

520         CONTINUE
C             WRITE(6,*)' '
            IF (ISTOPIMP .EQ. 1) THEN
C             WRITE(6,*)'Fraction of bainite+AF=',1.00D+00-MVF(J3)
             MVFBAF(ISTOP)=1.00D+00-MVF(J3)
             MVFRGM(ISTOP)=0.0



            ELSE
C             WRITE(6,*)'Retained Austenite+M=',1.00D+00-MVF(J3)
             MVFBAF(ISTOP)=0.0
             MVFRGM(ISTOP)=1.00D+00-MVF(J3)

             ENDIF
530         CONTINUE

1010        FORMAT('      ')
C##########################
C
      RETURN
C
5     FORMAT(F5.0,4F7.2,2D10.2,D10.2,F10.4,3F8.2,2D9.2,D10.3,D10.2)
```

```
6     FORMAT(//' CTEMP    VOL     VF    AREA      ANS     GV      GSTAR      ',
     &' XAGA       ',
     &' XGAG    TIME(I)   TIME3    TIME2 ',
     &'    ALP(I)     BI      K/s '/)
7     FORMAT(//20X,'Interface energy,                J/m**2= ',F10.3/
     &20X,          'Effective interface energy, J/m**2= ',F10.3//
     &20X,'Paraequilibrium Ae3 (Centigrade)',F5.0/
     &20X,'Temperature transformation stopped (Centigrade)',F5.0/
     &20X,'Fraction of boundary atoms forming nucleation sites',D10.3//
     &20X,'Austenite grain surface per unit volume      SV (1/m)',D10.3/
     &20X,'Lineal intercept, equiaxed austenite grains (microns)',F10.0//
     &20X,'Fiddle (1 means no fiddle factor) =',D12.4/
     &20X,'Nucleation stopped at fractional coverage = ',F8.3//)
28    FORMAT (/'     T10=',F10.6,
     &'      T20=',F10.6,'      WGAMMA=',F7.0,'  J/mol')
446   FORMAT('-----------------------------------',
     &'----------',
     &'----------------------------------')
445   FORMAT (4H     )
261   FORMAT (6H     C=,F8.4,6H    SI=,F8.4,6H    MN=,F8.4,
     &6H    NI=,F8.4,6H    MO=,F8.4,6H    CR=,F8.4,6H     V=,F8.4
     &,5X,'wt.%')
262   FORMAT (6H     C=,F8.4,6H    SI=,F8.4,6H    MN=,F8.4,
     &6H    NI=,F8.4,6H    MO=,F8.4,6H    CR=,F8.4,6H     V=,F8.4
     &,5X,'mole fraction')
      END
C
C*********************************************************************
      SUBROUTINE AAARG(ARG)
      DOUBLE PRECISION ARG
       IF(DABS(ARG) .LT. 1.0D-04) GOTO 1
       GOTO 2
1      ARG=0.0D+00
2      RETURN
      END
C*********************************************************************
```

```
      SUBROUTINE AARG(ARG)
C HELPS AVOID UNDERFLOW ERRORS IN EXPONENTIALS
      DOUBLE PRECISION ARG
      IF(ARG .GT. 173.0D+00) GOTO 1
      GOTO 2
1     ARG=179.0D+00
2     RETURN
      END
C*****************************************************************
C C AFEG AFEG LN ACTIVITY OF IRON IN GAMMA
      DOUBLE PRECISION FUNCTION AFEG(XEQ,AJ)
      DOUBLE PRECISION XEQ,AJ,DEQ,TEQ
      DEQ=DSQRT(1-2*(1+2*AJ)*XEQ+(1+8*AJ)*XEQ*XEQ)
      TEQ=5*DLOG((1-XEQ)/(1-2*XEQ))
      TEQ=TEQ+DLOG(((1-2*AJ+(4*AJ-1)*XEQ-DEQ)/(2*AJ*(2*XEQ-1)))**6)
      AFEG=TEQ
      RETURN
      END
C*****************************************************************
C Copyright Dr. H. K. D. H. Bhadeshia, University of Cambridge
C MUCG1.FOR
C calculation of XEQ and GMAX only. Adapted from MUCG46.FOR
C 5 July 1994
C
C Department of Materials Science and Metallurgy, Pembroke St. Cambridge CB2 3QZ
C
      SUBROUTINE AG(C,W,XBAR,T10,T20,KTEMP,XEQ,GMAX,FPRO,
     &              H,S,H1,S1,W1,F,AJ,AJ1)
      IMPLICIT REAL*8 (A-H,K-Z), INTEGER (I,J)
      DOUBLE PRECISION C(8)
      X1=C(1)
      XA=0.001D+00
      R=8.31432D+00
      W1=48570.0D+00
      H=38575.0D+00
      S=13.48D+00
```

```
      XEQ=0.1D+00
      IC=0
C
      T=KTEMP
      CTEMP=T-273.00D+00
C
      IF (T .LE. 1000.0) GOTO 20
      H1=105525.0D+00
      S1=45.34521D+00
      GOTO 19
20    H1=111918.0D+00
      S1=51.44D+00
C
19    F=ENERGY(T,T10,T20)
      AJ=1.0D+00-DEXP(-W/(R*T))
      AJ1=1.0D+00-DEXP(-W1/(R*T))
51    TEQ=R*T*AFEG(XEQ,AJ)-F
      IF (DABS(TEQ) .LT. 1.0) GOTO 52
      ETEQ=DAFEG(XEQ,AJ)*R*T
      XEQ=XEQ-TEQ/ETEQ
C Modified by K. Ichikawa Until ****
      IC=IC+1
      IF (IC .GE. 1000000) GOTO 55

C ****
      GOTO 51
52    AEQ=CG(XEQ,T,W,R)
      AFEQ=AFEG(XEQ,AJ)
      A=CG(X1,T,W,R)
      AFE=AFEG(X1,AJ)
C     Following "FPRO" was put according to Harry's direction
C     in order to get free energy change for growth.
C     FPRO is free energy change for ferrite growth.
C
c
      FPRO=R*T*(X1*(AEQ-A)+(1.0-X1)*(AFEQ-AFE))
```

```
C
C
C
      CALL GMAAX(A1,A,W1,F,R,T,X,AFE,H1,S1)
      GMAX=R*T*(A1-A)
C
60    RETURN

C55     WRITE(*,56)
55    CONTINUE
56    FORMAT(5X,'*** Calculations of XEQ and GMAX could not'/
     &       10X,' conpleted correctly  ***'//)

      GOTO 60

      END
C*************************************************************
      SUBROUTINE AL(XGAG,XBAR,XAGA,DIFF,CTEMP,ALPHA)
C Writing suppressed 5 July 1994
      IMPLICIT REAL*8(A-H,K-Z), INTEGER(I,J)
      DOUBLE PRECISION X2(22),Y2(22),X(60),Y(60),X1(3),Y1(3)
      GES=0.51466
C     GES IS A GUESS VALUE OF ALPHA1/(2*SQRT(D))
      I3=0
      J=0
      OMEGA=(XGAG-XBAR)/(XGAG-XAGA)
3     I3=I3+1
      DUM1=GES*DEXP(GES*GES)*(1.0D+00-DERF(GES))-(OMEGA
     &/DSQRT(3.14159D+00))
      X2(I3)=GES
      Y2(I3)=DUM1
C       WRITE(4,5)GES,DUM1
      DER=(DEXP(GES*GES)*(1.0D+00 + 2.0D+00*GES*GES))*
     &(1.0D+00-DERF(GES))-GES*2.0D+00/(DSQRT(3.14159D+00))
      I1=DINT(GES*1000000)
      GES=GES-DUM1/DER
```

```
      IF(GES .GT. 12.0) GOTO 1
      I2=DINT(GES*1000000)
      IF(I1 .EQ. I2)GOTO 2
      IF(I3 .GT. 20)GOTO 1
      GOTO 3
1     GES=0.51466
7     J=J+1
      DUM1=GES*DEXP(GES*GES)*(1.0D+00-DERF(GES))-(OMEGA
     &/DSQRT(3.14159D+00))
      DER=(DEXP(GES*GES)*(1.0D+00 + 2.0D+00*GES*GES))*
     &(1.0D+00-DERF(GES))-GES*2.0D+00/(DSQRT(3.14159D+00))
      X(J)=GES
      Y(J)=DUM1
      IF(J .EQ. 1) GOTO 7
      IF(DABS(Y(J)) .GT. DABS(Y(J-1)))GOTO 6
      GES=GES-0.5*DUM1/DER
      GOTO 7
6     X1(3)=X(J-1)
      X1(2)=X(J-2)
      X1(1)=X(J-3)
      Y1(3)=Y(J-1)
      Y1(2)=Y(J-2)
      Y1(1)=Y(J-3)
      CALL ANAL(3,0,CONST,SLOPE,CORR,X1,Y1)
      GES=-1.0D+00*CONST/SLOPE
      DUM1=GES*DEXP(GES*GES)*(1.0D+00-DERF(GES))-(OMEGA
     &/DSQRT(3.14159D+00))
      DO 10 J1=1,I3
      IF(DABS(DUM1) .GT. DABS(Y2(J1)))GOTO 9
      GOTO 10
9     GES=X2(J1)
      DUM1=Y2(J1)
10    CONTINUE
2     ALPHA=GES*2.0D+00*DSQRT(DIFF)
C       WRITE(4,4)CTEMP,ALPHA,DUM1
4     FORMAT(' CTEMP=', F8.0,10X,' ALPHA1, (cm/(sec)**.5)=',
```

```
     &D12.5,    10X,' DUM1=',D12.5/
     &/'******** ********** ********** ***********    ***********')
5      FORMAT(2D12.4)
       RETURN
       END
C*************************************************************************
       SUBROUTINE ALP11(W,XBAR,CTEMP,XAGA,XGAG,ALPHA)
C
C Modified to suppress writing. 5 July 1994
C
C 27 September 1985 same as .CONCDIF:RATE, BUT modified to
C allow easier low T calculations and provide iteration error messages
C TYPICAL DATASET
C 780 0.0100
C 740 0.0176
C 700 0.0266
C 660 0.0389
C 600 0.0552
C Modified 24-6-85 to include XINCR
C - this limits no. of Diff coeffs calculated for T¡700C
C PROGRAM TO CALCULATE PARABOLIC RATE CONSTANT, 4-1-84
C PROGRAM MODIFIED, 30-8-83, FOR ACCURATE XAPLPHA
C PROGRAM TO CALCULATE THE EFFECTIVE DIFFUSIVITY OF CARBON IN
C AUSTENITE, TAKING ACCOUNT OF THE FACT THAT THIS DIFFUSIVITY
C IS CONCENTRATION DEPENDENT.  USES SILLER AND MCLELLAN THEORY
C TO EXPRESS THE CONCENTRATION DEPENDENCE, AND LACHER ET AL
C  THEORY  TO  ALLOW  FOR  THE  EFFECT  OF  SUBSTITUTIONAL  ALLOYING
ELEMENTS
C ON THE ACTIVITY AND W OF CARBON IN AUSTENITE. **7 OCTOBER 1981**
C TEMPERATURE IS READ IN IN DEGREES CENTIGRADE
C  CARBON  CONTENT  READ  IN  AS  MOL  FRAC,  EXCEPT  FOR  THE  SUBROUTINE
OMEGA,
C WHERE THE CARBON CONTENT AND ALLOYING CONTENT IS READ IN AS WT PCT
IN
C THE FIRST LINE OF THE DATASET.
C  HH=PLANCKS  CONST.JOULES/SEC,KK=BOLTZMANNS  CONST.JOULES/DEGREE
```

```
KELVIN
C       D=DIFFUSIVITY OF CARBON IN AUSTENITE
C       Z=COORDINATION OF INTERSTIAL SITE
C       PSI=COMPOSITION DEPENDENCE OF DIFFUSION COEFFICIENT
C       THETA=NO. C ATOMS/ NO. FE ATOMS
C       ACTIV=ACTIVITY OF CARBON IN AUSTENITE
C       R=GAS CONSTANT
C       X=MOLE FRACTION OF CARBON
C       T=ABSOLUTE TEMPERATURE
C       SIGMA=SITE EXCLUSION PROBABLITY
C       W=CARBON CARBON INTERACTION ENERGY IN AUSTENITE
C
        IMPLICIT REAL*8(A-H,K-Y), INTEGER(I,J,Z)
        DOUBLE PRECISION DIFF(500), CARB(500)
        HH=6.6262D-34
        KK=1.38062D-23
        Z=12
        A5=1.0D+00
        R=8.31432D+00
        T=CTEMP+273.00D+00
        II2=0
C       WRITE(4,7)T,CTEMP,XBAR,XGAG,XAGA
        DASH=(KK*T/HH)*DEXP(-(21230.0D+00/T))*DEXP(-31.84D+00)
        DO 9    II=1,1000
        CARB(1)=XBAR
        IF (II .GT. 1)GOTO 1
        GOTO 8
1       IF((XGAG-XBAR) .LT. 0.005)GOTO 2
        GOTO 3
2       XINCR=0.0001D+00
        GOTO 4
3       XINCR=0.001D+00
4       CARB(II)=CARB(II-1)+XINCR
        IF (CARB(II) .GT. XGAG) GOTO 5
8       X=CARB(II)
        II2=II2+1
```

```
      THETA=X/(A5-X)
      ACTIV=CG(X,T,W,R)
      ACTIV=DEXP(ACTIV)
      DACTIV=DCG(X,T,W,R)
      DACTIV=DACTIV*ACTIV
      DACTIV=DACTIV*A5/((A5+THETA)**2)
      SIGMA=A5-DEXP((-(W))/(R*T))
      PSI=ACTIV*(A5+Z*((A5+THETA)/(A5-(A5+Z/2)*THETA+(Z/2)*(A5+Z/2)*
     &(A5-SIGMA)*THETA*THETA)))+(A5+THETA)*DACTIV
      DIFF(II)=DASH*PSI
9     CONTINUE
5     II3=0
C       CALL D01GAF(CARB,DIFF,II2,ANS,ERROR,II3)
      CALL TRAPE(CARB,DIFF,ANS,II2)
      ANS=ANS/(XGAG-XBAR)
C       WRITE(4,6)ANS,ERROR
      CALL AL(XGAG,XBAR,XAGA,ANS,CTEMP,ALPHA)
7     FORMAT(' ABSOLUTE TEMPERATURE, DEGREES KELVIN =',F8.1/
     &'              TEMPERATURE IN DEGREES CENTIGRADE =',F8.1/
     &' MOL FRAC CARBON IN ALLOY = ',F8.4/
     &' EQUILIBRIUM MOL FRAC CARBON IN AUSTENITE =',F8.4/
     &' EQUILIBRIUM MOL FRAC OF C IN FERRITE=',D12.4)
6     FORMAT(' INTEGRAL, XGAG-XBAR = ',D12.4, '  CM**2/SEC  ',
     &8HERROR = , D12.4)
      RETURN
      END
C*********************************************************************
      SUBROUTINE ANAL(J7,J9,CONST,SLOPE,CORR,X,Y)
      DOUBLE PRECISION AX,AX2,AY,AY2,AXY,CONST,CORR,SLOPE,
     &X(60),Y(60)
      INTEGER I,J8,J9,J7
      J8=J7-J9
      AX=0.0D+00
      AY=0.0D+00
      AX2=0.0D+00
      AY2=0.0D+00
```

```
      AXY=0.0D+00
      DO 1 I=1,J8
      AX=AX+X(I)
      AY=AY+Y(I)
      AXY=AXY+X(I)*Y(I)
      AX2=AX2+X(I)*X(I)
      AY2=AY2+Y(I)*Y(I)
1     CONTINUE
      CONST=(AY*AX2-AX*AXY)/(J8*AX2-AX*AX)
      SLOPE=((J8*AXY-AX*AY)/(J8*AX2-AX*AX))
      CORR=(J8*AXY-AX*AY)/(DSQRT((J8*AX2-AX*AX)*
     &(J8*AY2-AY*AY)))
C       WRITE(6,2)CONST,SLOPE,CORR
2     FORMAT('    INTERCEPT=',D12.4,'     SLOPE=',D10.3,
     &'     CORRELATION=',F8.4)
      RETURN
      END
C*****************************************************************
C
C Calculates time required to transform to a given volume fraction
C
      SUBROUTINE ATIM(SV,BI,TIME,ALP,VOL,XBARN,XAGA,XGAG,VMAX,WSI
     &,XBAR,XAGA1,XGAG1)
C
      IMPLICIT REAL*8(A-H,K-Z), INTEGER(I,J)
      DOUBLE PRECISION D(70),E(70)
C
          ADUM=1.0D-8
C
C This statement determines the entire accuracy at high cooling rates
          IF(VOL .LE. 1.0D-08) GOTO 4
C
          DTIME=TIME
          J=0
          I=0
C3          CALL AVOLF(AREA,ANS,VF,SV,BI,DTIME,ALP,
```

```
C     &                              DVOL,XBAR,XAGA,XGAG)
C############################
3               CALL AVOLFW2(AREA,ANS,VF,SV,BI,DTIME,ALP,
     &          DVOL,XBARN,XAGA,XGAG,WSI,VMAX,XBAR
     &          ,XAGA1,XGAG1)

C############################

          I=I+1
          D(I)=DVOL/VOL
          E(I)=DABS(D(I)-1.0D+00)
          E1=DABS(1.0/D(I)-1.0D+00)
          IF(DABS(D(I)) .GT. (1.0D+00+1.0D-11) ) GOTO 13
          IF(DABS(D(I)) .LT. (1.0D+00-1.0D-11) ) GOTO 13
          TIME=DTIME
          GOTO 2
13        IF(I .GT. 1 .AND. J .LT. 1)GOTO 10
          GOTO 11
10        IF(E(I) .GT. E(I-1))GOTO 12
          IF(E1 .GT. E(I-1)) GOTO 12
          GOTO 11
12        DTIME=DTIME*0.9D+00
C           CALL AVOLF(AREA,ANS,VF,SV,BI,DTIME,ALP,
C     &                              DVOL,XBAR,XAGA,XGAG)
C############################
                CALL AVOLFW2(AREA,ANS,VF,SV,BI,DTIME,ALP,
     &          DVOL,XBARN,XAGA,XGAG,WSI,VMAX,XBAR
     &          ,XAGA1,XGAG1)

C               AREA=AREA1
C               ANS=ANS1
C               VF=VF1
C               DVOL=DVOLW1
```

```
C############################

          IF((DVOL-VOL) .GT. 0.0D+00) GOTO 12
          J=J+1
          GOTO 3
C
C Newton's Iteritive method
C
11        DTIM1=DTIME-ADUM
          DTIM2=DTIME+ADUM
C           CALL AVOLF(AREA,ANS,VF,SV,BI,DTIM1,ALP,
C     &                          DVOL1,XBAR,XAGA,XGAG)

C############################
                CALL AVOLFW2(AREA,ANS,VF,SV,BI,DTIM1,ALP,
     &          DVOL1,XBARN,XAGA,XGAG,WSI,VMAX,XBAR
     &          ,XAGA1,XGAG1)

C                 AREA=AREA1
C                 ANS=ANS1
C                 VF=VF1
C                 DVOL1=DVOL11
C############################
C           CALL AVOLF(AREA,ANS,VF,SV,BI,DTIM2,ALP,
C     &                          DVOL2,XBAR,XAGA,XGAG)

C############################
                CALL AVOLFW2(AREA,ANS,VF,SV,BI,DTIM2,ALP,
     &          DVOL2,XBARN,XAGA,XGAG,WSI,VMAX,XBAR
     &          ,XAGA1,XGAG1)

C                 AREA=AREA1
C                 ANS=ANS1
C                 VF=VF1
```

```
C                   DVOL2=DVOL21
C##########################
            ADUM2=((DVOL-VOL)*(-2.0D+00*ADUM))/(DVOL1-DVOL2)
            IF(DABS(ADUM2) .GT. DTIME)GOTO 14
            DTIME=DTIME-ADUM2
            GOTO 3
14          DTIME=1.5D+00*DTIME
            GOTO 3
C
C VOL = volume fraction / equilibrium volume fraction
4           TIME=0.0D+00
C
C
2       RETURN
        END
C
C*****************************************************************
C
C Calculates time required to transform to a given volume fraction
C
        SUBROUTINE ATIMA(SV,BI,TIME,ALP,VOL,XBARN,XAGA,XGAG,VMAX,WSI
       &,XBAR,XAGA1,XGAG1)
C
        IMPLICIT REAL*8(A-H,K-Z), INTEGER(I,J)
        DOUBLE PRECISION D(5000),E(5000)
C
            ADUM=1.0D-8
C
C This statement determines the entire accuracy at high cooling rates
            IF(VOL .LE. 1.0D-08) GOTO 4
C
            DTIME=TIME
            J=0
            I=0
C3            CALL AVOLF(AREA,ANS,VF,SV,BI,DTIME,ALP,
C       &                               DVOL,XBAR,XAGA,XGAG)
```

```
C############################
3               CALL AVOLFW1(AREA,ANS,VF,SV,BI,DTIME,ALP,
     &           DVOL,XBARN,XAGA,XGAG,WSI,VMAX,XBAR
     &           ,XAGA1,XGAG1)

C############################

          I=I+1
          D(I)=DVOL/VOL
          E(I)=DABS(D(I)-1.0D+00)
          E1=DABS(1.0/D(I)-1.0D+00)
          IF(DABS(D(I)) .GT. (1.0D+00+1.0D-11) ) GOTO 13
          IF(DABS(D(I)) .LT. (1.0D+00-1.0D-11) ) GOTO 13
          TIME=DTIME
          GOTO 2
13        IF(I .GT. 1 .AND. J .LT. 1)GOTO 10
          GOTO 11
10        IF(E(I) .GT. E(I-1))GOTO 12
          IF(E1 .GT. E(I-1)) GOTO 12
          GOTO 11
12        DTIME=DTIME*0.9D+00
C           CALL AVOLF(AREA,ANS,VF,SV,BI,DTIME,ALP,
C    &                              DVOL,XBAR,XAGA,XGAG)
C############################
                CALL AVOLFW1(AREA,ANS,VF,SV,BI,DTIME,ALP,
     &          DVOL,XBARN,XAGA,XGAG,WSI,VMAX,XBAR
     &          ,XAGA1,XGAG1)

C############################



          IF((DVOL-VOL) .GT. 0.0D+00) GOTO 12
          J=J+1
          GOTO 3
C
```

```
C Newton's Iteritive method
C
11          DTIM1=DTIME-ADUM
            DTIM2=DTIME+ADUM
C             CALL AVOLF(AREA,ANS,VF,SV,BI,DTIM1,ALP,
C     &                           DVOL1,XBAR,XAGA,XGAG)

C############################
                CALL AVOLFW1(AREA,ANS,VF,SV,BI,DTIM1,ALP,
     &          DVOL1,XBARN,XAGA,XGAG,WSI,VMAX,XBAR
     &          ,XAGA1,XGAG1)

C############################
C             CALL AVOLF(AREA,ANS,VF,SV,BI,DTIM2,ALP,
C     &                           DVOL2,XBAR,XAGA,XGAG)

C############################
                CALL AVOLFW1(AREA,ANS,VF,SV,BI,DTIM2,ALP,
     &          DVOL2,XBARN,XAGA,XGAG,WSI,VMAX,XBAR
     &          ,XAGA1,XGAG1)

C############################
            ADUM2=((DVOL-VOL)*(-2.0D+00*ADUM))/(DVOL1-DVOL2)
            IF(DABS(ADUM2) .GT. DTIME)GOTO 14
            DTIME=DTIME-ADUM2
            GOTO 3
14          DTIME=1.5D+00*DTIME
            GOTO 3
C
C VOL = volume fraction / equilibrium volume fraction
4           TIME=0.0D+00
C
C
2       RETURN
        END
C
```

```
C*****************************************************************
      SUBROUTINE AVOLF(AREA,ANS,VF,SV,BI,TIME,ALP,
     &VOL,XBAR,XAGA,XGAG)
C
      IMPLICIT REAL*8(A-H,K-Z), INTEGER(I,J)
      DOUBLE PRECISION THETA(1000),FUN(1000)
C
          ILOOP=51
          AILOOP=ILOOP*1.0d+00
          ALP1=3.0D+00*ALP
          OMEGA=(XGAG-XBAR)/(XGAG-XAGA)
C
C Numerical integration using ILOOP-1 slices
C
      DO 1 I=1,ILOOP
          IDUM=I-1
          THETA(I)=IDUM/(AILOOP-1.0D+00)
          ARG=0.5D+00*3.14159D+00*BI*ALP1**2.0D+00*TIME**2.0D+00*
     &          (1.0D+00-THETA(I)**4.0D+00)
          CALL AARG(ARG)
          FUN(I)=1.0D+00-DEXP(-ARG)
1     CONTINUE
C
          CALL TRAPE(THETA,FUN,ANS,ILOOP)
          ARG=2.0D+00*SV*ANS*ALP*(TIME**0.5D+00)/OMEGA
          CALL AARG(ARG)
          VOL=1.0D+00-DEXP(-ARG)
          VF=VOL*OMEGA
          AREA=FUN(1)
C
      RETURN
C
C Page 68, Book 14, 20-12-1986, H. K. D. H. Bhadeshia
C AREA is the fraction of boundary covered
C TIME is in seconds
C VOl is volume fraction of ferrite/equilibrium vol. frac.
```

```
C VF is the actual volume fraction
C ALP is the one-dimensional parabolic thickening rate constant
C ALP1 is the one-dimensional parabolic lengthening rate constant
C BI is the grain boundary face nucleation rate per unit area per unit t
C XGAG, XAGA = equilibrium mol frac of carbon in gamma and alpha respect
C XBAR = average mol frac of carbon in alloy
C SV = austenite grain boundary area per unit volume (1/m)
C
      END
C
C**********************************************************************
C
C FUNCTION GIVING LFG   LN(ACTIVITY) OF CARBON IN AUSTENITE
      DOUBLE PRECISION FUNCTION CG(X,T,W,R)
      DOUBLE PRECISION J,DG,DUMMY,T,R,W,X
      J=1-DEXP(-W/(R*T))
      DG=DSQRT(1-2*(1+2*J)*X+(1+8*J)*X*X)
      DUMMY=5*DLOG((1-2*X)/X)+6*W/(R*T)+((38575.0)-(
     &13.48)*T)/(R*T)
      CG=DUMMY+DLOG(((DG-1+3*X)/(DG+1-3*X))**6)
      RETURN
      END
C
C**********************************************************************
C
C FUNCTION GIVING DIFFERENTIAL OF LN(ACTIVITY) OF CARBON IN AUSTENITE, L
C DIFFERENTIAL IS WITH RESPECT TO X
      DOUBLE PRECISION FUNCTION DCG(X,T,W,R)
      DOUBLE PRECISION J,DG,DDG,X,T,W,R
      J=1-DEXP(-W/(R*T))
      DG=DSQRT(1-2*(1+2*J)*X+(1+8*J)*X*X)
      DDG=(0.5/DG)*(-2-4*J+2*X+16*J*X)
      DCG=-((10/(1-2*X))+(5/X))+6*((DDG+3)/(DG-1+3*X
     &)-(DDG-3)/(DG+1-3*X))
      RETURN
      END
```

```
C
C*********************************************************************
C
C DAFEG DAFEG DIFFERENTIAL OF LN ACTIVITY OF IRON IN GAMMA
      DOUBLE PRECISION FUNCTION DAFEG(XEQ,AJ)
      DOUBLE PRECISION ETEQ,ETEQ2,DEQ,XEQ,AJ
      DEQ=DSQRT(1-2*(1+2*AJ)*XEQ+(1+8*AJ)*XEQ*XEQ)
      ETEQ=5*((1/(XEQ-1))+2/(1-2*XEQ))
      ETEQ2=6*((4*AJ-1-(0.5/DEQ)*(-2-4*AJ+2*XEQ+16*XEQ*AJ))
     &/(1-2*AJ+(4*AJ-1)*XEQ-DEQ))+6*(4*AJ/(2*AJ*(2*XEQ-1)))
      DAFEG=ETEQ+ETEQ2
      RETURN
      END
C
C*********************************************************************
C     ENERGY ENERGY
      DOUBLE PRECISION FUNCTION ENERGY(T,T10,T20)
      DOUBLE PRECISION T,T10,T20,F,T7
      T7=T-100*T20
      IF (T7 .LT. 300) GOTO 1
      IF (T7 .LT. 700) GOTO 2
      IF (T7 .LT. 940) GOTO 3
      F=-8.88909+0.26557*(T7-1140)-1.04923D-3*((T7-1140)**2)
      F=F+2.70013D-6*((T7-1140)**3)-3.58434D-9*((T7-1140)**4)
      GOTO 4
1     F=1.38*T7-1499
      GOTO 4
2     F=1.65786*T7-1581
      GOTO 4
3     F=1.30089*T7-1331
4     ENERGY=(141.0*T10 + F)*4.187
      RETURN
      END
C
C*********************************************************************
C Finds approximate temperature at which paraequilibrium ferrite
```

```
C formation first becomes possible
C H. K. D. H. Bhadeshia, 6 July 1994
C
      SUBROUTINE HIGH(C,W,T10,T20,HIGHT,ICI)
C
      IMPLICIT REAL*8(A-H,K-Z), INTEGER(I,J)
      DOUBLE PRECISION C(8)
C
       X1=C(1)
       XA=0.001D+00
       R=8.31432D+00
       W1=48570.0D+00
       H=38575.0D+00
       S=13.48D+00
       XEQ=0.05D+00
       IC=0
C
C      Modified following line from "DO 1 I=1183,973,-1" to
C      "DO 1 I=1183,893,-1", by K. Ichikawa on 31 Oct., 1994
C      and modified again to "DO 1 I=1183,879,-1".

      DO 1 I=1183,473,-1
C
       KTEMP=I
C
       T=KTEMP
C
        IF (T .LE. 1000.0) GOTO 20
          H1=105525.0D+00
          S1=45.34521D+00
        GOTO 19
20        H1=111918.0D+00
          S1=51.44D+00
C
19    F=ENERGY(T,T10,T20)
      AJ=1.0D+00-DEXP(-W/(R*T))
```

```
      AJ1=1.0D+00-DEXP(-W1/(R*T))
51    TEQ=R*T*AFEG(XEQ,AJ)-F
      IF (DABS(TEQ) .LT. 1.0) GOTO 52
      ETEQ=DAFEG(XEQ,AJ)*R*T
      XEQ=XEQ-TEQ/ETEQ
C Modified by K.Ichikawa until ***
      IC=IC+1
      IF (IC .GE. 1000000) GOTO 220
C ***
      GOTO 51
52      IF(XEQ .GE. X1) THEN
          HIGHT=KTEMP-273.15D+00
          GOTO 222
        ENDIF
1     CONTINUE
C
        IF(XEQ .LT. X1) THEN
C           WRITE(*,53)
53          FORMAT(5X,'*** Alloy cannot transform to ferrite'/
     &           10X,' at temperature as low as 473 K  ***'//)
            HIGHT=0.0D+00
        ENDIF
C
222     RETURN

C220   WRITE(*,221)
220    CONTINUE
221    FORMAT(5X,'*** Calculation of XEQ could not be'/
     &        10X,' conpleted correctly  ***'//)
       ICI=2
       GOTO 222
         END
C*****************************************************************
      SUBROUTINE ISONUC(TIME3,SV,BI,ALP,XBARN,XAGA,XGAG,A1,WSI,VMAX
     &,XBAR,XAGA1,XGAG1)
C
```

```
      IMPLICIT REAL*8(A-H,K-Z), INTEGER(I,J)
      DOUBLE PRECISION A(200)
C
      J2=50
      TINC=TIME3/J2
      TIME=0.0D+00
      SUM=0.0D+00
C
      DO 1 I=1,J2
12       TIME=TIME+TINC

C          CALL AVOLF(AREA,ANS,VF,SV,BI,TIME,ALP,VOL,XBAR,XAGA,XGAG)
C#########################
                 CALL AVOLFW2(AREA,ANS,VF,SV,BI,TIME,ALP,
     &           VOL,XBARN,XAGA,XGAG,WSI,VMAX,XBAR
     &           ,XAGA1,XGAG1)

C#########################

         IF(I .EQ. 1 .AND. AREA .GT. A1)GOTO 10
         IF(TIME .GT. TIME3)GOTO 2
         IF(AREA .GT. A1)GOTO 2
         GOTO 11
10       TINC=TINC/2000.0
         TIME=0.0D+00
         AREA=0.0
         GOTO 12
11       A(I)=(1.0D+00-AREA)*TINC*BI
         SUM=SUM+A(I)
C
1     CONTINUE
C
C2         WRITE(6,3)SUM
2        CONTINUE
         IF(SUM .EQ. 0.0)GOTO 9
3        FORMAT(20X,' Number of particles per unit area =',D12.4)
```

```
      DALPHA=(2.0D+00/(3.0D+00*SV*SUM))**0.333333
      DGAMMA=2.0D+00/(SV)
C       WRITE(6,8)DALPHA,DGAMMA
8     FORMAT(20X,' DALPHA =',D12.4,' m    DGAMMA = ',D12.4,' m')
C
C
9     RETURN
      END
C*****************************************************************
      SUBROUTINE
ISONUCA(TIME3,SV,BI,ALP,XBARN,XAGA,XGAG,A1,WSI,VMAX,XBAR
     &,XAGA1,XGAG1)
C
      IMPLICIT REAL*8(A-H,K-Z), INTEGER(I,J)
      DOUBLE PRECISION A(200)
C
      J2=50
      TINC=TIME3/J2
      TIME=0.0D+00
      SUM=0.0D+00
C
      DO 1 I=1,J2
12      TIME=TIME+TINC

C       CALL AVOLF(AREA,ANS,VF,SV,BI,TIME,ALP,VOL,XBAR,XAGA,XGAG)
C########################
              CALL AVOLFW1(AREA,ANS,VF,SV,BI,TIME,ALP,
     &        VOL,XBARN,XAGA,XGAG,WSI,VMAX,XBAR
     &         ,XAGA1,XGAG1)

C########################

      IF(I .EQ. 1 .AND. AREA .GT. A1)GOTO 10
      IF(TIME .GT. TIME3)GOTO 2
      IF(AREA .GT. A1)GOTO 2
      GOTO 11
```

```
10        TINC=TINC/2000.0
          TIME=0.0D+00
          AREA=0.0
          GOTO 12
11        A(I)=(1.0D+00-AREA)*TINC*BI
          SUM=SUM+A(I)
C
1       CONTINUE
C
2         CONTINUE

C2          WRITE(6,3)SUM
C           IF(SUM .EQ. 0.0)GOTO 9
C3          FORMAT(20X,' Number of particles per unit area =',D12.4)
C           DALPHA=(2.0D+00/(3.0D+00*SV*SUM))**0.333333
C           DGAMMA=2.0D+00/(SV)
C           WRITE(6,8)DALPHA,DGAMMA
C8          FORMAT(20X,' DALPHA =',D12.4,' m    DGAMMA = ',D12.4,' m')
C
C
9       RETURN
        END




C*************************************************************************
        SUBROUTINE NUC(SITE,GSTAR,CTEMP,GV,BI,DUMMY,FIDDLE,SIGMA)
        IMPLICIT REAL*8(A-H,K-Z), INTEGER(I,J)
C
        KELVIN=CTEMP+273.15D+00
        K=1.38062D-23
        H=6.6262D-34
        GSTAR=SIGMA**3.0D+00*DUMMY/(GV*GV)
C calculate number of sites pers unit area by dividing by the area
```

```
C   of an atom, taking width as 2.5d-10 metres. SITE is a fiddle factor
      NS=SITE/((2.5D-10)**2)
      Q=FIDDLE*2.4D+05/6.02217D+23
      ARG=(GSTAR+Q)/(K*KELVIN)
      CALL AARG(ARG)
      BI=(NS*K*KELVIN/H)*DEXP(-ARG)
C KELVIN = temperature in kelvin
C H, K = Planck constant, Boltzmann constant respectively
C Q = activation energy for self-diffusion of iron
C GSTAR = activation energy for grain boundary nucleation
C NS is the number of nucleation sites per unit area of boundary
C BI is the Grain boundary nucleation rate per second, per square meter
C SV is deleted from the equation of BI=(NS*K*KELVINE/H)*DEXP(-ARG),
C because Sally found the mistake of that on9 Jan. 1995. By K. Ichikawa.
C CTEMP is temperature in centigrade
C GV is gibbs free energy change per unit volume, for nucleation, J/m**3
C SIGMA is an interfacial energy per square meter
2     RETURN
      END
C*********************************************************************
      SUBROUTINE NUCC(SITE,GSTAR,CTEMP,GV,BI,SV,DUMMY,SIGMA)
      IMPLICIT REAL*8(A-H,K-Z), INTEGER(I,J)
      IF(CTEMP .GT. 721) GOTO 1
      IF(CTEMP .GT. 701) GOTO 2
      IF(CTEMP .GT. 681) GOTO 3
      IF(CTEMP .GT. 661) GOTO 4
      IF(CTEMP .GT. 641) GOTO 5
      IF(CTEMP .GT. 621) GOTO 6
      IF(CTEMP .GT. 601) GOTO 7
      IF(CTEMP .GT. 581) GOTO 8
      IF(CTEMP .GT. 561) GOTO 9
      IF(CTEMP .GT. 541) GOTO 10
1     BI=0.0D+00
      GOTO 11
2     BI=2.8D+05
      GOTO 11
```

```
3       BI=4.7D+06
        GOTO 11
4       BI=1.42D+07
        GOTO 11
5       BI=2.0D+07
        GOTO 11
6       BI=2.4D+07
        GOTO 11
7       BI=2.1D+07
        GOTO 11
8       BI=1.7D+07
        GOTO 11
9       BI=1.3D+07
        GOTO 11
10      BI=8.5D+06
11      RETURN
C KELVIN = temperature in kelvin
C H, K = Planck constant, Boltzmann constant respectively
C Q = activation energy for self-diffusion of iron
C GSTAR = activation energy for grain boundary nucleation
C NS is the number of nucleation sites per unit area of boundary
C BI is the Grain boundary nucleation rate per second, per square meter
C CTEMP is temperature in centigrade
C GV is gibbs free energy change per unit volume, for nucleation, J/m**3
C SIGMA is an interfacial energy per square meter
        END
C*************************************************************************
        SUBROUTINE OMEGA(C,W,XBAR,T10,T20,J)
C SUBROUTINE TO CALCULATE THE CARBON CARBON INTERACTION ENERGY IN
C AUSTENITE, AS A FUNCTION OF ALLOY COMPOSITION.  BASED ON .MUCG18
C THE ANSWER IS IN JOULES PER MOL.    **7 OCTOBER 1981**
        DOUBLE PRECISION C(8),W,P(8),B1,B2,Y(8),T10,T20,B3,XBAR
        INTEGER U,J
        B3=0.0D+00
        IF(J .EQ. 1) GOTO 2
        C(8)=C(1)+C(2)+C(3)+C(4)+C(5)+C(6)+C(7)
```

```
      C(8)=100.0D+00-C(8)
      C(8)=C(8)/55.84D+00
      C(1)=C(1)/12.0115D+00
      C(2)=C(2)/28.09D+00
      C(3)=C(3)/54.94D+00
      C(4)=C(4)/58.71D+00
      C(5)=C(5)/95.94D+00
      C(6)=C(6)/52.0D+00
      C(7)=C(7)/50.94D+00
2     B1=C(1)+C(2)+C(3)+C(4)+C(5)+C(6)+C(7)+C(8)
      DO 107 U=2,7
      Y(U)=C(U)/C(8)
107   CONTINUE
      DO 106 U=1,8
      C(U)=C(U)/B1
106   CONTINUE
      XBAR=C(1)
C Following 2 lines are eliminated after consulting Harry.
C 25 July 1996. K. Ichikawa
C       XBAR=DINT(10000.0D+00*XBAR)
C       XBAR=XBAR/10000
      B2=0.0D+00
      T10=Y(2)*(-3)+Y(3)*2+Y(4)*12+Y(5)*(-9)+Y(6)*(-1)+Y(7)*(-12)
      T20=-3*Y(2)-37.5*Y(3)-6*Y(4)-26*Y(5)-19*Y(6)-44*Y(7)
      P(2)=2013.0341+763.8167*C(2)+45802.87*C(2)**2-280061.63*C(2)**3
     &+3.864D+06*C(2)**4-2.4233D+07*C(2)**5+6.9547D+07*C(2)**6
      P(3)=2012.067-1764.095*C(3)+6287.52*C(3)**2-21647.96*C(3)**3-
     &2.0119D+06*C(3)**4+3.1716D+07*C(3)**5-1.3885D+08*C(3)**6
      P(4)=2006.8017+2330.2424*C(4)-54915.32*C(4)**2+1.6216D+06*C(4)**3
     &-2.4968D+07*C(4)**4+1.8838D+08*C(4)**5-5.5531D+08*C(4)**6
      P(5)=2006.834-2997.314*C(5)-37906.61*C(5)**2+1.0328D+06*C(5)**3
     &-1.3306D+07*C(5)**4+8.411D+07*C(5)**5-2.0826D+08*C(5)**6
      P(6)=2012.367-9224.2655*C(6)+33657.8*C(6)**2-566827.83*C(6)**3
     &+8.5676D+06*C(6)**4-6.7482D+07*C(6)**5 +2.0837D+08*C(6)**6
      P(7)=2011.9996-6247.9118*C(7)+5411.7566*C(7)**2
     &+250118.1085*C(7)**3-4.1676D+06*C(7)**4
```

```
      DO 108 U=2,7
      B3=B3+P(U)*Y(U)
      B2=B2+Y(U)
108   CONTINUE
      IF (B2 .EQ. 0.0D+00) GOTO 455
      W=(B3/B2)*4.187
      GOTO 456
455   W=8054.0
456   CONTINUE
      RETURN
      END
C
C*********************************************************************
      SUBROUTINE TIM(CULRAT1,TIME,AB2,LOWT,CURR,VOLT,SPEED,TINT,J)
      IMPLICIT REAL*8(A-H,K-Z),INTEGER(I,J)
C
C Find constants for particular welding process
C
        CALL HFLOW(J,C1,C2,EFF)
C
C Find cooling rate at intermediate temperature T=(HIGHT-LOWT)/2
C Units of cooling rate in K/s
C
        T= LOWT
        CULRAT1= CULRAT(T,TINT,C1,C2,CURR,VOLT,EFF,SPEED)
C
C Find time to cool between HIGHT and LOWT (units of time = s)
C
       TIME=(AB2)/CULRAT1
C
C
      RETURN
      END
C
C*********************************************************************
C
```

```
C       SUBROUTINE TRAPE
C
C       PURPOSE
C          TO COMPUTE THE VECTOR OF INTEGRAL VALUES FOR A GIVEN
C          GENERAL TABLE OF ARGUMENT AND FUNCTION VALUES.
C
C       USAGE
C             CALL TRAPE (X,Y,Z,NDIM)
C
C       DESCRIPTION OF PARAMETERS
C          X       - DOUBLE PRECISION INPUT VECTOR OF ARGUMENT VALUES.
C          Y       - DOUBLE PRECISION INPUT VECTOR OF FUNCTION VALUES.
C          Z       - THE RESULTING DP. VECTOR OF INTEGRAL VALUES. Z MAY BE
C                    IDENTICAL WITH X OR Y.
C          NDIM    - THE DIMENSION OF VECTORS X,Y,Z. NDIM MAX. 1000
C
C       REMARKS
C          NO ACTION IN CASE NDIM LESS THAN 1.
C
C       SUBROUTINES AND FUNCTION SUBPROGRAMS REQUIRED
C          NONE
C
C       METHOD
C          BEGINNING WITH Z(1)=0, EVALUATION OF VECTOR Z IS DONE BY
C          MEANS OF TRAPEZOIDAL RULE (SECOND ORDER FORMULA).
C          FOR REFERENCE, SEE
C          F.B.HILDEBRAND, INTRODUCTION TO NUMERICAL ANALYSIS,
C          MCGRAW-HILL, NEW YORK/TORONTO/LONDON, 1956, PP.75.
C
C     .....
C
      SUBROUTINE TRAPE(X,Y,ANS,NDIM)
C
C
      DOUBLE PRECISION X(1000),Y(1000),AZ(1000)
      DOUBLE PRECISION SUM1,SUM2,ANS
```

```
C
      SUM2=0.D+00
      IF(NDIM-1)4,3,1
C
C     INTEGRATION LOOP
    1 DO 2 I=2,NDIM
      SUM1=SUM2
      SUM2=SUM2+.5D+00*(X(I)-X(I-1))*(Y(I)+Y(I-1))
    2 AZ(I-1)=SUM1
    3 AZ(NDIM)=SUM2
      ANS=SUM2
    4 RETURN
      END
C*****************************************************************
C
      SUBROUTINE GMAAX(A1,A,W1,F,R,T,X,AFE,H1,S1)
      IMPLICIT REAL*8(A-H,K-Z)
C CALCULATION OF THE OPTIMUM NUCLEUS C CONTENT AND ACTIVITY OF C IN
C FERRITE NUCLEUS
C
C Estimate a value for X
C February 1991
       X=6.3998D-07*T-3.027D-04
       IF(X .LT. 0.1D-07)X=1.0D-08
       IF(X .GT. 0.32D-03)X=0.32D-03
C Estimation complete
C
      AJ1=1.0D+00-DEXP(-W1/(R*T))
1     D1=DSQRT(9.0D+00-6.0D+00*X*(2.0D+00*AJ1+3.0D+00)
     &+(9.0D+00+16.0D+00*AJ1)*X*X)
      B1=((D1-3.0D+00+5.0D+00*X)/(D1+3.0D+00-5.0D+00*X))
      B2=((3.0D+00-4.0D+00*X)/X)
      B3=(H1 - S1*T + 4.0D+00*W1)/(R*T)

      A1=DLOG(B1*B1*B1*B1*B2*B2*B2)+B3
C
```

```
      IF(X .GT. 1.0D-08)THEN
        A1FE=DLOG(1.0D+00-X)
      ELSE
        A1FE=X
      ENDIF
C
      TEST=F+R*T*(A1FE-AFE) - R*T*(A1-A)
C
C Newton iteration
C
      IF (DABS(TEST) .GT. 10.0) THEN
        DA1=(3.0D+00*X/(3.0D+00-4.0D+00*X))*(
     &  (4.0D+00*X-3.0D+00)/(X*X)-4.0D+00/X)
        DA2=(0.5D+00/D1)*(-12.0D+00*AJ1-18.0D+00+
     &  18.0D+00*X+32.0D+00*AJ1*X)
        DA2=4.0D+00*(((DA2+5.0D+00)/(D1-3.0D+00+5.0D+00*X))
     &  -((DA2-5.0D+00)/(D1+3.0D+00-5.0D+00*X)))
        DA1=DA1+DA2
        DA1FE=1.0D+00/(X-1.0D+00)
        ERROR=TEST/(R*T*(DA1FE-DA1))
        IF (ERROR .GT. X) ERROR = 0.3D+00*X
        X=DABS(X-ERROR)
        GOTO 1
      ENDIF
C End of iteration
      RETURN
      END
C*********************************************************************
C
C FUNCTION GIVING THE EQUILIBRIUM MOL.FRAC. CARBON IN ALPHA
C TEMP READ IN AS CENTIGRADE
C BASED ON MY PAPER ON FIRST ORDER QUASICHEMICAL THEROY,METSCI
      DOUBLE PRECISION FUNCTION XALPH(T)
      DOUBLE PRECISION T,CTEMP
      CTEMP=T/900.0D+00
      XALPH=0.1528D-02-0.8816D-02*CTEMP+0.2450D-01*CTEMP*CTEMP
```

```
     &-0.2417D-01*CTEMP*CTEMP*CTEMP+
     &0.6966D-02*CTEMP*CTEMP*CTEMP*CTEMP
      RETURN
      END
C
C*********************************************************************
      SUBROUTINE HFLOW(J,C1,C2,EFF)
      DOUBLE PRECISION C1,C2,EFF
      INTEGER J
      IF(J .EQ. 2) GOTO 2
      IF(J .EQ. 3) GOTO 3
      IF(J .EQ. 4) GOTO 4
      IF(J .EQ. 5) GOTO 5
      IF(J .EQ. 6) GOTO 6
      IF(J .EQ. 7) GOTO 7
      IF(J .EQ. 8) GOTO 8
      IF(J .EQ. 9) GOTO 9
      IF(J .EQ. 10) GOTO 10
      IF(J .EQ. 11) GOTO 11
      IF(J .EQ. 12) GOTO 12
      IF(J .EQ. 13) GOTO 13
      IF(J .EQ. 14) GOTO 14
      IF(J .EQ. 15) GOTO 15
      IF(J .EQ. 16) GOTO 16
C   Manual Metal Arc
      C1=1325.0
      C2=1.60
      EFF=0.775
      GOTO 22
C   Metal Cored Wire, CO2 shielding; SUSAN PARK
2     C1=4.452
      C2=2.411
      EFF=0.9
      GOTO 22
C   Metal Cored Wire, Fogon 20 shielding; SUSAN PARK
3     C1=28.535
```

```
      C2=2.064
      EFF=0.9
      GOTO 22
C  Tandem submerged arc
4     C1= 1.076
      C2= 2.6798
      EFF=0.9
      GOTO 22
C  Submerged Arc
5     C1=4359.0
      C2=1.51
      EFF=0.9
      GOTO 22
C  Vertical-Up MMA
6     C1=1125.0
      C2=1.7
      EFF=0.775
      GOTO 22
C  Bead on Plate FCAW Chakravati et al. Metal Const. 1985 p.178R
7     C1=206.1
      C2=2.0
      EFF=0.700
      GOTO 22
C  Bead on Plate Self-Sheilded Chakravati et al. Metal Const. 1985 p.178R
8     C1=173.4
      C2=2.0
      EFF=0.700
      GOTO 22
C  Bead on Plate SAW Chakravati et al. Metal Const. 1985 p.178R
9     C1=150.2
      C2=2.0
      EFF=0.950
      GOTO 22
C  Measured time-temperature Horizontal GMAW data EB, DTRC, NRL
C  Interpass temperature 150 C  Ed Metzbower
10    C1=24.013
```

```
      C2=2.2619
      EFF=0.755
      GOTO 22
C  Measured time-temperature Flat GMAW data EB, DTRC, NRL
C  Interpass temperature 150 C  Ed Metzbower
11    C1=23.172
      C2=2.2845
      EFF=0.755
      GOTO 22
C  Measured time-temperature Vertical GMAW data EB, DTRC, NRL
C  Interpass temperature 150 C Ed Metzbower
12    C1=8.3292
      C2=2.3884
      EFF=0.755
      GOTO 22
C  Measured time-temperature Vertical GMAW data EB, DTRC, NRL
C  Interpass temperature 93 C Ed Metzbower
C  At To=93 C1 values are 46.540, 41.806, and 36.104
C  At To=93 C2 values are 2.1996, 2.2217, and 2.1888 for
C  horizontal, flat, and vertical welds. There is only a small difference
C  in dT/dt for low To values.
13    C1=41.483
      C2=2.2030
      EFF=0.755
      GOTO 22

C  Computed time-temperature for laser weld 117000 W 5 mm/s EFF=0.50
C   Philips  data, modified laser.for program, centre of weldment
14    C1=498.42
      C2=2.0500
      EFF=0.50
      GOTO 22

C  Large heat input tandem submerged arc welding (130kJ/cm)
C  Data obtained by K. Ichikawa, Nippon Steel
15    C1= 46130.0
```

```
      C2= 1.10
      EFF=0.9
      GOTO 22

C  Large heat input tandem submerged arc welding (70kJ/cm)
C  Data obtained by K. Ichikawa, Nippon Steel
16    C1= 258600.0
      C2= 0.864
      EFF=0.9
      GOTO 22



22    RETURN
      END
C**********************************************************************
C     CULRAT CULRAT
      DOUBLE PRECISION FUNCTION CULRAT
     &(T,TINT,C1,C2,CURR,VOLT,EFF,SPEED)
C     FUNCTION TO GET COOLING RATE AT TEMPERATURE T
      IMPLICIT REAL*8 (A-H,O-Z)
      CULRAT=(T-TINT)**C2
      CULRAT=CULRAT*C1*SPEED/(CURR*VOLT*EFF)
      RETURN
      END
C
C**********************************************************************
      SUBROUTINE DEPLEC (C)
      IMPLICIT REAL*8(A-H,L-Z)
      DOUBLE PRECISION C(8)
C PROGRAM TO CALCULATE COMPOSITIONS FOR SOLUTE DEPLETED REGIONS
C M=MELTING POINT IN KELVIN, LIQUIDUS TEMPERATURE
C CARBON PARTITIONING IGNORED
C THERMODYNAMIC DATA FROM KIRKALDY AND BAGANIS
C SOLIDIFICATION AS DELTA FERRITE
```

```
C NOTICE: Originaly, the name of this subroutine is "HETRO"
C         which is made by Dr. H.K.D.H.Bhadeshia.
C
C     Modified by K. ICHIKAWA on 6 Dec. 1994.
C     Sinple empirical calculations of Liquidus Temperature.
C
C     LIQUID(Centigrade) is a liquidus temperature and is calculated
C     by very simple empilical approximation.
C
      CARBON=C(1)
      LIQUID=-81.13*CARBON+1538
C
      M=LIQUID+273
C       WRITE(*,2) M
      A=4.187D+00
      R=8.3143D+00
      PSI=DEXP((3.9*M-8200.0)*A/(R*M))
      PMN=DEXP((3100.0-2.308*M)*A/(R*M))
      PNI=DEXP((-2120.0-0.38*M)*A/(R*M))
      PCR=DEXP((2.19*M-4600.0)*A/(R*M))
      PMO=DEXP((2.29*M-6600.0)*A/(R*M))
      PV=DEXP((-5100.0+2.3*M)*A/(R*M))
      C(1)=C(1)
      C(2)=C(2)*PSI
      C(3)=C(3)*PMN
      C(4)=C(4)*PNI
      C(5)=C(5)*PMO
      C(6)=C(6)*PCR
      C(7)=C(7)*PV
      C(8)=1.0D+00-C(1)-C(2)-C(3)-C(4)-C(5)-C(6)-C(7)
2     FORMAT('    Data for Solute-Depleted Regions'/
     & ' Assumed Melting Point of Delta Ferrite=',F8.0,' K')
      RETURN
      END
C
C*********************************************************************
```

```
      SUBROUTINE SEGREC (C)
      IMPLICIT REAL*8(A-H,M-Z)
      DOUBLE PRECISION C(8)
C PROGRAM TO CALCULATE COMPOSITIONS FOR SEGREGATED REGIONS
C M=MELTING POINT IN KELVIN, LIQUIDUS TEMPERATURE
C CARBON PARTITIONING IGNORED
C THERMODYNAMIC DATA FROM KIRKALDY AND BAGANIS
C SOLIDIFICATION AS DELTA FERRITE

      CARBON=C(1)
      IF (CARBON .LE. 0.09) THEN
      SOLID=-477.78*CARBON+1538
      ELSE
      SOLID=1495
      ENDIF
      M=SOLID+273
C       WRITE(*,2) M
      A=4.187D+00
      R=8.3143D+00
      SPSI=DEXP((3.9*M-8200.0)*A/(R*M))
      SPMN=DEXP((3100.0-2.308*M)*A/(R*M))
      SPNI=DEXP((-2120.0-0.38*M)*A/(R*M))
      SPCR=DEXP((2.19*M-4600.0)*A/(R*M))
      SPMO=DEXP((2.29*M-6600.0)*A/(R*M))
      SPV=DEXP((-5100.0+2.3*M)*A/(R*M))
      C(1)=C(1)
      C(2)=C(2)/SPSI
      C(3)=C(3)/SPMN
      C(4)=C(4)/SPNI
      C(5)=C(5)/SPMO
      C(6)=C(6)/SPCR
      C(7)=C(7)/SPV
      C(8)=1.0D+00-C(1)-C(2)-C(3)-C(4)-C(5)-C(6)-C(7)
2     FORMAT('    Data for Solute-Segregated Regions'/
     & ' Assumed Solidus Temperature =',F8.0,' K')
      RETURN
```

```
      END
C*********************************************************************
C SUBROUTINE for building a equation "VF=a*T2+b*T+c"
C BY K.Ichikawa, 12 December 1994
C
      SUBROUTINE CURVE(J2,CTEMPS,VFS,A,I)
      IMPLICIT REAL*8(A-H,O-Z), INTEGER(I-N)
      DOUBLE PRECISION CTEMPS(100,100),VFS(100,100)
     &,A(100,3)
      NZ=0
C Count the number of zero in VFS(I)
      DO 1 M=1,J2
        IF (VFS(I,M) .LE. 0.0) THEN
        NZ=NZ+1
      ELSE
C Compute the regression of degree two with neglect the excessive
C zero in VF(I)
        CALL POLY(CTEMPS,VFS,J2-NZ+1,NZ,J2,A,I)
      ENDIF
1     CONTINUE
C       WRITE (*,10) A(I,1),A(I,2),A(I,3)
10    FORMAT (/'      A(1)='D20.6,
     &'      A(2)=',D20.6,'      A(3)=',D20.6)
      RETURN
      END
C*********************************************************************
C This SUBROUTINE computes the least squares regression of
C degree two. Input: NPNT (max 400) (x,y) pairs. Output: coefficients
C A(1) to A(3) of quadaratic polynomial y=A(1)+A(2)x+A(3)x**2.
      SUBROUTINE POLY(X,Y,NPNT,JZ,JE,A,I)
      IMPLICIT REAL*8(A-H,O-Z), INTEGER(I-N)
      DOUBLE PRECISION X(100,100),Y(100,100),A(100,3),COEF(3,3)
C
C     INITIALIZE VARIABLES
C
```

```
      SUMX    =  0.0D+00
      SUMY    =  0.0D+00
      SMSQX   =  0.0D+00
      SUMXY   =  0.0D+00
      SUMX3   =  0.0D+00
      SUMX4   =  0.0D+00
      SMX2Y   =  0.0D+00
C
C     INITIAL SUMMATIONS
C
      DO 20 M=JZ,JE
       SUMX    =  SUMX+X(I,M)
       SUMY    =  SUMY+Y(I,M)
       SUMXY   =  SUMXY+X(I,M)*Y(I,M)
       SMSQX   =  SMSQX+X(I,M)*X(I,M)
       SUMX3   =  SUMX3+X(I,M)*X(I,M)*X(I,M)
       SUMX4   =  SUMX4+X(I,M)*X(I,M)*X(I,M)*X(I,M)
       SMX2Y   =  SMX2Y+Y(I,M)*X(I,M)*X(I,M)
20    CONTINUE
C
C     SET-UP FOR FURTHER USE
C
      XPNT  =  NPNT
      RECIP   =  1.0D+00/XPNT
      SAVEA   =  SMSQX-((SUMX*SUMX)/XPNT)
      SAVEC   =  SUMXY-((SUMX*SUMY)/XPNT)
C
C     MEASURES OF CENTRAL TENDENCY AND DISPERSION
C
      XMEAN   =  SUMX/XPNT
      YMEAN   =  SUMY/XPNT
C
C
C     INITIALIZE VARIABLES
C
      DO 30 M=1,3
```

```
      DO 30 J=1,3
        COEF(M,J)=0.0D+00
30    CONTINUE
C
C
C     LINEAR REGRESSION
C
      COEF(2,1)=SAVEC/SAVEA
C
C     QUADRATIC REGRESSION
C
      TEMP      =  (SUMX*SMSQX)/XPNT
      TEMP1     =  SUMX3-TEMP
      COEF(3,2)=  (((SMX2Y-((SUMY*SMSQX)/XPNT))/TEMP1)-
     &COEF(2,1))/((
     &(SUMX4-((SMSQX*SMSQX)/XPNT))/TEMP1)-(TEMP1/SAVEA))
      COEF(2,2)=  (SAVEC-COEF(3,2)*(SUMX3-TEMP))/SAVEA
C
C
C     ESTIMATION OF REGRESSION COEFFICIENTS
C
      COEF(1,2)=  YMEAN-(COEF(2,2)*XMEAN)-(COEF(3,2)*(SMSQX*RECIP))
C
      A(I,1)=COEF(1,2)
      A(I,2)=COEF(2,2)
      A(I,3)=COEF(3,2)
      return
      end
C*************************************************************************
C This is a SUBROUTINE which calculates the sum of VF in segregated
C region and in depleted region.
C by K.Ichikawa on 14 Dec. 1994

      SUBROUTINE SUM(HIGHTD,LOWT,AB2,A,AD,HIGHT)
      IMPLICIT REAL*8(A-H,K-Z), INTEGER(I,J)
      DOUBLE PRECISION CTEMPT(2000),TVF(2000),A(3),AD(3)
```

```
      JT=((HIGHTD-LOWT)/AB2)+1
C     WRITE (*,30)
C      WRITE (*,20)
C      WRITE (*,40)
C      WRITE (*,50)

      DO 1 I=1,JT
         CTEMPT(I)=HIGHTD-AB2*(I-1)
C
         IF (CTEMPT(I) .GT. HIGHT) THEN
            TVF(I)=TVF1(AD,CTEMPT(I),HIGHTD)
C             WRITE(6,10) CTEMPT(I),TVF(I)
         ELSE
            TVF(I)=TVF3(A,AD,CTEMPT(I),HIGHT,HIGHTD)
C             WRITE(6,10) CTEMPT(I),TVF(I)
         ENDIF


10    FORMAT(F5.0,F7.2)
20    FORMAT('-----------------------------------',
     &'----------',
     &'----------')
30    FORMAT(4H     )
40    FORMAT(//'Total VF of Segregated and Depleted Regions'/)
50    FORMAT(//' CTEMP    VF'/)
1     CONTINUE
      RETURN
      END


C**********************************************************************
C This is a FUNCTION which calculates the regression of degree two.
C Caluculation at the Depleted Zone
C 14 Dec. 1994 by K.Ichikawa
```

```
      DOUBLE PRECISION FUNCTION TVF1(AD,X,HIGHTD)
      IMPLICIT REAL*8(T,X,H)
      DOUBLE PRECISION AD(3)

      IF (X .GT. HIGHTD) THEN
         TVF1=0.0
      ELSEIF (X .LE. -AD(2)/(2*AD(3))) THEN

         TVF1=(-AD(2)*AD(2)+4*AD(3)*AD(1))/(4*AD(3))



      ELSE
         TVF1=AD(1)+AD(2)*X+AD(3)*X*X
      ENDIF
      IF (TVF1 .LT.  0.0) THEN
         TVF1=0.0
      ENDIF
      RETURN
      END
C**********************************************************************
C This is a FUNCTION which calculates the regression of degree two.
C Caluculation at the Segregated Zone.
C 14 Dec. 1994 by K.Ichikawa


      DOUBLE PRECISION FUNCTION TVF2(A,X,HIGHT)
      IMPLICIT REAL*8(T,X,H)
      DOUBLE PRECISION A(3)

      IF (X .GT. HIGHT) THEN
         TVF2=0.0
      ELSEIF (X .LE. -A(2)/(2*A(3))) THEN

         TVF2=(-A(2)*A(2)+4*A(3)*A(1))/(4*A(3))
```

```
      ELSE
         TVF2=A(1)+A(2)*X+A(3)*X*X
      ENDIF
      IF (TVF2 .LT. 0.0) THEN
         TVF2=0.0
      ENDIF
      RETURN
      END
C**********************************************************************
C This is a FUNCTION which calculates the regression of degree two.
C Caluculation at the temperatures of Temp.¡=(Transformation Starting
C Temp. of Segregated Zone)
C 14 Dec. 1994 by K.Ichikawa

      DOUBLE PRECISION FUNCTION TVF3(A,AD,X,HIGHT,HIGHTD)
      IMPLICIT REAL*8(T,X,H)
      DOUBLE PRECISION A(3),AD(3)

      TVF3=TVF1(AD,X,HIGHTD)+TVF2(A,X,HIGHT)
      RETURN
      END

C**********************************************************************
      SUBROUTINE INITCC(C,CARBON,SI,MN,NI,MO,CR,V)

C This SUROUTINE stores the average chemical compositions.
C The function of this program is INITiarizing the Chemical
C Compositions to the average compositions.
C K. Ichikawa on 5 January, 1995
      IMPLICIT REAL*8(A-H,K-Z), INTEGER(I,J)
      DOUBLE PRECISION C(8)

        C(1)=CARBON
        C(2)=SI
        C(3)=MN
        C(4)=NI
```

```
      C(5)=MO
      C(6)=CR
      C(7)=V

      RETURN
      END
C*********************************************************************
      SUBROUTINE SCHEIL(CARBON,SI,MN,NI,MO,CR,V,C,I,N)
C
C     Sheil equation is applied in this subroutine by K. Ichikawa.
C     on 12 Jan. 1995.
C     However, g in original Sheil equation is substituted
C     to i/n-1/(2*n).
C     n is a number of division.
C     i means 'i'th  from the g=0.
C
C
      IMPLICIT REAL*8(A-H,K-M,O-Z), INTEGER(J,I,N)
      DOUBLE PRECISION C(7)
      CALL EDC(CARBON,SI,MN,NI,MO,CR,V,KC,KSI,KMN,KNI,KMO,KCR,KV)
      CSC =KC *C(1)*((1.00-((1.0*I/N)-(1.00/(2.00*N))))**(KC -1.00))
      CSSI=KSI*C(2)*((1.00-((1.0*I/N)-(1.00/(2.00*N))))**(KSI-1.00))
      CSMN=KMN*C(3)*((1.00-((1.0*I/N)-(1.00/(2.00*N))))**(KMN-1.00))
      CSNI=KNI*C(4)*((1.00-((1.0*I/N)-(1.00/(2.00*N))))**(KNI-1.00))
      CSMO=KMO*C(5)*((1.00-((1.0*I/N)-(1.00/(2.00*N))))**(KMO-1.00))
      CSCR=KCR*C(6)*((1.00-((1.0*I/N)-(1.00/(2.00*N))))**(KCR-1.00))
      CSV =KV *C(7)*((1.00-((1.0*I/N)-(1.00/(2.00*N))))**(KV -1.00))

      C(1)=C(1)
      C(2)=CSSI
      C(3)=CSMN
      C(4)=CSNI
      C(5)=CSMO
      C(6)=CSCR
      C(7)=CSV
```

```
      RETURN
      END
C*********************************************************************
      SUBROUTINE EDC(CARBON,SI,MN,NI,MO,CR,V,
     &KC,KSI,KMN,KNI,KMO,KCR,KV)
      IMPLICIT REAL*8(A-H,K-Z)

C PROGRAM TO CALCULATE Equivalent Distribution Coefficient
C M=MELTING POINT IN KELVIN, LIQUIDUS TEMPERATURE
C CARBON PARTITIONING IGNORED
C THERMODYNAMIC DATA FROM KIRKALDY AND BAGANIS
C SOLIDIFICATION AS DELTA FERRITE
C NOTICE: Originaly, the name of this subroutine is "HETRO"
C           which is made by Dr. H.K.D.H.Bhadeshia.
C
C       Modified by K. ICHIKAWA on 12 Jan. 1995.
C       Sinple empirical calculations of Liquidus Temperature.
C
C       LIQUID(Centigrade) is a liquidus temperature and is calculated
C       by very simple empilical approximation (L. SMRHA: Solidification and
C       crystallization of steel ingots, SNTL, Prague, 1983 (in Czech)).
C


      LIQUID=1537.0-
     &(88.0*CARBON+8.0*SI+5.0*MN+4.0*NI+2.0*MO+1.5*CR+2.0*V)



C
      M=LIQUID+273.0
C       WRITE(*,2) M
      A=4.187D+00
      R=8.3143D+00
      PC =1.0
      PSI=DEXP((3.9*M-8200.0)*A/(R*M))
      PMN=DEXP((3100.0-2.308*M)*A/(R*M))
```

```
      PNI=DEXP((-2120.0-0.38*M)*A/(R*M))
      PCR=DEXP((2.19*M-4600.0)*A/(R*M))
      PMO=DEXP((2.29*M-6600.0)*A/(R*M))
      PV =DEXP((-5100.0+2.3*M)*A/(R*M))

      KC =PC
      KSI=PSI
      KMN=PMN
      KNI=PNI
      KMO=PMO
      KCR=PCR
      KV =PV

2     FORMAT('    '/
     & ' Assumed Melting Point of Delta Ferrite=',F8.0,' K')
      RETURN
      END
C*************************************************************************
      SUBROUTINE DETN(C,SV,DUMM,SITE,
     &LOWT,J,CURR,VOLT,SPEED,TINT,CTEMP,
     &VFAW,VFA,VFW,VFBAF,VFRGM,
     &J2,HIGHT,J10,CTEMPW,IIMP,ISTOP)
C This SUBROUTINE calculates the value of "n" which is used to apply the
C Scheile's equation. By K. Ichikawa on 20 Jan. 1995

      IMPLICIT REAL*8(A-H,K-Z), INTEGER(I,J)
      DOUBLE PRECISION CTEMP(2000),C(8),
     &                 VFAW(200),VFA(200),VFW(200),VFBAF(200),VFRGM(200)

C       WRITE(*,446)
C       WRITE(*,500)

C Calculate the Chemical compositions in the most depleted region.
      CARBON=C(1)
      CALL EDC(CARBON,SI,MN,NI,MO,CR,V,
     &KC,KSI,KMN,KNI,KMO,KCR,KV)
```

```
      CC0 =KC* C(1)
      CSI0=KSI*C(2)
      CMN0=KMN*C(3)
      CNI0=KNI*C(4)
      CCR0=KCR*C(5)
      CMO0=KMO*C(6)
      CV0 =KV* C(7)

      C(1)=CC0
      C(2)=CSI0
      C(3)=CMN0
      C(4)=CNI0
      C(5)=CCR0
      C(6)=CMO0
      C(7)=CV0
C Calculate the VF in the most depleted region.
      CALL MAINCONP(C,SV, DUMM,SITE,
     &LOWT,J,CURR,VOLT,SPEED,TINT,CTEMP,
     &VFAW,VFA,VFW,VFBAF,VFRGM,
     &J2,HIGHT,ICI
     &,CARBON,SI,MN,NI,MO,CR,V,VW,CTEMPW,IIMP,ISTOP)
C Determin the "n". J10, in the following procedure, means the "n".

C      J10=1/VF(J2)
      J10=100
C       WRITE(*,560) J10
C       WRITE(*,446)

446   FORMAT('----------------------------------------',
     &'-------------------------',
     &'----------------------------------')


560   FORMAT('    '/
     & ' Determination of n.              n =',I5/)
```

```
500   FORMAT(//20X,'Calculations for determination of the value of "n".'/
     &20X,'(Calculation in the most depleted region.)')

      RETURN
      END

C*********************************************************************
C*********************************************************************
      SUBROUTINE
      SUMF(CTEMPE,VFEAW,VFEA,VFEW,VFEBAF,VFERGM,J10,ISUM)
      IMPLICIT REAL*8(A-H,K-M,O-Z), INTEGER(I,J,N)
      DOUBLE PRECISION CTEMPE(200),
     &VFEAW(200),VFAWI(200),
     &VFEA(200), VFAI(200),
     &VFEW(200),VFWI(200),
     &VFEBAF(200),VFBAFI(200),
     &VFERGM(200),VFRGMI(200)
C
C
C This SUBROUTINE can calculate the sum of VF which are divided by n.
C by K. Ichikawa on 12 Jan., 1995.
C
C Sum is made by numerically, so that any interpo. method is not
C adapted here.
C
C JN(I) is a number of calculation for the 'T'th divided segment.
C
C VFAWI(I), VFAI(I), VFWI(I), VFBAFI(I) and VFRGMI(I) will be
C used at the DO 110 loop later on.

      VFAWI(1) =VFEAW(1)
      VFAI(1)  =VFEA(1)
      VFWI(1)  =VFEW(1)
      VFBAFI(1)=VFEBAF(1)
      VFRGMI(1)=VFERGM(1)
C
```

```
      DO 10 I=2,J10
C SUM for alpha & alpha'W.
      VFAWI(I)=VFEAW(I)
      VFEAW(I)=VFEAW(I-1)+VFEAW(I)
C SUM for alpha only.
      VFAI(I)=VFEA(I)
      VFEA(I)=VFEA(I-1)+VFEA(I)
C SUM for alpha'W only.
      VFWI(I)=VFEW(I)
      VFEW(I)=VFEW(I-1)+VFEW(I)
C SUM for bainite & AF.
      VFBAFI(I)=VFEBAF(I)
      VFEBAF(I)=VFEBAF(I-1)+VFEBAF(I)
C SUM for retained austenite & martensite.
      VFRGMI(I)=VFERGM(I)
      VFERGM(I)=VFERGM(I-1)+VFERGM(I)
C
10    CONTINUE
      FVFAW =VFEAW(J10) /J10
      FVFA  =VFEA(J10)  /J10
      FVFW  =VFEW(J10)  /J10
      FVFBAF=VFEBAF(J10)/J10
      FVFRGM=VFERGM(J10)/J10
C
C Print the final results.
      IF (ISUM .EQ. 1) GOTO 70
      IF (ISUM .EQ. 2) GOTO 80
C %%%%%%%%%%%%%%%%%%%%%%%%%%%%%%%%%%%%%%%%
C70   WRITE(6,*)'  '
70    CONTINUE
C     WRITE(6,*)'  '
C     WRITE(6,*)'**************************************************'
C     WRITE(6,*)'*          Final Result of Calculations          *'
C     WRITE(6,*)'**************************************************'
C     WRITE(6,91)
C     WRITE(6,*)'VF'alpha+W=',FVFAW
```

```
C       WRITE(6,*)'VF alpha=',FVFA
C       WRITE(6,*)'VF W=',FVFW
C       WRITE(6,*)'VF bainite+AF=',FVFBAF
C       WRITE(6,*)'VF Retained gamma+matensite=',FVFRGM

        OPEN(20,FILE='resultbeta6')
        WRITE(20,*)FVFAW,' ',FVFA,' ',FVFW,' ',FVFBAF,' ',FVFRGM

C       WRITE(6,*)'  '
C       WRITE(6,*)'**************************Details in each solidification
C      & segment**************************'
C       WRITE(6,*)'Segment VF alpha+W VF alpha   VF W      VF B+AF    VF RA+
C      &M'

        DO 110 I=1,J10
C         WRITE(6,90)I,VFAWI(I),VFAI(I),VFWI(I),VFBAFI(I),VFRGMI(I)
110     CONTINUE

        GOTO 100
80       CONTINUE
C80      WRITE(6,92)
C       WRITE(6,90) FVF



93      FORMAT(F7.5,' ',F7.5,' ',F7.5,' ',F7.5)
90      FORMAT('  ',I3,'      ',F7.5,'    ',F7.5,'    ',F7.5,'    ',F7.5,
     &'    ',F7.5)

C %%%%%%%%%%%%%%%%%%%%%%%%%%%%%%%%%%%%%%%%%%%%%%%%%%%%%%%%%%%%%%%%%%%%%%%
91      FORMAT(//' Total volume fraction of each microstructual component
     & in the weld'/)
92      FORMAT(//' Total Volume Fraction of Widmanstatten Ferrite'/)
100     CONTINUE

        RETURN
        END
```

```
C***********************************************************************

C*************************************************************
C H. K. D. H. Bhadeshia, Diffusivity of carbon in austenite
C Department of Materials Science and Metallurgy
C Pembroke Street, Cambridge CB2 3QZ, U. K.
C 31 March 1987
C
C Program for the calculation of the diffusivity of carbon in austenite
C as a function of carbon concentration and temperature. Also accounts for
C the infulence of C, Mn, Si, Ni, Mo, Cr and V on the activity of carbon
C in austenite, and therefore on the diffusivity of carbon.
C
C WDIFF is the carbon--carbon interaction energy in austenite, not
C allowing for the presence of Mo, Cr or V
C
C diffusion coefficient in cm**/s
C
      SUBROUTINE DIFFUS(DIF,X,T,WDIFF)
      IMPLICIT REAL*8(A-H,O-Y), INTEGER(I-N,Z)
         W=WDIFF
         HH=6.6262D-34
         BOLTZ=1.38062D-23
         Z=12
         A5=1.0D+00
         R=8.31432D+00
C     D=DIFFUSIVITY OF CARBON IN AUSTENITE
C     Z=COORDINATION OF INTERSTIAL SITE
C     PSI=COMPOSITION DEPENDENCE OF DIFFUSION COEFFICIENT
C     THETA=NO. C ATOMS/ NO. FE ATOMS
C     ACTIV=ACTIVITY OF CARBON IN AUSTENITE
C     R=GAS CONSTANT
C     X=MOLE FRACTION OF CARBON
C     T=ABSOLUTE TEMPERATURE
C     SIGMA=SITE EXCLUSION PROBABLITY
C     W=CARBON CARBON INTERACTION ENERGY IN AUSTENITE
```

```
C
      DASH=(BOLTZ*T/HH)*DEXP(-(21230.0D+00/T))*DEXP(-31.84D+00)
      THETA=X/(A5-X)
      ACTIV=CG(X,T,W,R)
      ACTIV=DEXP(ACTIV)
      DACTIV=DCG(X,T,W,R)
      DACTIV=DACTIV*ACTIV
      DACTIV=DACTIV*A5/((A5+THETA)**2)
      SIGMA=A5-DEXP((-(W))/(R*T))
      PSI=ACTIV*(A5+Z*((A5+THETA)/(A5-(A5+Z/2)*THETA+(Z/2)*(A5+Z/2)*
     &(A5-SIGMA)*THETA*THETA)))+(A5+THETA)*DACTIV
      DIF=DASH*PSI
      RETURN
      END
C*****************************************************************
C
      SUBROUTINE PROGC(VMAX,T,XMAX,WDIFF,W,XBAR)
C Modified, 30-8-83, accurate XAPLPHA
C Modified, 30-8-83, accurate CAPILLARITY CONSTANT calculation
      IMPLICIT REAL*8 (A-H,K-Y), INTEGER(I,J,Z)
      DOUBLE PRECISION DIFF(1000),CARB(1000)
C CAPCON capillarity constant (normally written as capital gamma)
C XMAXR equlibrium concentration in austenite at plate tip of finite radius
C
      R=8.31432D+00
      RADIUS=0.0
      VMAX=0.0
      M1=0.00
C       WRITE(*,1009)
1009  FORMAT('**************************'/5H      )
      CTEMP=T
      T=T+273.00D+00
      II2=0
      XALPHA=XALPH(CTEMP)
C       WRITE(*,1005)T,CTEMP,XBAR,XMAX,XALPHA
      CALL RRAD(RADIUS,XMAX,XALPHA,XBAR,T,R,XMAXR,W)
```

```
1005  FORMAT(' ABSOLUTE TEMPERATURE, DEGREES KELVIN =',F8.1/
     &'              TEMPERATURE IN DEGREES CENTIGRADE =',F8.1/
     &' MOL FRAC CARBON IN ALLOY = ',F8.4/
     &' EQUILIBRIUM MOL FRAC CARBON IN AUSTENITE =',F8.4/
     &' EQUILIBRIUM MOL FRAC OF C IN FERRITE=',D12.4)
      DO 999 II=1,1000
      CARB(1)=XBAR
      IF (II .GT. 1)GOTO 1000
      GOTO 1001
1000  CARB(II)=CARB(II-1)+0.0001D+00
      IF (CARB(II) .GT. XMAXR) GOTO 1002
1001  X=CARB(II)
      II2=II2+1
      CALL DIFFUS(DIFF(II),X,T,WDIFF)
999   CONTINUE
1002  II3=0
C     CALL D01GAF(CARB,DIFF,II2,ANS,ERROR,II3)
      CALL TRAPE(CARB,DIFF,ANS,II2)
      ANS=ANS/(XMAXR-XBAR)
C       WRITE(*,1004)ANS,ERROR
1004  FORMAT(' INTEGRAL, XMAXR-XBAR = ',D12.4, '  CM**2/SEC   ',
     &8HERROR = , D12.4)
      CALL VEL4(VMAX,ANS,RADIUS,XMAX,XBAR,XALPHA)

C     Convert T to in degree C (by K. Ichikawa on 16 Feb 1996)
      T=T-273.00D-00
C
      RETURN
      END
C
C*********************************************************************

C H. K. D. H. Bhadeshia, November 1993
C Diffusion-controlled growth of parabolic cylinders, Trivedi analysis
C
      SUBROUTINE VEL4(VMAX,ANS,RADIUS,XMAX,XBAR,XALPHA)
```

```
      IMPLICIT REAL*8(A-H,K-Z), INTEGER(I,J)
C       WRITE(*,4)
4     FORMAT(/' DIFFUSION CONTROLLED GROWTH, TRIVEDI ANALYSIS')
C
C Numerical method constants.
C If the solution fails to converge, then DD should be changed
C to some smaller value. (April 1994)
      I2=1000
      DD=0.002
C
C Modification, 6 November 1993 to allow for the case when XALPHA ¿ XMAXC
        IF(XBAR .LE. XALPHA) THEN
          OMEG=0.99D+00
        ELSE
          OMEG=(XMAX-XBAR)/(XMAX-XALPHA)
        ENDIF
C
      P=(1.0D+00/8.0D+00)*(OMEG/(1.0D+00-OMEG))
      VMAX=(ANS*1.0D-04)*P/RADIUS
      VDUM=DD*VMAX
      VMAX=0.5*VMAX
      ANS=ANS*1.0D-04
C       WRITE(*,44)
44    FORMAT('      OMEGA       DUMMY       VMAX(M/S)       PECLET',
     &'       RAD(M)')
C
C Warning - the following polynomial has been derived for the
C OMEG range 0.4 to 1 only
C
      RAD=0.2026D+01-0.1917D+01*OMEG-0.8953D+00*OMEG*OMEG
     &     +0.3670D+01*OMEG*OMEG*OMEG
     &      -0.2519D+01*OMEG*OMEG*OMEG*OMEG
      RAD=10.0D+00**RAD
      RAD=RADIUS*RAD
C
      DO 1 I1=1,I2
```

```
      PECLET=VMAX*RAD/(2.0D+00*ANS)
      S2=-1.073019925D+00*(DLOG10(PECLET))-0.273767575D+00
      S2=10.0D+00**S2
      PI=3.14159D+00
      DUMMY=(DSQRT(PI*PECLET))*(DEXP(PECLET))*(DAERFC(DSQRT(P
      ECLET )))
     &        *(1.0D+00+(RADIUS/RAD)*OMEG*S2)
      DDD=DABS(100.0D+00*(DUMMY-OMEG))
        IF (DDD .GT. 0.05D+00) GOTO 55
C
C     Following WRITE Statement was deleted in oreder to avoid the too
C     much display of the OMEGA and so on. That WRITE Statement was moved
C     just before RETURN Statement so that only the final value can be
C     printed (by K. Ichikawa on 4 Dec. 1995).

C     WRITE(*,2)OMEG,DUMMY,VMAX,PECLET,RAD
2     FORMAT(7D12.4)
        IF (DDD .LT. 0.01D+00) GOTO 56
55    VMAX=VMAX+VDUM
1    CONTINUE


C56     WRITE(*,2)OMEG,DUMMY,VMAX,PECLET,RAD
56      CONTINUE
            RETURN

            END
C
C**********************************************************************
C
      SUBROUTINE RRAD(RADIUS,XMAX,XALPHA,XBAR,T,R,XMAXR,W)
      DOUBLE PRECISION RADIUS,XMAX,XBAR,T,R,SIG,MOLVOL,XMAXR
     &,XALPHA,RAD,OMEG,CAPCON,EPSI,W,DCG

      SIG=0.2
C SIG=INTERFACIAL ENERGY, JOULES PER METRE SQUARED
```

```
      MOLVOL=7.0894317D-06*(1.0D+00+3.549D-05*(T-298.0D+00))
C   MOLVOL = MOLAR VOLUME OF FERRITE
C RADIUS IS THE CRITICAL RADIUS FOR ZERO GROWTH
C RAD IS THE RATIO OF THE ACTUAL RADIUS TO THE CRITICAL RADIUS
C
C
      EPSI=XMAX*DCG(XMAX,T,W,R)
      CAPCON=(SIG*MOLVOL/(R*T))*((1.0D+00-XMAX)/(XALPHA-XMAX))
     &/EPSI
      RADIUS=CAPCON*XMAX/(XBAR-XMAX)
      OMEG=(XMAX-XBAR)/(XMAX-XALPHA)
      RAD=0.2026D+01-0.1917D+01*OMEG-0.8953D+00*OMEG*OMEG
     &+0.3670D+01*OMEG*OMEG*OMEG
     &-0.2519D+01*OMEG*OMEG*OMEG*OMEG
      RAD=10.00D+00**RAD
      RAD=RADIUS*RAD
      XMAXR=XMAX*(1.0D+00+(CAPCON/RAD))
C       WRITE(*,1)SIG,MOLVOL,RADIUS,XMAXR,CAPCON,EPSI
1     FORMAT(' INTERFACIAL ENERGY=',F8.4,' JOULES/METERS SQUARED'/
     &' MOLAR VOLUME OF FERRITE(METERS CUBED PER MOL)=',D15.6/
     &' GIBBS THOMPSON CRITICAL RADIUS(METERS)=',D15.6/
     &' EQUILIBRIUM CONC AT PLATE TIP, MOL FRAC, XMAXR=',D15.6/
     &' CAPILLARITY CONSTANT CAPCON,=',D15.6/
     &' NON-IDEALITY PARAMETER EPSI=',D15.6)
      RETURN
      END
C
C*********************************************************************
      DOUBLE PRECISION FUNCTION DAERFC(A)
      DOUBLE PRECISION A,DAERF
      DAERFC=1.0D+00-DAERF(A)
      RETURN
      END
C*********************************************************************
C   Error function
      DOUBLE PRECISION FUNCTION DAERF(Y)
```

```
      IMPLICIT REAL*8(A-H,O-Z)
      INTEGER              ISW,I
      DOUBLE PRECISION     P(5),Q(3),P1(8),Q1(7),P2(5),Q2(4)
C                                  COEFFICIENTS FOR 0.0 .LE. Y .LT.
C                                  .477
      DATA                  P(1)/-.44422647396874/,
     1                     P(2)/10.731707253648/,
     2                     P(3)/15.915606197771/,
     3                     P(4)/374.81624081284/,
     4                     P(5)/2.5612422994823D-02/
      DATA                  Q(1)/17.903143558843/,
     1                     Q(2)/124.82892031581/,
     2                     Q(3)/332.17224470532/
C                                  COEFFICIENTS FOR .477 .LE. Y
C                                  .LE. 4.0
      DATA                  P1(1)/7.2117582508831/,
     1                     P1(2)/43.162227222057/,
     2                     P1(3)/152.98928504694/,
     3                     P1(4)/339.32081673434/,
     4                     P1(5)/451.91895371187/,
     5                     P1(6)/300.45926102016/,
     6                     P1(7)/-1.3686485738272D-07/,
     7                     P1(8)/.56419551747897/
      DATA                  Q1(1)/77.000152935229/,
     1                     Q1(2)/277.58544474399/,
     2                     Q1(3)/638.98026446563/,
     3                     Q1(4)/931.35409485061/,
     4                     Q1(5)/790.95092532790/,
     5                     Q1(6)/300.45926095698/,
     6                     Q1(7)/12.782727319629/
C                                  COEFFICIENTS FOR 4.0 .LT. Y
      DATA                  P2(1)/-.22695659353969/,
     1                     P2(2)/-4.9473091062325D-02/,
     2                     P2(3)/-2.9961070770354D-03/,
     3                     P2(4)/-2.2319245973418D-02/,
     4                     P2(5)/-2.7866130860965D-01/
```

```
      DATA                Q2(1)/1.0516751070679/,
     1                    Q2(2)/.19130892610783/,
     2                    Q2(3)/1.0620923052847D-02/,
     3                    Q2(4)/1.9873320181714/
C                                 CONSTANTS
      DATA                XMIN/1.0D-8/,XLARGE/5.6875D0/
      DATA                SSQPI/.56418958354776/
C                                 FIRST EXECUTABLE STATEMENT
      X = Y
      ISW = 1
      IF (X.GE.0.0D0) GO TO 5
      ISW = -1
      X = -X
5       IF (X.LT..477D0) GO TO 10
      IF (X.LE.4.0D0) GO TO 25
      IF (X.LT.XLARGE) GO TO 35
      RES = 1.D0
      GO TO 50
C                                 ABS(Y) .LT. .477, EVALUATE
C                                 APPROXIMATION FOR ERF
10      IF (X.LT.XMIN) GO TO 20
        XSQ = X*X
        XNUM = P(5)
        DO 15 I=1,4
        XNUM = XNUM*XSQ+P(I)
15      CONTINUE
        XDEN = ((Q(1)+XSQ)*XSQ+Q(2))*XSQ+Q(3)
        RES = X*XNUM/XDEN
        GO TO 50
20      RES = X*P(4)/Q(3)
        GO TO 50
C                                 .477 .LE. ABS(Y) .LE. 4.0
C                                 EVALUATE APPROXIMATION FOR ERF
25      XSQ = X*X
      XNUM = P1(7)*X+P1(8)
      XDEN = X+Q1(7)
```

```
      DO 30 I=1,6
       XNUM = XNUM*X+P1(I)
       XDEN = XDEN*X+Q1(I)
30    CONTINUE
      RES = XNUM/XDEN
      GO TO 45
C                                  4.0 .LT. ABS(Y), EVALUATE
C                                  APPROXIMATION FOR ERF
35    XSQ = X*X
      XI = 1.0D0/XSQ
      XNUM = P2(4)*XI+P2(5)
      XDEN = XI+Q2(4)
      DO 40 I=1,3
       XNUM = XNUM*XI+P2(I)
       XDEN = XDEN*XI+Q2(I)
40    CONTINUE
      RES = (SSQPI+XI*XNUM/XDEN)/X
45     RES = RES*DEXP(-XSQ)
      RES = 1.0D0-RES
50    IF (ISW.EQ.-1) RES = -RES
      DAERF = RES
      RETURN
      END
C*====================================================================*
```

```
C Copyright Dr. H. K. D. H. Bhadeshia, University of Cambridge
C MUCG1.FOR
C calculation of XEQ and GMAX only. Adapted from MUCG46.FOR
C 5 July 1994
C
C Department of Materials Science and Metallurgy, Pembroke St. Cambridge CB2 3QZ
C
C SUBROUTINE for calculations of Widmanstatten Ferrite
C Originally name of the SUBROUTINE is AG but modified for
C the Widmanstatten Ferrite
C
```

```
C
      SUBROUTINE AGWF(C,W,XBAR,T10,T20,KTEMP,XMAX,GMAX)
      IMPLICIT REAL*8 (A-H,K-Z), INTEGER (I,J)
      DOUBLE PRECISION C(8)
      X1=C(1)
      XA=0.001D+00
      R=8.31432D+00
      W1=48570.0D+00
      H=38575.0D+00
      S=13.48D+00
      XEQ=0.1D+00
      IC=0
C
      T=KTEMP
      CTEMP=T-273.15D+00
C
      IF (T .LE. 1000.0) GOTO 20
      H1=105525.0D+00
      S1=45.34521D+00
      GOTO 19
20    H1=111918.0D+00
      S1=51.44D+00
C
C Following line 19 is modified from
C "F=ENERGY(T,T10,T20)" by K. ICHIKAWA
C on 17th JUly 1995.
C
19    F=ENERGY(T,T10,T20)+50.0D+00
      AJ=1.0D+00-DEXP(-W/(R*T))
      AJ1=1.0D+00-DEXP(-W1/(R*T))
51    TEQ=R*T*AFEG(XEQ,AJ)-F
      IF (DABS(TEQ) .LT. 1.0) GOTO 52
      ETEQ=DAFEG(XEQ,AJ)*R*T
      XEQ=XEQ-TEQ/ETEQ
C Modified by K. Ichikawa Until ****
      IC=IC+1
```

```
      IF (IC .GE. 1000000) GOTO 55

C ****
      GOTO 51
52    AEQ=CG(XEQ,T,W,R)
      AFEQ=AFEG(XEQ,AJ)
      A=CG(X1,T,W,R)
      AFE=AFEG(X1,AJ)
C
      CALL GMAAX(A1,A,W1,F,R,T,X,AFE,H1,S1)
      GMAX=R*T*(A1-A)
C




C Following line of "XMAX=XEQ" is added by K. ICHIKAWA
C for the calculation of Widmanstatten Ferrite on 17th
C July 1995.

      XMAX=XEQ


60    RETURN

C55     WRITE(*,56)
55    CONTINUE
56    FORMAT(5X,'*** Calculations of XEQ and GMAX could not'/
     &       10X,' conpleted correctly  ***'//)

      GOTO 60

      END
C*************************************************************
      SUBROUTINE WSTEMP(C,W,GMAX,GAAF,WS,HIGHT)
```

```
      IMPLICIT REAL*8 (A-H,K-Z), INTEGER (I,J)
      DOUBLE PRECISION C(8)

C     K. Ichikawa, University of Cambridge 13 Feb 1996.
C
C     Find the WS, maximum temperature at which Widmanstatten
C     transformation is possible.
C
C     All temperatures in Kelvine through out this subroutine.
C     TSTART is the temperature at which calculation for Widmanstatten
C     ferrite starts.
C
C     GMAX is maximum free energy change possible during the nucleation.
C     GAAF is free energy change for growth.
C



      CALL OMEGA(C,W,XBAR,T10,T20,0)
      CALL WHIGH(C,W,T10,T20,HIGHT,ICI)

      TSTART=HIGHT+273.18
      TSTOP=673.18


      DT=1.0
      J1=(TSTART-TSTOP)/DT

      DO 1 I=1,J1
      T=TSTART-DT*I

      GN=-2540.0+3.637*(T-273.18)


      CALL AG(C,W,XBAR,T10,T20,T,XEQ,GMAX,FPRO,
     &                H,S,H1,S1,W1,F,AJ,AJ1)
```

```
      GAAF=FPRO

      WS=T
      IF(GMAX .LE. GN .AND. GAAF .LE. -50.0)GOTO 10


1     CONTINUE

10    RETURN

      END

C*************************************************************
      SUBROUTINE WSNUCRATE(WSI,SV,T,GMAX)
      IMPLICIT REAL*8 (A-H,K-Z), INTEGER (I,J)

C
C Find the nucleation rate of Widman. ferrite.
C
C Based on the equation in (19) the paper, G.I.Rees and H.K.D.H.Bhadeshia,
C Bainite transformation kinetics Part 1 Modified model, Mat. Sci.
C and Tech. 1992, Vol.8, p985-993.
C
C U is the volume of a bainitic subunit
C
      CONSTR=2540.0D+00
      R=8.31432D+00
      U=(10.0D-06)*(10.0D-06)*(0.2D-06)
C     U=(10.0D-06)*(10.0D-06)*(0.2D-06)
C     In the original Harry's paper, K1DASHU = 33.90D+06
C                                    K2=2.065D+04
C     Modifying to fit the experimental data


      K1DASHUN=5.0D+05
```

```
      K2N=       0.155D+06

      K1DASHU=5.0D+05
      K1DASHU=K1DASHUN
      K1DASH =U*K1DASHU
      LBAR=2.0/SV
      K1=1.0/(LBAR*K1DASH)
      K2=0.15D+06
      K2=K2N
C
C
      WSI=K1*DEXP(-(K2)/(R*T)-K2*GMAX/(CONSTR*R*T))
C WSI is       nucleation rate per unit volume here.
      WSI=WSI/SV
C WSI is now nucleation rate per unit area.
C       WRITE(*,*)'WSI=',WSI

      RETURN

      END


C***********************************************************************
C***********************************************************************
       SUBROUTINE VWMAINCOMP(SV,CURR,VOLT,EFF,SPEED,TINT,
      &T,XMAX,WDIFF,W,XBAR,AB2,VF,J2,CTEMP,J,C,T10,T20,J3,VFW
      &,CTEMPW,HIGHT,IM,WS,JW,TIMED,TTIME,G,VMAX,WSIT)
       IMPLICIT REAL*8(A-H,K,L,O-Z), INTEGER(I,J,M,N)
       DOUBLE PRECISION CTEMP(1000),AC(8),BC(8),C(8),VF(1000)
      &,CTEMPW(1000),WSI(1000),VFW(1000),G(1000),
      &TIMED(1000),TTIME(1000)

C ############################
C CAUTION!!
C DEVFW(1000), DSVFW(1000) and DVFW(1000) are deleted from the above
C "DOUBLE PRECISION" because of the installation of the new concepts.
```

```
C K. Ichikawa 17 April 1996.
C ##########################

C Calculations for each cooling rate

      LW=0.0
      WFFT=400.0
      AB2=5.0
      JW=((WS-WFFT)/AB2)+1

      I=IM

      CTEMPW(I)=CTEMP(I)
      KTEMP=CTEMPW(I)+273.15D+00
C
C     Following CALL AGWF Statement was added to calculate the XMAX
C     by K. Ichikawa on 18 July 1995.
C
      CALL AGWF(C,W,XBAR,T10,T20,KTEMP,XMAX,GMAX)
C
      CTEMPWT=CTEMPW(I)
      CALL TIM(CULRAT1,TIMEI,AB2,CTEMPWT,CURR,VOLT,SPEED,TINT,J)

C Following "IF - ENDIF" is not necessary.
C
C       IF (I .EQ. 1) THEN
C       TIME(I)=TIMEI
C       ELSE
C       TIME(I)=TIMEI+TIME(I-1)
C       ENDIF
C
C     CONST1=tan(30degree)
C     C4: empirical constant for obtaining the actual volume fraction of
C         ferrite.
      A=2.0/((3.0)**(1/2))/SV
```

```
      L=2.0*A
      CONST1=(1/3)**(1/2)
      C4=1.0
C
C       T2 is cooling time

C       T2=(CURR*VOLT*EFF)/SPEED/C1/(1.0-C2)*
C       &((WFST-TINT)**(1.0-C2)-(WFFT-TINT)**(1.0-C2))
C
C Q is half-thickness of allotriomorphic ferrite
C
      Q=((3.0**(1/2))/2.0)*(1.0-(1.0-VF(J2))**(1/2))
C
C
      DO 10 ICONP=1,8
       AC(ICONP)=C(ICONP)
       IF(ICONP .EQ. 5 .OR. ICONP .EQ. 6 .OR. ICONP .EQ. 7) THEN
          BC(ICONP)=0.0
       ELSE
          BC(ICONP)=C(ICONP)
       ENDIF
10    CONTINUE

C
C       Following subroutine "OMEGA" was installed to get "WDIFF".

      CALL OMEGA(BC,WDIFF,XBARD,T10D,T20D,0)
C
      CALL PROGC(VMAX,CTEMPW,XMAX,WDIFF,W,XBAR)
      G(I)=VMAX

C ************** being Modified ********************************
C
C     Find the volume fraction of Widmanstatten ferrite,
C
C
```

```
C      BETA=(Thickness of Widman. ferrite)/(Length or Width)
C

       CALL WSNUCRATE(WSIT,SV,KTEMP,GMAX)
       WSI(I)=WSIT

       BETA=0.045

       IF (I .EQ. 1) THEN
        TIMED(I)=TIMEI

       ELSE

        TIMED(I)=(LN(1.0-VFW(I-1))/(-BETA*(G(I-1)**3)*
     &WSI(I-1)/4.0))**(1/4)
       ENDIF



       IF (I .EQ. 1) THEN
        TTIME(I)=TIMED(I)
       ELSE
        TTIME(I)=TTIME(I-1)+TIMED(I)
       ENDIF



C ********** being Modified again until @1@ **********
C ##########################
C Killed because of installation of new concept.
C K. Ichikawa on 16 April 1996.

C      DSVFW(I)=1.0-DEXP(-(BETA/4.0)*(G(I)**3)*WSI(I)*((TIMED(I))**4))
```

```
C        DEVFW(I)=1.0-DEXP(-(BETA/4.0)*(G(I)**3)*WSI(I)*
C      &((TIMED(I)+TIMEI)**4))

C         DVFW(I)=DEVFW(I)-DSVFW(I)

C          IF (I .EQ. 1) THEN
C           VFW(I)=DVFW(1)
C          ELSE
C

C          VFW(I)=DVFW(I)+VFW(I-1)
C         ENDIF
C ##########################


C ***** @1@ ************************************************
C
C          DSVFW(I)=1.0-DEXP(-(BETA/4.0)*(G(I)**3)*WSI(I)*((TIME(I))**4))
C
C          DEVFW(I)=1.0-DEXP(-(BETA/4.0)*(G(I)**3)*WSI(I)*
C      &((TIMED(I)+TIMEI(I))**4))
C
C          DVFW(I)=DEVFW(I)-DSVFW(I)
C
C
C          IF (I .EQ. 1) THEN
C           VFW(I)=DVFW(1)
C          ELSE
C
C
C          VFW(I)=DVFW(I)+VFW(I-1)
C          ENDIF
C
C
C ************** Being Modified ********************************
```

```
C       Followin equation did not agree very well with experimental data
C       by K. Ichikawa on 23 October 1995.
C
C       VW(I)=C4*G*(L-4.0*Q*CONST1)*TIME(I)*TIME(I)/L/L
C


C       Following WRITE STATEMENT were killed because of the instration
C       of Widmanstatten calc. program to the MAINCONP Program by K.
C       ICHIKAWA on 4 Dec. 1995.
C       WRITE(6,6)

C ############################
C Killed because of installation of new concept.
C K. Ichikawa on 16 April 1996.

C         WRITE(6,5)CTEMPW(I),VFW(I)

C ############################

C ***************************************************************
C
20      RETURN
C
5       FORMAT(F5.0,'    ',F7.5)
6       FORMAT(//' CTEMP      VW'/)
60      FORMAT(//'Widmanstatten Ferrite was impinged with
     &Allotriomorphic Ferrite'/)

80      FORMAT(//'Widmanstatten Ferrite was impinged with
     &Acicular Ferrite'/)

        END
C***************************************************************
C Finds approximate temperature at which paraequilibrium ferrite
```

```
C formation first becomes possible
C H. K. D. H. Bhadeshia, 6 July 1994
C
C This SUBROUTINE is made for the Widmanstatten Ferrite start temp.
C By K.Ichikawa on 8 Nov. 1995.
C
      SUBROUTINE WHIGH(C,W,T10,T20,HIGHT,ICI)
C
      IMPLICIT REAL*8(A-H,K-Z), INTEGER(I,J)
      DOUBLE PRECISION C(8)
C
       X1=C(1)
       XA=0.001D+00
       R=8.31432D+00
       W1=48570.0D+00
       H=38575.0D+00
       S=13.48D+00
       XEQ=0.05D+00
       IC=0
C
C      Modified following line from "DO 1 I=1183,973,-1" to
C      "DO 1 I=1183,893,-1", by K. Ichikawa on 31 Oct., 1994
C      and modified again to "DO 1 I=1183,879,-1".

      DO 1 I=1183,473,-1
C
       KTEMP=I
C
       T=KTEMP
C
        IF (T .LE. 1000.0) GOTO 20
          H1=105525.0D+00
          S1=45.34521D+00
        GOTO 19
20        H1=111918.0D+00
          S1=51.44D+00
```

```
C
19      F=ENERGY(T,T10,T20)+50.0D+00
        AJ=1.0D+00-DEXP(-W/(R*T))
        AJ1=1.0D+00-DEXP(-W1/(R*T))
51      TEQ=R*T*AFEG(XEQ,AJ)-F
        IF (DABS(TEQ) .LT. 1.0) GOTO 52
        ETEQ=DAFEG(XEQ,AJ)*R*T
        XEQ=XEQ-TEQ/ETEQ
C Modified by K.Ichikawa until ***
        IC=IC+1
        IF (IC .GE. 1000000) GOTO 220

C ***
        GOTO 51
52        IF(XEQ .GE. X1) THEN
            HIGHT=KTEMP-273.15D+00
            GOTO 222
          ENDIF
1       CONTINUE
C
          IF(XEQ .LT. X1) THEN
C               WRITE(*,53)
53              FORMAT(5X,'*** Alloy cannot transform to ferrite'/
     &             10X,' at temperature as low as 473 K   ***'//)
                HIGHT=0.0D+00
          ENDIF
C




222       RETURN
C220    WRITE(*,221)
220     CONTINUE
221     FORMAT(5X,'*** Calculation of XEQ could not be'/
```

```
     &        10X,' conpleted correctly  ***'//)
      ICI=2
      GOTO 222




        END
C*****************************************************************
C SUBROUTINE calculating the site saturation condition for the
C competitive growth of allotriomorphic and Widmanstatten
C ferrite on the austenite.
C
C K. Ichikawa on 29 Nov. 1995, modified from SUBROUNIE AVOLF
C
      SUBROUTINE SITESAT(AREA, ANS,VF,SV,BI,TIME,ALP,VOL,XBAR,
     &                   XAGA,XGAG,
     &                   TIMESAT,SATI,WSI,G)
C
      IMPLICIT REAL*8(A-H,K-Z), INTEGER(I,J)
      DOUBLE PRECISION THETA(1000),FUN(1000),
     &                 THETAW(1000),FUNW(1000)
C
C
C
          ILOOP=51
          AILOOP=ILOOP*1.0d+00
          ALP1=3.0D+00*ALP
          OMEGA=(XGAG-XBAR)/(XGAG-XAGA)

          ILOOPW=51
          AILOOW=ILOOPW*1.0d+00

          PI=3.141592654
          ETA=3.0
```

```
      BETA=0.045


C
C Numerical integration using ILOOP-1 slices
C
      DO 1 I=1,ILOOP
         IDUM=I-1
         THETA(I)=IDUM/(AILOOP-1.0D+00)
         ARG=0.5D+00*3.14159D+00*BI*ALP1**2.0D+00*TIME**2.0D+00*
     &        (1.0D+00-THETA(I)**4.0D+00)
         CALL AARG(ARG)
         FUN(I)=1.0D+00-DEXP(-ARG)

         IDUMW=I-1
         THETAW(I)=TIME*IDUMW/(AILOOPW-1.0D+00)

       ARGW=EXP((-WSI*BETA*G*(-THETAW(I)**3.0D+00
     &+TIME**3.0D+00))/3.0D+00)



         CALL AARG(ARGW)
         FUNW(I)=1.0D+00-DEXP(-ARGW)



1     CONTINUE
C


         CALL TRAPE(THETA,FUN,ANS,ILOOP)
         ARG=2.0D+00*SV*ANS*ALP*TIME**0.5D+00/OMEGA
         CALL AARG(ARG)
         VOL=1.0D+00-DEXP(-ARG)
         VF=VOL*OMEGA
```

```
            AREA=FUN(1)

C ?????????????????????????? Under Modification
C           CALL TRAPE(THETAW,FUNW,ANS,ILOOPW)
C
C           ARG=2.0D+00*SV*ANS*ALP*TIME**0.5D+00/OMEGA
C           CALL AARG(ARG)
C           VOL=1.0D+00-DEXP(-ARG)
C           VF=VOL*OMEGA
C           AREAW=FUNW(1)
C ??????????????????????????

C
C       RETURN
C
C Page 68, Book 14, 20-12-1986, H. K. D. H. Bhadeshia
C AREA is the fraction of boundary covered
C TIME is in seconds
C VOl is volume fraction of ferrite/equilibrium vol. frac.
C VF is the actual volume fraction
C ALP is the one-dimensional parabolic thickening rate constant
C ALP1 is the one-dimensional parabolic lengthening rate constant
C BI is the grain boundary face nucleation rate per unit area per unit t
C XGAG, XAGA = equilibrium mol frac of carbon in gamma and alpha respect
C XBAR = average mol frac of carbon in alloy
C SV = austenite grain boundary area per unit volume (1/m)

C
```

```
      SATI=AREA+AREAW


      IF(SATI .GE. 1.0) THEN
         TIMESAT=TIME
C          WRITE(*,20)TIMESAT
         GOTO 10
      ENDIF

10    RETURN
20    FORMAT(20X,'TIME for Site Sat. =',F8.4)
      END
C*****************************************************************
C SUBROUTINE transfers mole fraction of carbon to wt.%
C
C K. Ichikawa on 30 Dec. 1995
C
C Input C, XBARN as mole fraction, Output as wt.%.

      SUBROUTINE MOLTOWT(XBARN,C,CARBON,SI,MN,NI,MO,CR,V)
C
      IMPLICIT REAL*8(A-H,K-Z), INTEGER(I,J)
      DOUBLE PRECISION C(8)
C
C


      C(1)=XBARN*12.0115D+00
      C(2)=C(2)*28.09D+00
      C(3)=C(3)*54.94D+00
      C(4)=C(4)*58.71D+00
      C(5)=C(5)*95.94D+00
      C(6)=C(6)*52.0D+00
      C(7)=C(7)*50.94D+00
```

```
      C(8)=C(8)*55.84D+00
C
      TOTAL=C(1)+C(2)+C(3)+C(4)+C(5)+C(6)+C(7)+C(8)
C
      C(1)=C(1)/TOTAL*100.0
      C(2)=C(2)/TOTAL*100.0
      C(3)=C(3)/TOTAL*100.0
      C(4)=C(4)/TOTAL*100.0
      C(5)=C(5)/TOTAL*100.0
      C(6)=C(6)/TOTAL*100.0
      C(7)=C(7)/TOTAL*100.0
      C(8)=C(8)/TOTAL*100.0
C
      RETURN
      END
C*********************************************************************
C SUBROUTINE transfers mole fraction of carbon to wt.%
C
C K. Ichikawa on 23 Feb. 1996
C
C Input as mole fraction, Output as wt.%.

      SUBROUTINE MOLTOWTXBARN(XBARN,C)
C
      IMPLICIT REAL*8(A-H,K-Z), INTEGER(I,J)
      DOUBLE PRECISION C(8),CESC(8)
C
      CESC(2)=C(2)
      CESC(3)=C(3)
      CESC(4)=C(4)
      CESC(5)=C(5)
      CESC(6)=C(6)
      CESC(7)=C(7)
      CESC(8)=C(8)
C
      C(1)=XBARN*12.0115D+00
```

```
      C(2)=C(2)*28.09D+00
      C(3)=C(3)*54.94D+00
      C(4)=C(4)*58.71D+00
      C(5)=C(5)*95.94D+00
      C(6)=C(6)*52.0D+00
      C(7)=C(7)*50.94D+00
      C(8)=C(8)*55.84D+00
C
      TOTAL=C(1)+C(2)+C(3)+C(4)+C(5)+C(6)+C(7)+C(8)

C
      C(1)=C(1)/TOTAL*100.0
      C(2)=C(2)/TOTAL*100.0
      C(3)=C(3)/TOTAL*100.0
      C(4)=C(4)/TOTAL*100.0
      C(5)=C(5)/TOTAL*100.0
      C(6)=C(6)/TOTAL*100.0
      C(7)=C(7)/TOTAL*100.0
      C(8)=C(8)/TOTAL*100.0
C
      C(2)=CESC(2)
      C(3)=CESC(3)
      C(4)=CESC(4)
      C(5)=CESC(5)
      C(6)=CESC(6)
      C(7)=CESC(7)
      C(8)=CESC(8)
C
      RETURN
      END

C*****************************************************************
      SUBROUTINE AVOLFW2(AREA,ANS,VF,SV,BI,TIME,ALP,
     &VOL,XBARN,XAGA,XGAG,
     &WSI,G,XBAR,XAGA1,XGAG1)
C
```

```
C For the calcuration of Widmanstatten Ferrite Volume Fraction.
C Imitated from the SUBROUTINE AVOLF.
C
C Integration until the Widmanstatten Ferrite tip.
C
C K. Ichikawa, 11 April 1996.
C
      IMPLICIT REAL*8(A-H,K-Z), INTEGER(I,J)
      DOUBLE PRECISION FUN(1000),FUN2(1000),M(1000),
     &y1(1000),y2(1000)
C
          ILOOP=51
          AILOOP=ILOOP*1.0d+00
          ALP1=3.0D+00*ALP
C         BETA=0.05D+00 originally
          BETA=0.045D+00
          G1=BETA*G
          OMEGA=(XGAG-XBARN)/(XGAG-XAGA)
          OMEGAO=(XGAG-XBAR)/(XGAG-XAGA)

C
C Numerical integration using ILOOP-1 slices
C
      DO 1 I=1,ILOOP
          IDUM=I-1
          M(I)=IDUM/(AILOOP-1.0D+00)
          y1(I)=M(I)*ALP*TIME**0.5D+00
          y2(I)=(ALP*TIME**0.5D+00)+
     &          M(I)*(G*TIME-(ALP*TIME**0.5D+00))

C*Modified for the use of calculations of Widmanstatten ferrite
C until the next C*.
C Modified again for amending the fundamental mistake.
C 28 June 1996
          IF (G .EQ. 0.0D+00) THEN
          ARG =0.5D+00*3.14159D+00*BI*(ALP1**2.0D+00)
```

```
     &          *(TIME**2.0D+00)*
     &          (1.0D+00-(y1(I)/(ALP*TIME**0.5D+00))**4.0D+00)
          ARG2=0.0D+00

          ELSE
          ARG=0.5D+00*3.14159D+00*BI*(ALP1**2.0D+00)
     &          *(TIME**2.0D+00)*
     &          (1.0D+00-(y1(I)/(ALP*TIME**0.5D+00))**4.0D+00)+
     &          (1.0D+00/3.0D+00)*WSI*(G1)*(TIME**3.0D+00)*
     &          (1.0D+00-(y1(I)/(G*TIME))**3.0D+00)

          ARG2=(1.0D+00/3.0D+00)*WSI*(G1)*(TIME**3.0D+00)*
     &          (1.0D+00-(y2(I)/(G*TIME))**3.0D+00)
          ENDIF
C*
          CALL AARG(ARG)
          CALL AARG(ARG2)

          FUN(I) =1.0D+00-DEXP(-ARG )
          FUN2(I)=1.0D+00-DEXP(-ARG2)
1     CONTINUE
C

          CALL TRAPE(y1,FUN, ANS1,ILOOP)
          CALL TRAPE(y2,FUN2,ANS2,ILOOP)



     IF (G*TIME .GT. ALP*TIME**0.5D+00) THEN
      ANS=ANS1+ANS2
     ELSE
      ANS=ANS1
     ENDIF


          ARG=(2.0D+00*SV/OMEGA)*ANS
```

```
      CALL AARG(ARG)
      VOL=1.0D+00-DEXP(-ARG)
      VF=VOL*OMEGAO

      AREA=FUN(1)



C
      RETURN
C
C Page 68, Book 14, 20-12-1986, H. K. D. H. Bhadeshia
C AREA is the fraction of boundary covered
C TIME is in seconds
C VOl is volume fraction of ferrite/equilibrium vol. frac.
C VF is the actual volume fraction
C ALP is the one-dimensional parabolic thickening rate constant
C ALP1 is the one-dimensional parabolic lengthening rate constant
C BI is the grain boundary face nucleation rate per unit area per unit t
C XGAG, XAGA = equilibrium mol frac of carbon in gamma and alpha respect
C XBAR = average mol frac of carbon in alloy
C SV = austenite grain boundary area per unit volume (1/m)
C
C **********************************************************************
C Written by K. Ichikawa on 11 April 1996.
C
C WSI=Nucleation Rate of Widmanstatten Ferrite
C G=Growth Rate of Widmanstatten Ferrite
C PHI=y/(G*TIME)
C BETA=Geometrical Factor of Widmanstatten Ferrite (=0.05)
C
      END
C
```

```
C*********************************************************************
C*********************************************************************
      SUBROUTINE AVOLFW1(AREA,ANS,VF,SV,BI,TIME,ALP,
     &VOL,XBARN,XAGA,XGAG,
     &WSI,G,XBAR,XAGA1,XGAG1)
C
C For the calcuration of Widmanstatten Ferrite Volume Fraction.
C Imitated from the SUBROUTINE AVOLF.
C
C Integration until the Allotriomorphic Ferrite/Austenite Boundary
C
C K. Ichikawa, 11 April 1996.
C
      IMPLICIT REAL*8(A-H,K-Z), INTEGER(I,J)
      DOUBLE PRECISION FUN(1000),FUN2(1000),M(1000),
     &y1(1000),y2(1000)
C
          ILOOP=51
          AILOOP=ILOOP*1.0d+00
          ALP1=3.0D+00*ALP
          BETA=0.045D+00
          G1=BETA*G
          OMEGA=(XGAG-XBARN)/(XGAG-XAGA)
          OMEGAO=(XGAG-XBAR)/(XGAG-XAGA)

C
C Numerical integration using ILOOP-1 slices
C

      DO 1 I=1,ILOOP
          IDUM=I-1
          M(I)=IDUM/(AILOOP-1.0D+00)
          y1(I)=M(I)*ALP*TIME**0.5D+00
          y2(I)=(ALP*TIME**0.5D+00)+
     &          M(I)*(G*TIME-(ALP*TIME**0.5D+00))
```

```
C*Modified for the use of calculations of Widmanstatten ferrite
C until the next C*.
C Modified again for amending the fundamental mistake.
C 28 June 1996
      IF (G .EQ. 0.0D+00) THEN
      ARG =0.5D+00*3.14159D+00*BI*(ALP1**2.0D+00)
     &     *(TIME**2.0D+00)*
     &     (1.0D+00-(y1(I)/(ALP*TIME**0.5D+00))**4.0D+00)
      ARG2=0.0D+00

      ELSE
      ARG=0.5D+00*3.14159D+00*BI*(ALP1**2.0D+00)
     &     *(TIME**2.0D+00)*
     &     (1.0D+00-(y1(I)/(ALP*TIME**0.5D+00))**4.0D+00)+
     &     (1.0D+00/3.0D+00)*WSI*(G1)*(TIME**3.0D+00)*
     &     (1.0D+00-(y1(I)/(G*TIME))**3.0D+00)

      ARG2=(1.0D+00/3.0D+00)*WSI*(G1)*(TIME**3.0D+00)*
     &     (1.0D+00-(y2(I)/(G*TIME))**3.0D+00)
      ENDIF
C*
      CALL AARG(ARG)
      CALL AARG(ARG2)

      FUN(I) =1.0D+00-DEXP(-ARG )
      FUN2(I)=1.0D+00-DEXP(-ARG2)
1     CONTINUE
C
      CALL TRAPE(y1,FUN, ANS1,ILOOP)
      CALL TRAPE(y2,FUN2,ANS2,ILOOP)
```

```
      ANS=ANS1

         ARG=(2.0D+00*SV/OMEGA)*ANS


         CALL AARG(ARG)
         VOL=1.0D+00-DEXP(-ARG)
         VF=VOL*OMEGAO

         AREA=FUN(1)
C
      RETURN
C
C Page 68, Book 14, 20-12-1986, H. K. D. H. Bhadeshia
C AREA is the fraction of boundary covered
C TIME is in seconds
C VOl is volume fraction of ferrite/equilibrium vol. frac.
C VF is the actual volume fraction
C ALP is the one-dimensional parabolic thickening rate constant
C ALP1 is the one-dimensional parabolic lengthening rate constant
C BI is the grain boundary face nucleation rate per unit area per unit t
C XGAG, XAGA = equilibrium mol frac of carbon in gamma and alpha respect
C XBAR = average mol frac of carbon in alloy
C SV = austenite grain boundary area per unit volume (1/m)
C **********************************************************************
C Written by K. Ichikawa on 11 April 1996.
C
C WSI=Nucleation Rate of Widmanstatten Ferrite
C G=Growth Rate of Widmanstatten Ferrite
C PHI=y/(G*TIME)
C BETA=Geometrical Factor of Widmanstatten Ferrite (=0.05)
C
      END
C
```

```
C**********************************************************************

C**********************************************************************C
C To calculate the carbon concentration (mole fraction) at the
C   T-zero phase boundary at a specified temperature.
C
C H K D H Bhadeshia, University of Cambridge
C
      SUBROUTINE AXTO(H,S,H1,S1,XTO,T,W,W1,F,AJ,AJ1,STORE,XBARN,XBAR)
C
      IMPLICIT REAL*8(A-H,K-Z),INTEGER(I,J)
C
C XTO is the carbon concentration at the T-zero boundary
C T is the absolute temperature
C STORE is the stored energy in Joules per mole
C H, S, H1, S1, W, W1, F, AJ, AJ1 are thermodynamic quantities
C   defined in subroutines OMEGA, ENERGY and main program
C
C Initialize J
C
      J=0
C
C Calculate the driving force for the transformation of
C   austenite to ferrite without any change in chemical composition,
C   allowing for Zener ordering
C
C
##########################################################
########################
C Set the initial value of XTO in order to avoid the error.
C K.ICHIKAWA 28 May 1996.
C
C Modified on 24 June 1996 to XTO=XBAR.
C
C
C
```

```
      XTO=XBARN
C       XTO=XBAR

C
##################################################################
########################
C
      STORE=0.0
C
C In the following equation of "G=F+400.0", 400(J mol^-1) is
C a strain energy term due to the shape change.
C See H.K.D.H.Bhadeshia, Bainite in Steels, 1992.
C and H.K.D.H.Bhadeshia, Acta Metallurgica Vol. 29 pp.1117-1130,
C 1981.
C
C Following was previously "G=F+400.0". But it is modefied to
C "G=F".
C
C
      G=F+350.0
1     DFTO=FTO1(H,S,XTO,T,W,W1,H1,S1,G,AJ,AJ1)+STORE
C
C Solve for XTO using Newton's iterative method
C
        J=J+1
        IF (DABS(DFTO) .LE. 10.0D+00) GOTO 2
C
C Obtain differential of FTO1 with respect to XTO
C
      G9=G91(XTO,T,W,W1,H1,S1,G,H,S,AJ,AJ1)
C
C Modify original guess of XTO, assuming that convergence occurs
C  within nine iterations
C
        IF (J .GE. 9) GOTO 2
        XTO=XTO-DFTO/G9
```

```
      IF (XTO .LE. 1.0D-12) GOTO 3
      GOTO 1
3     XTO=0.0000D+00
C
2        RETURN
         END
C
C*********************************************************************
C
C*********************************************************************
C
C To calculate the differential of FTO1 with respect to XTO
C  see subroutine FTO1 for description of parameters
C The differentiation is used in order to apply the Newton Iteration
C
C Unpublished work, H. K. D. H. Bhadeshia, University of Cambridge
C  See laboratory book 5B
C
      DOUBLE PRECISION FUNCTION G91(XTO,T,W,W1,H1,S1,F,
     &                              H,S,AJ,AJ1)
CCCC
      DOUBLE PRECISION R,XTO,T,W,W1,H1,S1,F,AJ,AJ1,FD,FD1,DT5,
     &DT6,DZEN1,DZEN2,DZEN3,V1,V2,V3,V4,V5,V6,V7,V8,V9,G1,
     &DZEN6,DZEN7,DZEN8,H,S
C
C MOdified by K. Ichikawa on 30 May 1996.
C R is the universal gas constant
C
      R=8.31432
C
      FD=DSQRT(1.0-2.0*(1.0+2.0*AJ)*XTO+(1.0+8.0*AJ)*XTO*XTO)
      FD1=DSQRT(9.0-6.0*XTO*(2.0*AJ1+3.0)+(9.0+16.0*AJ1)*XTO*XTO)
C
      DT5=28080.0*XTO/(1.0-XTO)
      DT6=T/DT5
C
```

```
      IF (DT6 .GT. 1.0) GOTO 48
      IF (DT6 .LT. 0.25) GOTO 47
C
      DZEN1=0.2307+42.7974*DT6-233.8631*(DT6**2)+645.4485*(DT6**3)
     &-954.3995*(DT6**4)+711.8095*(DT6**5)-211.5136*(DT6**6)
      DZEN2=-2.6702+45.6337*DT6-225.3965*(DT6**2)+567.7112*(DT6**3)
     &-771.6466*(DT6**4)+538.1778*(DT6**5)-151.3818*(DT6**6)
C
      GOTO 46
C
47    DZEN2=1.0
      DZEN1=3.295
46    DZEN3=(((DZEN2*XTO)**2)*(-50898.56)/(1.0-XTO))+DZEN1*T*XTO*
     &(0.6623741)
C
      DZEN3=DZEN3*4.187
      GOTO 45
48    DZEN3=0.0
C
45    V1=FD-1.0+3.0*XTO
      V2=FD+1.0-3.0*XTO
      V3=1.0-2.0*AJ+(4.0*AJ-1.0)*XTO-FD
      V4=2.0*AJ*(2.0*XTO-1.0)
      V5=FD1-3.0+5.0*XTO
      V6=FD1+3.0-5.0*XTO
      V7=(XTO-1.0-2.0*AJ+8.0*XTO*AJ)/FD
      V8=(9.0*XTO-9.0-6.0*AJ1+16.0*AJ1*XTO)/FD1
      V9=H1-(H)-(S1-(S))*T-6.0*W+4.0*W1
      G1=2.0+DLOG(XTO**2)+4.0+DLOG((1.0-XTO)**4)
     &-10.0-DLOG((1.0-2.0*XTO)**10)
     &-DLOG((V1/V2)**6)-6.0*((XTO/V1)*(V7+3.0+V1*(3.0-V7)/V2))
     &+DLOG((V3/V4)**6)-
     &6.0*((1.0-XTO)/V3)*(4.0*AJ*(1.0-(V3/V4))-V7)
     &+3.0*(DLOG(3.0-4.0*XTO)-4.0*XTO/(3.0-4.0*XTO))
     &+DLOG((V5/V6)**4)+4.0*(XTO
     &/V5)*(V8+5.0+(V5/V6)*(5.0-V8))
```

```
      IF (DT6 .GT. 1.0) GOTO 90
      DZEN6=(-3.3948+13.6112*DT6-13.4376*(DT6**2))*T/(28080.0*
     &((1.0-XTO)**2))
      DZEN7=(-3.3118+15.7462*DT6-23.2449*(DT6**2))*T/(28080.0*
     &((1.0-XTO)**2))
      DZEN8=50898.0*((DZEN2*XTO)**2)/((1.0-XTO)**2)+(-50898.0*(2*
     &DZEN2*DZEN6*(XTO**2)+2.0*XTO*(DZEN2**2))/(1.0-XTO))+DZEN1
     &*T*0.6623741+DZEN7*T*XTO*0.6623741
      GOTO 91
90    DZEN8=0.0
C
91    G91=V9+R*T*G1+DZEN8-F
C
        RETURN
        END
C
C*********************************************************************
C
C*********************************************************************
C
C To calculate the free energy change accompanying the transformation
C from austenite to ferrite of the same chemical composition, including
C a Zener ordering term. The latter describes the ordering of carbon
C atoms, that leads the body-centered cubic lattice of ferrite becoming
C body-centered tetragonal. The degree of ordering increases as the
C carbon concentration increases, or as the transformation temperature
C decreases.
C
C H. K. D. H. Bhadeshia
C
C Department of Materials Science and Metallurgy
C Pembroke Street, Cambridge CB2 3QZ, U. K.
C 31 March 1987
C
C MOdified by K. Ichikawa on 30 May 1996.
C
```

```
C
C References:
C
C   C. Zener Trans. AIME 167 (1946) 550.
C
C   J. C. Fisher, Metals Transactions 185 (1949) 688-690.
C
C   H. K. D. H. Bhadeshia and D. V. Edmonds
C    Acta Metallurgica 28 (1980) 1265-1273.
C    Also see laboratory book 7.
C
      DOUBLE PRECISION FUNCTION FTO1(H,S,X,T,W,W1,H1,S1,F,AJ,AJ1)
C
      DOUBLE PRECISION R,X,T,T60,ZEN1,ZEN2,ZENER,
     &                 W,W1,H1,S1,F,AJ,AJ1,D,D11,H,S
C
      D=DSQRT(1.0D+00-2.0D+00*(1.0D+00+2.0D+00*AJ)*X
     &+(1.0D+00+8.0D+00*AJ)*X*X)
      D11=DSQRT(9.0D+00-6.0D+00*X*(2.0D+00*AJ1+3.0D+00)
     &+(9.0D+00+16.0D+00*AJ1)*X*X)
C
C Units of T = Kelvin
C
C Calculate T60, which is the value of the actual temperature T
C    divided by the critical temperature beyond which there is no
C    Zener ordering. X is the mole fraction of carbon in the ferrite.
C If T60¿1, the transformation occurs above the ordering temperature
C    and Zener ordering does not occur.
C
      T60=T*(1.0D+00-X)/(28080.0D+00*X)
C
      IF (T60 .GT. 1.0) GOTO 18
C
C Calculate the contribution to the free energy change due to
C   Zener ordering.
C
```

```
      IF (T60 .GT. 0.25) GOTO 17
C
C Polynomial fit to data in Table 2 of Fischer (1949)
C
      ZEN1=0.2307+42.7974*T60-233.8631*T60*T60+645.4485*T60*T60*T60
     &-954.3995*(T60**4)+711.8095*(T60**5)-211.5136*(T60**6)
      ZEN2=-2.6702+45.6337*T60-225.3965*T60*T60+567.7112*(T60**3)
     &-771.6466*(T60**4)+538.1778*(T60**5)-151.3818*(T60**6)
      GOTO 16
C
17    ZEN2=1.0D+00
      ZEN1=3.295
C
16    ZENER=(((ZEN2*X)**2)*(-50898.56)/(1.0-X))+ZEN1*T*X*0.6623741
C
C convert from calories per mole to Joules per mole
      ZENER=ZENER*4.187
      GOTO 15
C
18    ZENER=0.0
C
C Calculation of the Zener ordering term complete
C
C R is the universal gas constant
15    R=8.31432
C
C calculate the free energy change accompanying the change from
C austenite to ferrite of the same composition, including a Zener
C ordering term. See Bhadeshia and Edmonds (1980)
C
      FTO1=X*R*T*DLOG(X*X)+X*(H1-(H)-(S1-(S)
     &)*T+4.0*W1-6*W)-R*T*(1.0-X)*DLOG((1.0-X)**4)+
     &5.0*R*T*(1.0-2.0*X)*DLOG(1.0-2.0*X)
     &-R*T*X*DLOG(((D-1.0+3.0*X)/(D+1.0-3.0*X))**6)
     &-R*T*(1.0-X)*DLOG(((1.0-2.0*AJ+(4.0
     &*AJ-1.0)*X-D)/(2.0*AJ*(2.0*X-1.0)))**6)+
```

```
     &3.0*R*T*X*DLOG(3.0-4*X)+R*T*
     &X*DLOG(((D11-3.0+5.0*X)/(D11+3.0-5.0*X))**4)+
     &(1.0-X)*F+ZENER
C
C
          RETURN
          END
C
C**********************************************************************
C
```

REFERENCES

Aaronson, H. I. and Wells, C.: *Transactions of Metallurgical Society of AIME* **206** (1956) 1216–1223.

Abson, D. J., Dolby, R. E. and Hart P. H. M.: *Trends in steels and consumables for welding,* Paper 25, The Welding Institute (1979) 75–101.

Abson, D. J.: *Nonmetallic Inclusions in Ferritic Steel Weld Metals–A review,* IIW Document IX-1486-87 (1987).

Adams, C. M.: *Welding Journal* **31** (1958) 210s–215s.

Ali, A. and Bhadeshia, H. K. D. H.: *Materials Science and Technology* **6** (1990) 781–784.

American Institute of Physics: *American Institute of Physics Handbook, 3rd ed.,* ed., Gray, D. E., McGraw-Hill (1972).

Andrews, K. W.: *Journal of the Iron and Steel Institute* **203** (1965) 721–727.

ASME CASE 2098-1, American Society for Mechanical Engineers (1991).

ASTM designation E 112-82, American Society for Testing and Materials.

Ashby, M. F. and Ebeling, R.: *Transactions of the Metallurgical Society of AIME* **236** (1933) 1396–1404.

Atkinson, C.: *Acta Metallurgica* **15** (1967) 1207–1221.

Avrami, M.: *Journal of Chemical Physics* **7** (1939) 1103–1112.

Avrami, M.: *Journal of Chemical Physics* **7** (1940) 212–224.

Babu, S. S., Bhadeshia H. K. D. H. and Svensson L. -E.: *Journal of Materials Science Letters* **10** (1991) 142–144.

Babu, S. S. and Bhadeshia, H. K. D. H.: *Journal of Materials Science Letters* **14** (1995) 314–316.

Babu, S. S., David, S. A., Vitek, J. M., Mundra, K. and DebRoy, T.: *Materials Science and Technology* **11** (1995) 186–199.

Bailey, N.: *The Welding Institute Research Report,* No. 26/1976/M (1976).

Bailey, N. and Jones, S. B.: *Welding Journal* **51** (1978) 217s–231s.

Bhadeshia, H. K. D. H. and Edmonds, D. V.: *Metallurgical Transactions* **10A** (1979) 895–907.

Bhadeshia, H. K. D. H. and Edmonds, D. V.: *Acta Metallurgica* **28** (1980) 1265–1273.

Bhadeshia, H. K. D. H.: *Acta Metallurgica* **29** (1981a) 1117–1130.

Bhadeshia, H. K. D. H.: *Metal Science* **15** (1981b) 175–177.

Bhadeshia, H. K. D. H.: *Metal Science* **15** (1981c) 178–180.

Bhadeshia, H. K. D. H.: *Metal Science* **15** (1981d) 477–479.

Bhadeshia, H. K. D. H.: *Metal Science* **16** (1982a) 159–165.

Bhadeshia, H. K. D. H.: *JOURNAL DE PHYSIQUE* **43, C4** (1982b) 443–448.

Bhadeshia, H. K. D. H., Svensson, L.–E. and Gretoft, B. A.: *Acta Metallurgica* **33** (1985a) 1271–1283.

Bhadeshia, H. K. D. H.: *Materials Science and Technology* **1** (1985b) 497–504.

Bhadeshia, H. K. D. H.: *Progress in Materials Science* **29** (1985c) 321–386.

Bhadeshia, H. K. D. H., Svensson, L.–E. and Gretoft, B.: *Journal of Materials Science* **21** (1986a) 3947–3951.

Bhadeshia, H. K. D. H., Svensson, L. E. and Gretoft, B.: *Preprints Part 1, Third International Conference on Welding and Performance of Pipelines,* London, The Welding Institute, 18–21 November (1986b), (17-1)–(17-10).

Bhadeshia, H. K. D. H., Svensson, L.–E. and Gretoft, B.: *Welding Metallurgy of Structural Steels,* ed. Koo, J. Y., AIME, Warrendale (1987) 517–529.

Bhadeshia, H. K. D. H.: *Phase Transformations '87,* ed. Lorimer G. W., Institute of Metals, London (1988) 309–314.

Bhadeshia, H. K. D. H. and Christian, J. W: *Metallurgical Transactions* **21A** (1990) 767–797.

Bhadeshia, H. K. D. H.: *Bainite in Steels,* The Institute of Materials (1992).

Bhadeshia, H. K. D. H. and Svensson, L.–E.: *Modelling the evolution of microstructure in steel weld metal, Mathematical modelling of weld phenomena,* ed. Cerjak, H. and Easterling, K. E., The Institute of Materials (1993) 109–180.

Bhadeshia, H. K. D. H.: *Thermodynamics, Cambridge Program for Industry text, "Modelling Phase Transformations of in Steel",* 20–22 March, (1995a).

Bhadeshia, H. K. D. H.: *2nd Griffith Conference on Fracture on Micromechanisms of Fracture and Their Structural Significance* (1995b) 15–24.

Bhadeshia, H. K. D. H., MacKay, D. J. C. and Svensson L.–E.: *Materials Science and Technology* **11** (1995) 1046–1051.

Bhadeshia, H. K. D. H.: *Materials World,* November (1996) 943–645.

Bhadeshia, H. K. D. H.: *Displacive Phase Transformations and Their Applications in Materials Engineering,* ed. Inoue, K., Mukherjee, K., Otsuka, K. and Chen, H., The Minerals, Metals & Materials Society , (1998) 69–78.

Blackburn, J. M., Vassilaros, M., Brandemarte, A., Fox, A. and Franke, G.: *Welding and Weld Automation in Shipbuilding,* ed. DeNale, R., The Minerals, Metals & Materials Society (1996) 167–186.

Bradley, J. R., Rigsbee, J. M. and Aaronson, H. I.: *Metallurgical Transactions* **8A** (1977) 323–333.

Buck, P.: *MSc thesis,* Colorado School of Mines, Golden, Colorado (1984).

Cahn, J. W.: *Acta Metallurgica* **4** (1956a) 449–459.

Cahn, J., W.: *Acta Metallurgica* **4** (1956b) 572–575.

Christian, J. W.: *The Theory of Transformations in Metals and Alloys, Part 1 Equilibrium and General Kinetic Theory, 2nd ed.,*Pergamon Press Ltd, Oxford (1975).

Carapella, L. A.: *Metals Progress* **46** (1944) 108.

Chijiiwa, R., Tamehiro, H., Yoshida, Y., Funato, K., Uemori, R. and Horii, Y.: *Shinnittetsu Gihou,* Nippon Steel Corporation, Tokyo, Japan **No. 348** (1993) 55–62.

Clyne, T. W. and Kurz, W.: *Metallurgical Transactions* **12A** (1981) 965–971.

Coates, D. E.: *Metallurgical Transactions* **4** (1973) 2313–2325.

Cochrane, R. C. and Kirkwood, P. R.: *Trends in steels and consumables for welding,* Paper 35, The Welding Institute (1979) 103–121.

Cool, T.: *Ph. D. Thesis,* University of Cambridge (1996).

Cool, T. and Bhadeshia, H. K. D. H.: *Materials Science and Technology* **12** (1996) 40–44.

Cottrell, C.L. M.: *Iron and Steel Institute Special Report* **76** (1962) 1–6.

DeHoff, R. T. and Rhines, F. N.: *Quantitative Microscopy,* McGraw Hill, New York (1968).

Devillers, L., Kaplan, D., Marandet, B., Ribes, A. and Ribound, P. V.: *The Effects of Residual, Impurity and Microalloying Elements on Weldability and Weld Properties,* Paper 1, The Welding Institute (1984) 1-1–1-11.

Devletian, J. H., Singh, D. and Wood, W. E.: *Trends in Welding Research, Proceedings of the 4th International Conference,* Gatlinburg, TN (1995) 341–346.

Devletian, J. H., Singh D. and Wood, W. E.: *Welding and Weld Automation in Shipbuilding,* ed. DeNale, R., The Minerals, Metals & Materials Society (1996) 151–166.

Dieter, G. E.: *Mechanical Metallurgy, 2nd ed.,* McGraw-Hill, New York, NY (1976) 261–80.

Dilthey, U., Pavlik, V. and Reichel, T.: *Mathematical Modelling of Weld Phenomena 3,* ed. Cerjak, H., The Institute of Materials (1997) 85–113.

Dixon, B.: *Australian Welding Journal* **Summer** (1981) 23s–30s.

Dowling, J. M., Corbett, J. M., and Kerr, H. W.: *Metallurgical Transactions* **17A** (1986) 1611–1623.

Dubé, C. A.: *Ph. D. Thesis,* Carnegie Institute of Technology, Pittsburgh, PA (1948).

Dubé, C. A., Aaronson, H. I. and Mehl, R. F.: *Revue de Metallurgie* **No. 3** (1958) 201–210.

Dunne, D. P. and Wayman, C. M.: *Metallurgical Transactions* **2** (1971) 2327–2341.

Enomoto, M.: *Metallurgical Transactions* **22A** (1991a) 1235–1245.

Enomoto, M.: *Tetsu-to-Hagané* **77** (1991b) 735–745.

Enomoto, M.: *Materia Japan,* The Japan Institute of Metals **33** (1994) 147–154.

Evans, G. M.: *Welding Journal* **62** (1983) 313–320.

Evans, G. M.: *OERLIKON–Schweißmitt* **48** (1990) 15–31.

Evans, G. M.: *OERLIKON–Schweißmitt* **49** (1991) 18–33.

Evans, G. M.: *Welding Journal* **October** (1995) 249s–261s.

Farrar, R. A. and Zhang, Z.: *Materials Science and Technology* **12** (1995) 759–764.

Fonda, R. W., Spanos, G. and Vandermeer, R. A.: *Trends in Welding Research, Proceedings of the 4th International Conference,* Gatlinburg, TN (1995) 277–282.

Fox, A. G., Eakes, M. W. and Franke, G. L.: *Welding Journal* **October** (1996) 330s–342s.

Franklin, A. G.: *Journal of the Iron and Steel Institute* **207** (1969) 181–186.

Friedel, J.: *Dislocations,* Addison–Wesley (1964) 189.

Fick, J. I. J. and Rogerson, J. H.: *Low Carbon Structural Steels for Eighties,* The Institute of Metallurgist, London (1977) 41–50.

Fiore, S. R.: *Welding and Weld Automation in Shipbuilding,* ed. DeNale, R., The Minerals, Metals & Materials Society (1996) 135–150.

Fisher, J. C.: *Metals Transactions* **185** (1949) 688–690.

Garland, J. G. and Bailey, N.: *The Welding Institute Research Report,* No. 25/1976/M (1976).

Garland, J. G. and Kirkwood, P. R.: *Metal Construction* **7** (1975) 275–283.

Gilbert, A. and Owen, W. S.: *Acta Metallurgica* **10** (1962) 45–54.

Ghosh, G. and Olson, G. B.: *Proceedings of ICOMAT'92, International Conference on Martensitic Transformations,* Monterey, Institute for Advanced Studies, CA, USA, (1993) 353–358.

Ghosh, G. and Olson, G. B.: *Acta Metallurgica et Materialia* **42** (1994) 3361–3370.

Grange, R. A. and Stewart H. M.: *Transactions of the American Institute of Mining and Metallurgical Engineer* **167** (1946) 467–501.

Gretoft, B., Bhadeshia, H. and Svensson, L.–E.: *Acta Stereologica* ESS IV-2, Göteborg (1985) 365–371.

Gregg, J. M. and Bhadeshia, H. K. D. H.: *Acta Metallurgica et Materialia* **42** (1994a) 3321–3330.

Gregg, J. M. and Bhadeshia, H. K. D. H.: *Metallurgical and Materials Transactions* **25A** (1994b) 1603–1611.

Grong, O. and Matlock, D. K.: *International Metals Reviews* **31** (1986) 27–48.

Grong, Ø.: *Metallurgical Modelling of Welding,* The Institute of Materials (1994).

Handbook of Chemistry and Physics, 57th ed., ed. Weast, R. C., CRC Press, Ohio (1977).

Hehemann: *Phase Transformations,* American Society for Metals (1970).

Hillert, M.: *Internal Report,* Swedish Institute Metal Research (1953).

Hillert, M.: *Jernkontrets Annaler* **141** (1957) 757–785.

Hollomon, J. H. and Jaffe, L. D.: *Ferrous Metallurgical Design,* Wiley, New York (1947) 47.

Homma, H., Wakabayashi, M. and Mori, N.: *Preprint of the National Meeting of Japan Welding Society, Autumn* **31** (1982) 56–57.

Honeycombe, R. W. K. and Bhadeshia, H. K. D. H.: *Steels, Microstructure and Properties, 2nd ed.,* Edward Arnold (1995).

Horii, Y.: *Recent Development on Controlling the Microstructure and Toughness of Low Alloy Weldments, Proceedings of "Nishiyama-Kinen-Gijutu-Kouza" (Nishiyama Memorial Technical Lecture),* The Iron and Steel Institute of Japan, 15 February **No. 128** (1989) 39–76.

Horii, Y., Ohkita, S. and Wakabayashi, M.: *Proceedings of the First Pacific Asia Offshore Mechanics Symposium,* Seoul, Korea, June (1990) 103–107.

Horii, Y. and Ohkita, S.: *Journal of the Japan Welding Society* **60** (1991) 632–636.

Horii, Y.: *Dr. Thesis,* Osaka University, Japan (1995a).

Horii, Y., Ichikawa, K., Ohkita, S., Funaki, S. and Yurioka, N.: *Quarterly Journal of Japan Welding Society* **31** (1995b) 500–507.

Horii, Y., Ohkita, S., Shinada, K. and Koyama, K.: *Shinnittetsu Gihou,* Nippon Steel Corporation, Tokyo, Japan **No. 355** (1995c) 13–19.

Hsieh, K., C., Babu, S. S., Vitek, J. M. and David, S. A.: *Materials Science and Engineering A* **215** (1996) 84–91.

Hultgren, A.: *Transactions of the American. Society for Metals* **39** (1947) 915–968.

Hultgren, A.: *Jernkontorets Annaler* **135** (1951) 403–483.

Ichikawa, K., Horii, Y., Akechi, S. and Kobayashi, J.: *Welding Journal* **July** (1995) 230–238.

Ichikawa, K., Horii, Y., Motomatsu, R., Yamaguchi, M. and Yurioka, N.: *Quarterly Journal of Japan Welding Society* **14** (1996) 27–32.

Ichikawa, K.: *Unpublished work* (1997).

Ichikawa, K.: *Unpublished work* (1998).

Iezawa, T., Inoue, T., Hirano, O., Okazawa, T. and Koseki, T.: *Tetsu-to-Hagané* **79** (1993) 1108–1114.

Ikeda, R., Oi, K., Yasuda, K. and Nakano, Y.: *Preprints of the National Meeting of Japan Welding Society* **60** (1997) 240–241.

Ishida, K.: *Journal of Alloys and Compounds* **220** (1995) 126–131.

Ito, Y. and Nakanishi, M.: *Journal of Japan Welding Society* **44** (1975) 815–821.

Japanese Industrial Standard (JIS) G3106, Japanese Standards Association (1992).

Jang, J. and Indacochea, J. E.: *Journal of Materials Science* **22** (1987) 689–700.

Jones, S. J. and Bhadeshia, H. K. D. H.: *Acta Materialia* **45** (1997a) 2911–2920.

Jones, S. J. and Bhadeshia, H. K. D. H.: *Metallurgical and Materials Transactions A* **28A** (1997b) 2005–2013.

Kasuya, T. and Yurioka, N.: *Welding Journal* **March** (1993) 107s–115s.

Kaufmann, L. and Cohen, M.: *Progress in Metal Physics* **7** (1958) 165–246.

Kayali, E. S., Pacey, A. J. and Kerr, H. W.: *Canadian Metallurgical Quarterly* **23** (1984) 227–236.

Kihira, H. and Matsuda, F.: *Transactions of Japan Welding Research Institute* **2-2** (1973) 83–95.

Kirkaldy, J. S.: *Canadian Journal of Physics* **36** (1958) 907–916.

Kirkaldy, J. S., Thomson, B. A. and Baganis, E. A.: *Prediction of multicomponent equilibrium and transformation diagram for low-alloy steel, Hardenability concept with applications to steels,* AIME, USA (1978).

Kluken, A. O. and Grong, Ø.: *Metallurgical Transactions* **20A** (1989) 1335–1349.

Kluken, A. O. and Grong, Ø.: *Trends in Welding Research, Proceedings of the 3th International Conference,* Gatlinburg, TN (1993) 569–574.

Komizo, Y.: *JWS (Japan Welding Society) BULLETIN, Japan Welding Society* No. 13 September (1994) 151–153.

Koseki, T., Ohkita, S. and Yurioka, N.: *Science and Technology of Welding and Joining* **2** (1997) 65–69.

Kurz, W. and Fisher, D. J.: *Fundamentals of Solidification, 3rd ed.,* TRANS TECH PUBLICATIONS (1992).

Kusunoki, Y and Umemoto, M.: *Current Advances in Materials and Processes, Report of the ISIJ Meeting* **6** (1996) A-25.

Lazor, R. B. and Kerr, H. W.: *Pipeline and Energy Plant Piping: Design and Technology,* Pergamon Press, Toronto, Canada (1980) 141–149.

Lehmann, J., Gaye, H., Yamada, W. and Matsumiya, T.: *Proceedings of the 6th International Iron and Steel Congress,* Nagoya, Japan, October, The Iron and Steel Institute of Japan (1990) 256–263.

MacKay, D. J. C.: *Neural Computation* **4** (1992a) 415–447.

MacKay, D. J. C.: *Neural Computation* **4** (1992b) 448–472.

MacKay, D. J. C.: *Neural Computation* **4** (1992c) 720–736.

MacKay, D. J. C.: *Darwin College Journal, March* **4** (1993) 81.

MacKay, D. J. C.: *ASHRAE (American Society of Heating, Refrigerating and Airconditioning Engineers) Transactions* **100** (1994) 1053–1062.

MacKay, D. J. C.: *Network : Computation in Neural Systems* **6** (1995) 469–505.

MacKay, D. J. C.: *Maximum Entropy and Bayesian Methods, Fundamental Theories of Physics, 62,* ed., Heidbreder, G. R., Kluwer Academic (1996).

MacKay, D. J. C.: *Bayesian Non-Linear Modelling with Neural Networks, Mathematical Modelling of Weld Phenomena 3,* ed. Cerjak, H, The Institute of Materials (1997) 359–389.

Magee, C. L.: *Ph. D. Thesis,* Carnegie Institute of Technology, Pittsburgh, PA (1966).

Masumoto, I. and Imai, K.: *Journal of the Japan Welding Society* **39** (1970) 565–575.

Matsuda, H.: *Yousetuyakingaku,* Nikkan-Kougyou-Shinbunsha, Tokyo, Japan (1972).

Mills, A. R., Thewlis, G. and Whiteman, J. A.: *Materials Science and Technology* **3** (1987) 1051–1061.

Morgan–Warren, E. J. and Jordan, M. F.: *Metals Technology* **1** (1974) 271–278.

Mori, N., Homma, H., Ohkita, S. and Wakabayashi, M.: *Journal of the Japan Welding Society* **50** (1981) 174–181.

Mori, N., Homma, H., Wakabayashi, M., Ohkita, S. and Saito, S.: *Seitetsu Kenkyu,* Nippon Steel Corporation **307** (1982a) 104–116.

Mori, N., Homma, H. and Wakabayashi, M.: *Preprint of the National Meeting of Japan Welding Society, Spring* **30** (1982b) 64–65.

Morita, Z., Tanaka, T., Imai, N., Kiyose, A. and Katayama, Y.: *Transactions of ISIJ* **28** (1988) 198–205.

Mullins, W. W. and Sekerka, R. F.: *Journal of Applied Physics* **34** (1963) 323–329.

Nakao, Y., Oshige, H., Noi, S. and Nishi, Y: *Quarterly Journal of the Japan Welding Society* **3** (1985) 773–781.

Nehrenberg, A. E.: *Transactions of the American Institute of Mining and Metallurgical Engineers* **167** (1946) 494–498.

Ohhama, N., Tobishima, N., Motomatsu, R., Suzuki, T., Ichikawa, K. and Horii, Y.: *Reprints of the National Meeting of Japan Welding Society* **57** (1995) 292–293.

Ohkita, S., Homma, H., Tsushima, S. and Mori, N.: *IIW Document. II-1070-86,* (1986).

Ohshita, S., Yurioka, N., Mori, N. and Kimura, T.: *Welding Journal* **May** (1983) 129s–136s.

Oi, K., Ikeda, R., Kawabata, T. and Amano, K.: *Preprints of the National Meeting of Japan Welding Society* **60** (1997) 242–243.

Okumura, M.: *Dr Thesis,* Osaka University, Japan (1990).

Olson, G. B.: *Personal communication to Bhadeshia, H. K. D. H.* (1995).

Olson, D. L., Liu, S., and Edwards, G. R.: *Physical Metallurgical Concerns in the Modelling of Weld Metal Transformations, Mathematical modelling of weld phenomena,* ed. Cerjak, H and Easterling, K. E., The Institute of Materials (1993) 89–108.

Payson, P. and Savage, C. H.: *Transactions of the American Society for Metals* **33** (1944) 261–280.

Phillips, R. H. and Jordan, M. F.: *Metals Technology* **4** (1977) 396–405.

Puls, M. P. and Kirkaldy, J. S.: *Metallurgical Transactions* **3** (1972) 2777–2794.

Purdy, G. R., Weichert, D. and Kirkaldy, J. S.: *Transactions of the Metallurgical Society of AIME* **230** (1964) 1025–1934.

Reck, V. Jr.: *Master's Thesis,* Naval Postgraduate School, Monterey, CA (1995).

Reed, R. C. and Bhadeshia, H. K. D. H.: *Materials Science and Technology* **8** (1992) 421–431.

Rees, G. I. and Bhadeshia, H. K. D. H.: *Materials Science and Technology* **8** (1992) 985–993.

Rees, G. I. and Bhadeshia, H. K. D. H.: *Materials Science and Technology* **10** (1994) 353–358.

Rees, G. I.: *Widmanstätten Ferrite, Cambridge Programme for Industry text, "Modelling Phase Transformations in Steels",* 20–22 March (1995).

Ricks, R. A., Howell, P. R. and Barrite, G. S.: *Journal of Materials Science* **17** (1982) 732–740.

Robson, J. D. and Bhadeshia, H. K. D. H.: *Calphad* **20** (1996) 447–460.

Robson, J. D. and Bhadeshia, H. K. D. H.: *Materials Science and Technology* **13** (1997a) 631–639.

Robson, J. D. and Bhadeshia, H. K. D. H.: *Materials Science and Technology* **13** (1997b) 640–644.

Rosenthal, D.: *Welding Journal* **21** (1941) 220s–234s.

Rowland, E. S. and Lyle, S. R.: *Metal Progress* **47** (1945) 907–912.

Rowland, E. S. and Lyle, S. R.: *Transactions of American Society for Metals* **37** (1946) 27–47.

Russell, K. C.: *Acta Metallurgica* **17** (1969) 1123–1131.

Saito, Y.: *Materials Science and Engineering* **A223** (1997) 134–145.

Sakumoto, Y., Keira, K., Mochizuki, H., Tahara, T. and Hagiwara, K.: *Shinnittetsu Gihou,* Nippon Steel Corporation, Tokyo, Japan **No. 344** (1992) 31–39.

Samsonova, G. V.: *Fiziko-khimicheskie svoistva okislov,* Moscow, Izdatel'stvo Metallurgiya (1969).

Sandvik, B. J. P.: *Metallurgical Transactions A* **13A** (1982) 777–800.

Sato, K., Mukai, Y. and Toyota, M.: *Yousetsu-kougaku,* Rikougakusha, Japan (1981).

Savage, W. F. and Aaronson, A. H.: *Welding Journal* **45** (1966) 85–90.

Scheil, E.: *Archiv für das Eisenhüttenwesen* **12** (1935) 565–571.

Scheil, E.: *Bemerkungen zur Scichtkristallbildung,* Zeitschrift für Metallkunde **34** (1942) 70–72.

Sekiguchi, H., Masumoto, I. and Imai, K.: *Journal of the Japan Welding Society* **35** (1966) 1025–1032.

Shimomura, J., Tani, H., Kooriyama, T., Sato, S. and Ueda, S.: *Kawasaki Steel Giho,* Tokyo, Japan **20** (1988) 189–196.

Shinoda, T., Hoshino, K., Yamashita, R. and Ono, H.: *Quarterly Journal of The Japan Welding Society* **8** (1990) 21–25.

Shipway, P. H. and Bhadeshia, H. K. D. H.: *Materials Science and Engineering A* **223** (1997) 179–185.

Siller, R. H. and McLellan, R. B.: *Transactions Metallurgical Society of AIME* **245** (1969) 697–700.

Siller, R. H. and McLellan, R. B.: *Metallurgical Transactions* **1** (1970) 985–988.

Singh, S. B. and Bhadeshia, H. K. D. H.: *Materials Science and Engineering* **A245** (1998) 72–79.

Smrha, L.: *Solidification and crystallisation of steel ingot (in Czech),* SNTL, Prague (1983).

Sneider, G. and Kerr, H. W.: *Canadian Metallurgical Quarterly* **23** (1984) 315–325.

Spanos, G. and Hall, M. G.: *Metallurgical and Materials Transactions* **27A** (1996) 1519–1534.

Steven, W. and Haynes, A. G.: *Journal of the Iron and Steel Institute* **183** (1956) 349–359.

Sundman, B., Jansson, B. and Andersson, J.–O.: *Calphad* **9** (1985) 153–190.

Surian, E., Trotti, J., Cassanelli A. and De Vedia, L. A.: *Welding Journal* **March** (1994) 45s–53s.

Svensson, L.–E., Gretoft, B. and Bhadeshia, H. K. D. H.: *Scandinavian Journal of Metallurgy* **15** (1986) 97–103.

Svensson, L.–E. and Gretoft, B.: *Welding Journal* **December** (1990) 454s–461s.

Swallow, E. and Bhadeshia, H. K. D. H.: *Materials Science and Technology* **12** (1996) 121–125.

Thewlis, G.: *Joining & Materials* **2** (1998a) 25–32.

Thewlis, G.: *Joining & Materials* **2** (1998b) 125–129.

Thewlis, G.: *Materials Science and Technology* **10** (1994) 110–125.

Taguchi, I., Hamada, H. and Tani, S.: *NIPPON STEEL TECHNICAL REPORT, July* (1985) 59–68.

Touloukian, Y. S., Powell, R. W., Ho, C. Y. and Klemens, P. G.: *Thermophysical Properties of Matter, The TPRC Data Series Vol. 1, Thermal Conductivity, Metallic Elements and Alloys,* IFI/PLENUM, New York, Washington (1970).

Townsend, R. D. and Kirkaldy, J. S.: *Transactions of American Society for Metals* **61** (1968) 605–619.

Trivedi, R.: *Metallurgical Transactions* **1** (1970) 921–927.

Trivedi, R. and Pound, G. M.: *Journal of Applied Physics* **38** (1967) 3569–3576.

Uchino, K.: *Dr Thesis,* Kyushu University, Japan (1997) 41–48.

Umemoto, M., Ohtsuka, H. and Tamura, I.: *Proceedings of International Conference on HSLA Steels,* eds. Dunne, O. P. and Chandra, T. Wollongong, Australia, printed by South Coast Printers (1984) 107–112.

Umemoto, M.: *Tetsu-to-Hagané* **81** (1995) 157–166.

Underwood, E. E.: *Quantitative Stereology,* Adison-Wesley Publishing Co., London (1970).

Van der Ven, A. and Delaey, L.: *Progress in Materials Science* **40** (1996) 181–264.

Vercesi, J. and Surian, E.: *Welding Journal* **June** (1996) 191s–196s.

Watanabe, I. and Kojima, T.: *Journal of Japan Welding Society* **49** (1980) 772–780.

Watanabe, J., Takai, K. and Nagumo, M.: *Tetsu-to-Hagané* **82** (1996) 947–952.

Watson, J. D. and McDougall, P. G.: *Acta Metallurgica* **21** (1973) 961–973.

Wayman, C., M.: *Introduction to the Crystallography of Martensite,* Macmillan, New York (1964).

Welding Handbook, 7th ed., Vol.1, American Welding Society, ed. Weisman, C., Florida (1981) 79.

Wilkinson, F. J., Cottrell, C. L. M. and Huxley, H. V.: *British Welding Journal* **5-12** (1958) 557–562.

Yamamoto, K., Hasegawa, T. and Takamura, J.: *ISIJ International* **36** (1996) 80–86.

Yang, J. R. and Bhadeshia, H. K. D. H.: *Materials Science and Technology* **5** (1989) 93–97.

Yang, J. R. and Chang, L. C.: *Materials Science and Engineering A* **223** (1997) 158–167.

Yurioka, N., Suzuki, H., Ohshita, S. and Saito, S.: *Welding Journal* **June** (1983) 147s–153s.

Yurioka, N., Okumura, M., Kasuya, T. and Ohshita, S.: *Welding Note, 3rd ed.,* Nippon Steel Corporation (1985).

Yurioka, N., Okumura, M., Kasuya, T. and Cotton, H. J.: *Metal Construction* **19** (1987) 217R–223R.

Yurioka, N.: *Journal of the Japan Welding Society* **61** (1992) 288–304.

Zener, C.: *Transactions of the American Institute of Mining and Metallurgical Engineers* **167** (1946) 550–583.

Zener, C.: *Journal of Applied Physics* **20** (1949) 950.

Zhang, S., Hattori, N., Enomoto, M. and Tarui, T.: *ISIJ International* **36** (1996) 1301–1309.

Zhang, Z. and Farrar, R. A.: *Materials Science and Technology* **12** (1996) 237–260.